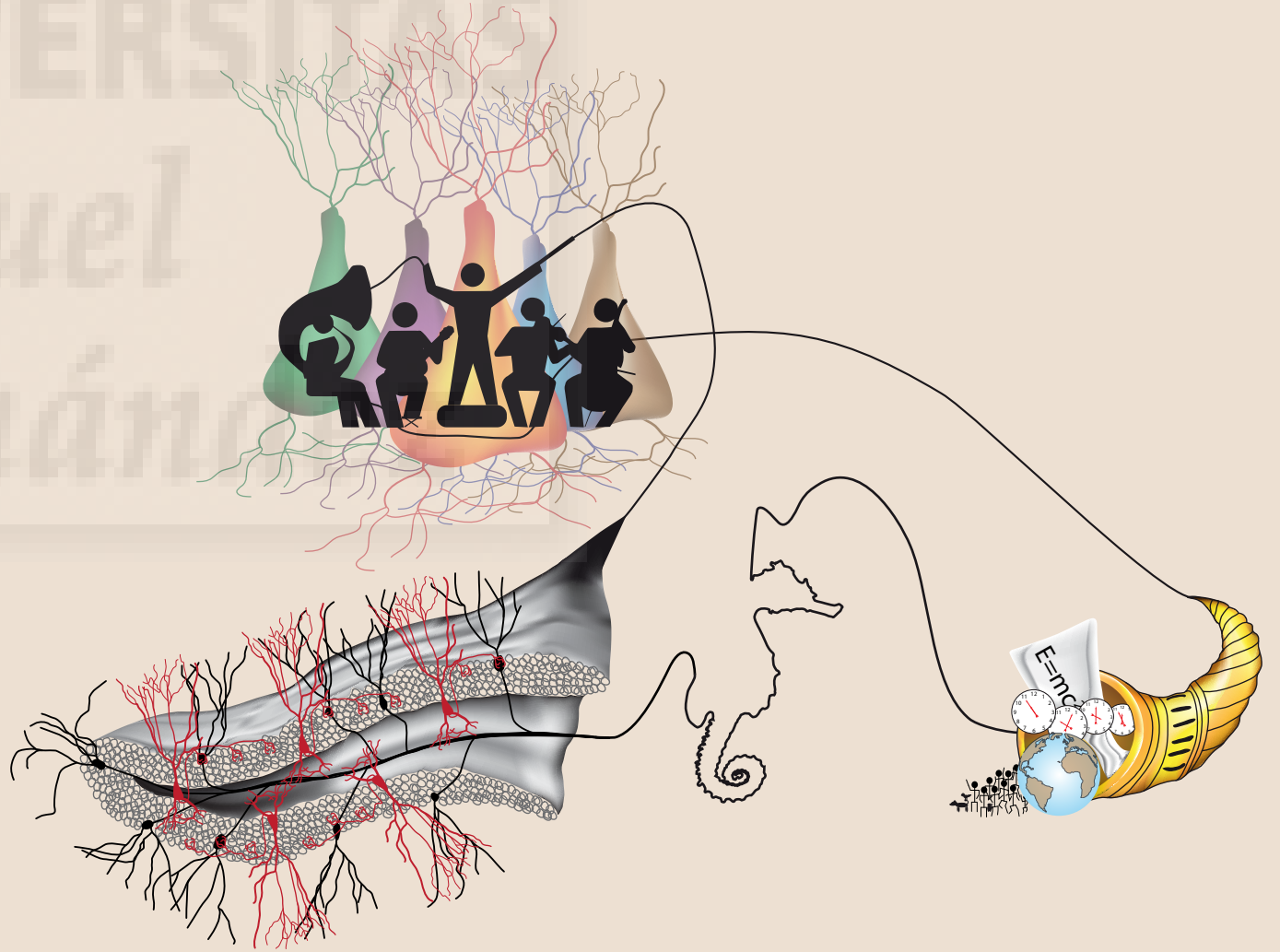UNIVERSITAS
Miguel Hernández

Instituto de Neurociencias (CSIC-UMH)
Programa de Doctorado en Neurociencias
Universidad Miguel Hernández, Alicante (España).

Hilar parvalbumin interneurons control functional connectivity associated to spatial memory encoding.

JOSÉ MARÍA CARAMÉS TEJEDOR   2018

TESIS DOCTORAL

José María Caramés Tejedor
Alicante, 2018.

EXCELENCIA SEVERO OCHOA

CSIC
Consejo Superior de Investigaciones Científicas

CSIC
UNIVERSITAS
Miguel Hernández
INSTITUTO DE NEUROCIENCIAS

GOBIERNO DE ESPAÑA
MINISTERIO DE EDUCACIÓN, CULTURA Y DEPORTE

Instituto de Neurociencias (CSIC-UMH)
Programa de Doctorado en Neurociencias
Universidad Miguel Hernández, Alicante (España).

Hilar parvalbumin interneurons control functional connectivity associated to spatial memory encoding.

Doctoral thesis
presented by
José María Caramés Tejedor

Director:
Dr. Santiago Canals Gamoneda, CSIC.

Academic tutor:
Prof. Juana Gallar Martínez, UMH.

San Juan de Alicante, 2018.

To who it may concern:

The doctoral thesis developed by me, José María Caramés Tejedor, entitle *Hilar parvalbumin interneurons control functional connectivity associated to spatial memory encoding*, included the following publication in the annex (section X), in which I am the second author.

Complete reference:

Pérez-Cervera L, Caramés J.M., Fernández-Mollá, L.M., Moreno, A., Fernández, B., Pérez-Montoyo, E., Moratal, D., Canals, S. and Pacheco-Torres, J. (2018). *Mapping functional connectivity in the rodent brain using electric-stimulation fMRI.* Methods Mol. Biol. 1718: 117-134. Chapter 8.

<u>doi:</u> 10.1007/978-1-4939-7531-0_8.

This publication will not be used in any other thesis.

José María Caramés Tejedor.

A QUIEN CORRESPONDA:

Prof. Miguel Valdeolmillos López, Coordinador del Programa de Doctorado en Neurociencias del Instituto de Neurociencias, Centro Mixto de la Universidad Miguel Hernández-UMH y la Agencia Estatal Consejo Superior de Investigaciones Científicas-CSIC,

CERTIFICA:

Que la Tesis Doctoral *"Hilar parvalbumin interneurons control functional connectivity associated to spatial memory encoding"* ha sido realizada por D. José María Caramés Tejedor (DNI 80159781-C) bajo la dirección del Dr. Santiago Canals Gamoneda y da su conformidad para que sea presentada a la Comisión de Doctorado de la Universidad Miguel Hernández

Para que así conste a los efectos oportunos, firma el presente certificado en San Juan de Alicante a 05 de Julio de 2018.

Miguel Valdeolmillos López.

A QUIEN CORRESPONDA:

Dr. Santiago Canals Gamoneda, científico titular del Consejo Superior de Investigaciones Científicas,

Autoriza la presentación de la Tesis Doctoral titulada "*Hilar parvalbumin interneurons control functional connectivity associated to spatial memory encoding*", realizada por D. José María Caramés Tejedor (DNI 80159781-C) bajo su inmediata dirección y supervisión en el Instituto de Neurociencias de Alicante, centro mixto CSIC-UMH, y que presenta para la obtención del grado de Doctor por la Universidad Miguel Hernández.

Y para que así así conste, y a los efectos oportunos, firma el presente Certificado en San Juan de Alicante, a 05 de Julio de 2018.

Santiago Canals Gamoneda.

AGRADECIMIENTOS.

En primer lugar, me gustaría agradecer enormemente a mi director de tesis, Santiago Canals, por su confianza, apoyo, paciencia y enseñanzas durante los 4 años que he pasado en su laboratorio. Espero que no se haya arrepentido muchas veces de haberme aceptado cuando trasladé la beca FPU y comencé a hacer este trabajo de tesis con su supervisión. Su apoyo ha sido fundamental para llevar a cabo tanto la tesis como todas las actividades que he hecho durante este tiempo (cursos, congresos, etc.). Santiago; gracias. Valoro muchísimo la oportunidad de poder haber realizado este trabajo en tu laboratorio, y tu guía para llevarlo a buen puerto. Ha sido un director de tesis fantástico y en estos años he podido comprobar que también una gran persona. Gracias.

También me gustaría agradecer especialmente, y con mucho cariño, a mi tutora académica, Juana Gallar. Aunque la beca FPU obligue a dar clases universitarias según BOE, soy muy consciente que ha sido gracias a ella que he podido tener esa grata experiencia docente. Sin ella, iniciarme en las prácticas docentes hubiera sido mucho más difícil. Además, contar con su experiencia y ayuda en las primeras clases ha sido, personal y profesionalmente, enormemente gratificante y es un modelo a seguir en el ejercicio profesional, académico y, sobre todo, en el trato personal. En este sentido, también tengo que agradecer a Mari Carmen Acosta, quien también me ha ayudado, y de quien es posible aprender tanto. Ambas también mediaron en el reconocimiento administrativo de las horas lectivas, aspecto que está(ba) en el limbo burocrático. Muchas gracias Juana y Mari Carmen, ha sido un privilegio poder aprender de vosotras.

Por otra parte, también quiero hacer mención a mis compañeras/os de laboratorio. Andrea, Andrés y Andrés, Antonio, Begoña, Corinne, Laura, Silvia, Víctor, a los que hemos acogido durante un tiempo, como Cristian, y las nuevas incorporaciones, Encarni y Selim. También a Jesús Pacheco, que me enseñó casi todo lo que sé de la parte práctica de la resonancia magnética; siempre se quedó más tiempo del que le correspondía si era necesario y siempre me trató con franco cariño. Gracias a todos; sin todos/as y cada uno de vosotros/as, el camino realizado para hacer la tesis no hubiera sido igual. Es posible que la tesis hubiera salido adelante, pero desde luego no hubiera sido tan enriquecedor, ni llevadero. Es genial venir a trabajar todos los días, fines de semana, festivos, etc., si al lado hay gente como vosotros. Mención especial para Elena y para Raquel. Las dos tuvieron la mala pata de comenzar a hacer el máster con mi "ayuda" (en caso de que lo mío pueda considerarse ayuda). Realmente el que se vió enriquecido por su presencia fui yo. Por mi parte, no hubiera podido tener mejores compañeras. Elena ha estado principalmente implicada en los experimentos de conducta; de hecho, la idea del SETAmaze (tarea de conducta explicada en la presente tesis) es una idea conjunta de los dos que involucra 5 horas de tren a Barcelona, un poco de fastidio-coraje porque no nos convenciera nada que hubiéramos visto en la bibliografía y alguna cerveza. Raquel llegó al laboratorio cuando se iba a comenzar a analizar histológicamente el experimento de cFos. Siempre está con una enorme sonrisa en la cara y desprende una ilusión por aprender que alegra. De ellas he aprendido mucho, y conocerlas ha sido enriquecedor, tanto laboral (¡los colores, los colores!) como personalmente. A todas/os vosotras/os, de corazón; gracias.

También a mis compañeros/as de otros laboratorios, y de aquellos en los que he estado antes. Son demasiados para mencionarlos a todos/as, pero que sepáis que me acuerdo y os llevo conmigo. Mención especial para Alfredo Espinet, que me aceptó en un laboratorio de aprendizaje por primera vez, arriesgándose a que la liara, como siempre ocurre al comenzar a

"gatear científicamente", y a Luis J. Santín y Carmen Pedraza, del departamento de Psicobiología de la Universidad de Málaga, que me enseñaron las primeras técnicas al uso para ahondar en el estudio del sistema nervioso vinculado a procesos cognitivos.

Por último, a mi familia cercana. Ellos/as saben quienes son. Sí quiero mencionar a Julián, que no ha podido verme defender la tesis, pero que tanto ha influido positivamente en mi. Siento que parte de lo que soy se lo debo a él, y por tanto parte de esta tesis es realmente suya.
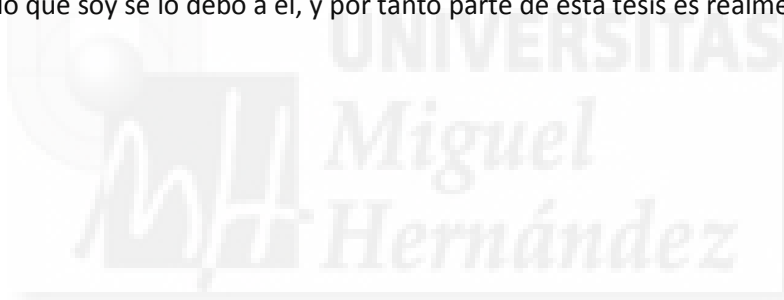
"Unos van por el ancho campo de la ambición soberbia; otros, por el de la adulación servil y baja; otros, por el de la hipocresía engañosa, y algunos, por el de la verdadera religión; pero yo, inclinado de mi estrella, voy por la angosta senda de la caballería andante, por cuyo ejercicio desprecio la hacienda; pero no la honra. […] Si el que esto entiende, si el que esto obra, si el que desto trata merece ser llamado bobo, díganlo vuestras grandezas".

Don Quijote de la Mancha, libro 2, cap. 32.

IV

INDEX.

LIST OF FIGURES.

INTRODUCTION.

MATERIAL AND METHODS.

RESULTS.

ABSTRACT.

ABSTRACT.

Episodic memory requires hippocampus and its interactions with other structures, as the prefrontal cortex. Inactivation of synapses either in hippocampus or prefrontal cortex prevents memory formation. However, synapse potentiation (i.e. in the form of LTP) not only enhances synaptic strength but also reorganizes hippocampal functional connectivity so that it alters its interactions with other structures. We hypothesize that synaptic plasticity, trough its action on the excitation/inhibition balance, redistributes activity in the system to enhance functional coupling in a distributed network of structures required for memory formation.

In this thesis I study the role of hilar parvalbumin-expressing interneurons on either intra-hippocampal as well as extra-hippocampal long-range functional connectivity, and how, through this mechanism, they influence spatial memory encoding, consolidation and/or retrieval. We also investigate whether hilar parvalbumin (PV) interneurons control the size of the formed memory engram. We hypothesize that the inhibition of hilar PV basket cells enhances activity propagation, facilitating the encoding of new dentate gyrus-dependent memories in a brain-wide distributed network. This hypothesis is based on previous findings showing that synaptic plasticity in the dentate gyrus, in the form of LTP in the perforant pathway, alters the excitation/inhibition balance.

To commit our investigation, we combine pharmacogenetic (Designer Receptors Exclusively Activated by Designer Drugs, DREADDs, able to excite or inhibit the containing neurons) expressed on the hilar PV interneurons in mice, with *in vivo* electrophysiological recordings in dentate gyrus, CA1 and prefrontal cortex, fMRI and standard and custom-designed behavioural tasks to dissects different aspects of the memory formation. To evaluate the engram size, we analysed cFos labelling in dentate gyrus and hippocampus after the experimental animals carried out the behavioural task.

Briefly, our data confirm that hilar PV basket interneurons control the output of dentate gyrus granule cells, not affecting its dendritic properties. Inhibition of hilar PV interneurons makes the granule cells to fire in response to smaller stimulation currents and with shorter delays, so that dentate gyrus-to-hippocampus propagation increases, enhancing the intra-hippocampal connectivity and, very impressively, also the extra-hippocampal long-range connectivity with the prefrontal cortex, medial temporal lobe structures and other areas related to different aspects of memory and learning. This increased connectivity reminds to the one obtained after LTP induction, but we do not induce LTP to get it; we only decrease granule cell perisomatic tone. Importantly, behavioural testing in the same animals shows that inhibition of hilar PV interneurons also enhances the spatial memory encoding, but not consolidation, nor its retrieval. This enhanced encoding is accompanied by improved pattern separation when confronting animals with similar contexts, ruling out a possible effect of disinhibition in memory generalization. Further cFos analysis supported this conclusion, by showing that PV-cells inhibition does not change the size of the engrams recruited during memory formation. On the contrary, activation of hilar PV interneurons impairs granule cells fire, decreasing functional connectivity and precluding encoding, even though granule cells dendrites and engram size remained intact.

These data point to the hilar PV interneurons as regulators for intra- and extra-hippocampal functional connectivity, demonstrating that perisomatic inhibition controlling granule cell firing at the local level, and not synaptic plasticity, *per se*, in granule cells, determines the efficiency of new information encoding in hippocampal memory engrams. We hypothesize that the

described mechanism, nailed down to a single cell type (PV-interneurons), in a defined brain region (dentate gyrus) and a particular cognitive function (episodic memory formation) may represent a more general mechanism to regulate information flows in the wide brain network.

RESUMEN.

La memoria episódica require del hipocampo y de sus interacciones con otras estructuras, como corteza prefrontal. Si las sinapsis se inactivan en alguna de estas estructuras, la memoria se impide. Sin embargo, la potenciación de las sinapsis (tras LTP) no sólo mejora las sinapsis, también reorganiza la conectividad hipocampal de manera que su interacción con otras estructuras también mejora. Hipotetizamos que esta redistribución de la actividad en el sistema se basa en la ratio excitación/inhibición.

El presente trabajo estudia las implicaciones funcionales que tienen las interneuronas del hilus que expresan parvalbúmina (PV), sobre la conectividad funcional del giro dentado y del hipocampo, sobre su conectividad con otras estructuras y sobre la codificación, consolidación y recuperación de la memoria espacial, y sobre la separación de patrones; funciones asociadas al giro dentado. Además, también estudiamos si la regulación de las interneuronas parvalbúmina del hilus condiciona el tamaño del engrama mnémico. La hipótesis que nos guía es que la inhibición de estas neuronas facilita la propagación de la actividad neuronal, facilitando la codificación de memorias dependientes de giro dentado. Nos basamos en que la inducción de LTP causa un aumento de la excitación, pero también reduce el tono inhibitorio local, de manera que la modulación de poblaciones neuronales inhibitorias concretas podría tener efectos similares.

Para llevar a cabo la investigación, combinamos farmacogenética (DREADDs, del acrónimo Designer Receptors Exclusively Activated by Designer Drugs, que tienen capacidad para excitar o inhibir a las neuronas que los contienen), expresados en las neuronas parvalbúmina del hilus en ratones, con registros electrofisiológicos *in vivo* en giro dentado, CA1 y corteza prefrontal, imagen por resonancia magnética funcional y tareas conductuales que nos permiten estudiar distintos aspectos de la memoria. Para evaluar el tamaño del engrama evaluamos el marcaje con cFos en giro dentado e hipocampo, una vez que los ratones finalizaron la tarea de conducta.

Brevemente, nuestros datos indican que las neuronas parvalbúmina del hilus controlan el disparo de las granulares del giro dentado sin afectar funcionalmente a sus dendritas. La inhibición de las interneuronas PV hace que las granulares disparen más fácilmente y con menor latencia, en respuesta a una menor estimulación, incrementando la propagación giro dentado-hipocampo y, sorprendentemente, también la conectividad del hipocampo con otras estructuras como corteza prefrontal, regiones del lóbulo temporal medial y otras también involucradas en diferentes aspectos del aprendizaje y la memoria. Esta conectividad aumentada recuerda a la obtenida tras la inducción de LTP, pero en este trabajo no inducimos LTP para obtenerla; disminuimos la inhibición perisomática sobre las células granulares del giro dentado. La inhibición de las neuronas PV del hilus también favorece la codificación de la memoria espacial, sin afectar ni a su consolidación, ni a su recuperación. Esta codificación aumentada permite una mejor separación de patrones cuando se testa enfrentando una retención favorecida a largo plazo, con una tarea espacial a corto plazo. Este dato es coherente con que la inhibición de las neuronas PV del hilus no cambia el tamaño del engrama marcado con cFos. Por el contrario, la activación de las neuronas PV del hilus dificulta el disparo de las neuronas granulares sobre sus dianas hipocampales, disminuyendo la actividad interna del hipocampo e impidiendo la codificación de la memoria, incluso aunque las dendritas de las células granulares y el tamaño del engrama permanecen intactos.

Estos datos apuntan a que las interneuronas PV del hilus son unos controladores clave en la regulación de la conectividad intra- y extra-hipocampal, demostrando que la inhibición perisomática local sobre las células granulares, y no la plasticidad sináptica en células granulares, *per se*, determina la eficiencia de la entrada de nueva información en los engramas de memoria hipocampales. Hipotetizamos que el mecanismo aquí descrito, apuntando a una población concreta (interneuronas PV$^+$), en una región definida (giro dentado) y relacionada con una función cognitiva específica (codificación de memoria episódica), puede representar un mecanismo más general que regule el tránsito de información en redes neuronales.

I.- INTRODUCTION.

1.1- Memory. Historical review.

1.1.1.- First studies – until 1st half of XX century.

Before starting, I would like to beg the pardon of many other scientists that preceded in memory study and are not included here. For sure their works influenced the persons named herein (and many others; it is a collective work), but to dive in the historical part of the study of the memory is not the point of the present PhD thesis. The sole objective is to contextualize the experimental work presented herein.

In science, we progress by adding a small step to those that others did before us. There are some notions of classic philosophers and physicians that boarded the memory, during classic era and medieval age[1]. However, its systematic study started very recently.

At the end of the XIX century, something was changing in the academic environment. Psychology was just born in Wilhelm Wunt's physiology laboratory in Leipzig (1879), creating the first laboratory of experimental psychology and getting separated from the general physiology in its object of study; focused on the cognitive functions and brain. Also, Jean Marie Charcot (1825-1893), teaching in the Salpêtrière, was founding the modern neurology. Many relevant figures for the incipient cognitive function studies were his pupils, like William James, Alfred Binet, and Joseph Babinski, among others. Clinical physicians were approaching the study of the central nervous system doing more structured observation regarding the language[2,3], memory — Korsakoff syndrome was characterised in 1887; Armand-Ribot wrote the first attempt to study the memory in term of modern neuroscience in 1881; Alzheimer defined the disease that takes his name in 1901—, and other cognitive functions. In that period, Richard Wolfman Semon (1859-1918) proposed the term "engram"[4] to refer to the lasting physical changes that occur in the brain in response to the experience. He proposed that once formed, an engram become dormant, but may be awakened by the presentation of parts of the original (or similar) event. Bibliography considers Semon as the pioneer of the word "engram", to refer the physical-cellular neuronal changes associates specifically with a particular memory[5]. Despite the concept of "physical changes related to specific functions", in a more generalized way, was proposed before by Ramón y Cajal[6]. He observed that the brain does not grow in size or weight with the acquisition of knowledge, so it means that the learning has to cause some physical changes, not related to new neurons. Based on that, Santiago Ramón y Cajal pronounced the sentence "cada persona puede llegar a ser, si se lo propone, el arquitecto de su propio cerebro", now in the main entrance of the Ramón y Cajal Hospital, in Madrid. Nowadays, the concept of engram refers to the concrete neurons that participate in a specific function, as a particular memory.

Contemporaneously, Camilo Golgi (1873)[7] discovered the Golgi staining method that allowed the anatomists to go deeper in the brain at cellular level. Ramón y Cajal improved the protocol and started with the description of the nervous system[8], both at the cellular and the network levels — when possible, due to the limitation of the technique — (Figure 1.1). He also glimpsed functional implications emerging from the anatomic structure. As result of his work, he proposed the neuron theory, now corroborated. Because of that, he is considered the pioneer of the modern neuroscience and the maximum exponent of the conjunction between the academic interest on brain's anatomy, cognitive functions (as evidenced by his interest in the incipient psychology) and neurology, in the initial steps of the modern neuroscience.
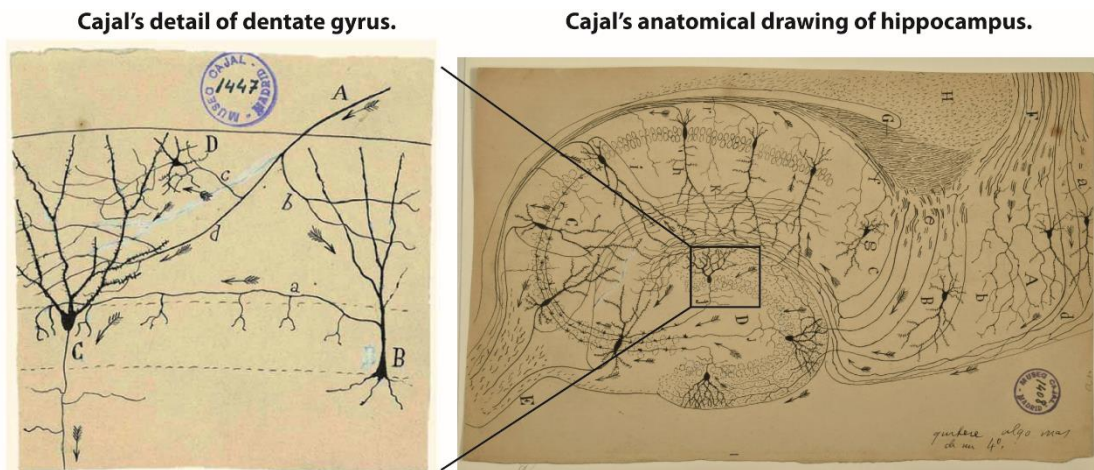
Figure 1.1. Cajal's drawing of anatomical and networks features of the dentate gyrus and the hippocampus. Arrows indicate the hypothesized by Cajal information flow, pointing for the first time to local and across-regions neuronal networks underlying to functions. Left: detail of the dentate gyrus local network. A are perforant pathway fibres, B is a hilar basket cell, innervating C, a granule cell. Both B and C are innervated by perforant pathway, coming from the entorhinal cortex, as seen in the right. Right: horizontal anatomical drawing of the hippocampal formation. Arrows indicate hypothesized information flow based on the anatomical connections between individual neurons. Modified from Sotelo (2003)[9].

As reaction for early clinical descriptions, there were no problems in accepting that some cognitive functions, like language, were localized in the brain (V.g.: Wernicke or Broca's aphasias). For some others, its localizationist acceptation was not that easy, in spite its equal clinical evidence (V.g.: Harlow's observations on Phineas Gage regarding social behaviour, 1848)[10]. Following the localizationist stream, academics tried to find the place for the memory. With little success. Memory, as a whole, seemed to be elusive to specific lesions in a particular area[5,11]. Some authors, as Lashley (1890-1958, Donald Hebb's mentor and student of John B. Watson, the famous psychologist), proposed that memory should be a distributed process in the neuronal system, in line with Semon's ideas.

Following the distributed processing ideas, Lashley's student, the Canadian neuropsychologist Donald Hebb, proposed the currently named Hebb's law, by which the synaptic strengthening between groups of neurons that are active during an event (corresponding to the engram formation) increases if its activation is coincident in time and space. It provides the basis for the memory acquisition. The reactivation of this ensemble (or part of it) makes available the remembering. However, Donald Hebb forgot to mention his tutor, Lashley, influence on his ideas on how plastic changes could lead to a memory. They had a complicated relationship (according to Orbach[12], who was the last postdoctoral fellow in Lashley's lab). Nevertheless, Donal Hebb did recognize the influence of Cajal's pupil, Rafael Lorente de Nó, who years before wrote about cell assemblies. According to Hebb himself[13], the cell assembly was a development of Rafael Lorente de No's 1930 work on self-exciting reverberatory circuits[14].

It is possible that after years of hard work, Hebb, influenced by Lorente de Nó, got inspired suddenly and independently (or as a consequence of reading others), and wrote the Hebb's law. In science, we tend to assign much work to one particular person, while the reality is that many people work hard in a topic, until finally one of them give the final step, taking all the credit. I think Donal Hebb gave the final step and, in his book *The organization of the behaviour: a neuropsychological theory*[15], materialized the academic environmental idea that

plastic changes between neurons happen when neurons get activated jointly both in time and space, and it creates memory (which is, of course, meritorious). Donald Hebb also proposed cell assemblies, which is a group of interconnected neurons that are simultaneously active during an event, as the responsible for mainteining activity within the network transiently. It would allow the event to have an internal representation in our brains during a short period, which has been related to short-term memory.

Years later, Wilder Graves Penfield (1891-1976) observed the reaction of several epileptic patients after electrical stimulation while functional and electrically mapping its brain to localize the seizure focus. Patients referred that they had "familiarities related to previous experiences"[16]. For instance, one of them (patient RW) reported: "my mother is telling my brother he has got his coat on backwards". That situation happened just before the patient went to the clinic. That was the first time that an artificially evoked memory was observed, and it happened while Penfield was stimulating in the temporal lobe. The hunt for the memory system was getting on the track.

By that time, experimental psychologist Brenda Milner (1918 -) started to work in Penfield's lab. She observed that two patients with temporal lobotomy had memory loss. After she informed about that, William Scoville invited her to evaluate Henry Molaison (patient HM). By the time Lashley concluded that specific engram memory location was elusive, Scoville and Milner[17] presented the cognitive outcomes of 10 patients that underwent temporal lobe resections. By comparing their neuropsychological results with surgery damages, they concluded that medial temporal lobe, including the hippocampus and adjacent temporal lobe structures, was a crucial component for the memory. Milner merged neurosurgery and neuropsychology to dive in the memory location, and built the foundations of decades of studies on the field. Its epitome came with the hand of the patient HM report[18], worldwide known. She observed that HM has no difficulties in some assignments, for instance, instrumental tasks —like mirror-drawing—, but it was impossible for him to recall the declarative information, even regarding the task or his participation on it. Milner emphasized that understanding a specific role of particular brain structure in memory requires careful consideration of the kind of memory tested. So, she emphasized the idea of the existence of different kinds of memories. Her results provide the cornerstone for the following theories of multiple memory systems. Also, Milner pointed to the temporal nature of the memory, due that HM could remember events that happened a long time before the surgery, but not anything that experienced after it (the now classical division between long-term and short-term memory).

In her studies, the hippocampal formation and temporal lobe areas surrounding it were key components for the memory. So that, in spite of the traditional notion of a distributed process (getting force nowadays), memory research focused specially in the hippocampus from that moment on (still in our days).

1.1.2.- 2nd half of XX century.

After Milner's studies, there was an increasing interest in the hippocampus and its relation with memory. It will be discussed in section 1.2, memory and hippocampal formation (below), so that here we only express the general context.

Using selective anatomical tracers, the anatomists dove into every time finer details of the brain connectivity, revealing local networks in a specific brain area and long-range connectivity between areas. Classical neurotransmitter systems were discovered during this period, together with its receptors. As result of its discovery, neurons were categorized in two big groups: excitatory neurons, mainly glutamatergic, that activate the ones that receive the neurotransmitter; and inhibitory neurons, mainly GABAergic, that inhibit their targets (reviewed in Florey, 1991[19]; Watkins, 2000[20]). Neuromodulators, like dopamine, serotonin, noradrenaline and acetylcholine, were also discovered during this period. It is necessary to say that Ramón y Cajal already had suggested the existence of different kinds of neuronal populations based on the local neural networks[21]. The neurotransmitter discovery allowed the division of neuronal population according to their neurochemical features, which was also related to the excitatory/inhibitory function they played in the system.

One inflexion point happened in 1973 when Tim Bliss and Terje Lømo[22] informed that the application of high-frequency trains in the perforant pathway of the rabbit induces plastic changes in dendrites. It provokes an increased neuronal Excitatory Post-Synaptic Potentials (EPSP), and Population Spikes (PS), recorded in the same area when stimulated afterwards. We go more in-depth in that point in section 1.3, synaptic plasticity and memory (below). It could be the Hebb's law demonstration and provoked an increasing interest in the understanding of how different areas may change activity, underlying to cognitive processes.

Related to this, it was also a growing interest in the development of new techniques, and its application on neuroscience, like the functional Magnetic Resonance Imaging (fMRI). Comparative science divisions tried to extrapolate human results to animal models, and *vice versa*. Many behavioural tasks were standardised to study memory processes. Those tasks, taking good note of Milner's reports, tried to be specific for the study of different memory subtypes. This way, we can find tasks to evaluate instrumental/operant memory[23] spatial memory[24], object recognition[25], fear conditioning[26], between many others. The development of behavioural tasks allowed us to have tools to study isolated sub-divisions of memory while modulating, pharmacologically or electrically, the activity of neurons. It was especially useful when combined with genetic modulation in rodents — the first one was achieved in 1974[27] and widely extended during the 90's—, that allowed us to study the effect of specific proteins or receptor on memory and learning. The development of these techniques allowed the community to focus on the proteomic regulation of local synaptic plastic changes related to memory.

1.1.3.- Last studies. Optogenetics and pharmacogenetics tools.

New tools have appeared in neuroscience in the last years, as optogenetics[28] and pharmacogenetics[29]. These new tools overpass previous technical limitations, allowing us to have new results. For instance, one of the main disadvantages of the genetic manipulation in mice is that it affects the whole brain, not only to the region of interest. Also, mutated mice strains may develop compensatory functional changes during the maturation that could affect the results. Another disadvantage of other experimental approaches, as the electrical stimulation, is that it excites all the neurons and fibres nearby the stimulation place, independently of its biochemical nature. With optogenetics and pharmacogenetics, we can activate only one specific subset of neuron in one particular area.

The optogenetic approach bases on the artificial expression of an opsin —a protein that reacts to specific light wavelength— in a specific subset of neurons. It is achieved by direct genetic manipulation or using viral vectors (lentivirus or adeno-associated vectors, AAVs), containing opsin genetic code to be included in the vector's cellular targets[30]. The use of viral vectors to express mutated proteins in a particular neuronal population can be nonCRE-dependent or CRE-dependent[31]. NonCRE-dependents entail a specific virus to detect one particular neuronal target, while CRE-dependents require mice strains that express CRE recombinase under the control of specific neuronal promoters. CRE-dependent viruses infect all the neurons nearby the injection point, but its genetic information is only readable by those neurons that express CRE recombinase. So that opsins are expressed only on the CRE-expressing neurons. Then, by placing an optic fibre into the brain, coupled to a light source of different wavelengths, we can activate or inhibit opsin-expressing neurons (depending on the opsin itself and the light wavelength applied, for a review see Deisseroth, 2015[32]; Deisseroth and Hegemann, 2017[33]), having high specificity over the neuronal population modulation and high temporal control.

Pharmacogenetic tools bases on a very similar protocol than optogenetics. However, instead of an opsin, it is expressed another protein (called DREADD; from Designer Receptors Exclusively Activated by Designed Drug) that respond to an external ligand/drug that is, otherwise, inert for the rest of the neuronal receptors[29,34,35] (described more in-depth in material and method, section 3.1). Pharmacogenetic also allows the modulation of a specific subset of neurons, through the activation of different G-protein inner cascades associated to the DREADDs. The injection of the external ligand leads to excitation if the mutated protein activates Gq-cascade, or to inhibition, if the mutated protein activates Gi-cascade[36]. Once injected, external ligand activity takes for several hours. DREADDs approach applied on memory and learning are newer than the optogenetic and has been less used on the field.

Both techniques have created a revolution in neuroscience due that they allow the functional dissection of a specific subset of neurons in freely moving animals, *in vivo* and *in vitro*. They can be combined with previous behavioural tasks and/or molecular approaches invented in the past decades to study memory.

This way, for instance, combining optogenetic, behaviour and neuronal activity molecular markers, Susumu Tonegawa and colleagues were able to label a specific engram associated to a specific emotional-spatial memory[37,38]. After having labelled the engram associated to a fear-context conditioned response, they placed the animal in a non-conditioned space and turned the laser on, to activate the previously conditioned engram; animals evidenced the freezing behaviour associated with the conditioned memory. To achieve it, they took advantage of the Immediate-Early genes (IEGs), in particular cFos, to label engram cells implicated in a particular

memory. The neuronal activation, due to the entrance of Ca^{2+} inside the neurons, leads to a molecular cascade associated with the IEGs[39]. Most commonly IEGs used to label neuronal activation is cFos (for a review Minatohara et al., 2016[39]). Tonegawa and cols made the mice to express opsins, under the control of cFos IEG expression, only in those neurons that were actives when animals carried out a fear conditioning task[37,38], thanks to their precise timing control on opsin expression related to cFos activity. This way they could control the memory engram activation by flashing with optogenetic on the neurons that encoded this information. It seems that Semon's and Lashley's ideas are back again. The activation of a neuronal engram in the hippocampus activated a specific memory. It evidenced the importance of hippocampal formation on memory and learning again.

1.2.- Memory and hippocampal formation.

1.2.1.- Memory.

Memory is fundamental to human life. Memory is the ability to acquire, consolidate and recall information. However, how our brain does such a thing? The answer is especially tough due that memory is not a homogeneous concept. Qualitatively diverse types of memory enable us to acquire and use a repository of knowledge; so that we can evocate the consequences of past behaviours and to plan for the future. These different memory systems operate semi-independently, involving distinct but overlapping brain networks.

Diverse forms of memory include the temporal dissociation between short and long-term memory and the qualitatively distinct systems of long-term memory (LTM)[40]. Different theoretical frameworks of LTM distinguish perceptual representations, semantic and episodic memory[41], declarative memory[42,43], spatial memory[44], the learning of actions and habits[45,46], emotional memory[47] and others. Cutting across these distinctions is the explicit vs implicit memory expression[48]. Mnemic processes include the differentiation between **encoding, consolidation and retrieval** (for a review, Wang and Morris, 2010[49]). The encoding is the conversion of sensorial inputs into the neural code substrate and its integration into single neuronal trace for initiating the memory processes. Whereas the consolidation refers to the time after the encoding, before settling the information, in which interfering material could impair the recall of the target memory at a later time[50]. After encoding and consolidation, memory system also requires the retrieval of the memory; that is the ability to recall the previously saved memory. Clinical and experimental data support its differentiation, having proposals for different brain mechanism for its implementation in the brain.

Many efforts were made to compile the clinical and experimental data related to memory. One of them is the Tulving's serial, parallel, independent (SPI) framework[41] and the idea that hippocampal memory includes the ability to remember events and episodes that take place in a specific location[51–53]. This theory also holds that medial temporal lobe structures, especially the hippocampal formation, are crucial for memory encoding, in line with Milner reports. SPI framework emphasizes that the encoding is automatic, referred to episodic memory — the conjunction of where-when-what events— and related to the hippocampal formation[54]. This theory combines the role of plastic synaptic changes in the neural mechanisms of cellular consolidation[55] and the critical role of mental schemas, or engrams, in systems consolidation[56], recognizing the fact that other brain structures also contribute to episodic memory via their

role in executive function and working memory[57]. So this theory merges the role of synaptic tagging without forgetting the implication of the rest of the network(s) connected to the hippocampal formation. Also, it emphasises that episodic learning is automatic and not necessary goal-directed.

Automatic encoding vs goal-seeking tasks.

Concerning episodic memory, the unexpected environmental events happen, and it may be useful to encode what, where and when they happened. Even though the animal had no intention of learning them, nor was motivated to do so, it encodes it. This is automatic or incidental encoding[58]. On the other hand, the animal also may be engaged in a goal-seeking activity, looking for tracks that could be relevant to solve a specific task, having strong inner motivation. This behaviour engages in intentional or controlled processing that is both, task-specific and goal related. In the latter one, the behaviour is a medium to get the goal; while in the first there is not apparent reinforcement, and the learning is spontaneous. There is evidence for this distinction in nonhuman primates[54] and rodents[59,60]. It is important for the present work because the automatic encoding has been related to the hippocampus and especially to the dentate gyrus[49], while the goal-directed one has been more related to the prefrontal cortex (PFC)[61,62]. Of course, PFC may play a critical role in automatic episodic memory encoding as well, and in particular, its communication with the hippocampus and related to consolidation[56,63], but it does so especially when subjects engage in a more prospective learning task; as it is when animals internally are willing to get a specific goal.

It is uncertain what incidental episodic-like learning for animals is. The requirements are that the encoding should be fast, lack of clear motivation or incentive and not require intricate planning. One standardized behavioural task that fit with these criteria is the novel object recognition task[25], or its variant, the **Novel Location of the Object** (see material and methods section 3.1, behaviour). This task has also been associated directly with dentate gyrus function[64–66], being more necessary as we increase the difficulty of the spatial task[64]. This task also allows the experimental segregation for encoding, consolidation or retrieval[67,68].

After sensorial information arrives at associative areas, it is channelled to the hippocampal formation, via entorhinal cortex[69]. Once there, to achieve the mnemic representation in the system, there are two neural mechanisms proposed[70]: a) a cellular one, that includes protein synthesis and synaptic plasticity, and b) a system mechanism, that reflex the dynamic interaction between interconnected neurons populations, especially within hippocampus and neocortex. Cellular consolidation reflects processes that happen at the single cells level involving signal-transduction pathways and gene activation, whereas systems consolidation involves an interaction between distinct brain areas.

Cellular changes will be discussed more in-depth in section 1.3.

From a system level perspective, the standard theory asserts that it is a process that involves dynamic interactions between the hippocampus and the cortex, especially prefrontal cortex[71]. Some data support that the information would be processed first in the hippocampus, and then its anatomical and functional long-range interactions gradually enable the transient of the memories to the cortex. From neocortex, information would be later used for memory retrieval[42], despite some long-lasting traces may remain in the hippocampus, and are required for some aspects of the whole memory, for instance, for the spatial memory traces[72]. However, other data support that the cortex can also be a primary "learner" with the capacity to express immediate changes in neocortical connectivity that decay rapidly unless the new hippocampal inputs interleave within activated cortical frameworks[56].

Hippocampus on spatial-episodic memory.

Clinical and experimental data support the hippocampus implication on spatial-episodic memory[17,73]. For instance, the hemodynamic response in hippocampal formation increases when humans recall recent events memories, and decreases with the age of the events[74,75]. This temporal gradient suggests that the hippocampal formation participates more in the encoding and that the long-term memory traces gradually consolidate in distributed cortical areas[42], explaining the recall of old memories in the presence of lesions in the hippocampal formation.

However, other data report amnesic patients with horizontal gradients of retrograde amnesia (no associated timing curves), even in patients with medial temporal lobe damage[76]. However, Nadel and Moscovitch (1997)[72] and Moscovitch et al. (2006)[77] support that although the gist of the memory may be intact after hippocampal formation damage, the detail and vividness of memory requires the hippocampus[78]. In line with the latter authors, it was also suggested that hippocampus is always required for storage and retrieval of allocentric and spatial memories[79], whereas semantic memory is interceded by the neocortex, subject to the completion of a systems consolidation process after learning. It has also been proposed that the hippocampal formation is required to reinforce the initially weak connections among cortical modules/areas that are encoding in parallel[56,80].

These, and many other data, make most, if not all, the people working in the memory field consider the hippocampal formation as a particularly important node for automatic encoding of relational events[53], objects-in-places[81], and goals-in-places[82], having an enormous implication in the spatial processing of memories.

1.2.2.- Hippocampal formation.

Giulio Cesare Aranzi named the hippocampus in 1564. It takes the name from the ancient Greek, meaning seahorse, because of the distinctive anatomical shape (Figure 1.2). The first detailed anatomical studies were done by Santiago Ramón y Cajal[21] and then by Lorente de Nó[83], who subdivided the hippocampus into four parts: CA1, CA2, CA3 and CA4 (Figure 1.2). The nomenclature CA comes from *Cornu Ammonis* (*cornu* = horn; *Ammon* = goat, from the Phoenician), associated to the Greek mythological representation of the *cornucopia*, due to the characteristic form of hippocampus' creases. Nowadays, the nomenclature has changed a bit, because, for instance, there is no clear differentiation for CA4, and CA3 (a, b and c) has occupied its space (Figure 1.2).
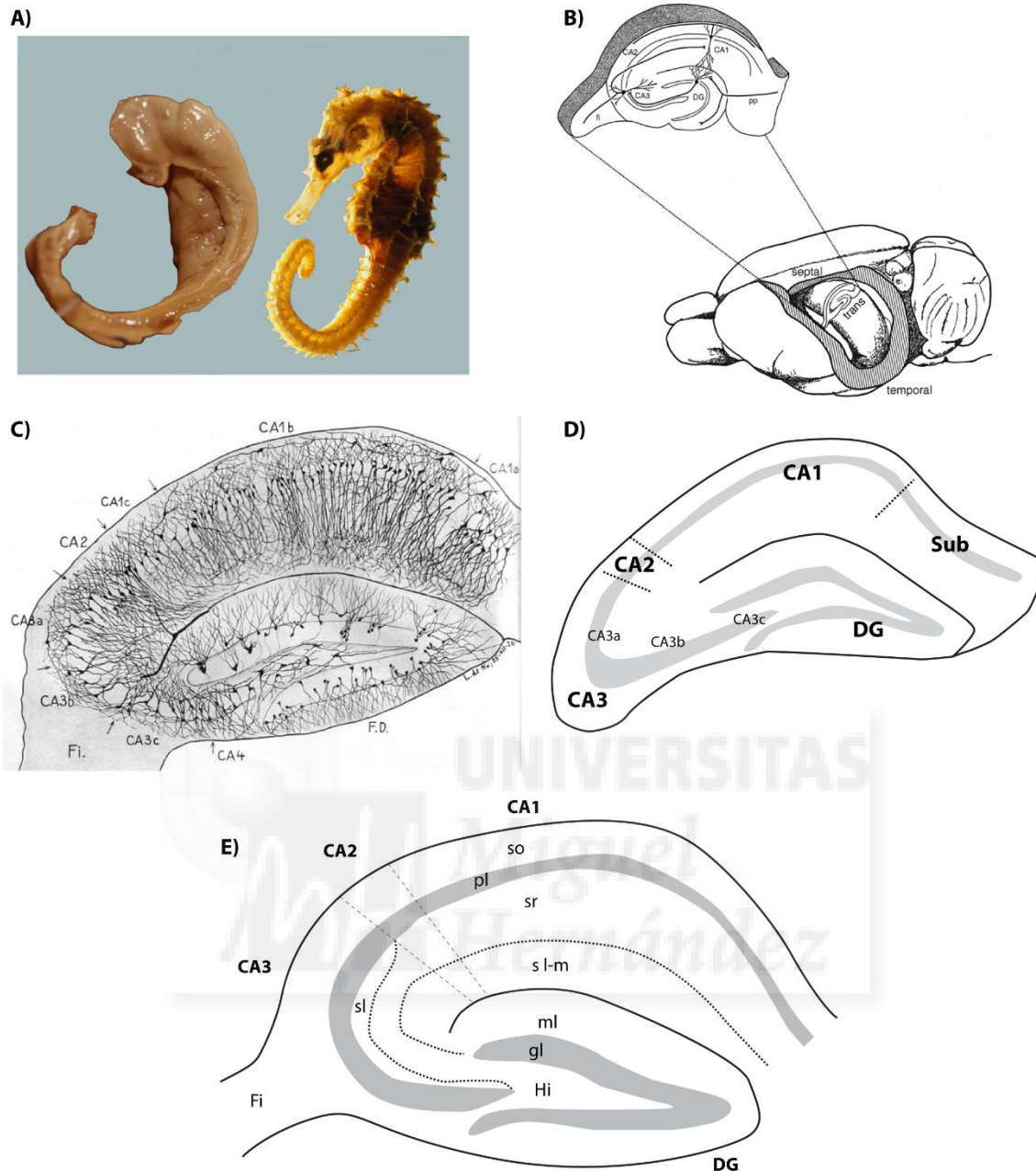
Figure 1.2. Anatomical external features of the hippocampus and its divisions. A) Anatomical similarities between anatomical brain region "hippocampus" (left) and a seahorse (right). B) Hippocampus position in the rat/mouse brain and a coronal section extracted. C) Dentate gyrus and hippocampus coronal section drawing, and its subdivisions, in CA1a, b, c, CA2, CA3a, b, c and CA4, as established by Lorente de Nó in 1934. D) Scheme of dentate gyrus and hippocampal subdivisions as accepted nowadays. E) Hippocampal subdivisions in layers; so = stratum oriens, pl = pyramidal layer, sr = stratum radiatum, s l-m = stratum lacunosum-moleculare, sl = stratum lucidum, ml = molecular layer, gl = granular layer, Hi = hilus, Fi = fimbria. A, B and C modified from Andersen et al., 2007[11].

The hippocampal formation includes the hippocampus, the subicular complex, the entorhinal cortex and the dentate gyrus. The entorhinal cortex is considered an interface between cortical information and the hippocampus. It is part of the neocortex and can recognize ensembles of sensorial inputs, including its spatial properties[84]. The entorhinal cortex is connected to the hippocampus and dentate gyrus, been its primary provider of afferences, through the perforant pathway[69]. Especially relevant for this thesis is the dentate gyrus (boarded deeply in section 1.4). From dentate gyrus, the connections flow to CA3, and then to

CA1. CA3 and CA1 contact with extrahippocampal regions and to subicular complex (that includes subiculum, para-subiculum and pre-subiculum). Subicular neurons send projections to entorhinal cortex[85], from where it could re-enter in hippocampus, creating a closed loop of neural information processing, that has been proposed theoretically (together with prefrontal-hippocampus connectivity) as a putative base for the short-term retention of information required for working memory[86,87].

Both hippocampus and dentate gyrus have a very well established laminated cellular structure, very well conserved amongst mammals. The reason for the relatability is that the hippocampus is phylogenetically quite old, as it is considered part of the archicortex/allocortex. Because the well preserved structural features of the hippocampus in all the species, from now on this work will focus on mice's hippocampal formation as it is the animal model used. The anatomical names and terms are also valid for human's hippocampus, as well as for other rodents[88,89].

Overview of the hippocampus and dentate gyrus anatomy.

Dentate gyrus and hippocampus, in mice, are located bilaterally in the medial temporal lobe, extending its "banana" shape volume from posterior-ventral-lateral to anterior-dorsal-medial position, just below the *corpus callosum* in its anterior extension. Because its peculiar shape, after applying a coronal or horizontal cut in the brain, hippocampus and dentate gyrus can be distinguished because its confronted C-shaped anatomies (Figure 1.2), although C-shape dentate gyrus is sharper, forming an almost V-shape.

Dentate gyrus anatomy is discussed below (see section 1.4), but briefly, it contains molecular layer, granule cell layer and hilus (also called polymorphic layer). Hippocampus is divided currently in CA3, CA2 and CA1. Each one of them can be further subdivided based on anatomical connections (Figure 1.2E) and gene expression. Regarding the layers, we distinguish (from external to internal): the *alveus*, formed by the axons of pyramidal neurons in their way to form the fimbria-fornix pathway; the *stratum oriens*, containing apical dendrites of CA pyramidal cells; the pyramidal cell layer, containing somas of the CA pyramidal cells; the *stratum radiatum*, containing the basal dendrites of CA pyramidal cells. In CA3, between the pyramidal cell layer and the *stratum radiatum* there is the *stratum lucidum*, formed by the terminations of dentate gyrus granule cells axons (called mossy fibres) over the proximal part of CA3 pyramidal neurons; and finally the *stratum lacunosum-moleculare*, immediately adjacent to the hippocampal fissure, that separate CA1 field and dentate gyrus, that is obliterated.

Excitatory neurons somas are located in granule cell layer (dentate gyrus granule cells) and pyramidal cell layer (pyramidal cells). Principal cells in DG and CA1 have no projections back to its efferent regions, which give the hippocampus a mostly unidirectional flow of electrical information, which together with the very well defined laminar distribution provides a unique region to be used for mapping electrically the neural properties that underlie the neuronal transmission[11,90].

Surrounding the excitatory neurons there many types of interneurons both in the hippocampus and in the dentate gyrus[91,92]. Given its importance for this work, they are explained in depth in section 1.5.

The hippocampal formation has four principal efferent bundles: the fimbria-fornix pathway, the dorsal commissure, the ventral commissure, and the angular bundle[11].

Briefly, the *fimbria-fornix pathway* provides inputs from, and afferents to, subcortical areas[93]. This pathway is a double sense pathway, formed by 1) axons that enter in the hippocampus extending obliquely in the alveus, from medial to lateral, and 2) axons from hippocampal CA pyramidal layer and subiculum in route to subcortical terminations. Fibres in the fimbria are organized topographically, and the entering ones come mainly from septal nuclei, thalamus and hypothalamus[94].

Dorsal and *ventral hippocampal commissures* pathways are formed by axons that cross the midline carrying information from the contralateral hippocampus (CA1 and CA3 mainly), dentate gyrus (mossy cells axons), presubiculum and entorhinal cortex. Most of this fibres have a homotopic origin from the contralateral hippocampal formation.

Last, but not least, the *angular bundle* comprises fibres from and to cortical and subcortical areas interconnected with the entorhinal cortex[11] and fibres that connect entorhinal cortex, presubiculum and parasubiculum with dentate gyrus granule cells[95,96], CA3 and CA1. It is the main route taken by fibres originating from the ventrally situated entorhinal cortex as they travel to septotemporal levels of other hippocampal formation fields. This bundle is the principal route for neocortical inputs reaching dentate gyrus and the hippocampus; sensorial cortical inputs, as visual or other contextual/spatial information, arrive at the entorhinal cortex, where it is processed and transmitted to the hippocampus and dentate gyrus. A minority of entorhinal fibres also reach the hippocampus via the alveus, thought the temporoammonic alvear pathway[8]. However, the majority of entorhinal cortex fibres entering in dentate gyrus and hippocampus form the perforant pathway, which receives this name because its axons traverse or perforate the subiculum and the hippocampal fissure in their way to its targets. The perforant pathway is the primary input into the dentate gyrus[8]. It arises mainly from cells located in layer II of the entorhinal cortex, although a minor component comes from layer V and VI[97]. In the molecular layer, the entorhinal terminals are strictly confined to the outer two thirds, where they form asymmetrical excitatory synapses. These contacts occur on granule cell spines, and also, and importantly for this work, on hilar basket cells interneurons —most of them are parvalbumin positives[92]—. The perforant pathway can be divided into two parts based on the region of origin and pattern of termination: lateral perforant pathway and medial perforant pathway. The first one starts in the lateral entorhinal cortex, terminates in the most superficial third of the molecular layer in dentate gyrus and projects also to CA3 and CA1. While the latter one starts in the medial entorhinal cortex, terminate in the middle third of the molecular layer and projects also to CA3 but and less extent to CA1[11].

Internal hippocampal refers to the local networks and circuits formed therein in the hippocampus and dentate gyrus. They can be subdivided into connectivity between different hippocampal gyrus regions and local cellular connectivity.

By one hand, regarding the intra-hippocampal and dentate gyrus networks (between its subdivisions), we found three circuits: the trisynaptic, the disynaptic and the monosynaptic connection (Figure 1.3A). The trisynaptic circuit comprises unidirectional connections that from the entorhinal cortex, via the perforant pathway, arrives at the dentate gyrus, it excites granule cells that connect with CA3 pyramidal neurons, and these send projections to CA1 pyramidal neurons, via Schaffer collaterals. The disynaptic circuit comprises axons that go directly from entorhinal cortex to CA3, and from here to CA1 pyramidal neurons. Finally, the temporoammonic monosynaptic connection goes directly from entorhinal cortex to CA1 pyramidal neurons. It is necessary to mention that around the 4% of CA3 pyramidal neurons show a high level of recursion coming from other CA3 pyramidal neurons, which is thought to be the neuronal substrate for pattern completion and the storage of related memories[98]. From CA3 and CA1 electrical signals can flow out from the hippocampus to other hippocampal formation areas (as subicular complex, coming back to entorhinal cortex) or to other subcortical or cortical extra-hippocampal regions. Dorsal and ventral hippocampus are also in contact by the longitudinal pathway, that is a distributed bundle of collateral axons that runs between the dorsal and the ventral CA3 pyramidal neurons[99].

On the other hand, local cellular connectivity refers to those connections created at the intra-nodal level, in between different types of neurons. This local connectivity is crucial to understand how activity propagates in the system[100–103]. *Grosso modo*, we distinguish two big subtypes of local networks: feedforward and feedback networks (Figure 1.3B-C). Feedforward networks are those in which a given input activates both the excitatory neuron and the GABAergic local interneuron that directly inhibit the excitatory population activated with the same input. Feedback networks are those in which a given input activates an excitatory neuron (A) locally, which activates an inhibitory GABAergic interneuron, placed sequentially, that in turn inhibit the very same excitatory neuron that was first activated (neuron A)[104]. Feedforward and feedback networks —and others, as the lateral inhibitory networks— are combined simultaneously in the same local nodes, thanks to the diversity of neurons, and coordinate activity within the node.

Both kinds of inhibitory networks combine neurons with different targets: perisomatic or dendritic, accomplishing different roles. Interneurons in local networks also established inhibitory contacts between them, and moreover, some of them express electrical gap junctions so that they can coordinate firing[91,105]. Introducing in depth all of this issues would distract from the main topic of the present thesis work, but as herein we present an experimental work that modulates the activity of parvalbumin hilar GABAergic interneurons, at least we need to mention its role in the circuit we modulate. They are implicated in both feedforward and feedback inhibition, thanks to its anatomical features, and innervate perisomatically its dentate gyrus granule cells targets (see dentate gyrus section 1.4, below). Hilar PV-basket cells neurons are explained in detail in section 1.5.1.
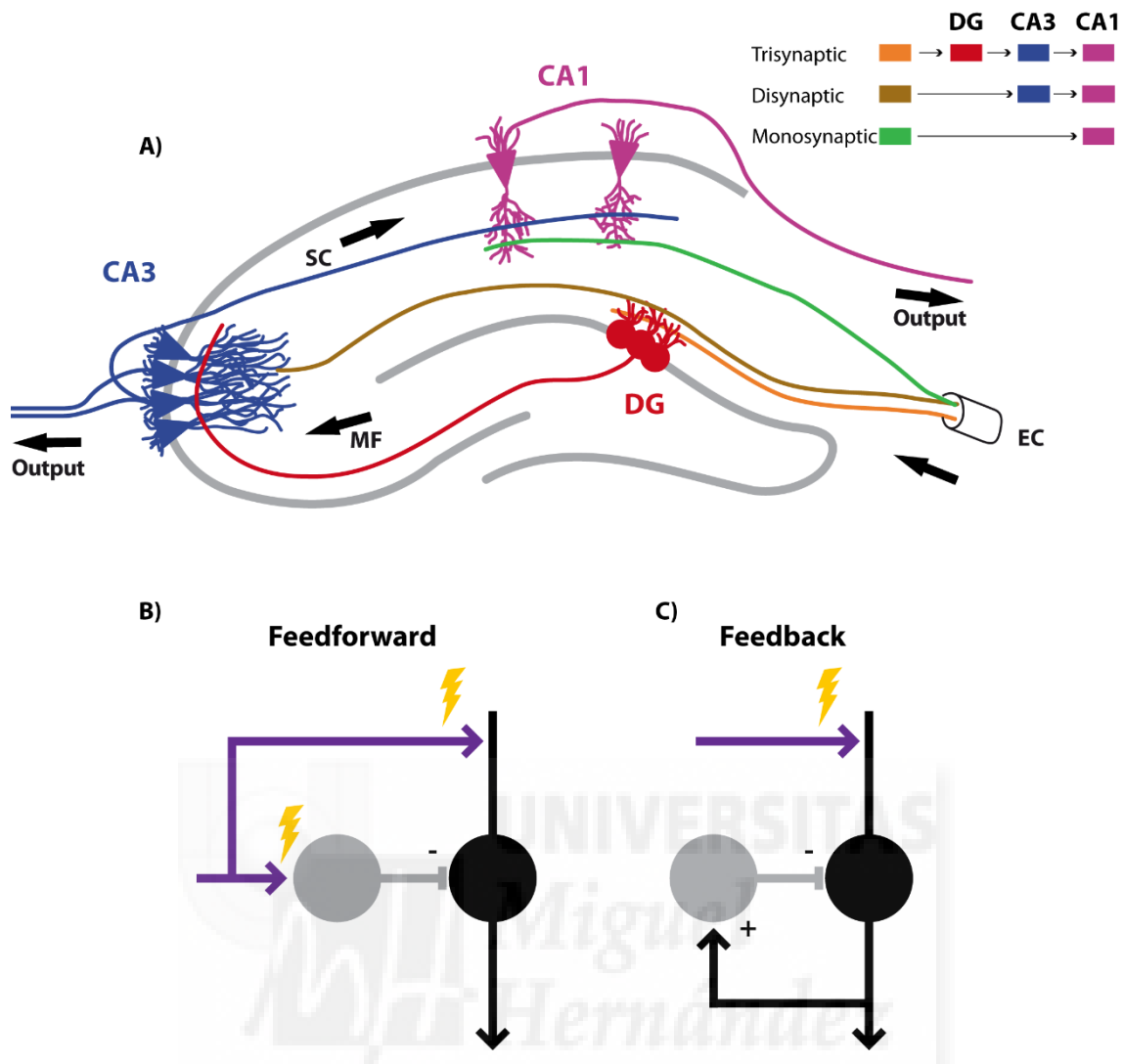
Figure 1.3. Neuronal networks in the hippocampus and inhibitory circuits. A) Schematic representation of main inner hippocampal circuits: trisynaptic, disynaptic and temporoammonic monosynaptic. Fibres from EC contact mainly with dentate gyrus, and less extensively to CA3 and CA1 directly. From dentate gyrus, mossy fibres contact with CA3, and CA3 pyramidal neurons emit the Schaffer collaterals to CA1. Axons from CA3 and CA1 form the output of the hippocampus. EC = entorhinal cortex, PP = perforant pathway, DG = dentate gyrus, MF = mossy fibres, SC = Schaffer collaterals. B) Schematic representation of a classical feedforward inhibitory network. C) Schematic representation of a classical feedback inhibitory network. Grey circle indicates inhibitory interneuron; black circle represents excitatory neuron; purple lines show excitatory afferents on the network.

Outputs from the hippocampus.

CA3 and CA1 pyramidal neurons are the only ones that project to the outside of the hippocampus, creating its long-range connections. These connections are monosynaptic to cortical areas, which are supposed to support consolidation and recall of memories, or polysynaptic. There are three main targets from the hippocampus, whether they use the fimbria-fornix pathway or the angular bundle (previously explained): 1) to cortices, as temporal, parietal sensorial cortices and frontal cortex, 2) to other medial temporal lobe structures as subiculum, entorhinal cortex, and 3) to subcortical areas —as thalamus, hypothalamus, amygdala, nucleus accumbens and septal nuclei—[106]. Figure 1.4 illustrates a simplified scheme of its anatomical connections.

Something to keep in mind for the present work is that dentate gyrus does not send axons to any extra-hippocampal areas directly; dentate gyrus granule cells have only one external output, to CA3, and one local target, the hilus, contacting on interneurons and mossy cells. Mossy cells also connect with local interneurons and with contralateral granule cells.
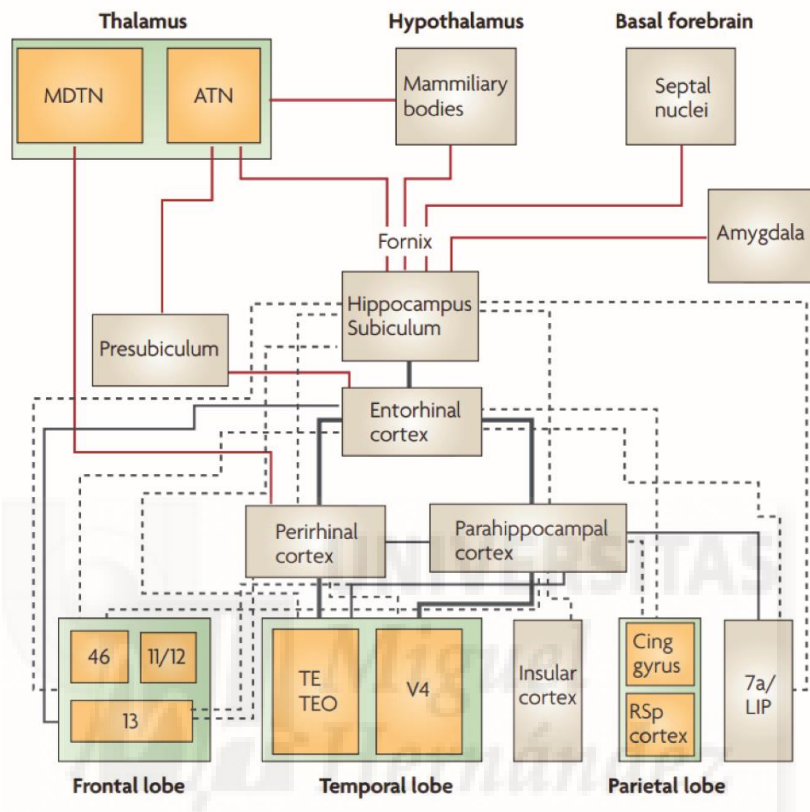
Figure 1.4. Hippocampal connections from and to cortical and subcortical areas. Subcortical ones are indicated in red; cortical connections are in black. Thickness approximates the strength of the connections. Most of the neocortical inputs enter in the hippocampal formation through the entorhinal cortex; while outputs mostly leave hippocampus through the subiculum and then to frontal, parietal and temporal lobe, including entorhinal, perirhinal and parahippocampal cortices, as indicated by discontinuous lines. Subcortical connections are bidirectional. 7a/LIP = lateral intraparietal area, RSp = retrosplenial cortex, Cing. gyrus = cingular gyrus, TE and TEO= inferior temporal areas, V4 = visual area 4, numbers in frontal cortex indicate numbers according to Brodmann areas: 46 = dorso-lateral prefrontal cortex; 11/12 = medial and lateral orbitofrontal cortex, 13 = anterior insular cortex. Extracted from Bird and Burguess (2008)[106].

1.3.- Synaptic plasticity and memory.

Talking about memory nowadays is talking about synaptic plasticity. A quick search in PubMed with the terms "plasticity" AND "memory" give us 13.849 results. In 1973, Bliss and Lomo discovered the long-term potentiation (LTP) in the dentate gyrus of the rabbit. LTP is considered the proof of the Hebb's law and consists on the increasing excitatory efficiency on the synapses after the application of an artificial stimulation train at high frequencies[22,107]. Five years later, Klein and Kandel described the modification of synaptic strength after basic learning in *Aplysia Californica*[108]. Nowadays, the LTP phenomenon is a candent topic in neurobiology, with some discussions, as its presynaptic or postsynaptic site of expression (for a

review, see Padamsey and Emptage, 2013[109]). LTP has been studied widely in the hippocampus, although it occurs virtually in all the excitatory NMDA-dependent synapses in the brain[110], being involved in many neural functions, from visual cortical plasticity to sensitization to pain, and others[111]. However, it is not that clear how plastic changes control activity propagation at the level of circuits (for a review on that topic, Andersen et al. 2017[112]).

1.3.1.- Properties of LTP plastic changes.

LTP occurs at synapses that are repeatedly active, increasing their efficiency. It swells the sensitivity to neurotransmitters by increasing receptor number in the postsynaptic terminal and/or increasing neurotransmitter release by the pre-synaptic terminal[113]. It raises the essential link between protein synthesis, cellular changes and functional properties in the circuits.

LTP is input specific and induce plastic changes that happens selectively on those synapses that allow specific routes to become potentiated[114]. It is a requirement for the learning and memory because the internal representation of the environment must be encoded in a definite pattern of spatial and temporal neural events. As LTP plastic changes are input-specific, it gives the possibility to be clustered on sequential activations representing external world, being as different as possible from other surrounded cluster of connectivity, which represents others concept/events.

Related to the clustering of interconnected synapses, it emerges the concept that the LTP allows the associativity. It requires that at least two different, but adjacent, circuits of concatenated neurons may influence each other, so that the activation of one of them, increase the probability of firing in the other one[115,116]. This property is crucial because it provides a synaptic mechanism for binding simultaneously coincident information from events and related knowledge.

The most common LTP mechanism is NMDA receptor-dependent[55,117,118]. These ionotropic glutamate receptors are voltage-dependent, and Mg^{2+} blocks its interior in normal conditions. Only the co-activation of pre and post-synaptic terminal can release the Mg^{2+} from the channel. It happens when an efferent fibre fire at high frequency. The low delay between one pulse and the next one (and successive) makes the glutamate to arrives at the synapse when the previous neurotransmitter release has activated adjacent AMPA receptors, which lead to a postsynaptic inner cascade that displace the Mg^{2+} from the NMDA receptor. Then the Ca^{2+} may enter inside the neuron, given the NMDA high permeability to Ca^{2+}, mobilizing a protein-kinase reaction cascade necessary for LTP plastic changes[119]. Some of them involve AMPA receptors, which are transported to the synaptic cleft. So that, next time presynaptic terminal releases glutamate, the higher number of AMPA receptors result in increased efficiency in neurotransmission (Figure 1.5).

However, this mechanism is not the only one, as LTP can occur as well without NMDA receptor mediation at least in some synapses, for instance, in dentate gyrus to CA3 projections[120].
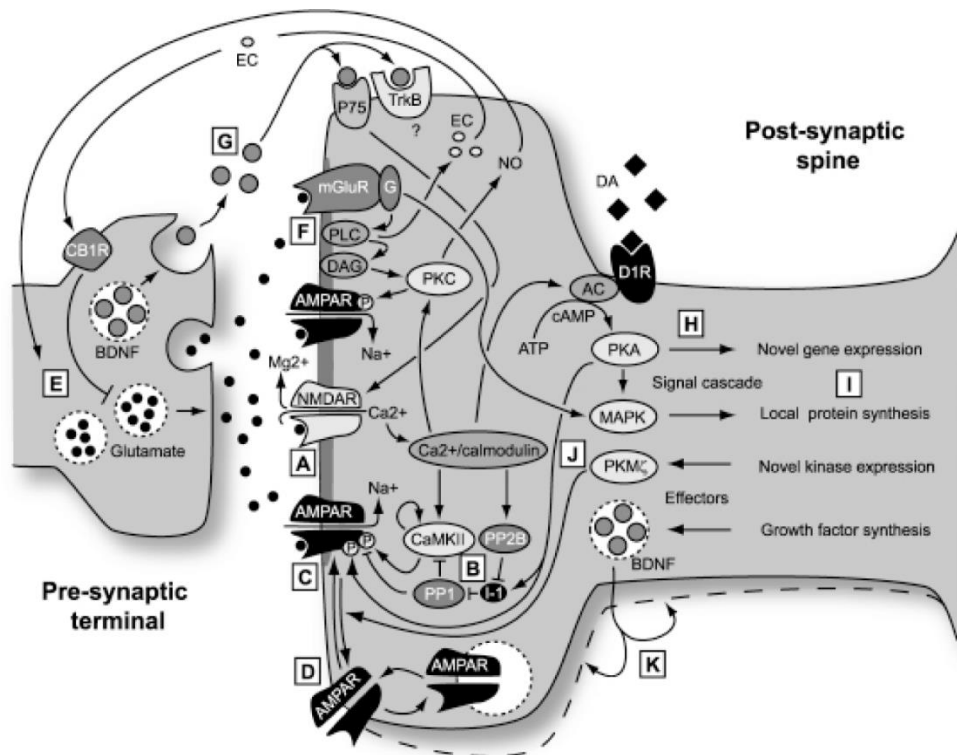
Figure 1.5. Schematic mechanisms of LTP and LTD. A) NMDA receptor activation, under the pre and post-synaptic coincident activity, eject the Mg^{2+} ion that blocks the channel, allowing Ca^{2+} to enter. B) Ca^{2+} mobilizes Ca^{2+}/Calmodulin complex which activates seconds messenger cascades, conditioned by the dynamic Ca^{2+} transient so that low and prolonged Ca^{2+} levels induce LTD, and brief but steeper transients induce LTP. C) Phosphorylation of AMPA receptors expresses LTP. De-phosphorylation causes LTD. D) Trafficking AMPA receptors from and to the membrane regulate LTP (increasing number in the membrane) and LTD (decreasing number in the membrane). E) presynaptic mechanisms promoting sustained firing rate also promotes LTP. F) LTD also is associated with mGluR type 1. Its activation leads to a reduced conductance in AMPA receptors. H-K) Longer lasting forms of LTP and LTD requires new protein synthesis, either locally or in other cell areas, mediated by different molecules as PKA, MAPK, PKM or BDNF (extracted from Bliss and Cooke, 2011[121]).

1.3.2.- Long Term Depression and depotentiation.

Another form of plasticity, opposite to the LTP, is the Long-Term Depression (LTD), a plastic process that decreases the synaptic efficacy and is induced by low-frequency stimulation[122,123]. It reduces the number of AMPA receptors from the membrane surface, by its internalization (Figure 1.5). We should not confound with "depotentiation", which is the decay of the LTP and implies the normal loss of the synapse strengthening induced by LTP[124]. Both, depotentiation and LTD, have been related to the loss of memories, although its exact neurobiological features and its role in memory are still under debate[125,126].

LTD is mainly glutamatergic NMDA receptor-dependent and $Ca2^+$ levels dependent. The low-frequency stimulation protocols cause lower levels of $Ca2^+$ in the postsynaptic targets, which would lead to internalization of AMPA receptors[110]. Another explanation is that LTD mechanism depends on mGlu receptors[127], whose activation leads to the mobilization of calcium-sensitive kinases that finally phosphorylate AMPA receptors, reducing conductance in the membrane, or even reducing spine's size[110]. Although its role in learning and memory is not as well characterized as its counterpart LTP, the theory holds that LTD has a role in forgetting, or at least in controlling the learning. If in the system would only exist LTP, at a

certain point the system would saturate (it only gets potentiated)[128]. Another possible role of LTD is in stabilizing the level of excitation that would help to prevent abnormal neuronal activity that could lead to altered states, as epilepsy[129].

1.3.3.- Synaptic plasticity and networks connectivity.

Little is known about how synaptic plastic changes affect to the information transmission at the level of the circuits.

In the first article about LTP[22] the authors informed about an increased efficiency in the Excitatory Post-Synaptic Potential (EPSP) recorded in the molecular layer of the dentate gyrus (as a reflex of dendritic integration) that leads to a major Population Spike (PS). It was called the EPSP to PS potentiation. However, and mostly neglected, in the majority of the cases this relation was non-linear, showing a bigger PS than the predicted by the increased EPSP slope.

"In the majority of cases [...], the potentiation of the population spike could not be explained wholly in terms of potentiation of the EPSP". Bliss and Lomo, 1973, 344 p.

It implies that other factors than the increased excitability of glutamatergic synapses affect the network consequences of the LTP. These others aspect may have implications for memory and learning as well. For instance, LTP induction induces changes at inhibitory synapses of principal neurons[130] or in the excitatory synapses of the interneurons[131]. Also, synaptic plasticity may affect differently to distinct neuronal populations[132]. High-frequency stimulation induces potentiation in excitatory synapses, but same protocols do different things in inhibitory interneurons, by virtue of different composition in the glutamatergic receptors[133,134], or different proteomic machinery or membrane potential[113]. Also, LTP and LTD may occur in inhibitory synapses (not only in the traditional excitatory ones)[130,132,135]. It implies that LTP/LTD may modulate activity at the level of the network, and not only at local synaptic level.

To emphasize the relationship between local LTP and functional network changes, Canals et al. (2009)[136] probed that there is a functional reorganization of the circuit after the induction of LTP in one particular node. They implanted stimulating electrodes into rats' perforant pathway and acquired fMRI images while stimulating, before and after LTP induction. Before LTP, only the hippocampus and the dentate gyrus showed Blood Oxigenated-Level Dependent (BOLD) signal. After LTP induction, there was not only a local BOLD increase in those structures, which is expected, but also it appears an extra-hippocampal BOLD activity in other distant regions, in which authors didn't induce LTP (as prefrontal cortex, nucleus accumbens, amygdala, and others)[136]. These data suggest that in spite the LTP is a local phenomenon, its effects on the local circuitry goes beyond the local processing and affect the functionally related circuit. Further experiments proved that the dentate gyrus is the structure that changes the activity the most after LTP induction —following the same protocol in high-resolution fMRI[137]—, and also that the LTP induction in dentate gyrus causes a decrease of inhibitory tone, mainly the perisomatic one, together with the well-known increased efficiency of excitatory transmission in the dendrites.

The topic of this piece of work is not related to plastic changes *per se*, but regarding the consequences of synaptic plasticity in the dentate gyrus on long-range functional connectivity and the role of inhibition. Canals' laboratory pointed interneurons as critical regulators for understanding the information flow on the hippocampal trisynaptic circuit, its long-range

connectivity and its functional implications on memory and learning. In this thesis we modulated the activity of some hilar interneurons (parvalbumin-expressing interneurons), with pharmacogenetic tools (DREADDs), to address its functional consequences over the learning and memory. We combine pharmacogenetic with *in vivo* electrophysiological recordings in anaesthetized mice, fMRI, behaviour and engram labelling, in the way described in material and methods. The anatomical structure in which we focused is the dentate gyrus. So in the next two sections, we focus on the dentate gyrus and its interneurons populations.

1.4.- Dentate gyrus.

1.4.1.- Anatomic overview.

The dentate gyrus is part of the hippocampal formation. It has a V- or U- shaped structure (depending on the anterior-posteriority and the kind of cut applied to the brain) and comprises three layers, called (from outside to inside): molecular layer, granule cell layer and hilus, also called hilar region or polymorphic layer (Figure 1.6).

Molecular layer is the external part of the dentate gyrus, and it is mostly occupied by dendrites of dentate gyrus granule cells, and of some hilar interneurons. It is further divided into two parts depending on the receptor field that the afferent axons innervate. In that sense, we distinguish 1) the two outer third in the molecular layer, where inputs from entorhinal cortex arrive; lateral entorhinal cortex innervates the most external third in the molecular layer, and medial entorhinal cortex innervates the middle one (Figure 1.6). And 2) the inner third, where commissural afferents from the contralateral hippocampus arrive[11]. Granule cells dendrites are cone-shaped, directed toward the exterior portion of the molecular layer and are more extensive in the supralaminar blade of the granule layer, than in the infralaminar blade[138].

Granule cell layer is the intermediate one between the molecular layer and the hilus. This layer contains the somas of granule cells, that are the principal excitatory neurons in dentate gyrus and the only excitatory neurons that project to other areas (hilar mossy cells are also excitatory but project to ipsi- or contralateral dentate gyrus). Granule cells somas are highly compacted in the granular layer and can be segregated in supralaminar and infralaminar blade, having differential anatomical and functional properties[138,139]. Dentate gyrus granule cells are highly hyperpolarized and show rare firing rate, but when it does, it does in burst having a strong influence on their postsynaptic CA3 targets[140]. Axons of granule cells are called the mossy fibres and innervate CA3 fields. Supralaminar blade mainly innervates CA3a subdivision, also CA3b, mostly bypassing CA3c; while infralaminar blade innervates CA3c preferentially, an area not involved in auto-associative networks related to learning[141].

The hilus forms the internal part of the dentate gyrus. It takes its name due to the axons of the granule cells, that get adjacent one from each other so that it gives a filamentous appearance (hilus, from the Latin *hilum*, meaning thread/strand). It is also called polymorphic layer because of the diversity of neurons it presents. Axons of the granule cells pass through the hilus on their way to CA3. In the hilus, they emit collaterals to GABAergic interneurons and mossy cells. Part of those collaterals contact with hilar basket cells, forming feedback inhibition circuits. Those are important for this work because we will focus on interneurons regulation, and especially in the hilar PV^{+} cells, which most of them are basket cells[92]. Hilar interneurons will be boarded deeply in section 1.5.
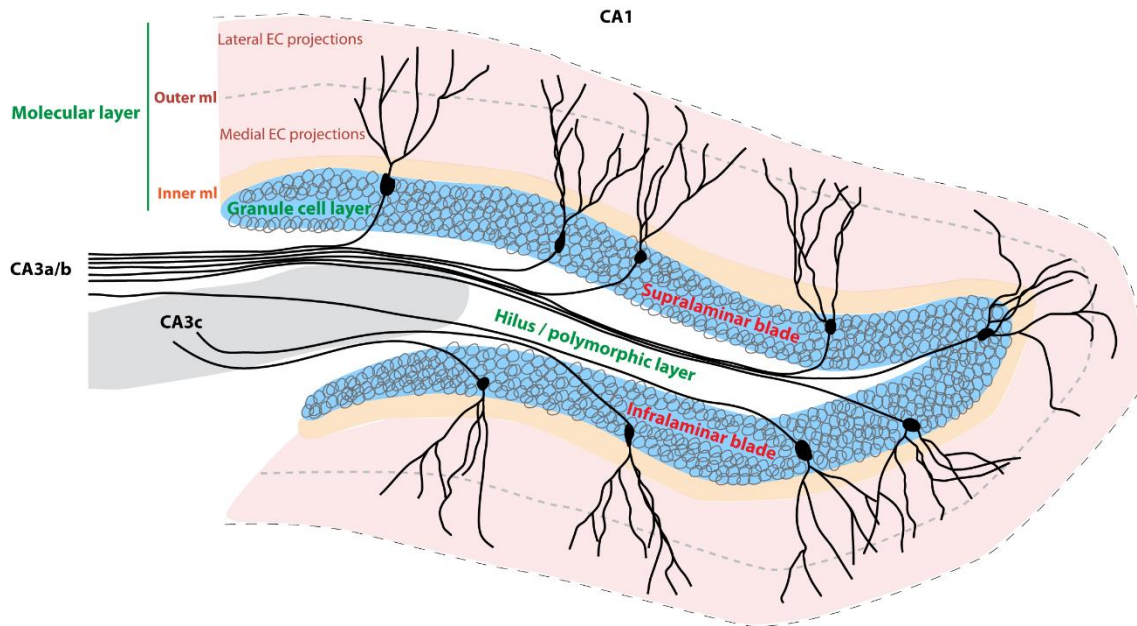
Figure 1.6. Schematic anatomical detail of the dentate gyrus. Drawing of a coronal view of dentate gyrus. CA = *Cornu Ammonis*, ml = molecular layer, EC = entorhinal cortex.

1.4.2.- Afferences to the dentate gyrus.

Entorhinal cortex projections to the dentate gyrus.

Dentate gyrus receives inputs mainly from the entorhinal cortex through the perforant pathway[8]. The projection to dentate gyrus arises mainly from layer II of the entorhinal cortex, and a minor component from layers V and VI. Its terminals are confined to the outer two-thirds of the molecular layer, contacting with dendrites of granule cells and some interneurons subtypes, as the apical dendrite of the parvalbumin basket cells. Lateral entorhinal cortex generates the lateral perforant pathway that terminates in the outer third of the molecular layer. Medial entorhinal cortex generates the medial perforant pathway that terminates in the middle third of the molecular layer. The perforant pathway is part of the angular bundle previously explained in section 1.2.2. Although the majority of fibres in the perforant pathway come from the entorhinal cortex, it also comprises some axons coming from the presubiculum and parasubiculum, which enters in the molecular layer and ramifies between the lateral and medial termination sites[95]. As subiculum receives direct projections from the anterior thalamic nucleus, these fibres provide a putative functional link between the thalamus and dentate gyrus, via subiculum.

Basal forebrain projection from the septal nuclei.

The dentate gyrus also receives afferents from subcortical regions as the medial septal nucleus and the diagonal band of Broca, via the fimbria-fornix pathway, branching in the hilus with cholinergic and, in less proportion, GABAergic synapses[142]. Cholinergic projections contact mainly with granule cells with asymmetrical and presumably excitatory contacts. Only 5-10% of

cholinergic contacts are on interneurons. GABAergic projections terminate preferentially on GABAergic hilar interneurons, forming symmetrical synapses, presumably inhibitory.

Supramammillar and other hypothalamic projections.

Hypothalamic afferents to dentate gyrus arises mainly from the suprammillar area. They terminate densely in the molecular layer, just superficial to the granule cells, and lightly in the hilus. These projections to the dentate gyrus arise from calretinin and substance P neurons[143] and use glutamate as the primary neurotransmitter[144]. More hypothalamic nuclei project to the dentate gyrus; however, its diffusiveness and lack of distinguished biochemical markers made its study difficult.

Brain stem nuclei projections.

Dentate gyrus also receives projections from the brainstem nuclei, as locus coeruleus (noradrenergic), ventral tegmental area (minor projection, dopaminergic) and raphé nuclei (serotonergic)[145–147]. All of them terminate primarily in the hilar region of the dentate gyrus, on interneurons in general, and basket cells in particular. It points to these neurotransmitter systems as modulators of hilar interneurons controlling the information flow in the dentate gyrus.

1.4.3.- Inner connectivity in the dentate gyrus.

Once the external inputs arrive into the dentate gyrus, they are processed conditioned by the endogenous features of granule cells and dentate gyrus interneurons and its inner connectivity.

Dentate Gyrus granule cells.

Dentate gyrus granule cells have some unique features, as the mossy fibres extensions contacting in the CA3 thorny excrescences, its few and disperse multi-sites connections on CA3 (boarded in section 1.4.4) and some particular electrophysiological characteristics[140]. They also present neurogenesis even during the adulthood (at least in rodents). They have an elongated cell body, 10 μm width and 18 μm height[148], tightly packed in granule cell. Its dendrites extend into molecular layer, where they receive inputs from entorhinal cortex, from the contralateral dentate gyrus and from dendritic-target hilar interneurons.

Neurogenesis in the dentate gyrus has been related to several aspects of learning and memory, as pattern separation/completion for associative memories[149], memory consolidation[150] and others (for a review; Abrous and Wojtowicz, 2015[151]; Deng et al., 2010[152]). Neurogenesis is also related with the high inhibitory control that the dentate gyrus granule cells present; the more mature the neuron is, the more inhibited[153,154]. It has significant implications; maybe the newborn neurons may encode new information efficiently due to the less inhibitory tone, and eventually, after a period in which they become progressively more

and more inhibited, they can retain this information for a variable period[154]. Interestingly, the total number of neurons do not vary with age under typical experimental conditions[155], but it may increase by environmental factors, which affect whether the proliferation or the survival[156,157].

Dentate gyrus granule cells are highly hyperpolarized; its resting membrane potential is around -80/-85 mV. Its membrane resistance in around 122 ± 13 MΩ and the temporal window for synaptic integration is $\tau_m = 16 \pm 1$ ms (similar to pyramidal neurons in CA3 and CA1). The combination of low membrane resistances and highly negative resting potential support the idea of the K^+ selective leak conductance as responsible for its features[158]. Also, the current and voltage threshold is more positive than most of the neurons, showing a high action potential threshold[158]. All together help the very low firing rate exhibited by dentate gyrus granule cells. Regarding dendritic integration, dentate gyrus granule cells show comparable synaptic excitation to CA3 and CA1 pyramidal cells —which exclude dendritic synaptic differences as responsible in firing rate—, and a higher ratio of excitation versus hyperpolarizing inhibition (probably required to more easily overpass its hyperpolarization)[158].

Dentate gyrus granule cells present low-frequency firing, virtually 0 Hz —we need to go to the order of minutes to see them spontaneously firing[140]—. Despite their meagre firing rate, if they do, they do in bursts, having an enormous and super-effective influence on CA3 targets. Granule cells are exposed to barrages of fast AMPA-mediated excitatory postsynaptic currents (EPSCs), coming mainly from entorhinal cortex; and inhibitory postsynaptic currents (IPSCs), due to local inhibitory interneurons. EPSCs have coherence with the field potential in theta frequency, while IPSCs do in gamma range. The classic view in the theory point to glutamatergic entorhinal cortex, or cholinergic input coming from medial septum, as driver for the theta activity[159–161], while gamma is a local phenomenon driven by GABAergic interneurons[162]. Gamma power, related to inhibitory interneurons activity (especially fast-spiking basket-cells), is higher in granule cells than in other excitatory neurons[140,158], while theta power remains equal. It indicates a higher local inhibitory control over granule cells than the generally applied in the brain.

Interestingly for this work, even though gamma activity in dentate gyrus rely on local inhibition, entorhinal cortex lesions reduce it, when it should only compromise excitation[163]. This, and other data point to an interrelationship between this two, spectrally and mechanistically distinct, rhythms that coexist in the dentate gyrus. Theta-gamma coupling oscillations are in the point of view of computational models, merged with experimental data, as the basis for the temporal encoding of information[164] and the facilitation of the communication between areas[165]. Research has pointed especially to the GABAergic fast-spiking interneurons, parvalbumin basket cells, as a critical generator of gamma oscillations[162,166,167].

Theta-gamma coupling activity, related to excitatory-inhibitory synaptic events, is also affected by cable filtering[168,169], because dendro-somatic transfer impedance is highly frequency and location dependent[168,170]. Thus, proximal inputs provide signals in gamma frequency, related to basket cells perisomatic inhibitory contacts, and distal inputs may provide signals in theta frequency with more efficiency, related to the entorhinal inputs over granule cells.

Related to local inhibitory activity controlling granule cells, dentate gyrus interneurons in general, and parvalbumin basket cells in particular, are boarded deeply in section 1.5., given its great importance for this work.

Internal microcircuits depend on the number neurons subtypes included on them. There still is an academic discussion on how many interneurons subtypes exist and how exactly they connect in the dentate gyrus (for a review Freund and Buzsaki, 1996[91]; Pelkey et al., 2017[92]). However, in the dentate gyrus, and for this work, may be sufficient with the division of granule cells projections to the hilus, basket cells perisomatic innervation over granule cells and hilar interneurons projections to the molecular layer (Figure 1.7). Those divisions comprise the population we focus on this piece of work; the parvalbumin basket cells in the hilus.

Granule cell projections to the hilus.

Granule cells axons, called mossy fibres[8], have unusually large buttons that form *en passant* synapses in CA3 (around 15-20 per mossy fibre), but they also set collaterals into the hilus, contacting with interneurons and mossy cells. Each mossy fibre may have even seven collaterals into the hilus, with a total length of around 2.3 mm[171], which point to the importance of the feedback inhibitory circuits on the regulation of granule cells activity.

Mossy fibres collaterals branch in the hilus and gives rises to around 200 small synaptic varicosities, forming contacts with proximal dendrites of hilar mossy cells[172], basal dendrites of inhibitory basket cells, and other interneurons subtypes[173] as the Hilar Perforant Path-Associated cells (HIPP). It is necessary to note that while contacts with CA3 pyramidal neurons are 15-20, contacts in the hilus are around 200, and most of them are over inhibitory interneurons populations[173]. Some collaterals may enter in the granule cells layer itself (never in the molecular layer) and contact also with proximal apical dendrites of parvalbumin basket cells[174].

Basket cells perisomatic innervation over granule cells.

Basket cells are located below the granule cell layer and extend its axon all along the granule cell layer, establishing GABAergic perisomatic contacts[175,176]. Some contacts may be in the proximal dendrites of granule cells as well. Hilar basket cells present an apical dendrite that ramifies in the molecular layer and is innervated by entorhinal afferents; and a basal dendrite inside the hilus, innervated by granule cells axons, mossy cells and by GABAergic interneurons[174]. The polysynaptic contacts are evidence of complex inhibitory/dis-inhibitory mechanisms controlling information flow in the dentate gyrus, whose functional implications are mainly unknown.

There is a substantial difference in number between the granule cells and the basket cells. However, its axonal plexus ramifies densely in the local circuit, so that each basket cell contacts with around 10.000 granule cells, 7-10 contacts with each one, even at 1-1.5 mm distance away[174]. This finding, together with their high firing frequency and precise timing[177], point them as perfect regulators of granule cells activity.
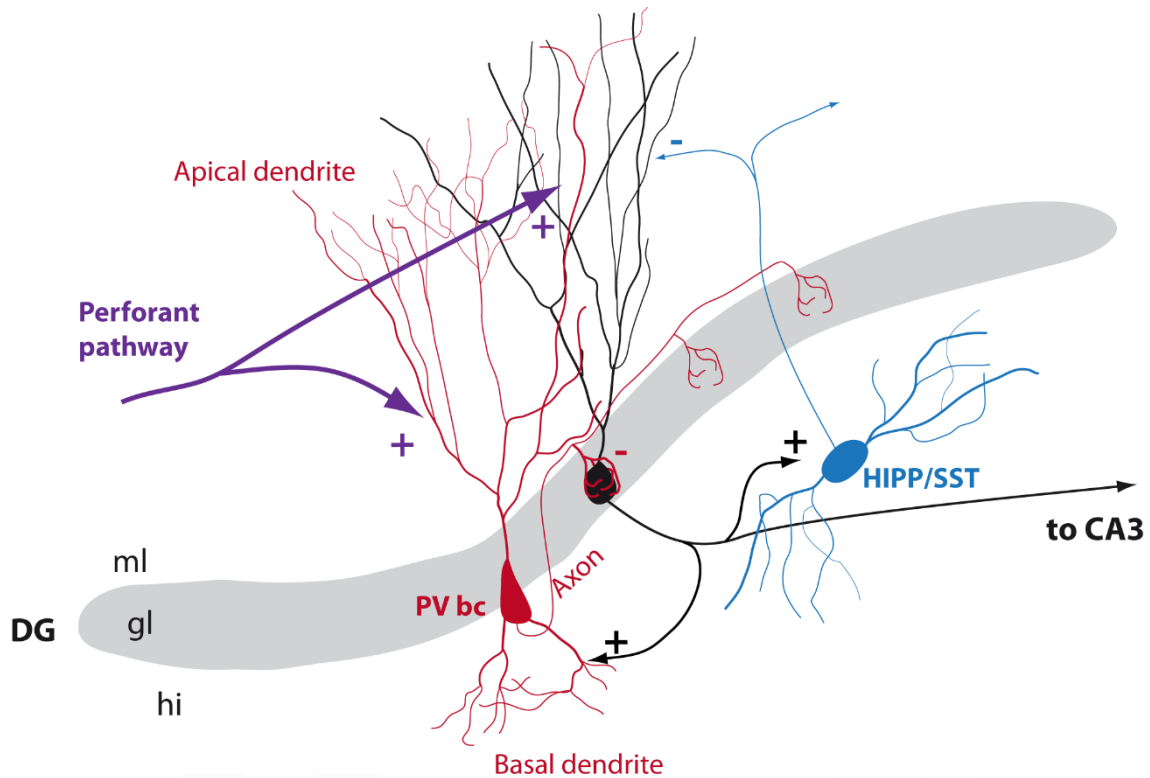
Figure 1.7. Schematic representation of classical inner microcircuits in the dentate gyrus. Perforant pathway fibres (purple) activates both granule cell (black) and apical dendrite of parvalbumin basket cells interneurons (PVbc; in red), which inhibit perisomatically the granule cells. Granule cells firing activates PVbc and hilar perforant pathway-associated cells, related to somatostatin biomarker (HIPP/SST; in blue), which inhibit granule cell dendritically. Kindly note that PVbc mediates feedforward and feedback inhibition, while HIPP/SST neurons do so only in feedback inhibition. It is a classical and simplified scheme of the dentate gyrus inner circuitry. Other interneurons subtypes inclusion would distract from the explanation of PVbc role in the circuit regulating granule cells activity. DG = dentate gyrus, ml = molecular layer, gl = granule cell layer, hi= hilus, CA3 *cornu ammonis* 3. + Indicates activation, - indicates inhibition.

Hilar interneurons projections to the molecular layer.

Hilar Perforant Path-associated cells (HIPP) cells, identified by the expression of somatostatin (SST), provide the GABAergic projections to the molecular layer. They represent 16% of the interneurons in the hilus[178,179]. Its dendrites are located exclusively in the hilus, where they receive projections from granule cells, mossy cells and other interneurons[91]. HIPP cells extend their axons to the outer two third of the molecular layer, inhibiting distal dendrites of granule cells, and mediate in feedback inhibition over granule cells (Figure 1.7). Interestingly, HIPP axon-terminal fields and mossy cell plexus are complementary in their respective innervating regions, suggesting that both cell types may be another excitation/inhibition regulatory system over the dentate gyrus granule cells[11].

1.4.4.- Efferent projections from the dentate gyrus.

Dentate gyrus does not project to any other area than the CA3, through the mossy fibres. They contact on the CA3 field in the stratum lucidum, close to the pyramidal layer. The dentate gyrus projection ends abruptly at the beginning of CA2, being one of the main features that differentiate CA3 from CA2. CA3 can be further subdivided, from proximal to distal with respect to the dentate gyrus, in CA3c, CA3b and CA3a. CA3c is even inside the hilus and receives inputs mainly from granule cell placed in the infralaminar blade. CA3c pyramidal cells have not auto-associative recurrent networks related to associative learning and memory[141]. Some infralaminar layer cells axons cross the pyramidal cell layer in CA3c and also contact on CA3a, and CA3b[171]. Granule cell in supralaminar blade mainly innervate CA3a, the most distal section, also CA3b, and mostly bypass CA3c[139,141].

Mossy fibres give rise to complex en passant presynaptic terminals called mossy fibres expansions[180]. They may be even 8 μm large, but the majority range between 3-5 μm. These expansions form irregular, sophisticated and very characteristic synapses with the CA3 pyramidal cell proximal dendritic spines, called thorny excrescences. These synapses may have more than one contact per mossy fibre expansion but in the same pyramidal dendritic tree. Each granule cells contact only with 15-20 pyramidal neurons, with these super-effective synapses with multi-release sites in the mossy fibre expansions. Each CA3 pyramidal cell may receive input from about 72 granule cells, while granule cells-to-CA3 pyramidal cells ratio range from 12:1 in the septal hippocampus to 2:3 in its temporal pole[174]. These peculiarities have attracted the attention of many scientists (since Marr, 1971[98]), who point to the CA3 region, together with its recurrent connections, as responsible for pattern completion; and to the dentate gyrus for pattern separation.

Mossy fibres release mainly glutamate, as evidenced by its asymmetric synapses and biochemical markers. However, they are also immunoreactive for several other neuroactive substances, as dynorphin, GABA and cholecystokinin (CCK)[181,182]. Between all of them, the most interesting could be the co-immunoreactivity for GABA; although granule cells do not demonstrate mRNA for the synthetic GABA related enzymes GAD65 or GAD67, prolonged stimulation of the perforant pathway may induce GAD mRNA expression. It is thought to be involved in plasticity and in controlling the excitation, in case of over-activation related to epilepsy[183,184].

1.4.5.- Dentate gyrus functions.

Dentate gyrus receives multiple convergent sensory inputs through the entorhinal cortex. It includes vestibular, olfactory, visual, auditory and somatosensory inputs, in conjunction with spatial grid cells information[185]. This conjunction between sensory and spatial information explains why most of the studies relate dentate gyrus with spatial-context memory, although some of them also integrate non-spatial but context-dependent information[186,187]. This spatial functions associated to dentate gyrus include pattern separation[188,189], grid to cell code conversion[185,190] and the encoding of new spatial memories by associating sensory-specific inputs and contextual information converging in the same cell[191,192].

Many articles relate the dentate gyrus with pattern separation. This attention comes from Marr's theory (1971), who developed a computational model that pointed to CA3 as the

central node for pattern completion —mainly because its recurrent collaterals—, and to the dentate gyrus as the primary node for pattern separation —due to its sparse connectivity, its high number of neurons and its precise and super-effective connections on the CA3[98,193]—. Marr's theory focused more in the pattern completion than in the dentate gyrus function, relegating the latter as "helper" of CA3 in case of complex spatial situations with high overlapping similitudes; which could lead to a CA3 recurrence failure. It raised the idea of dentate gyrus requirement is directly proportional to the grade of similitude of the contextual information; so to say, directly proportional to the difficulty of the spatial task. Experimental data support pattern separation associated with the dentate gyrus[64,188,194]. For instance, damage in rat's dentate gyrus reduces its ability to detect object movements concerning previous positions. Also, dentate gyrus granule cells respond when the environment is suffering progressive and soft changes, but do not when the same environment changes drastically[188]. Moreover, in humans, pattern separation tasks increase BOLD response in dentate gyrus and CA3. Also, the dentate gyrus participation in non-spatial pattern separation has been discarded: 1) temporal pattern separation is mediated by CA1[64], 2) separation of purely visual patterns is linked to perirhinal cortex[195], 3) discrimination between rewards is accomplished by the amygdala[196], and 4) motor separation pattern is related to the caudate nucleus[197].

Even though the majority of the research focuses on pattern separation, not all the studies agree in considering it as the only dentate gyrus function[198–200]. For instance, Lee and Jung (2017)[200] propose that dentate gyrus bind different sensorial information, including spatial one, "packing" them into discrete patterns, first in the dentate gyrus and then transferring it into the rest of the trisynaptic circuit. As a result of this binding, it emerges the pattern separation, because different sensorial conjunctions result on discrete separation of patterns; but as a consequence of the "packing" of sensory-spatial memories, not as a property *per se*. In that sense, Morris et al. (2013)[199] found that dentate gyrus lesions compromise learning in odour-context association tasks, not requiring pattern separation. It supports the role of the dentate gyrus in binding sensory-spatial information. Also, Buckmaster and Schwartzkroin (1994)[198] suggested that the dentate gyrus may participate in associative learning as well, due that mossy cells-to-granule cells express NMDA synaptic plasticity[201]. Actually, LTP presence in dentate gyrus would be detrimental to pattern separation because it tends to attract similar patterns together by enhancing synapses that are common with similar patterns[202].

All these data point to the dentate gyrus participating in contextual memories formation and discrimination. It does so by itself or by modulating hippocampus activity. Hippocampus and dentate gyrus contribute by combining object and place information via conjunctive processing[203,204]. Following this idea, Spanswick and Sutherland (2010)[205], demonstrated that animals with dentate gyrus lesions showed problems in recognizing new positions of the objects in context-dependent tasks, but did the standard object-recognition task correctly. Morris et al. (2012)[206] replicated the spatial-dependent memory deficits after dentate gyrus lesions.

Some other works claim that the dentate gyrus may contribute to temporal associative integration for events and temporal cue-recall sequences based on the newborn neurons in the dentate gyrus[207]. As time passes, the young neurons mature or die. When new events happen together in time, they may be encoded within the same young neurons. The concatenated replenishing of neurons, memorizing new events, may be the substrate for temporal orthogonalization and the episodic memory. In that sense, dentate gyrus lesions

disrupt the temporal association between spatial events presented within 3 minutes[207]. This implication for storing spatial and temporal aspect of events also links dentate gyrus with episodic and working memory[208,209].

To summarize dentate gyrus function; most of the research focuses exclusively on pattern separation since Marr's proposals (1971). However, being plausible, it could be due to a consequence of a more extend implication on sensorial-spatial processing, converging spatial inputs with context-related information. Dentate gyrus importance increase as function of the difficulty of the task, so that its implication is more evident when the spatial task requires some grade of overlapping inputs. Dentate gyrus may modulate CA3 activity, where auto-associative memories are thought to take place. However, the specific way in which dentate gyrus does it is unknown. Some experimental data and computational models point to the theta-gamma coupling activity, related to the excitation/inhibition ratio, as an essential key to understand the electrical activity flow, underlying to its functions and especially to memory.

1.5.- Interneurons and inhibition.

We still don't have a unique classification for all the interneurons, but several that, altogether, allow its study and the communication between professionals. We can classify them according to the anatomical features, by which we distinguish interneurons based on its shape, position and connectivity —as basket cells interneurons, axo-axonic cells, Hilar Commisural-Associational Pathway-related interneurons (HICAP), Hilar Perforant Path-associated cells (HIPP) and others—, or based on the molecular marker they express —as parvalbumin (PV), somatostatin (SST), cholecystokinin (CCK), vasointestinal peptide (VIP), among others—. These neurons with different biochemical markers correspond (although not entirely) with some of the anatomical classifications. For instance, PV interneurons usually are associated with hilar basket cells; while SST interneurons mostly correspond with the HIPPs anatomical subtype[91]. In addition to their specific biochemical marker, most, if not all, of the interneurons are GABAergic, co-labelling for GABA related molecules, like glutamic acid decarboxylase (GAD). The total number of interneurons in the hippocampus range from 7%[210] and 11%[211]. Interneurons can also be classified based on its electrophysiological properties, so that we differentiate, for instance, fast-spiking interneurons, to point neurons with low inter-spike delay and high firing frequencies. The electrophysiological studies have led to an incredibly high number of different subdivisions[212]. The high complexity of the interneurons' classification in specific networks nodes gives rise to the idea that maybe they can be only be clustered attending to a combination of electrophysiological, anatomical and biochemical factor[212], giving a high number of entities.

Not trying to classify them, we will focus on hilar PV expressing interneurons of the dentate gyrus, most of them correspond to the anatomical pyramidal basket cell subtype[92] and with the fast-spiking electrophysiological phenotype[213], because they are the target population for this work. Other subtypes will also be mentioned briefly.

1.5.1.- Dentate gyrus interneurons.

Hilar PV pyramidal basket cells.

Most of the basket cells in the hippocampus and dentate gyrus match with PV labelling[92,214], in spite some basket cells do not, and co-label with CCK instead (16%). Some bistratified interneurons (not mentioned in deep) also form a low portion of total PV interneurons[92]. PV+ and CCK+ basket cells differ in their electrophysiological properties, even though they both are basket-cells. CCK+ interneurons fire in a less reliable manner, not being coupled to the gamma oscillation in the network and generate fluctuating, asynchronous and less timed inhibition on their targets[213]. This two biochemically distinct basket cells probably are playing different roles in the network fluctuations. Because of that, and due to that we modulate only the PV+ interneurons activity in this work, we are going to focus on the PV+ majority of the basket cells.

PV-expressing basket cells (PVbc) present pyramidal shape cells bodies ranging from 25 to 35 μm ø, located along the deep surface of the granule cell layer, although some of them can be found embedded in the granule cells layer itself. The name of the basket is due to the characteristic perisomatic plexus over its neuronal targets, which surround the soma forming a kind of basket[8]. The first description of the pyramidal basket cells and defined them as having a unique an-spiny dendritic tree ramified in the molecular layer (its apical dendrite), whose functional property is to provide feedforward inhibition over its granule cells targets. Lorente de Nó[83] distinguished also the basal dendrite, that may vary in number from two to five branches, sited in the hilus, and receive inputs from granule cells, so that it allows the basket cell to mediate also in feedback inhibition. This basal dendrite also receives inputs from other cells types, as the hilar mossy cells or inhibitory interneurons[91]. In total hilar basket cells receive inputs from; 1) entorhinal cortex, via perforant pathway, 2) contralateral dentate gyrus, via commissural association fibres, 3) dentate gyrus granule cells, through the mossy fibres, 4) CA3 pyramidal neurons, via its back projections to mossy cells and then to baskets cells, 5) from others PVbc, and 6) from other hilar interneurons[91]. Lorente de Nó (1934) defined basket-cells as free of spines, however, recent research presented in FENS forum 2016, not yet published to our knowledge, by the group of Marlene Bartos, probed that exists two different populations of parvalbumin-expressing basket cells; an-spiny and spiny basket cells, whose functional and electrophysiological differences are still under study.

Axonal arbours of the basket cells ascend through the granule cells layer, distribute long horizontal branches superficially to the granule cell layer, and emit a large number of collaterals that descend into the granule cell layer, where they form a dense perisomatic plexus in the proximal dendrites of granule cells, with GABAergic inhibitory type 2 synapses (Figure 1.8). Perisomatic contacts are optimal to control the timing of action potentials in target cells[215,216]. Each axon branch around 1.5 mm along the septotemporal axis, and around 44 mm long in total, with a high number of synaptic buttons[176]. This large axonal dimensions and the high number of contacts over its targets seem to compensate the low number of hilar basket cells neurons: its ratio with respect granule cells range from 1:100 to 1:180 in the supralaminar blade, and around 1:300 in the infralaminar blade[11]. However, each PVbc may contact with even 10.000 granule cells, 7-10 perisomatic contacts per neuron, at 1-1.5 mm distance away[174].

Hilar PV basket cells are estimated in around 14% of the total number of interneurons in the hippocampus and dentate gyrus[217]. However, its exact number is controversial because, at

mature stages, PV expression levels are dynamic, related with the activity in the circuits they are embedded in[218], which could elicit differential staining. It also may reflect functional dynamical properties at the level of the networks. In that sense, it is worthy to note that PV basket cells can be recruited by different combinations of inputs and may serve dynamic functions in the circuitry, contributing with rapid and timed inhibition on their postsynaptic cells[219,220].

Excitatory synaptic inputs rapidly activate PV-expressing interneurons, which generate high-frequency trains of action potentials phase-locked to fast network oscillations. It provides fast, stable and precise-in-time inhibitory output onto their target cells[213]. It is possible because they have low input resistance, R_{in} ~80 MΩ, and fast membrane time constant, τ_m ~10 ms, which conditions low specific membrane resistance, R_m ~10–15 kΩ,[220,221]. The recruitment of PV basket cells by entorhinal cortex afferents elicits short-latency feedforward inhibition[216], whereas, activation in dentate gyrus cells activates feedback inhibition and modulate the duration of the discharge period in the target cells. Interestingly, while multiple pulse activity usually leads to a depression in the firing rate, same multiple pulse activity leads to a reliable activation of PV basket cells[222]. Altogether, these data indicate that PV basket cells rapid and reliably translate excitatory inputs into a fast inhibitory control on its targets, controlling activity propagation in the node they are embedded in[219,220].

PVbc dendrites have large diameters[223]. As the anatomical parameters also condition the neuronal electrophysiological properties, synaptic currents integration in the soma are quicker than in other interneuron types[224]. The combination of large dendritic diameter, low attenuation of activity propagation and low R_m support fast propagation of EPSPs in PVbc. It helps to the fast-spiking characteristics of these cells. Moreover, the fast τ_m define narrow time windows for temporal summation[224]. They also express low densities of voltage-dependent Na^+ conductance at their dendrites, but high densities of voltage-dependent K^+, mostly Kv3-type channels[225]. K^+ channels facilitate the decay time course of EPSPs at apical dendrites, so that temporal precision is enhanced. Furthermore, the density of K^+ channels declines with distance from the soma, indicating that acceleration of EPSPs will be more profound at proximal than at distal dendrites (Figure 1.8).

The majority of excitatory synapses in interneurons, in general, contain four subunits of postsynaptic AMPA receptors: GluR1, GluR2, GluR3 and GluR4[226]. Dentate gyrus fast-spiking cells, presumably PVbc, express low-levels of GluR2[227]. It is associated with fast deactivation kinetics. AMPA receptors lacking GluR2 subunit also show a Ca^{2+} permeability several times larger than the standard[227]. Its activation has been related to LTP induction mechanism[228], which point to the PVbc interneurons as candidates to be regulated by plastic changes, having unknown functional implications at the level of the networks.

Action potentials of PV basket cells have short half-durations (< 0.4 ms) and propagate rapidly (~0.25 m s^{-1}) with minimal failure rate along the axon[220]. Thus, they support rapid and reliable transduction of signals from the input to the release site, occurring with minimal fluctuation and low failure rates[221].

Figure elements (labels within illustration):

A)

apical dendrite

K⁺ Kv3 type channels, a.u.

Axon extension in the DG = 1.5 mm
Axon total lenght = 44 mm
Number of contacts per gc = 7-10
Number gc contacted = around 10.000
Ratio PVbc/gc (supralaminar) = 1:140
Ratio PVbc/gc (infralaminar) = 1:300

ml

perisomatic plexus

gl

hi

25-35 µm ø soma

Low input resistant; aprox. 80 MΩ
Fast membrane constant; 10 ms
Low membrane resistant; 10 –15 kΩ
Low Na⁺ conductancie in dendrites

50 mV
200 ms
800 pA

basal dendrite

B)

C)

Na⁺/Ca²⁺

GluR1   GluR3

GluR2 GluR4
GluR1 GluR3

Low GluR2 subunit levels
fast deactivation kinetic
high Ca²⁺ permeability

AMPA receptor

Figure 1.8. Detailed illustration of a hilar parvalbumin basket cell. A) Detailed draw representing anatomical and electrophysiological features of hilar PVbc interneurons. Black indicates dendrites and soma; blue line indicates axonal arbour and perisomatic plexuses. Colour bars indicate the density of potassium Kv3 channels from the soma. *In vitro* data (right) taken from Yexica et al., (2008)[229]. B) Amplification of the squares in A, focusing on PV basket cells dendritic synapses. C) Magnification of the synaptic membrane of PVbc, representing characteristics heterotetramers AMPA receptor on its surface; containing GluR1, GluR2, GluR3 and GluR4 subunits. AMPA receptors on PV basket cells show low levels of GluR2 subunit, which provokes fast deactivation kinetic and high Ca²⁺ permeability. DG = dentate gyrus, gc = granule cell, PVbc = parvalbumin basket cell, ml = molecular layer, gl= granule cell layer, hi = hilus.

Other interneurons.

Classifications based on the anatomy.

Classically, the anatomical classification (Figure 1.9) segregates dentate gyrus interneurons in:

- Hilar Perforant Path-associated cells (HIPP cells). This type has 2-3 primary dendrites that start from the poles of its fusiform soma, sited in the hilus. They run in parallel to the granule cell layer blade and spread for nearly its entire length. Its branch coincides with the

distribution of mossy fibres collaterals in the hilus. The main feature of these cells is the presence of long, thin and often branched spines in the soma and dendrites. Its axon ascends into the outer two third of the molecular layer (exactly where perforant pathway fibres arrive) and innervates with symmetric inhibitory type 2 synapses on granule cell dendrites, having a highly disperse distribution (with even 100.000 synapses)[11]. Occasionally they also contact with other interneurons subtypes[176]. Some collaterals of the HIPP cells may also arrive at CA1 region and subiculum[230]. This anatomical subtype often is associated with the SST biochemical phenotype. HIPP cells are likely to mediate dendritic feedback inhibition of granule cells[231].

- Hilar Commisural-Associational Pathway-related cells (HICAP) are multipolar cells with thin and sparsely spiny dendrites that extend both in the hilus and in the inner third of the molecular layer (where commissural fibres arrive)[230]. Their soma is in the subgranular zone, from where the axon ascends and branch in a Y-shaped manner in the middle third in the molecular layer. Their axons possess a large number of buttons that tend to be confined in the inner third of the molecular layer, forming symmetric synapses in proximal dendrites of granule cells[230]. HICAP cells termination seems to have a preference for large calibre granule cells spiny dendrites[231].

- The Axo-Axonic, or chandelier, interneurons somas are within the granule cells layer and extend their dendrites both in the molecular layer (apical dendrite), that reach mainly the outer third, and in less number in the hilus (basal dendrite)[232]. They have a pyramidal-like soma, and its axon innervates mainly the axon cone on the granule cells targets, in a characteristic termination that gives rise to its name, with 4-12 buttons aligned parallel to the axon initial segment of granule cells and of other hilar interneurons. Some granule cells receive axo-axonic innervation from several chandelier interneurons[233]. This termination on the axon initial segment is unique among interneurons subtype having enormous influence in blocking the firing of the target neurons.

There are other interneurons anatomical subtypes in the hilar region of the dentate gyrus, as neurons with axons and dendrites in molecular layer (MOPP cells)[230], hilar neurons with specific projections to subiculum and hippocampus[234], hilar interneurons with unknown projections[235,236], and others (Figure 1.9. For a review: Freund and Buzsaki, 1996[91]; Pelkey et al., 2017[92]). However, boarding all of them would distract from the introductory overview, and it could be counterproductive for the present thesis.

The anatomical classification co-exists with interneurons division based on its biochemical markers (Figure 1.9). Some subdivisions have a kind of overlapping coincidence with the anatomical classifications, but they do not always march perfectly. For instance, basket cells are linked to PV- and CCK-expressing (16%) interneurons or HIPP cells mostly are hilar SST expressing cells. However, VIP-expressing interneurons have not, to my knowledge, specific anatomical subtype to be associated with. Neither the calbindin or the calretinin ones. The classifications based on the biochemical marker divided interneurons into:

- Somatostatin-positive interneurons have been associated with HIPP anatomical subtype[237]. Their somas and dendrites are in the hilus, where they receive input of the granule cell mossy fibres, mossy cells and other interneurons subtypes. Its axons ramify in the outer two-thirds in the molecular layer, where afferents from entorhinal cortex arrive. A small proportion of cells emits collateral to contralateral dentate gyrus and CA1[238]. Their similarities with HIPP anatomical subtype make them be used as synonymous, being probably the most straight-forward of all the bridges between anatomical-biochemical classifications. Giving its connections, they seem implicated in feedback dendritic inhibition.

- Calbindin-positive interneurons form the group with the lowest number of neurons in the dentate gyrus, but interestingly they are placed in the molecular layer (3-20 per slice) and the hilus (3-10 per slice). Their dominant dendritic orientation can be horizontal or vertical and its axon, in the dentate gyrus, has not been reconstructed yet. Calbindin is a marker also of granule cells, so it is not specific to interneurons, and this feature makes its study harder[239].

- Calretinin-positive interneurons may be spiny or an-spiny. Spiny ones are mostly in regions where receive innervation from mossy fibres; in hilus and CA3. In the dentate gyrus, dendrites are confined in the hilus. Its axon was not visualized by immunostaining yet, due to its high myelinisation, but at least some of them project to contralateral dentate gyrus[91]. However, in CA3 has been intracellularly injected with biocytin and its axons arborized in stratum lacunosum-moleculare, and in the outer third of the dentate gyrus molecular layer[91]. The GABAergic nature of the spiny calretinin interneurons is controversial; some articles have probe negative co-staining with GABA makers[240], but negative staining does not necessarily mean negative expression, it could be due to low levels of GABA or GAD. Spine-free calretinin interneurons in the hippocampus, on the other hand, receive inputs mainly from extra-hippocampal projections, from not established sites, and innervate mainly other interneurons. They are also GABA negative[91].

- Neuropeptide Y immunoreactive interneurons in the dentate gyrus are mostly in the hilus, but some of them are in the molecular layer. They have a pyramidal shape soma and two dendrites branches; the basal one is restricted to the hilus, receiving inputs mainly from mossy fibres, and the apical one ascends to the molecular layer. This subtype is similar to the previously explained basket cells, but the axons form a dense plexus in the outer third in the molecular layer, gradually losing density in the middle one and sparsely in the inner third. Some fibres cross to contralateral dentate gyrus[91].

- Vasointestinal peptide (VIP) positive interneurons are GABAergic and are present in all the layers in the dentate gyrus[241], although they tend to be more numerous within or nearby granule cells layer. Their morphology and laminar distribution are quite variable; the most frequent type of VIP interneurons has a bifurcated dendritic tree, with predominant radial orientation, which extends toward the pial surface. Cells within or below the granule cell layer

tend to have pyramidal shape somas with rich basal dendrites. In deep hilus, some VIP cells have multipolar dendrites that may be very long. Axons from VIP interneurons mainly innervate other interneurons subtypes placed in hilus, or in the molecular layer, and also some of them innervate other VIP positive interneurons[242]. Due to its connectivity, and its inhibitory controls over other interneurons, VIP expressing neurons are thought to be regulators of the inhibition in local networks. It was confirmed at least in cortical networks[243], pointing to VIP interneurons as "switchers" for other inhibitory interneurons populations.

There are more interneuron subtypes, including enkephalin positive interneurons, neurokinin immunoreactive neurons, nitric-oxide synthase interneurons, among others. However, even less is known about them, and they will not add anything else to the present work, despite its academical interest.

Anatomical division of interneurons

1.- PV bc	4.- CCK bc
2.- Axo-axonic	5.- HIPP
3.- Bistratified	6.- HICAP

Biochemical division of interneurons

1.- PV$^+$	4.- Calretinin$^+$	7.- VIP$^+$
2.- Calbindin$^+$	5.- CCK$^+$	
3.- NPY$^+$	6.- SST$^+$	
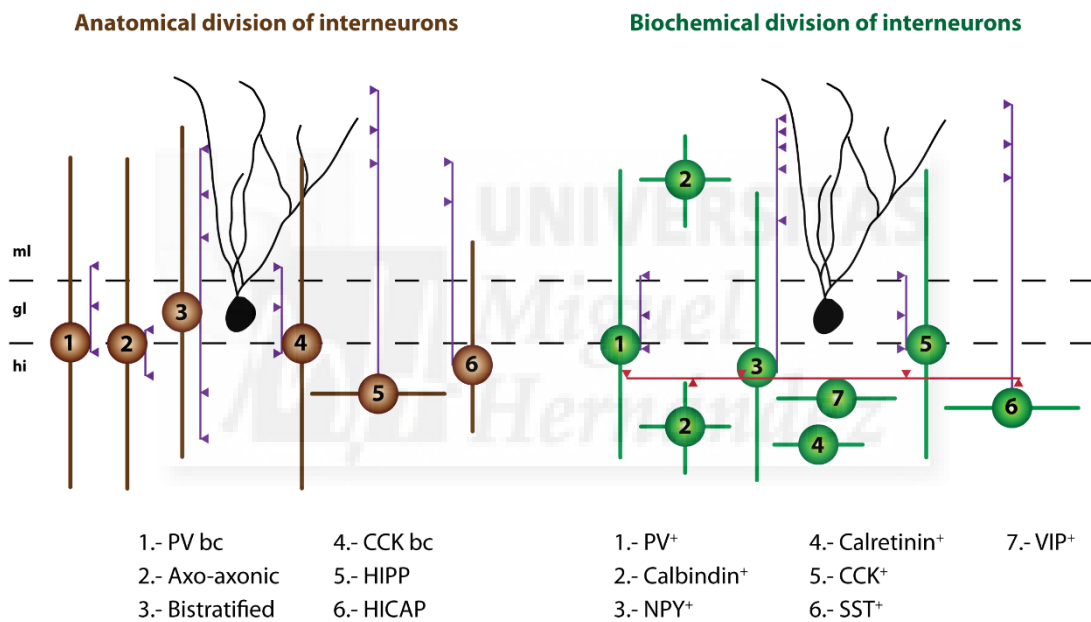
Figure 1.9. Schematic representation of main hilar interneurons. Black neurons represent excitatory granule cells. Left: anatomical classification of hilar interneurons. Brown circles indicate soma position, brown lines indicate dendrites and purple lines indicate axons and its innervation area. Right: interneuron classification based on biochemical markers. Green circles indicate soma position, green lines indicate dendrites and purple lines indicates axons and its innervation area. Red line is the axon of VIP interneurons, which inhibit other inhibitory interneurons. PV = parvalbumin, CCK = cholecystokinin, bc = basket cell, HIPP = hilar perforant pathway-associated cells, HICAP = hilar commissural associational pathway-related cells, NPY = neuropeptide Y, SST = somatostatin, VIP = vasointestinal peptide, ml = molecular layer, gl = granule cell layer, hi = hilus.

Inhibition was classically seen as mere compensation over the excitability in the neurons. Even nowadays some authors argue that inhibition, *per se*, serves no functional role beyond homeostatic inhibition after excitation[244]. Nevertheless, strong evidence coming from experimental data, computational models and theoretical proposals point to the role of inhibition as essential for neural computations and for providing temporal windows that allow neuronal functional coupling both locally and, by controlling local processing, affecting long-range connectivity[245,246].

The synchronization of neuronal ensembles is crucial for information processing. The researchers that support that the inhibition in the system plays a vital role point to the interneurons as critical players in coordinating this processing. The synchronous firing of neurons generates neural oscillations that we can measure in extracellular local field potential (LFP) recordings under certain conditions[247]. The first division of neural oscillations was done by Berger in 1929, who divided rhythms in alfa (<12Hz) and beta (>12Hz). The convention of naming neuronal oscillations based on its frequency remains nowadays but has varied in its classification (for a review Colgin, 2016[248]). In the hippocampus, most relevant frequency bands are theta, which goes from 4 to 10 Hz, and gamma, >30 Hz. Gamma is further divided into low gamma (30-50 Hz), mid (50-90 Hz) and fast (90-150 Hz)[249]. PVbc in particular basket cells are strongly phase locked related to gamma activity[250]. And, the fast-spiking perisomatic targeting, matching with PVbc connections, are essential for generating gamma rhythms[167,251,252]; its silencing impair gamma oscillations, while its activation induce them[253,254]. Gamma oscillations, and so the PVbc, can control their targets firing rate, being an essential requirement for the synchronization of principal cell assemblies and the emergence of fast network activity patterns[162].

Theta-gamma oscillations have an essential role in dentate gyrus function: they may represent a reference signal for temporal encoding "clusters" of information regarding contextual aspects[164]. Local interneurons gamma activity, in particular, may facilitate communication between principal neurons by synchronizing them[165,255], and high perisomatic inhibition may select cells that receive the highest excitation by a "winner takes all" mechanism[256]. Such a mechanism may be particularly useful in the dentate gyrus, where it could potentially participate in spatial mnemic processes[185,188]. It could be done thanks to gamma oscillation filtering —especially related to fast-spiking basket cells interneurons—. Then, if the granule cells fire, its amplification in bursts generate a highly efficient output onto CA3 pyramidal neurons. After overpassing inhibition, granule cells sparseness and its particularities described above may help to efficiently transmit information to CA3 pyramidal cells, having a high capacity of modifying CA3 processing. In this way, the dentate gyrus may work as a filter that selects salient inputs that are then conveyed to CA3, where they can be efficiently stored in the CA3-CA3 network by heterosynaptic potentiation[257].

When inhibitory interneurons fire they release GABA, which activate $GABA_A$ receptors on their postsynaptic targets, leading to hinder firing (or even blocked) during 10-40 ms after interneuron activation, being maximum at 20 ms. Also, the same initial release of GABA activates $GABA_B$ autoreceptors in the same inhibitory interneuron that release it, from 60 ms to 200 ms after GABA discharge, being maximum at around 100 ms[258]. It paradoxically leads to an inhibition of the interneuron, dis-inhibiting its postsynaptic targets and facilitating its firing. It implies that interneurons, in general, may both; impair or facilitate post-synaptic target

firing, and control themselves directly, through GABA$_B$ auto-receptors[91,92]. Both mechanisms may help, thought the inhibition of the inhibitory interneurons, to the plasticity and the effective coordination between nodes in the brain. Importantly, GABA$_B$ interneurons dis-inhibition over its targets, given its 60-200 ms delay, fits with theta frequencies of 5-10 Hz. Regarding that point, some articles point to the importance of the theta cycle on the modulation of synaptic plasticity[259,260] and in the coupling between brain nodes, including the hippocampus[261]. Theta-gamma activity is particularly important when animals are exploring new environments[163], in which in vivo data probed that gamma oscillations during exploration occurs in all hippocampal subfields, but has their maximum power (mV/mm3) in the dentate gyrus[163], and especially in the hilus.

The coupling between excitation (that stimulates GABAergic interneurons and projects to other areas) and inhibition (that regulate the timing in which excitatory neurons may, or may not, to fire) has been called the excitation/inhibition balance (or E/I ratio). Considering the critical role of interneurons in controlling neuronal networks, it does not surprise its implications in brain disorders, including neurologic and psychological ones[92].

Coming from hippocampal studies, inhibition, and especially gamma oscillations, is basis for numerous cognitive functions, such memory and spatial navigation[262,263], learning and retrieval of information[264], attention, conceptual categorization[265], spatial representations[266], working memory[266,267] and, importantly for this work, environmental novelty detection, for which, in addition to the hippocampal dopaminergic innervation[268], it is supposed to exist a temporal shutdown of specific inhibitory interneurons[269], not yet established, that may aid to new memory encoding and trace persistence. It is also possible that inhibition may help to the plasticity-related events by regulating the timing of neural events[270].

Nevertheless, the specific function of specific interneuron populations in specific cognitive processes has not been related (to our knowledge). Here we study the role of hilar PVbc interneurons on the control of the dentate gyrus activity, the intra-hippocampal activity propagation in the trisynaptic circuit, its extra-hippocampal long-range functional connections, its implications on the encoding, consolidation and retrieval of new spatial memories, and on pattern separation. We also study the role of hilar PVbc modulation on the cells recruitment for specific contextual-dependent engrams.

II.- HYPOTHESIS.

Hypothesis.

Memory formation relays on some cellular and network mechanisms that interact to coordinate distributed cognitive process. Between all these elements, the present thesis work focuses on the regulation of excitation/inhibition balance as a putative mechanism to coordinate memory formation in the hippocampal formation. The hypothesis is that synaptic plasticity associated with memory encoding reorganizes functional connectivity in the system through the regulation of the excitation/inhibition ratio in the dentate gyrus. Thus, functional coupling in a network of mesocorticolimbic structures necessary for learning would be under the control of hippocampal interneurons. We further hypothesize that perisomatic inhibiting basket cells are strategically located to exert this control and, therefore, modulating their activity would impact on long-range functional connectivity and memory formation.

III.- OBJECTIVES.

Objectives.

1.- To study how the local inhibitory network in the dentate gyrus, more specifically basket cell interneurons, influence activity propagation in the hippocampus.

2.- To investigate whether modulation of dentate gyrus basket cells may influence the hippocampal long range functional connectivity to extrahippocampal areas.

3.- To elucidate the functional consequences of 1 and 2 on spatial memory encoding, consolidation and retrieval.

4.- To assess the size of the engram associated to memory encoding when modulating basket cells activity in the dentate gyrus.

5.- To examine the effect of dentate gyrus basket cell activity modulation on contextual pattern separation.
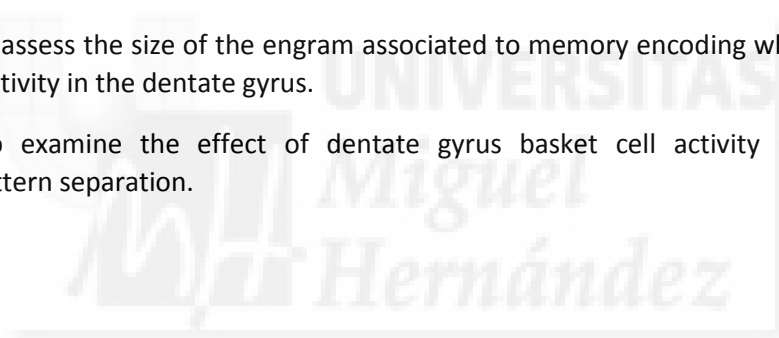
IV.- MATERIAL AND METHODS.

To achieve objective 1, we combined pharmacogenetic (DREADDs), targeting hilar PV+ interneurons, with LFP electrophysiological recordings on dentate gyrus and CA1 region while stimulating in the perforant pathway of anaesthetised mice.

To attain objective 2, we used same DREADDs than before but adding LFP recordings in the prefrontal cortex and also fMRI acquisitions while stimulating at 10 or 20 Hz in the perforant pathway.

To accomplish objective 3, we combined animals with same hilar PV interneurons infected with mutated proteins for pharmacogenetic (DREADDs), with a spatial memory dependent behavioural task as the Novel Location of the Object (NLO), discarding meddling of anxiety or other parameters in our data.

To get objective 4, we merged NLO behavioural task, while modulating hilar PV inhibitory cells, with cFos labelling and its posterior histological analysis.

Last, but not least, to reach objective 5 we develop a new behavioural task to evaluate long-short memory interactions while mice perform an assignment that requires pattern separation. Mice carried out this task under hilar PV interneurons modulation conditions. Control parameters from pilot studies are presented as well.

Objectives 1 to 3 were jointly confronted in a large experiment (EXPERIMENT 1). Objectives 4 and 5 were confronted in separate experiments, EXPERIMENT 2 and EXPERIMENT 3, respectively.

3.1.- EXPERIMENT 1.

3.1.1.- Animals.

134 mice, both males and females, two months old at the beginning of the experiments, were randomly assigned to 3 groups (Sham group, PV-Inhibition or PV-Activation, depending on the virus injected; see DREADDs section, below). No differences were found between sex unless otherwise specified (included as a co-variable in the statistical analysis). Mice were initially from the line 129P2-Pvalb$^{tm1(cre)Arbr}$/J (Jackson Laboratories, RRID: IMSR_JAX:008069) but bred and housed in the centre facilities. They were housed in groups of 3-5, with 12-12 h light/dark cycle, lights on at 8:00, at 23 ± 2°C of temperature and free access to food and water. Mice strain is known as PV-Cre line, and express CRE recombinase under the control of the parvalbumin promotor. For the behavioural experiments, the light/dark cycle was progressively inverted. All the experiments were following Spanish law (53/2013) and European regulations (EU Directive 2010/63/EU) and were approved by the CSIC ethical committee.

Due to several reasons described below, in its correspondent section, some animals were finally removed from the groups giving a total number of mice of 122, males (n=75) and females (n=47).

3.1.2.- DREADDs, Designer Receptors Exclusively Activated by Designer Drugs.

To modulate the hilar PV interneuron activity in the PV-cre mice we used cre-dependent adeno-associated viral vectors (AAVs) containing DREADDS (UNC Gene Therapy Vector Core, University of North Caroline, North Caroline, USA), injected intracerebrally in the dentate gyrus (see Surgery for injecting AAVs section, below), so that DREADDs were expressed in the hilar PV cells. The specificity on the hilar PV cells was confirmed histologically (Figure 3.1). A batch of mice were operated but no injected with viral vectors, forming the Sham operated group.

DREADDs allow us to modulate specifically the infected population of neurons, in our case the hilar PV interneurons. This method bases on the mutation of a G protein couple receptor, activated by an exogenous agonist, Clozapine-N-Oxide (CNO, ref: BML-NS105-0025, ENZO Life Science Inc., New York, USA), which otherwise is inert[36]. This very same mutated G protein coupled receptor cannot be activated by the usual endogenous ligand, acetylcholine[36,271]. So that, by expressing DREADDs in the PV interneurons of the hilus we have the tool to modulate specifically their activity after the injection of CNO (1 mg/kg, i.p.). This effect takes around 25 minutes to get the peak and is sustained for several hours *in vivo*[29,34,35].

They are different subtypes of DREADDs depending on the kind of mutated G protein receptor, and so the inner signal transduction cascade the CNO activates. In between all the options we selected DREADDs AAV5-hSyn-DIO-**hM3D(Gq)**-mCherry, to activate PV interneurons, or AAV5-hSyn-DIO-**hM4D(Gi)**-mCherry, to inhibit them. hM3D(Gq) nomenclature means that is a mutated receptor originally coming from the **h**uman **M**uscarinic receptor type **3**, mutated to become **D**READD, coupled to **Gq** Protein. Same logic applies to hM4D(Gi): **h**uman **M**uscarinic receptor type **4**, **D**READD, coupled to **Gi** protein. Thanks to its respective G-Protein type coupled hM3D(Gq) DREADD leads to neuronal excitation while hM4D(Gi) leads to neuronal inhibition[29,271].

A batch of mice was infected in the hilus with AAV5-hSyn-DIO-**hM3D(Gq)**-mCherry, forming the **PV-Activation** group, and other group was infected with AAV5-hSyn-DIO-**hM4D(Gi)**-mCherry, forming the **PV-Inhibition group**. The remaining mice were equally operated but did not received viral infusion, forming the Sham-operated group (controls).

3.1.3.- Surgery for injecting AAVs.

Two months old mice were anaesthetized with isofluorane (Laboratorios Esteve, Murcia, Spain) 4%, 0.8 L/min oxygen for induction, and then fixed in a stereotaxic set up (David Kopf Instruments, California, USA) over a heating pad at 37°C. Isofluorane was kept at 1-2%, 0.8 L/min oxygen, for maintenance. After opening the skin, we did a 700 µm Ø trepan in the skull with a milling cutter (Ref: FST 19007-07, Finest Science Tools, FST, Heidelberg, Germany) attached to a cordless micro drill (Ref: 58610V, Stoelting Co., Illinois, USA). Coordinates for the injections, from Bregma, were -2 mm AP, ±1.4 mm LM, +2 mm DV (Keith and Paxinos, 2008). Then we gently introduced a micropipette (Ref: 4878, World Precision Instruments, WPI, London, UK) through the trepan, into the brain. Micropipette was filled with mineral oil and viral vectors containing DREADDs (see above). Oil and DREADDS were separated with 1 µl of air. Micropipette was attached to a pump infusion Nanoliter 2010 Injector (WPI) coupled to the stereotaxic frame and was previously pulled in a P-2000 puller (Sutter Instruments

Company, California, USA). We placed the tip of the micropipette in the hilus and very gently injected 0'5 µl of DREADD viral vectors per hemisphere. Once done, we waited 10 minutes before elevate the micropipette 200 µm up and waited for others 10 minutes before very gently removing totally the micropipette. The correct anatomical infection in the hilus was confirmed histologically (Figure 3.1C).

After closing the skin with silk thread we administered subcutaneously analgesic, Buprenorphine (Dechra Veterinaria Products SLU, Barcelona, Spain), and antibiotic, Syvaquinol (Laboratorios Syva S.A.U., León, Spain), to the mice and we controlled their recovery (3 weeks). We checked their welfare especially during three days after the surgery and we injected analgesic if necessary until their full recovery. All the clothes, smells, noise, gloves and rooms used for this surgery were controlled and were as different as possible than the ones used for the normal handling and especially during the behavioural experiments. Light/dark cycle was progressively inverted after this point for the behavioural experiments.
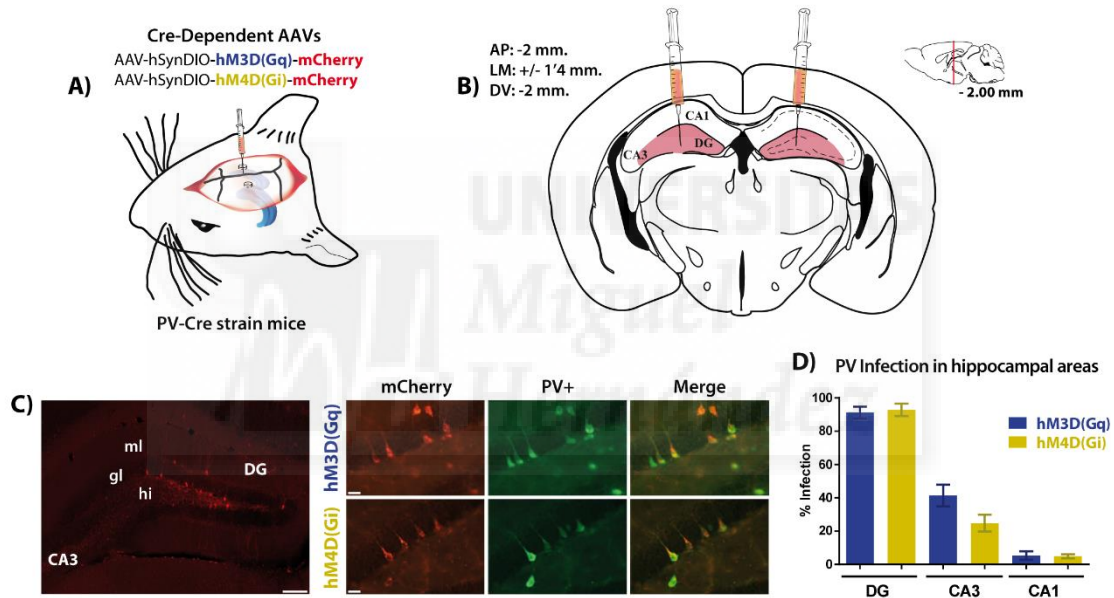
Figure 3.1. AAVs injection surgery and infection on the hilar PV interneurons. A) Schematic representation of the bilateral dentate gyrus infection with cre-dependent viral vector used in PV-cre mice strain. B) Schematic representation of the infection on the coronal section, coordinates respect bregma. C) Confirming micro pictures of the infected area (left, 10x, scalebar=100 µm) and of the infection's specificity over the PV interneurons in both groups (right, 40x, scalebar=25 µm). mCherry labels AAVs infection, green is Alexa 488 secondary antibody labelling PV cells after inmunohistochemistry. D) Quantification of the infection percentage per hippocampal area.

3.1.4.- Behaviour.

Mice carried out the behavioural task one month after the surgery. As general consideration for all the behavioural experiments, the CNO injections were made sequentially (13 minutes of difference between each animal) to respect the timing for entering into the arena. Also, we took care of injecting the animals in other room, as different as possible that the one in which we carried out the behaviour, with different gloves and the body covered with a white wrapper. It was done to avoid stress during the behavioural experiments. Behaviour was carried out with the priceless help of Elena Pérez Montoyo, as part of her master thesis work.

Novel Location of the Object task (NLO).

After animal's habituation to the experimenter and the experimental room, mice were introduced into an empty arena (50x50x30 cm) with spatial cues in the walls (Figure 3.2A-B), softly illuminated (luxes: 23 in the centre, ± 2 in the corners), and were free to explore during 2 trials of 5 minutes each. Initial control parameters about movement, locomotion, thigmotaxis and exploratory behaviour were analysed during the habituation, and we checked that the animals were actually habituated at the end of those trials. 24 h later we introduced two identical objects in opposite corners (13'5 cm away from the walls) that the animals were free to explore until they reach 20 seconds of exploration between both, or until they spend 10 minutes as total time in the arena[272]. This session is called the familiarization phase, and it is related to the encoding of new contextual information of the objects and its location. 24 h after the encoding we displaced one of the objects to a new location (another corner, 13'5 cm away from the walls and 15 cm away from the other object) and we again tested the animals, with the same criteria. It is called the test-24h phase. If the animals remember were the object was, they tend to explore more the object in the new location. We set the time that the animals explore the object in the new location divided by the total time of exploration of both objects as exploration index of the mice spatial memory. The distance between object was specially selected to be challenging for the mice to realize the movement of the objects[64] so that the task is dentate gyrus dependent[66]. Animals were introduced in the arena so that its initial distance with respect to the objects was equal. Objects and arena were cleaned with 70% ethanol in between animals to avoid odour tracks.

By repeating this protocol, but changing the temporal moment of the CNO injection, we could modulate the PV interneurons activity during the encoding, during the consolidation or during the retrieval of the contextual memory, as well as in control conditions (injecting saline) (Figure 3.2A-B). To modulate hilar PV interneuron activity during the encoding we injected CNO 90 minutes before the animal entered in the arena for the familiarization phase —so CNO modulates hilar PV interneurons during the encoding of contextual information regarding the object and its location—. One week later we repeated the experiment with the same animals but injecting saline (0'9%) instead of CNO; so animals were control of themselves. To modulate the PV interneuron activity during the consolidation first we let the animals to explore the objects during the familiarization phase, and 10 minutes after its encoding we injected CNO. Finally, to modulate hilar PV interneurons during the retrieval of the memory we let the animals to encode and consolidate normally, and we injected CNO 90 minutes before the mice entered in the arena for the test-24h session.

Animals that underwent the task while modulating the PV interneurons during the encoding and in control condition were the same batch (n=39), 1 week between experiments, but using different objects —their locations were counterbalanced—. Animals for consolidation (n=42) and retrieval modulation (n=41) experiments formed other batches but they were littermates and under the same conditions.

Animals with less than 8 seconds of exploration, between both objects, were removed of the analysis, as exclusion criteria, due to lack of exploration —to avoid bias in the exploration index ratio—. Before starting with the experiments we carried out some pilot studies to set the behavioural conditions and to confirm that all the settings were correct in our hands (data not shown). We confirmed specially that 15 cm of distance between objects was enough for the animal to discriminate the movement, in line with the bibliography[64,66].

Exploration was considered when the animal was facing the object and actively touching or sniffing the object. This criterion is more restricted than the normally used (2 cm). Performance was videotaped and data extraction for objects exploration was done manually. The experimenter was blind to the experimental conditions. The results were contrasted between two members of the lab and no differences were found in the objects exploration preference.

Elevated plus maze (EPM).

To avoid anxiety interferences in our interpretations, the animals that carried out the NLO modulating the retrieval also underwent the Elevated Plus Maze task (n=41; Sham, PV-Inhibition and PV-Activation groups, Figure 3.2C). After they ended the NLO task, still under CNO effects, they were carried to the adjacent room, in where they were introduced gently in the centre of an elevated and cross-shaped arena. Two of the arms had walls (closed arms), and the other two had not (open arms). They were videotaped for 5 minutes, and its performance tracked with commercial software (Smart Video Tracking Software, Panlab, Barcelona, Spain). Then we compared the time that the animal spent in the open arms vs in the closed arms as index of the anxiety[273,274]. We also checked for other parameters as the number of entrances in each arm and distance travelled.
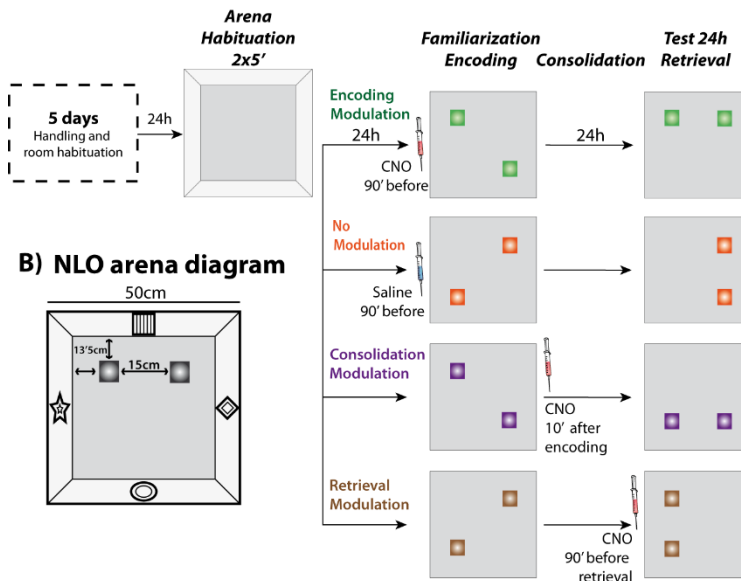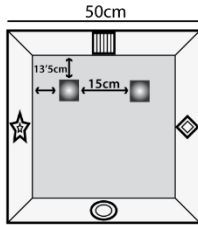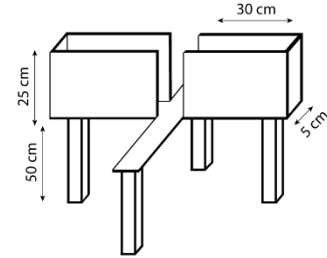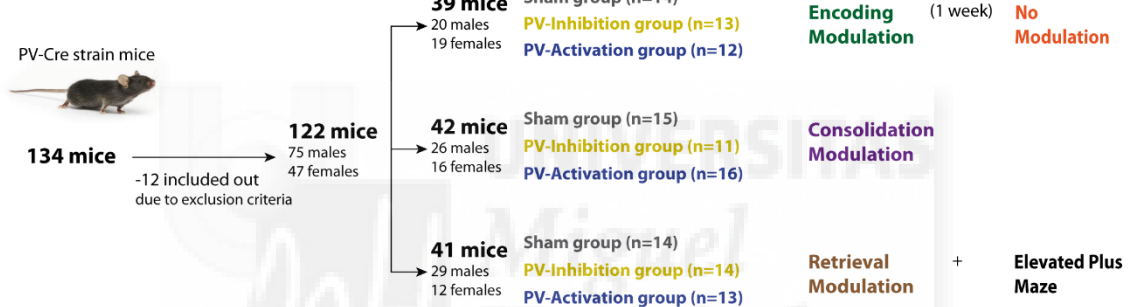
Figure 3.2. Behavioural tasks and mice used for contextual learning studies and anxiety. A) schema of the protocols implemented for studying the hilar PV interneuron modulation on encoding, consolidation and retrieval, or in control condition, by changing the CNO injection temporally or injecting saline. B) Schematic representation of the arena used for the NLO experiments. C) drawing of the Elevated Plus Maze used to evaluate anxiety. D) Diagram of the mice used for the behavioural experiments.

After behaviour tests, mice were divided to underwent either *in vivo* electrophysiology or fMRI experiments.

3.1.5.- *In vivo* electrophysiology.

Surgery for in vivo electrophysiology.

Mice were anaesthetized with urethane (1.4 g/kg, i.p.; Sigma Aldrich, Madrid, Spain). Some preliminary experiments (n=25) were done to set stimulating protocols and the best urethane dose, which is not trivial in mice, prior to the proper experiments (data not shown). The most suitable dose for the strain used was 1.4 g/kg with 1/5 of reinforcement if necessary 90 min after the first injection. After checking the lack of reflexes in mice, animals were placed and fixed in a stereotaxic frame (Narishigue, Tokyo, Japan). The skin of the head was cut, the scalp and the periosteum were separated and we did three 1'8 mm Ø trepan in the skull with a

milling cutter (Ref: FST 18004-18, FST, Heidelberg, Germany) attached to a cordless micro drill (Stoelting Co.) in the same coordinates used to introduce the electrodes (shown below). Then we introduced one bipolar stimulating electrode (10-15 kΩ, 325 μm Ø, WPI, ref. TM53CCNON) in perforant pathway (from bregma, in mm: -4.3 AP, +2.5 ML, +1.4 DV, 12° angle), and two recording probes (single shank, 50 μm contact spacing, 32 channels; NeuroNexus Technologies, Michigan, USA) were targeted to the prefrontal cortex (from bregma, in mm: +2 AP, +0.2 ML, +2.5 DV) and hippocampus (from bregma, in mm: -2 AP, +1.5 ML, -2 DV), including CA1 and dentate gyrus regions. Recording and stimulating electrodes were implanted following stereotaxic standard procedures and optimized based on the online recording to have the best quality of the signal in the dentate gyrus, CA1 and prefrontal cortex, taking into account specially the typical evoked potential in dentate gyrus[275] (Figure 3.3A-C). An Ag/AgCl wire (WPI) was placed in contact with the skin and used as a ground. The position of the electrodes was further confirmed *post mortem* thanks to the prior immersion in DiI-ethanol solution of recording electrodes.

Stimulating protocols and recordings.

The stimulating electrode was connected to a pulse generator and current source (STG2004, Multichannel Systems, Reutlingen, Germany) controlled by MC_Stimulus software (Multichannel System). Electrophysiological data from the recording probes were filtered (0.1-3 kHz), amplified and digitalized (20-32 kHz sampling rate, depending on the recording protocol itself) and analysed off-line using the Spike2 software (Cambridge Electronic, Cambridge, UK) or MatLab (The MathWorks Inc., Natick, MA, USA). For evaluating the Excitatory Post-Synaptic Potential (EPSP) we measured the maximum slope of the evoked potential in molecular layer (for dentate gyrus) or *stratum radiatum* (for CA1). And as reflex of the Population Spike (PS) we measured the amplitude of the spike recorded in hilus (for dentate gyrus) or in pyramidal layer (for CA1) (Figure 3.3C).

All electrophysiological protocols (Figure 3.3D-I, table 1) were recorded in the same animals before and after CNO injection. Also, after recording the post-CNO protocols, we induced LTP using standard theta burst stimulation in perforant pathway[276], consistent on five trains of pulses (100 Hz, lasting 30 ms) at 150 ms interval, and repeated three times in 1 minute. 30 and 60 minutes after LTP induction we recorded again spontaneous activity, subthreshold evoked potentials and an Input-Output curve. Then the animal was perfused and the brain extracted for histology (see histology section, below).
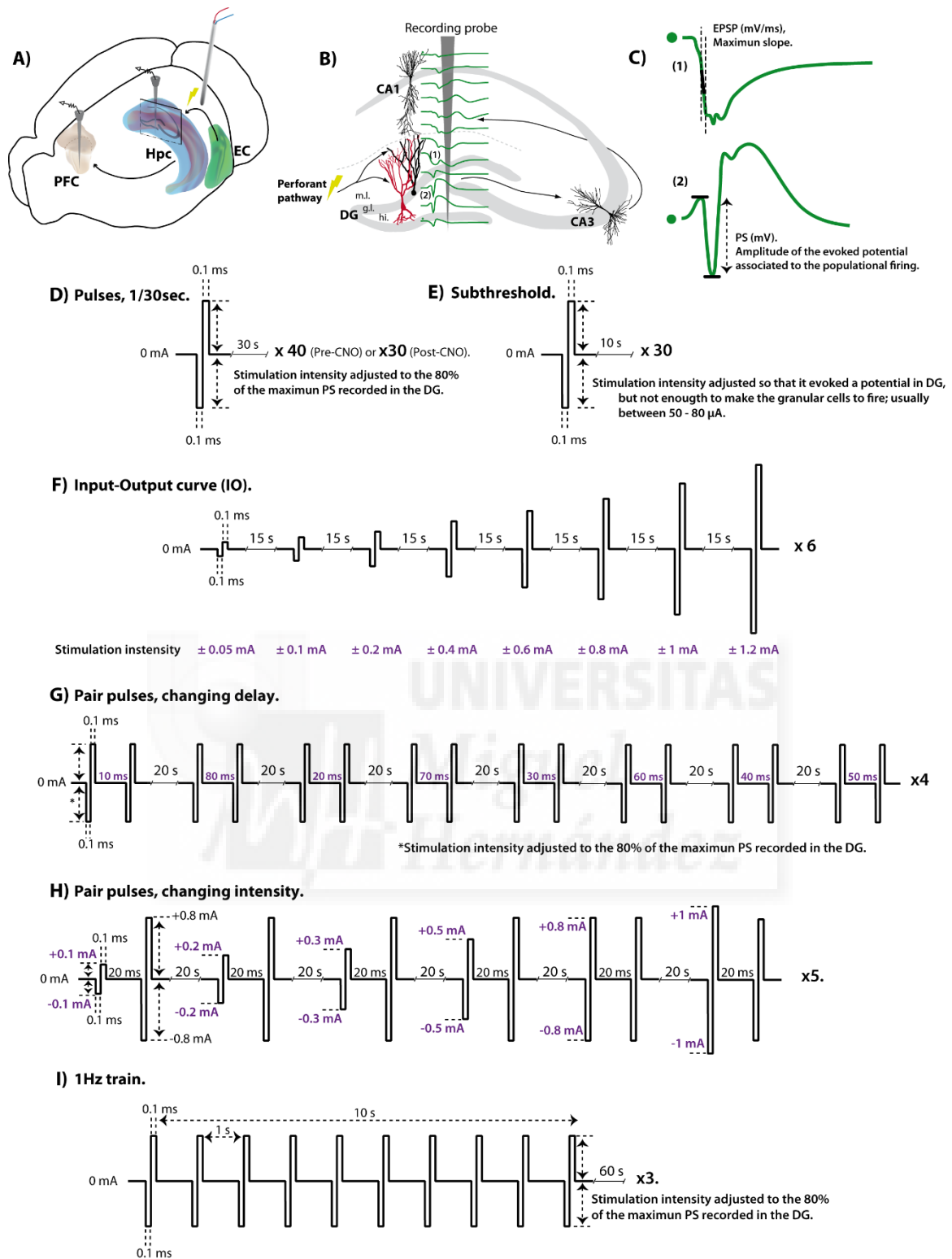
Figure 3.3. *In vivo* **electrophysiological recordings and stimulation protocols.** A) Scheme of the electrodes position for *in vivo* electrophysiological recordings. PFC: prefrontal cortex; Hpc: Hippocampus; EC: entorhinal cortex. B) Drawing of the recording probe placed in hippocampus and dentate gyrus (DG) and CA1 with over-imposed evoked LFPs recordings, together with a scheme of the trisynaptic circuit, involving DG, CA3, and CA1. Numbers indicate the example EPSP evoked potential in the anatomical region where the specific channel of the probe is (1), and the same for the PS (2). C) Waveform of EPSP (1) and PS (2) evoked potentials, indicating the parameter extracted from each one of them as reflect of dendritic currents generated in molecular layer (EPSP), measured as the maximum slope, and as reflect of granule cells population firing, measured as the amplitude of the population spike (PS). D-I) Schematic representation of the protocols applied in perforant pathway before and after CNO injection. Order of application specified in Table 1.

Table 1. **Temporal order for *in vivo* electrophysiology stimulation protocols.** Organized in columns: first the stimulating protocols Pre-CNO (left column), then Post-CNO (middle column) and finally Post-LTP induction (right column). Grey columns' numbers indicate the duration; white columns contain the protocols names. Empty spaces indicate resting time in between stimulation protocols.

Pre-CNO		Post-CNO		Post-LTP	
30'	Tissue resting.	15'	Pulses, 1/30sec.	30'	
20'	Pulses, 1/30sec.	5'	Continuous recording.	5'	Continuous recording.
5'	Continuous recording	15'	Pulses, 1/30sec.	5'	Subthreshold.
5'	Subthreshold.	5'	Continuous recording.	10'	Input-Output curve.
10'	Input-Output curve.	15'	Pulses, 1/30sec.	10'	
1'		5'	Continuous recording.	5'	Continuous recording.
12'	Pair pulses, changing delay.	5'	Subthreshold.	5'	Subthreshold.
1'		10'	Input-Output curve.	10'	Input-Output curve.
12'	Pair pulses, changing intensity.	1'			
1'		12'	Pair pulses, changing delay.		
3'	1Hz train stimulation.	1'			
1'		12'	Pair pulses, changing intensity.		
5'	Continuous recording.	1'			
	CNO injection (1mg/kg, i.p.)	3'	1Hz train stimulation.		
		1'			
		5'	Continuous recording.		
			LTP INDUCTION.		

3.1.6.- Functional Magnetic Resonance Imaging.

Surgery for fMRI experiments.

For the fMRI experiments mice were also anaesthetized with 1.4 g/kg of urethane, and after confirming the lack of reflexed, they were fixed in a stereotaxic frame (Narishigue). The skin of the head was cut, the scalp and the periosteum were separated, and we did two 1'8 mm Ø trepan in the skull with a milling cutter (ref: 18004-18, FST) attached to a cordless microdrill (Stoelting Co.). Blood cleaning is fundamental for this procedure, due that the presence of iron may disturb magnetic signals[277]. We cleaned the mice's skull with oxygenated water before opening the trepans, and we always cleaned as much as possible any blood track during the surgery. One of the trepans was in the skull above the hippocampus (coordinates from bregma are -2 AP, +1.5 ML, -2 DV) and the other above the perforant pathway (with coordinates for the electrode implantation, in mm from bregma: -4.3 AP, +2.5 ML, +1.4 DV, -12° angle).

We introduced one recording probe (same as the one used for electrophysiology: single shank, 50 µm contact spacing, 32 channels; NeuroNexus Technologies) targeted to the hippocampus, allowing us to record evoked potentials in the dentate gyrus, to facilitate the optimization of the stimulation point in the perforant pathway with the stimulating electrode.

To make the stimulation compatible with fMRI, we used custom made carbon fibres electrodes as described elsewhere[278,279] for rats, and optimized for mice as part of this work, which is not trivial for fMRI experiments[277]. Briefly, individual 7 µm diameter carbon fibres (Goodfellow Cambridge Limited, Cambridge, UK) were bundled and introduced into a pulled double borosilicate capillary (WPI, ref. TST150-6") with $\simeq$ 200µm tip diameter and electrical impedance of 40-65 kΩ. Tip was bent in a flame to form a 90º angle to minimize the distance between the head of the animal and the magnetic resonance imaging array coil once implanted. A regular wire connector was couple to the pipette, linked to the carbon fibres

using silver conductive epoxy resin (ref: 186-3616, RS components, Madrid, Spain) and isolated with rapid epoxy resin (Araldite, Basel, Switzerland).

The electrode was placed in the perforant pathway (Figure 3.4A) and the optimization was guided by the evoked potential recorded in dentate gyrus. Once optimized, we removed gently the recording electrode and the carbon fibre electrode was secured to the skull with super-bond C&B dental cement (Sun Medical Co. LTD, Moriyana, Shiga, Japan). We also placed an intraperitoneal cannula (1'5 m long) to inject CNO later on, from outside of the fMRI apparatus. Then the animals were carried to the fMRI facilities in the centre, where they were placed in a custom made animal holder with adjustable bite and ear bars and positioned into the horizontal 7-T scanner (Biospec 70/30, Bruker Medical, Ettlingen, Germany). Animals were constantly supplied with 0.8 L/min O_2 through a mask and temperature were controlled between 36.5 and 37.5 ºC with a water heat-pad.

fMRI data aquisition and stimulating protocols.

Functional images acquisition was performed in 12 coronal slices using a GE-EPI protocol applying the following parameters: field of view (FOV) 25x25 mm, slice thickness, 1 mm; matrix, 96x96; segments, 1; FA 60°; time echo (TE), 15 ms; time repetition (TR), 2000 ms. T_2-weigthed anatomical images were collected using a rapid acquisition relaxation enhanced sequence (RARE): FOV, 25x25 mm; 12 slices; slice thickness, 1mm; matrix, 192x192; TE_{eff}, 56 ms; TR, 2 s; RARE factor, 8. A 1H mouse brain received, only phased-array, coil with integrated combiner and preamplifier, and no tune/no match, was employed in combination with the actively detuned transmit-only resonator (Bruker BioSpin MRI GmbH, Germany).

fMRI data were analyzed offline using our lab own software developed in MatLab, which included Statistical Parametric Mapping packages (SPM8, www.fil.ion.ucl.ac.uk/spm). After linear detrending, temporal (0.015-0.2 Hz) and spatial filtering (3x3 gaussians kernel or 1.5 sigma) of voxel time series, a general linear model (GLM) was applied with two model shifted forward in time; hemo model for hippocampus Region of Interest (ROI) and fhemo model for the rest of the brain. This segregation responds to the differential hemodynamic response observed in hippocampus vs the rest of the brain in our anaesthetized mice, being the response in hippocampus slower than in the rest of the brain. Functional maps were generated from voxels that had a high significant component for the model ($p < 0.01$) and were clustered together in space.

Region of interests were extracted according with a mice atlas[280] overimposed on the functional maps, and were used to compute the volume of brain tissue activated in absolute terms (number of voxels actives above the statistical threshold in each ROI). ROIs included hippocampus, prefrontal cortex (prelimbic, infralimbic, orbitofrontal and cingular cortex), medial temporal lobe structures (entorhinal cortex, subiculum, presubiculum, pirirhinal cortex and ectorhinal cortex), subcortical structures (amygdala, basal nucleus and accumbens nucleus) and cortical areas (visual cortex, auditive cortex, sensory cortex, associative areas and motor cortex) (Figure 13). We calculated the number of active voxels before and after CNO injection (1 mg/kg, i.p.) when stimulating at 10 Hz or 20 Hz in the perforant pathway (4 sec. ON, 26 sec. OFF) (Figure 3.4B-D).

After acquiring all the required series for the fMRI study, animals were perfused and their brains extracted (see histology section, below).
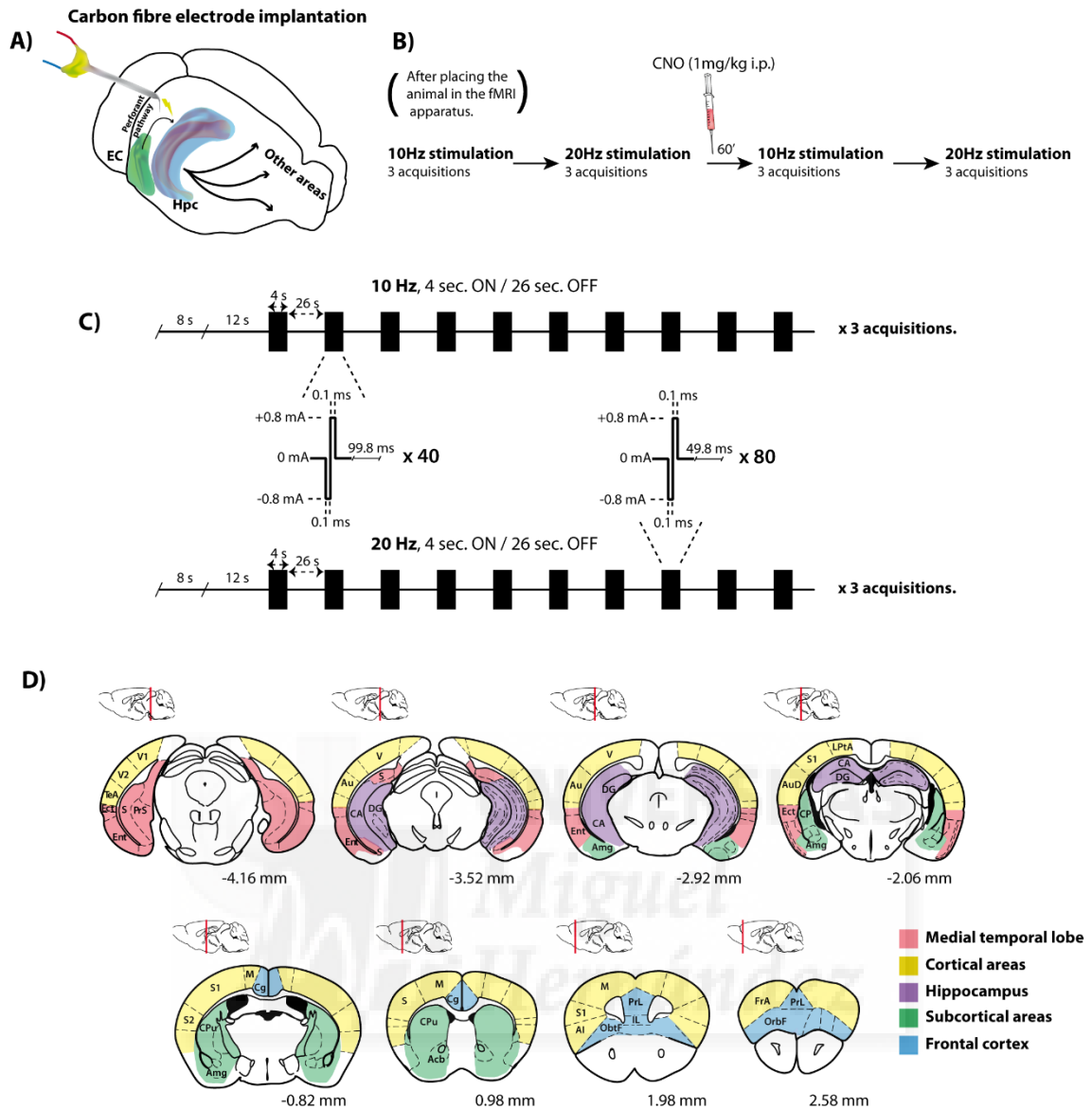
Figure 3.4. fMRI experiments preparation and ROIs. A) Schematic representation of carbon fibre implantation in the perforant pathway. B) Timeline of stimulation protocols in fMRI experiments. C) fMRI stimulating protocols representation at 10Hz and 20Hz, 4 sec. ON, 26 sec. OFF. D) Schemas of the ROIs used for fMRI data analysis. Active above the threshold voxels in each ROI were clustered in space and its number compared before and after CNO injection for each stimulating protocol. Medial temporal lobe included Ect, ectorhinal cortex; Ent, entorhinal cortex; PrS, presubículum; and S, subículum. Cortical areas included AI, agranular insular cortex; Au, auditory cortex; AuD, dorsal secondary auditory cortex; FrA, frontal association cortex; LPtA, lateral parietal association cortex; M, motor cortex; S1, primary sensory cortex, S2, secondary sensory cortex; TeA, temporal association cortex; V1, primary visual cortex and V2, secondary visual cortex. Hippocampus included DG, Dentate Gyrus; and CA, cornus ammonis. Subcortical areas included Amg, amygdala; CPu, caudo-putamen nucleus; and Acb, nucleus accumbens. Frontal cortex included Cg, cingulate cortex; IL, infralimbic cortex; PrL, prelimbic cortex; and OrbF, orbitofrontal cortex. Distances in mm with respect Bregma (Paxinos and Franklin, 2012)[280].

3.1.7.- Histology.

After the *in vivo* electrophysiology or the fMRI experiments the animal were perfused with 20 ml of room temperature saline (0'9%) and 50 ml of 4°C 4% paraformaldehyde (PFA; BDH prolabo, VWR chemicals, Lovaina, Belgium) to check the correct infection of the DREADDs and the position of the electrodes. Brains were extracted and kept in PFA 4% for at least 24h at 4°C and then cut in fixed material vibratome (VT 1000S, Leica, Wetzlar, Germany) in 80 μm slices. 6-8 slices containing hippocampus were selected and used for underwent a standard protocol for fluorescent immunohistochemistry against PV (primary antibody: mouse anti-PV, 1:5000, ref. 235, Swant, Switzerland; secondary antibody: Alexa 488 goat anti-mouse, 1:500, ref. A11029, Thermo Fisher Scientific, MA, USA). Slices were then mounted in slides with antifadding medium and covered for the posterior analysis under the microscope. We checked the anatomical accuracy of the infection by looking the expression of the DREADDs reporter mCherry, and the specificity over the PV neurons by checking the co-labeling of mCherry and PV immunohistochemical labelling. Animals with incorrect infection were removed from all the analysis.

3.1.8.- Statistic.

All the statistical data were analysed and plotted using GrahPad Prism 7 software (GraphPad Software Inc., La Jolla, CA, USA) or SPSS v20 software (IBM, New York, USA). First we did an exploratory analysis of the data to visually detect abnormalities as missing values, outliers, etc. in which skewness and kurtosis index were checked to be between -2 and +2 to be considered acceptable in order to be able to probe normality of the distribution[281]. All the data were then checked for the parametric-test requirements, including normality (D'Agostino-Pearson test and Shapiro-Wilk test) and homoscedasticity (F of Levene test). In case the data passed all the analysis to proceed with parametric statistic we applied two ways ANOVA, unless otherwise specified, due that we are working with factors *group*, with 3 levels (3 groups; Sham, PV-Inhibition and PV-Activation), and *time*, 2 levels (before and after CNO injection). We applied a Bonferroni *post hoc* analysis for multiple comparisons with alfa adjusted to Bonferroni. We also calculated partial *eta* square as $SS_{effect} / (SS_{effect} + SS_{error})$ for effect size of the ANOVA, and the power of the effect (1-β) using GPower software (University of Düsseldorf, Düsseldorf, Germany). Partial *eta* square (η_p^2) indicates the variance explained by the studied factor over the dependent variable after excluding variance explained by other predictors. It can be interpreted qualitatively as large if partial *eta* square > 0.13[282], although always taking into account the *n* of the group. If, by any reason, partial *eta* square could not be used, then we express the R squared indicator (r^2), being similar to *eta* square, but needing > 0.30 values for indicating large effects. On the other hand, the power effect (1-β) is an invert indicator of committing a type II error (accepting the null hypothesis while false).

Data were plotted using GraphPad Prism 7 software (GraphPad Software Inc.) and figures were created with Adobe Illustrator software (Adobe Systems Incorporated, San José, California, EEUU).

3.2.- EXPERIMENT 2.

3.2.1.- Animals.

29 animals, both males (n=16) and females (n=13), 2 months old at the beginning of the experiments, were randomly assigned to 4 groups: Sham (n=8), PV-Inhibition (n=9), PV-Activation (n=8) and home-cage group (n=4) (Figure 3.5). Groups were exactly the same than previously explained (in section 3.1, animals, above), with the addition of the home-cage group, that was composed by animals that did not performed the behavioural task (see section Behaviour, below). Mice were the same strain than previous experiment; originally from the line 129P2-Pvalb$^{tm1(cre)Arbr}$/J (Jackson Laboratories, RRID: IMSR_JAX:008069) but bred and housed in the centre facilities. They were housed in groups, with 12-12 h light/dark cycle, lights on at 8:00, at room temperature (23 ± 2 ºC) and free access to food and water. For the behavioural experiments the light/dark cycle was progressively inverted. All the experiments were in accordance with Spanish laws (53/2013) and European regulations (EU directive 2010/63/EU).

3.2.2.- DREADDs, Designer Receptors Exclusively Activated by Designer Drugs.

Exactly as explained above (section 3.1.2, DREADDs).

3.2.3.- Surgery for injecting AAVs.

Exactly as explained above (section 3.1.3, surgery for injecting AAVs).

3.2.4.- Behaviour.

One month after the surgery, mice performed the behavioural task. As in previous experiments, we were careful to take measures to avoid stress in the mice, as explained before. Avoiding stress was especially crucial in this experiment due that cFos labels neuron's activation, independently of its cause, and we wanted that cFos labelling were related only to the encoding of the spatial task; not to the anxiety after the CNO injection. It was controlled experimentally in the handling, but also we let 155 minutes between injection and brain extraction so that cFos related with the injection was mostly degraded. We also included the home-cage group —that received CNO injection, with the same timing, but did not carry out the behavioural task— as a negative control for the cFos expression. The injections of CNO (1 mg/kg, i.p.) were made sequentially in all the animals in order to respect the timing for entering in the arena and the brain extraction.

After the surgery recovery, mice got very well habituated to the handling and experimental room. Then Sham, PV-Inhibition and PV-Activation mice were introduced sequentially into an empty arena (50x50x30 cm) with spatial cues in the walls and softly illuminated (luxes: 23 in the centre ± 2 in the corners). Arena was the same that used for previous experiments. Mice were free to explore the empty arena during 2 trials of 5 minutes each. We checked that the animals were actually habituated to the arena at the end of those trials. 24h later we injected CNO (1 mg/kg, i.p) 90 minutes before animals were free to explore again the arena, in which we had introduced 2 identical objects in opposite corners (13'5 cm away from the walls; as in previous experiments) for 5 minutes. 60 minutes after, animals were carried to the perfusion room for brain extraction (see histology section, below). Home-cage group received CNO injection, but did not carry out behaviour (Figure 3.5), and their brain was extracted with the same timing, with respect their CNO injections, that for the rest of the groups. This way, home-cage group is a negative control that allow us to compare the effectivity of the behavioural task in inducing cFos expression.

We confirmed that all the animals had explored the objects at less 8 seconds. Animal with less exploration were removed of the analysis (n=3), as exclusion criteria to avoid bias in the cFos expression.
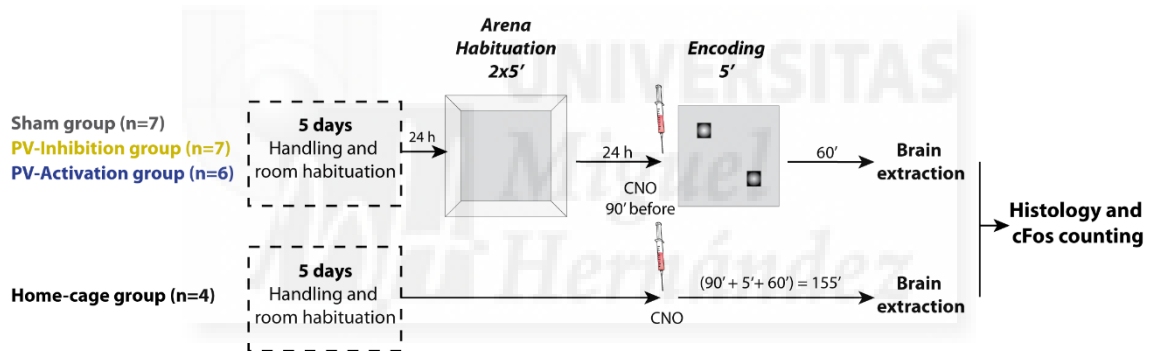
Figure 3.5. Time line of cFos experiments. Experimental groups (Sham, PV-Inhibition and PV-Activation) did the behavioral task while home-cage group did not. CNO injection timing was equal for all the groups with respect its brain extraction.

3.2.5.- Histology.

60 minutes after the mice ended the behavioural task, animals were deeply anaesthetized with pentobarbital (20 mg/ml, i.p.) (Ventoquinol E.V.S.A. laboratories, Madrid, Spain), perfused intracardially with 10 ml of saline (0'9%) and 50 ml of 4% of PFA (BDH prolabo, VWR chemicals) at 4°C. Brains were extracted and kept in PFA 4% for 24h at 4°C and then cut in fixed material vibratome (Leica) in 50 µm slices. 12-18 slices containing dorsal hippocampus were selected and used for underwent a standard protocol for immunohistochemistry against cFos (primary antibody: guinea pig anti-cFos, 1:400, ref. 226004, Synaptic Systems, Göttinger, Germany; secondary antibody: Alexa 488 donkey anti-guinea pig, 1:500, ref. 706-545-148, Jackson ImmunoResearch, Suffolk, United Kingdom). Slices were then mounted in slides with antifadding medium and covered for the posterior analysis under the microscope. We checked the anatomical accuracy of the infection by looking the expression of the virus reporter mCherry. Animals with incorrect infection were removed of the all the analysis (n=2).

cFos labelled cells were counted optically in 12-18 slices per brain with the priceless help of Raquel García Hernández, as part of her master thesis work. Counting was carried out by two trained researchers, in blind for the experimental condition, in granular layer of dentate gyrus, and pyramidal layer in CA3 and CA1, for the 4 groups, in both hemispheres, using a fluorescence microscope (model DM4000B, Leica). Also, Raquel Hernández did another automatic counting in parallel with the help of Imaris software (Bitplane AG, Rucih, Switzerland) to confirm the counting using two methods (data not shown). First, images were taken with the aid of the fluorescence microscope previously named coupled to Neurolucida software (MicroBrightField Inc., Wetzlar, Germany) at 20x/0.50 dry objective, with the same acquisition setting for all the animals. Those images were taken from 4 representative slides per animal, in every group. Then the number of neurons labelled was estimated using an automatic spot-detection algorithm integrated in the Imaris 7.0.0 software. Also, Imaris software allowed the analysis of the intensity of the labelling of each hippocampal and dentate gyrus neuron from the mentioned slices.

Optical counting of the number of neurons per slice were averaged by animal, and then by group, to avoid an overestimation of the *n* for the statistical analysis. However, when scoring the intensity of the labelling each neuron has a different value, so we considered each neuron as an individual for the population. And the values were averaged directly per group. Intensity values were extracted from random samples in each group: 51 cells in DG, and 85 cells in CA3 for Sham group; 67 cells in DG and 104 cells in CA3 for PV-Inhibition group; and 96 cells in DG and 106 in CA3 from PV-Activation group.

3.2.6.- Statistics.

After preliminary analysis of the data, as explained in section 3.1.8 (statistic), we applied an unpaired *t*-test between home-cage and Sham group to test whether or not the behavioural task induces cFos expression in the hippocampus in normal conditions. Once confirmed, to test how modulating the hilar PV interneurons affects to the cFos expression we applied a one-way ANOVA test between Sham, PV-Inhibition and PV-Activation groups. For some analysis, specified in the results, we did a non-parametric Kruskall-Wallis test instead of the ANOVA because some data failed the normality test (Shapiro-Wilk, $p < 0.05$, and kurtosis value < 2). We applied a Tukey *post hoc* analysis after the ANOVA, or Dunn's test after the Kruskall-Wallis, with alpha adjusted with Bonferroni. We also calculated partial eta square as $SS_{effect} / (SS_{effect} + SS_{error})$, for effect size, and the power of the effect $(1-\beta)$. For intensity labelling analysis each neuron was consider an individual for the total *n*. Neurons for analysing intensity were extracted from 2 randomize sliced per group.

3.3.- EXPERIMENT 3

3.3.1.- Animals.

75 PV-Cre strain mice (same than previous experiments), both females (n=28) and males (n=47) were used for this sets of studies. No differences between sex unless otherwise specified. Animals were housed in groups, with 12-12 h light/dark cycle, lights on at 8:00, at room temperature (23 ± 2 ºC) and free access to food and water. For the behavioural experiments the light/dark cycle was progressively inverted. All the experiments were in accordance with Spanish law (53/2013) and European regulations (EU directive 2010/63 EU). Mice were subdivided into 3 different batch, for different experiments:

1.- 21 mice were used to evaluate the normal performance of non-operated mice in the task. 4 of them were excluded of the analysis according with the same criteria applied before (lack of exploratory behaviour) or due to unexpected events during the behavioural sessions in the animal house facilities. These animal correspond to the "control experiment" (see behavioural protocol, below).

2.- 44 mice were injected with AAV containing DREADDs in the hilus and then randomly assigned into 3 groups: Sham (n=15), PV-Inhibition group (n=14) and PV-Activation group (n=15). 2 mice of each group were finally removed by virtue of the same exclusion criteria than before or due to incorrect infection in hilar region (confirmed afterwards with histology). These animals correspond to the "DREADDs hilar PV interneurons modulation experiment" (see behavioural protocol, below)

3.- 10 mice were injected with AAV5-hSyn-DIO-hM4D(Gi)-mCherry in the hilus and then used in the behavioural task with and without PV interneurons inhibition —being controls of themselves—. 2 mice were extracted for the analysis due to the same exclusion criteria. These mice performed the behavioural task as the groups in 2, but the first movement of the object was displaced 10 cm. instead of 5 cm (see behavioural protocol, below). These animals correspond to the "Hilar PV cell inhibition experiment, with 10 cm of displace".

Besides another batch of 20 mice was previously used in two pilot studies to set the experimental conditions for the behavioural task (data not shown).

3.3.2.- DREADDs, Designer Receptors Exclusively Activated by Designer Drugs.

Exactly as explained above (section 3.1.2, DREADDs).

3.3.3.- Surgery for injecting AAVs.

Exactly as explained above (section 3.1.3, surgery for injecting AAVs).

3.3.4.- Behavioural task.

Behavioural protocol and arena were developed to assess pattern-separation associated with the recognition of novel object locations in the environment. The rational is to assess whether memories are generalized (pattern separation lost) as a consequence if inhibitory manipulation in the dentate gyrus. We call it SETAmaze, for Spatial Evaluation Task, and alluding to its mushroom shape ("seta" in Spanish) of the maze.

Arena.

Behavioural arena (Figure 3.6A) consists in a semi-circular white methacrylate box (Aries, Alicante, Spain; 70 cm Ø, walls 40 cm) and, in the middle of the straight wall, an inter-trial entering box (10x10x15cm), separated from the semi-circular area by a manually elevated door, which allow the animal to go in or out from one section of the task to the other. Interior of the arena was sanded to avoid lux reflection. Walls was entirely coated in black with vinyl (AsVinilo, Madrid, Spain) on the outside to avoid differential illumination (luxes inside the box were 14 ± 1'5). In the inside part of the walls, we placed spatial cues. The arena was also elevated 2 cm, with rubber feet, from the table in which it was for the behavioural experiments. This elevation allowed us to place magnets below the arena ground in the exact point in which we put the objects inside the semi-circular arena. Objects also had a magnet at the bottom (orientated so that it felt attraction to the magnet placed below the ground). This way objects were easy to move and, more importantly, were placed in the same point for all the animals, maintaining the same distances in each moving. Magnets in the bottom were embedded in a custom made piece with the 3D printer (MakerBot Replicator tm2, Desktop 3D printer, New York, USA), that enter in a hole in the bottom of the objects, and were fixed with epoxy resin (Araldite), dried to avoid smells. Epoxy was sanded to enclose the magnet-in-the-object to the magnet-below-the-ground as much as possible. Objects were at 10 cm from the walls. The semi-circular shape allowed us to maintain them equidistant from the wall, to control thigmotaxis, and from the initial point where the mouse enter in the arena —to avoid preferences for any object based on the distance, or the perceived size of the object, instead of spontaneous attraction for one or other object in the task—. Also, the mice, during the habituation sessions, were trained to walk from one chamber to the other by their own will, which is an advantage over other behavioural tasks that force the entering by placing the animal in one specific point in the arena (usually carrying them by the tail).

Behavioural protocols.

Behavioural tasks with the SETAmaze (Figure 3.6B-E) were divided in three protocols, corresponding with the animal groups explicited in section 3.3.1 (Figure 3.7F).

Control experiments.

After one week of habituation to the handling and the experimental room, mice were then allowed to enter in the custom-made behavioural arena, empty of objects, for five sessions. Each session consisted of 5 minutes in the semi-circular piece and 1 minute in the inter-trial

entering box (Figure 3.6D-E). Animals started in the entering box. 24h later we repeated the habituation with another five sessions. The goal of the habituation is that the animals get familiar with the arena and learn that they could go in and out from one chamber to the other only when the door that connects both is open.

24 h after the second habituation session, we introduced two identical objects in the semi-circular piece 10 cm away from the walls, 10 cm away one from the other, placed in a straight line with the entrance point of the mice, 25 cm away from the entering point. The animals were free to explore both during 5 minutes. Then the door that connects both chambers was opened, and animals returned to the inter-trial box for 1 minute. During that minute one of the objects (counterbalanced) was displaced 5 cm away from the other, in arc respect to the entrance and maintaining the 10 cm respect to the wall. Then the door was opened again, and the animals were free to explore both objects again. This process was repeated four times until the object was displaced 20 cm away from the starting point. The idea is that, by changing little by little the position of the object, we can evaluate the distance at which the animals realize the movement of the object, as evidence of the recognition of a new spatial pattern (confronting the previous memory of the spatial distribution of objects in the arena with the new distribution). We set the exploration time of the moved object relative to the total time of exploration of both objects, as an index of contextual discrimination.

For the half of the animals (n=8) the object was moved from the centre of the arena to the corner, and for the other half (n=9) the object was displaced from the corner to the centre, to avoid a possible bias introduced by the corner. Left-right object movement was counterbalanced.

DREADDs hilar PV interneurons modulation experiment.

All the steps were equal than before until the second habituation session (included). For this experiment, we used AAV injected mice with DREADD expressed in hilar PV interneurons and Sham operated animals.

24 h after the last session of habituation, experimental mice were injected with CNO (1 mg/kg, i.p.), and 90 minutes later they were put inside the entering box of the SETAmaze to enter in the semi-circular arena, in where we had put the two identical objects. Once the door was open and the animal entered, they encoded the object's new spatial information. Animals were free to explore for 5 minutes. Then the animals were taken out from the arena and returned to their home-cage. This way PV interneurons activity were modulated only during the encoding of the starting position of the objects. 24 later mice entered again in the SETAmaze, but the initial position of one of the object was displaced 5 cm further away from the other. Then the task continued as usual —5 minutes of exploration in the semi-circular arena, 1 minute in the inter-trial box while the object was displaced other 5 cm and so on—. This process was repeated three times, 5 cm of displacement until the object was 20 cm away from the starting point (3 times x 5 cm = 15 cm + 5 initial cm = 20 cm).

The idea is that we could evaluate the long-term spatial memory encoded under CNO modulation on hilar PV interneurons, and its interactions with a short-term memory task involving spatial pattern separation by measuring the distance at which the animals realize the movement of the object.

Hilar PV cell inhibition experiment, with 10 cm of displace.

All the steps were equal than before until the second habituation session (included). For this experiment, we used AAV injected mice with hSyn-DIO-**hM4D(Gi)**-mCherry DREADD expressed in hilar PV interneurons (only for inhibition). Same animals did the task with and without CNO injection.

24 h after the second session of habituation, animals were injected with CNO (1 mg/kg, i.p.), and 90 minutes later they were put inside the entering box of the SETAmaze to explore the two identical objects we had introduced in the same starting position than before. Animals were free to explore both during 5 minutes. Then the animals were taking off and returned to their home-cages. 24 h later mice were put back in the entering box for performing the rest of the test trials. The objects were displaced 10 cm directly from the initial position (instead of 5 as in the previous experiment) and then moved from 5 cm in 5 cm, to a maximum distance of 20 cm from the position they had encoded under hilar PV inhibition. One week later, we repeated the task with the same animals, with other objects (its movement was counterbalanced), and injecting saline instead of CNO.
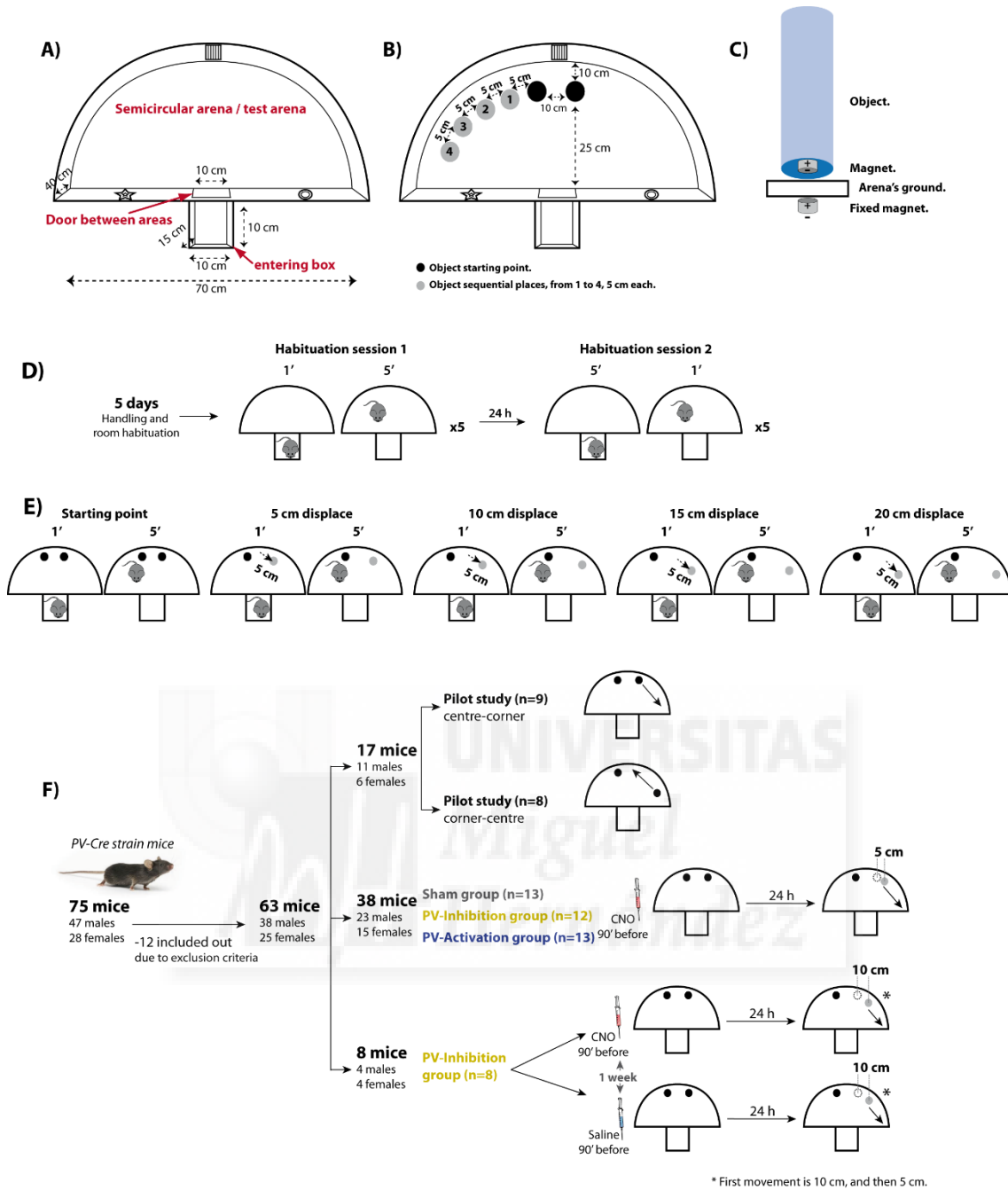
Figure 3.6. SETAmaze experiments. A) Schematic representation of the SETAmaze arena. B) Schematic representation of the starting position of the objects (black rounds), distance to each other, to the walls, to the mice's entrance, and the distance of object's sequential movements during the test (grey rounds). C) Illustration of the position of the magnets to ensure objects' sites. Fixed magnets were placed below the ground in the exact position where the objects are placed during the test. D) Diagrams to illustrate the habituation sessions. E) Diagrams to illustrate test trials. F) Scheme of mice used for the SETAmaze experiments, its assignment, and the test variations that each one of the group carried out after its habituation to the maze.

3.3.5.- Statistics.

All the statistical data were analysed and plotted using GrahPad Prism 7 software (GraphPad Software Inc.) or SPSS v20 software (IBM). First we did an exploratory analysis of the data to visually detect abnormalities as missing values, outliers, etc. Skewness and kurtosis index were checked to be between -2 and +2 to be considered acceptable for parametric comparisons[281]. All the data were then checked for the parametric-test requirements, including normality (D'Agostino-Pearson test and Shapiro-Wilk test) and homoscedasticity (F of Levene test). In case the data passed all the analysis to proceed with parametric statistic we applied a two ways ANOVA analysis.

The reasons for choosing this statistic were:

1.- Control experiment. We compared the exploratory index or the total exploration time (as dependent variable) of the factor group (2 levels: those mice that underwent the test with the object being moved from the centre to the corner, and those that did it being the movement from the corner to the centre), and the factor position of the object (5 levels: starting position, and 5, 10, 15 or 20 cm of object's displacement).

2.- DREADDs hilar PV interneurons modulation experiment. We compared exploratory index or total exploration time of the factor group (3 levels: Sham, PV-Inhibition or PV-Activation) with the factor position of the object (5 levels: starting position, and 5, 10, 15 or 20 cm of displacement).

3.- DREADDs hilar PV interneurons only inhibition experiment, with 10 cm of displace. We compared the exploratory index or total exploration time for the factor position of the object (4 levels: starting point, and 10, 15 or 20 cm of displacement) in the same animals but in two different moments (1 week of difference; with CNO or saline injection).

We applied multiple comparison Bonferroni *post-hoc* analysis, in case of statistical differences, with alfa adjusted to Bonferroni. We also calculated partial eta square as SS_{effect} / (SS_{effect} +SS_{error}) for effect size of the ANOVA and the power of the effect ($1-\beta$) using GPower software (University of Düsseldorf). Data were plotted using GraphPad Prism 7 software (GraphPad Software Inc.) and figures were created with Adobe Illustrator software (Adobe Systems Incorporated).

V.- RESULTS.

5.1 Electrophysiology.

5.1.1- Dentate gyrus electrophysiology.

Evoked potentials.

EPSP remains equal in all the groups after hilar PVbc modulation.

After perforant pathway stimulation (Figure 5.1A), LFPs recorded in the molecular layer of the ipsilateral dentate gyrus revealed the EPSP, an extracellular population readout of the synaptic activity. EPSP slope is maximal in the mid-molecular layer of the dentate gyrus, corresponding with the termination field of the medial perforant pathway, and increased with the stimulation intensity. This response, known as input-output curve, was not affected by any of the experimental manipulations (Figure 5.1B); nor in the Sham [$F_{7,40}$ = 0.56, p = 0.78], nor in the PV-Inhibition [$F_{7,40}$ = 0.21, p = 0.98], nor in the PV-Activation group [$F_{7,40}$ = 0.03, p = 0.99]; in any intensity applied (Figure 5.1C-D). This result is not surprising based on the PV basket cells (PVbc) cells connections, which innervate perisomatically their targets, so that the dendrites should be, and are, functionally intact. However, it needs to be demonstrated and has important implications in conjunction with other data presented herein. The no-changes in the EPSP slope reflect equal dendritic integration in dentate gyrus granule cells before/after CNO injection, in all the groups equally.

Figure 5.1. Evoked synaptic responses in dentate gyrus after hilar PV+ cells modulation. A) Schematic representation of the recording and stimulation sites during the Input-Output protocol. EC = entorhinal cortex; Hpc = Hippocampus; PFC = prefrontal cortex. B) Schematic representation of the recording probe placed in the hippocampus and dentate gyrus with over-imposed evoked potential after perforant pathway stimulation (in green). PV cells are marked in red. The point indicates the channel extracted for evaluating EPSP slope. C) Representative waveforms of the EPSP recorded in molecular layer in the dentate gyrus, before (in black) and after (in colour) PV interneurons modulation with CNO injection (1 mg/kg, i.p.). Scalebars indicates 1 ms and 1 mV. D) Quantification of the deepest slope of the EPSP in the Input-Output curve protocol. Sham n = 6, PV-Inhibition n = 6, PV-Activation group n = 6.

In addition to previous data showing that the synaptic response is intact after hilar PV cell modulation, synapses may be potentiated in all the groups equally, as the EPSP slope increases 60 minutes after LTP induction (Figure 5.2). EPSP in Sham group increases [$F_{7,40}$ = 5.34, p = 0.0002, η_p^2 = 0.32, 1-β = 0.96] in an Input-Output curve at 0.2 mA stimulation intensity [t_{40} = 4.06, p = 0.0018], 0.4 mA [t_{40} = 5.06, p < 0.0001], 0.6 mA [t_{40} = 6.34, p < 0.0001], 0.8 mA [t_{40} = 6.45, p < 0.0001], 1 mA: [t_{40} = 5.8, p < 0.0001] and 1.2 mA [t_{40} = 5.43, p < 0.0001]. In PV-Inhibition group EPSP also increases after LTP [$F_{7,40}$ = 32.46 p < 0.0001, η_p^2 = 0.45, 1-β = 1], at 0.4 mA [t_{40} = 9.16, p < 0.0001], 0.6 mA [t_{40} = 13.44, p < 0.0001], 0.8 mA [t_{40} = 13.18, p < 0.0001], 1 mA: [t_{40} = 12.69, p < 0.0001] and 1.2 mA [t_{40} = 12.9, p < 0.0001]. Also EPSP increases in PV-Activation after LTP induction [$F_{7,40}$ = 36.2 p < 0.0001, η_p^2 = 0.46, 1-β = 1], at 0.2 mA [t_{40} = 6.54, p < 0.0001], 0.4 mA [t_{40} = 11.52, p < 0.0001], 0.6 mA [t_{40} = 14.52, p < 0.0001], 0.8 mA [t_{40} = 14.95, p < 0.0001], 1 mA [t_{40} = 15.57, p < 0.0001] and 1.2 mA [t_{40} = 14.92, p < 0.0001]. We also evaluated the EPSP 30 minutes after LTP inductions obtaining the same results (data not shown for simplicity). These data indicate that the synapses become equally potentiated by LTP in all the groups. Overall these results –perhaps not surprisingly, but importantly– suggest that modulating soma-targeting basket cells make the dendritic function to remain preserved.

Dentate gyrus EPSP after LTP induction, post-CNO injection.
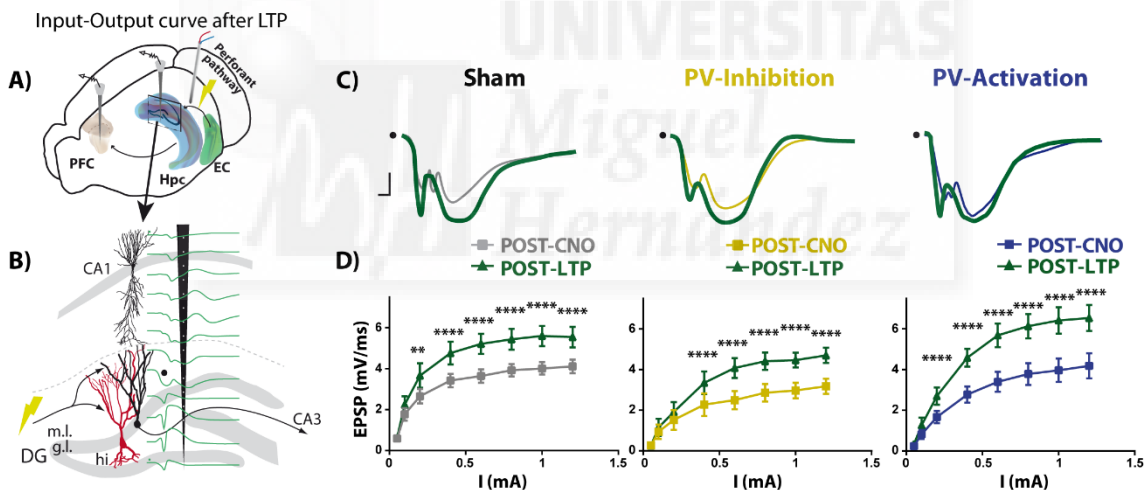
Figure 5.2. EPSP evoked potential in dentate gyrus after LTP induction, post-CNO injection. A) Schematic representation of the recording and stimulation sites during the Input-Output protocol applied 60 min after LTP induction. EC = entorhinal cortex; Hpc = hippocampus; PFC = prefrontal cortex. B) Schematic representation of the recording probe placed in the hippocampus and dentate gyrus with over-imposed evoked potential after perforant pathway stimulation (in green). PV cells are marked in red. Point indicates the channel extracted for evaluating EPSP slope. C) Representative waveforms of the EPSP recorded in the molecular layer in dentate gyrus after CNO injection (in colour; grey, yellow or blue, depending on the group) and 60 minutes after LTP induction (in green). Scalebars indicates 1 ms and 1 mV. D) Quantification of the EPSP maximum slope in response to perforant pathway Input-Output stimulation protocol 60 minutes after LTP induction. ** = 0.003, **** < 0.0001. Sham n = 6, PV-Inhibition n = 6, PV-Activation group n = 6.

The population spike (PS) in dentate gyrus reflects the coordinated firing of dentate gyrus granule cells, evoked by the perforant pathway stimulation in our experimental conditions (Figure 5.3A-B). As for the EPSP, the PS spike amplitude increases with stimulation intensity and is not affected by CNO injection in Sham group [$F_{7,40}$ = 1.58, p = 0.18] (Figure 5.3C-D). However, PV-Inhibition group increases dentate gyrus PS after CNO injection [$F_{7,40}$ = 3.97, p = 0.002, η_p^2 = 0.29, 1-β = 0.99] (Figure 5.3C-D). This increase is significant from low stimulation intensities in the Input-Output curve protocol, even at 0.2 mA [t_{40} = 5.75, p < 0.0001], and qualitatively become almost saturated soon, presenting a kind of *plateau* in its graphical progression (Figure 5.3D) at 0.4 mA [t_{40} = 5.72, p < 0.0001], 0.6 mA [t_{40} = 4.44, p = 0.0005], 0.8 mA [t_{40} = 3.98, p = 0.0022], 1mA [t_{40} = 2.89, p = 0.04] and 1.2 mA [t_{40} = 3.04, p = 0.03]. On the other hand, PV-Activation group shows decreased PS amplitude after CNO injection [$F_{7,40}$ = 4.81, p = 0.0005, η_p^2 = 0.31, 1-β = 1], those differences are evidenced at higher intensities than 0.6 mA [t_{40} = 4.28, p = 0.0009], 0.8mA [t_{40} = 5.29, p < 0.0001], 1mA [t_{40} = 4.84, p = 0.0002] and 1.2 mA [t_{40} = 4.60, p = 0.0003] (Figure 5.3C-D).

We also measured the latency at which PS appears. It does not change before and after CNO injection in Sham group [$F_{4,25}$ = 1.93, p = 0.13], nor in the PV-Activation group [$F_{4,25}$ = 0.37, p = 0.82]. However, the PS latency in PV-Inhibition group decrease around 0.5 ms after CNO injection when we inhibit the PVbc interneurons [$F_{4,25}$ = 50.65, p < 0.0001, η_p^2 = 0.4, 1-β = 1], being evident at 0.4 mA stimulation intensity [t_{25} = 3.84, p = 0.0037], 0.6 mA [t_{25} = 4.22, p = 0.0015], and 0.8 mA [t_{25} = 2.92, p = 0.03], having tendency at 1 mA [t_{25} = 2.56, p = 0.08] and 1.2 mA [t_{25} = 2.4, p = 0.12]. Only the stimulation intensities that evoked reliable PS before and after CNO injection were taken for the analysis of the latency (> 0.4 mA).

Taken together these data indicate that by decreasing PVbc perisomatic inhibition, granule cells firing is facilitated. It increases the amplitude of PS evoked potentials and decreases its latency. On the contrary, increasing the PVbc perisomatic inhibition impairs granule cells firing, as evidenced by the depression of PS amplitude. The comparably smaller effect of PV cell inhibition vs excitation (smaller effect of PS amplitude and no effect on latency) probably reflects the already high basal inhibitory tone in the DG. CNO injection, alone, does not induce any observable change in our conditions.
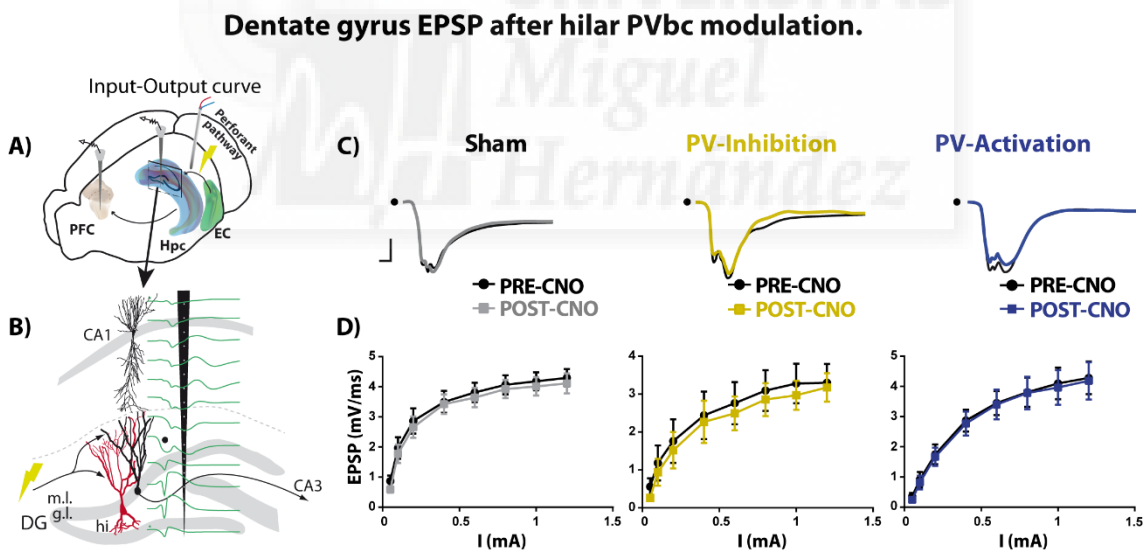
Granule cell PS after hilar PVbc modulation.
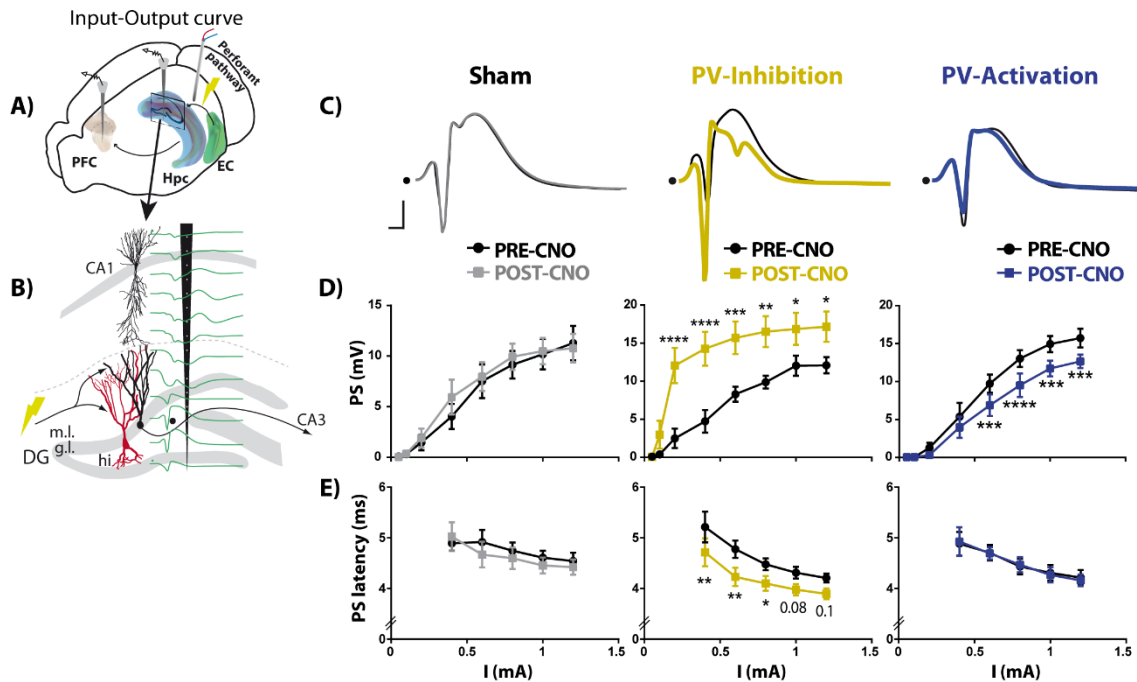
Figure 5.3. PS evoked potential in the dentate gyrus after PV cells modulation. A) Schematic representation of the recording and stimulation sites during the Input-Output protocol applied. EC = entorhinal cortex; HPC = hippocampus, PFC = prefrontal cortex. B) Schematic representation of the recording probe site with over-imposed evoked potential after perforant pathway stimulation (in green). Point indicates the channel extracted for evaluating PS amplitude. C) Representative waveforms of the PS recorded in hilus before (in black) and after CNO injection (in colour). Scalebars indicates 2 ms and 4 mV. D) Quantification of the PS amplitude before and after CNO injection. E) Quantification of the PS latency of the data in D, only reliable PS evoked intensities before and after CNO injection were taken for its analysis. * < 0.05, ** <0.01, *** < 0.001, **** < 0.0001. Sham n = 6, PV-Inhibition n = 6, PV-Activation group n = 6.

Differential effects of PS amplitude after LTP, post-PVbc modulation.

LTP induction in Sham group increases the PS [$F_{7,40}$ = 5.55, p = 0.0002, η_p^2 = 0.33, 1-β = 0.99] at 0.1 mA stimulation intensity [t_{40} = 3.09, p = 0.02], 0.2 mA [t_{40} = 5.76, p = 0.0001] and 0.4 mA [t_{40} = 4.65, p = 0.0003], until it becomes saturated compared with PS amplitude recorded before LTP induction (Figure 5.4C-D, left). Nevertheless, in the PV-inhibition group, LTP induction is not able to further increase the PS amplitude, which appears to saturate at low stimulation intensities as a consequence of perisomatic desinhibition (Figure 5.4C-D, middle) [$F_{7,40}$ = 0.99, p = 0.45]. On the other hand, PS amplitude increases in the PV-Activation group, even if we previously increase the PVbc perisomatic tone over granule cells [$F_{7,40}$ = 2.82, p = 0.017, η_p^2 = 0.24, 1-β = 0.87], although it has less statistical power, likely reflecting the increased difficulty of granule cells firing. It was observed at 0.2 mA stimulation intensity [t_{40} = 3.5, p = 0.009] and 0.4 mA [t_{40} = 2.9, p = 0.04] (Figure 5.4C-D, right).

LTP induction also reduced PS latency in the Sham group [$F_{4,25}$ = 647.6, p < 0.0001, η_p^2 = 0.48, 1-β = 0.99] in all the stimulation intensities studied; 0.4 mA [t_{25} = 14.35, p < 0.0001], 0.6 mA [t_{25} = 11.74, p < 0.0001], 0.8 mA [t_{25} = 11.39, p < 0.0001], 1 mA: [t_{25} = 9.71, p < 0.0001] and 1.2 mA [t_{25} = 9.7, p < 0.0001]; in the PV-inhibition group [$F_{4,25}$ = 106.6, p < 0.0001, η_p^2 = 0.45, 1-β = 0.99], also in all the stimulation intensities studied; 0.4 mA [t_{25} = 5.52, p < 0.0001], 0.6 mA [t_{25} = 3.85, p = 0.0034], 0.8 mA [t_{25} = 3.53, p < 0.008], 1 mA: [t_{25} = 3.09, p = 0.025] and a tendency at

1.2 mA [t_{25} = 2.77, p = 0.056]; and in PV-Activation group [$F_{4,25}$ = 224, p < 0.0001, η_p^2 = 0.47, 1-β = 0.99], also at 0.4 mA [t_{25} = 8.52, p < 0.0001], 0.6 mA [t_{25} = 7.75, p < 0.0001], 0.8 mA [t_{25} = 6.69, p < 0.0001], 1mA [t_{25} = 5.49, p < 0.0001] and 1.2 mA [t_{25} = 4.99, p = 0.0002] (Figure 5.4E). Only those intensities that evoked a reliable PS before and after LTP were taken into account.

Taking together these data indicate that LTP induction increase granule cells PS in control and PV-Activation group, but not in PV-Inhibition group, in which the PS is saturated when decreasing the perisomatic inhibition of the PV cells. LTP also decreases firing latency, whether it increases in amplitude or not, pointing to the regulation of firing latency as another consequence of the LTP induction. Interestingly, it does so in a less evident manner in the PV-inhibition group, in which PS delay was already a bit reduced (Figure 5.4E, middle), pointing to the inhibitory tone as a critical factor to regulate the PS latency as well.

Granule cells PS after LTP induction, post-CNO injection.
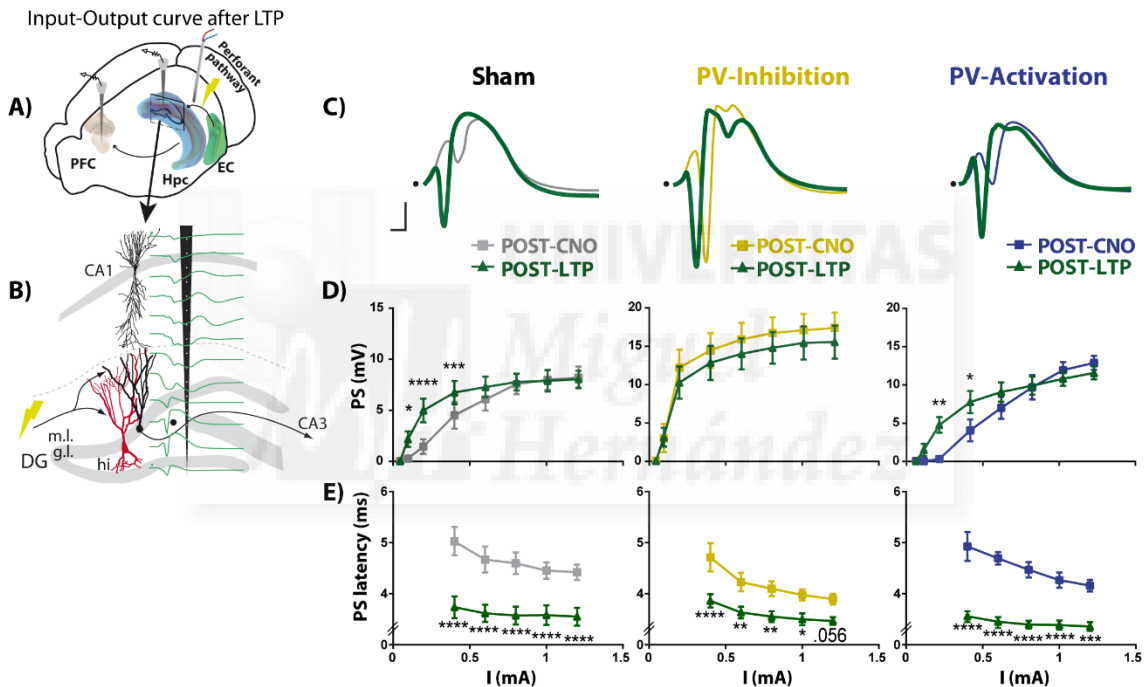
Figure 5.4. PS evoked potential in the dentate gyrus after LTP induction, post-CNO injection. A) Schematic representation of the recording and stimulation sites during the Input-Output protocol applied. EC = entorhinal cortex; Hpc = hippocampus, PFC = prefrontal cortex. B) Schematic representation of the recording probe placed in hippocampus and dentate gyrus with over-imposed evoked potential after perforant pathway stimulation (in green). Point indicates the channel extracted for evaluating PS amplitude. C) Representative waveforms of the PS recorded in hilus after CNO injection (1 mg/kg, i.p.), before LTP (in colour; grey yellow or blue, depending on the group) and after LTP (in dark green). Scalebars indicates 2 ms and 4 mV. D) Graphical quantification of the PS amplitude before and after LTP induction following the same colour code. E) Graphical quantification of the PS latency of the same data in D. Only reliable PS evoked intensities were taken for its analysis. * < 0.05, ** <0.01, *** < 0.001, **** < 0.0001. Sham n = 6, PV-Inhibition n = 6, PV-Activation group n = 6.

Briefly, pair pulses in a delay-change protocol consists on the application of two consecutive stimulations within a range of temporal intervals between them (10-80 ms). It is regularly used to study feedback inhibition, because the application of the first pulse, or conditioning pulse, elicits a first population spike (PS1) which activates feedback inhibition mediated by $GABA_A$ heteroreceptors and $GABA_B$ autoreceptors (the latter, due to their presynaptic location, causes dis-inhibition over the granule cells targets as explained in section 1.5.2). When the second pulse is applied 20-40 ms after PS1, the amplitude of the PS2 is largely reduced due to the $GABA_A$ mediated inhibition. However, if the second pulse is applied > 60 ms after PS1, it elicits a larger PS2 than PS1, because of $GABA_B$ heteroreceptor dis-inhibit the targets[258] (Figure 5.5A).

In Sham group, nor PS1 [$F_{7,40}$ = 0.63, p = 0.72], neither PS2 [$F_{7,40}$ = 2.14, p = 0.07] change before and after CNO injection (Figure 5.5B, left).

Regarding PV-Inhibition group, inhibition of PV cells leads to an increased PS1 when comparing before-after CNO injection [$F_{7,40}$ = 132.1, p < 0.0001, η_p^2 = 0.45, 1-β = 0.99], but surprisingly there is no differences in the kinetic of the PS2 before and after CNO injection [$F_{7,40}$ = 1.41, p = 0.22] (Figure 5.5B, middle). PS2 amplitude does not increase due to $GABA_B$ disinhibition either. It could be due to a saturation of the granule cell PS after PVbc inhibition, or to decreased $GABA_B$ autoreceptor activity. To address that point we re-adjusted the stimulation intensity so that PS1 amplitude postCNO was equal to PS1 pre-CNO in four animals (Figure 5.5C). Results indicate a clear reduction of $GABA_B$ mediated dis-inhibition [$F_{7,24}$ = 229.4, p < 0.0001, η_p^2 = 0.48, 1-β = 1] after 40 ms [t_{24} = 12.72, p < 0.0001], 50 ms [t_{24} = 28.6, p < 0.0001], 60 ms [t_{24} = 32.46, p < 0.0001], 70 ms [t_{24} = 32.11, p < 0.0001] and 80 ms [t_{24} = 26.36, p < 0.0001].

On the other hand, the PV-Activation group shows a reduced PS1 amplitude post-CNO compared with pre-CNO [$F_{7,40}$ = 305.4, p < 0.0001, η_p^2 = 0.46, 1-β = 0.99], but PS2 is also reduced [$F_{7,40}$ = 47.04, p < 0.0001, η_p^2 = 0.35, 1-β = 0.99], but only after 50 ms [t_{40} = 4.31, p = 0.0008], 60 ms [t_{40} = 3.75, p = 0.0044], 70 ms [t_{40} = 5.68, p < 0.0001] and 80 ms [t_{40} = 6.26, p < 0.0001] (Figure 5.5B, right), again at latencies that point to $GABA_B$ inhibition regulation, although this reduction may reflect a diminished granule cells activity as well.

Dentate gyrus PS during pair pulses inhibition stimulation protocol 10-80 ms.
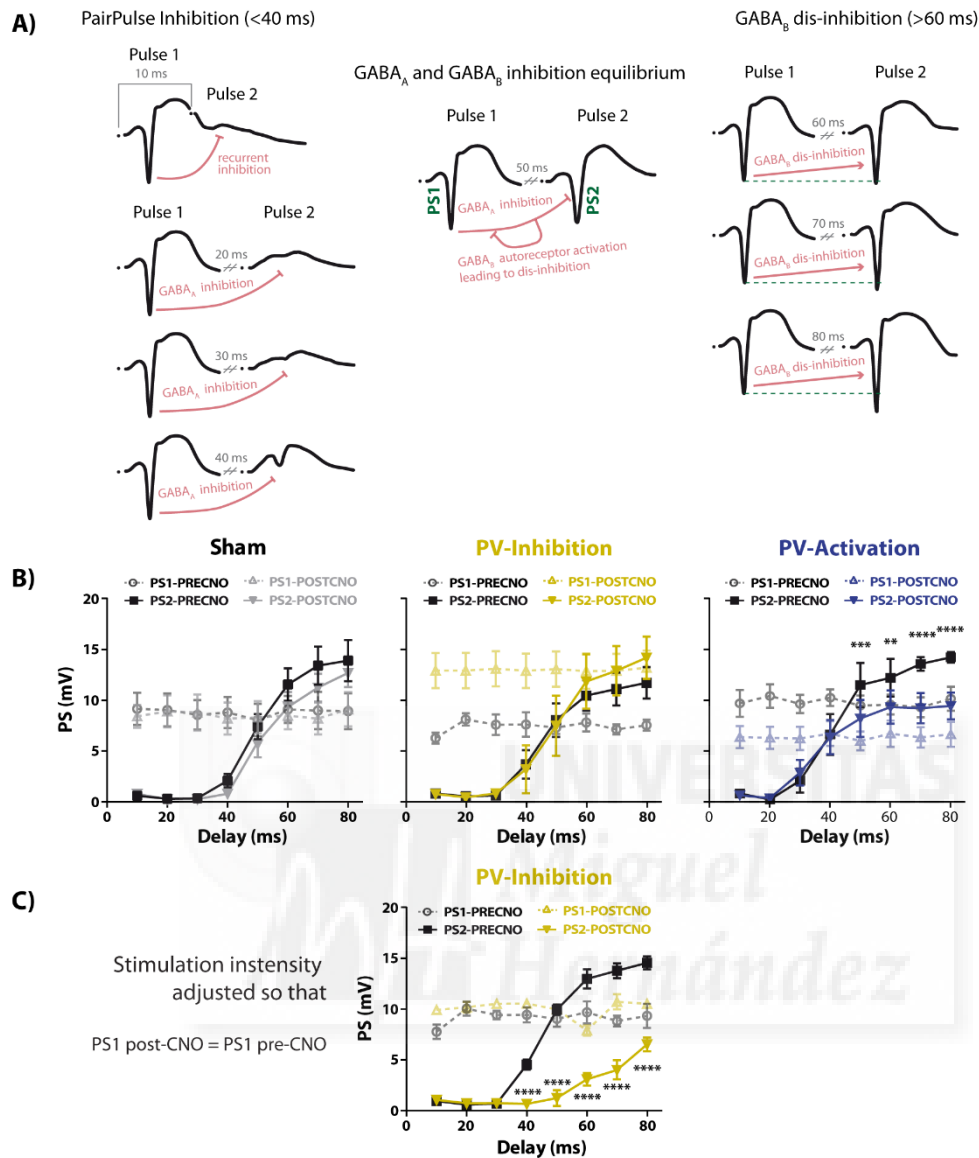
Figure 5.5. Dentate gyrus PS during pair-pulses stimulation protocol, with delay change, before and after CNO. A) Waveform examples of a typical evoked potentials in our pair-pulses protocol, from 10 to 80 ms of interval between pulses, extracted from Sham group. PS extracted form same recording channels than in Figures 4.3 and 4.4. B) Quantifications of PS amplitude, per group. Sham n=4, PV-Inhibition n=6, PV-Activation n=6. Discontinuous traces indicate first pulses PS amplitude. C) Quantification of PS amplitude of PV-Inhibition group (n=4) when adjusting stimulation so that PS1 pre and post-CNO were equal. All the represented statistic is made comparing PS2 before and after CNO injection. ** <0.01, *** < 0.001, **** < 0.0001.

To summarize: PSs in Sham group does not change with the CNO injection and evokes the typical response expected when applying the pair-pulses protocol. Regarding experimental groups, one problem we found is that there were variations in amplitude on PS1 before and after CNO injection, which may condition the PS2 changes. Some animals of PV-Inhibition group even evidenced multiple spikes eventually. They were no more than two but sufficient to affect direct interpretations of the analysis of this pair pulse protocol. It might mask the feedback inhibition-related changes in PS2, leading us to putative miss-interpretations. Nevertheless, the analysis allows us to discard feedback GABA$_A$ mediated inhibition changes in

our results when modulating PV interneurons —based on the virtually 0 mV PS in all the groups before 40 ms inter-pulses latency—. After 50 ms (GABA$_B$ dis-inhibition latencies), PS2 PV-Inhibition group shows no differences before-after CNO injection (Figure 5.5B), when applying same stimulation intensity. However, if we reduce the stimulation intensity to adjust PS1 at equal amplitude (pre- and post-CNO), then PS2 is reduced after CNO injection (Figure 5.5C). PV-Activation group PS2 decreases in amplitude after CNO injection. It could reflect diminished GABA$_B$ function or decreased *per se* PS because PV interneurons activation impairs granule cells firing.

Evoked potentials after Pair Pulse stimulation with varying intensities.

Briefly, pair pulses changing intensity protocol consists on the application of two consecutive electrical pulses with fixed temporal delay (20 ms, in the peak of the GABA$_A$ mediated inhibition) and fixed stimulation intensity of the second pulse (0.8 mA), but varying the intensity of the first pulse (ranging 0.1-1 mA) (Figure 5.6A). If the conditioning pulse does not evoke a PS in the first response (low intensities, 0.1 mA), it potentiates the second PS due to a calcium accumulation mechanism in the presynaptic terminal. However, if the conditioning pulse evokes a PS1, then feedback inhibition through GABA$_A$ receptor will depress the PS2. So that PS1 blocks the PS2, by virtue to GABA$_A$ feedback inhibition. By regulating first pulse intensity, and recording the variations of PS2 we can study presynaptic facilitation induced by calcium accumulation or feedback inhibition mediated by GABA$_A$ (Figure 5.6B).

Application of this protocol doesn't change PS2 in Sham group before vs after CNO injection [$F_{5,24}$ = 1.61, p = 0.19]. However, PS2 in PV-Inhibition group does change [$F_{5,30}$ = 5.19, p = 0.0015, η_p^2 = 0.31, 1-β = 0.98] being higher post-CNO when we apply 0.1 mA in pulse 1 [t_{30} = 3.37, p = 0.012] and lower at 0.2 mA [t_{30} = 3.79, p = 0.0049]. PS2 in PV-Activation also present differences pre- and post-CNO [$F_{5,30}$ = 12.4, p < 0.0001, η_p^2 = 0.40, 1-β = 0.99]. This differences are evident in the same stimulation intensities than PV-Inhibition group (0.1 mA, 0.2 mA) but inversely; PS2 in PV-Activation group at 0.1 mA decreases postCNO [t_{30} = 5.99, p < 0.0001] and increases at 0.2 mA [t_{30} = 4.78, p = 0.0003] (Figure 5.6C). EPSP does not change, again, in any group (Sham [$F_{5,24}$ = 0.57, p = 0.71], PV-Inhibition [$F_{5,30}$ = 1.45, p = 0.23] and PV-Activation [$F_{5,30}$ = 0.39, p = 0.84]) (Figure 5.6D).

Dentate gyrus PS and EPSP during pair pulses inhibition stimulation with intensity change.
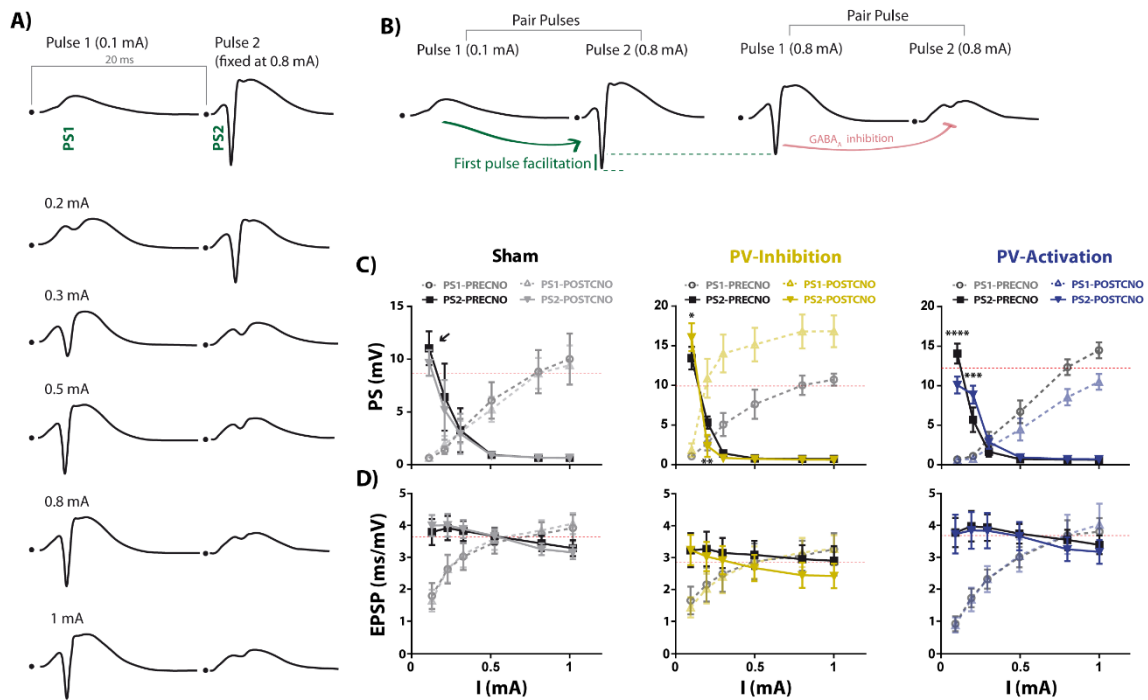
Figure 5.6. Dentate gyrus evoked potentials during pair-pulses stimulation protocol, changing stimulation intensity, before and after CNO. A) Representative waveform of the evoked potentials during pair pulses protocol, changing intensity and fixed interval between pulses. Extracted from Sham group. PS analysed for the same channel than in figures 5.3 and 5.4. B) Representative waveform showing the expected first pulse facilitation of the second PS (left, in green) and GABA$_A$ mediated feedback inhibition of the second spike, after PS1 (right, in red). C) Graphical quantifications of PS1 (discontinuous lines) and PS2 (continuous lines), before and after CNO injection, per group. Statistical analysis was made, and is represented, comparing PS2 before (in black) and after (in colour) CNO injection. Arrow indicate the point in which first pulse facilitation is evidenced in Sham group. D) Same than C, but representing EPSP. * < 0.05, ** <0.01, *** < 0.001, **** < 0.0001. Sham n = 5, PV-Inhibition n = 6, PV-Activation group n = 6. Discontinuous red line indicates the value obtained at 0.8 mA intensity with single pulse stimulation.

Contrasts between PS1 before and after CNO injection graphically show no differences in Sham group, while PS1 is highly increased in PV-Inhibition group and decreased in PV-Activation group after CNO injection (Figure 5.6C). Statistic not shown for simplicity, to avoid redundancy (it confirms the previously explained results in section 5.1.1) and to not to distract from the main point of this section; the comparison of the evoked response motivated by the second pulse.

Taking together the data indicate that the EPSP does not change in any group (Figure 5.6D). PS2 in Sham group does not change either, and it presents the expected first pulse facilitation and GABA$_A$ feedback inhibition. This GABA$_A$ inhibition is also evident in the experimental groups after PS1 appears, before and after CNO injection, without differences. Nevertheless, the pair pulse facilitation in the experimental groups, before first stimulating pulse evoke PS does change after CNO injection. First pulse increases in PV-Inhibition group, and decreases in PV-Activation group. The second pulse decreases in PV-Inhibition group, and increases in PV-Activation group. These significant differences may reflect a differential PS2 modulation by increased or decreased PS1 (depending on the group), more than a direct effect of PV interneurons over the pair pulse facilitation. PS1 modulation can explain all the significant differences. It makes tough the conclusion over pulse facilitation in experimental groups. What

we can extract from the data is that EPSP does not change in any group (again) and that GABA$_A$ feedback mediated inhibition seems to be not affected (although we cannot completely discard it), pointing indirectly, to the feedforward inhibitory circuits as responsible for the results presented herein.

Temporal course for EPSP and PS changes after CNO injection.

We recorded single pulse evoked potentials during minutes 0-15, 20-35 and 40-55 post-CNO to study the temporal course of CNO injection. We applied 1 pulse every 30 seconds with stimulation intensity adjusted to 80% of the maximum PS (Figure 5.7A). After CNO injection, repeated measures one-way ANOVA in Sham group probes that PS and EPSP does not vary with the time (PS [$F_{3.69,18.46}$ = 1.22, p = 0.33], EPSP [$F_{3.9,19.5}$ = 1.7, p = 0.19]). PV-Inhibition group PS increases with the time [$F_{3.07,15.38}$ = 7.71, p = 0.002, η_p^2 = 0.14, 1-β = 1], while EPSP again does not change [$F_{2.88,14.11}$ = 1.59, p = 0.23]. PV-Activation group PS decrease with the time [$F_{2.47,12.4}$ = 9.9, p = 0.0018, η_p^2 = 0.25, 1-β = 1], while EPSP, again, remain unaffected [$F_{3.74,17.37}$ = 1.24, p = 0.32] (Figure 5.7B-C).

To compare distinct temporal courses between different groups we did a normalized transform with respect the initial measures mean of PS and EPSP applying same stimulation intensity without CNO effects (normalized transform value = data of PS or EPSP for a given pulse – mean of the PS or EPSP without CNO effects, per animal). Comparison of PS temporal courses between groups (Figure 5.7D-E) show robust differences between groups [$F_{2,15}$ = 34.99, p < 0.0001, η_p^2 = 0.37, 1-β = 0.96]. Multiple comparison between PV-Inhibition and PV-Activation groups with Sham, by temporal points, show that PV-Inhibition PS is higher than the one in control conditions from 20 minutes on (p = 0.01), and become stable at around 30 minutes after CNO injection (p < 0.001). PV-Activation PS, on the other hand, decrease significantly after a bit more time, around 25 minutes after CNO injection (p = 0.01), but become stable with approximately the same latency, around 30 minutes after CNO injection (p < 0.001). There are no statistical differences between EPSPs normalized values between groups [$F_{2,15}$ = 0.38, p = 0.68].

Around 20-25 minuts after CNO i.p. administration, changes in PS amplitude are detected in both PV-Inhibition (p = 0.01) and PV-Activation groups (p = 0.01), reach a plateau after approximately 30 min of injection (p < 0.001) and remain stable for the duration of the experiment; and at least 10 h according with the bibliography[29,34].
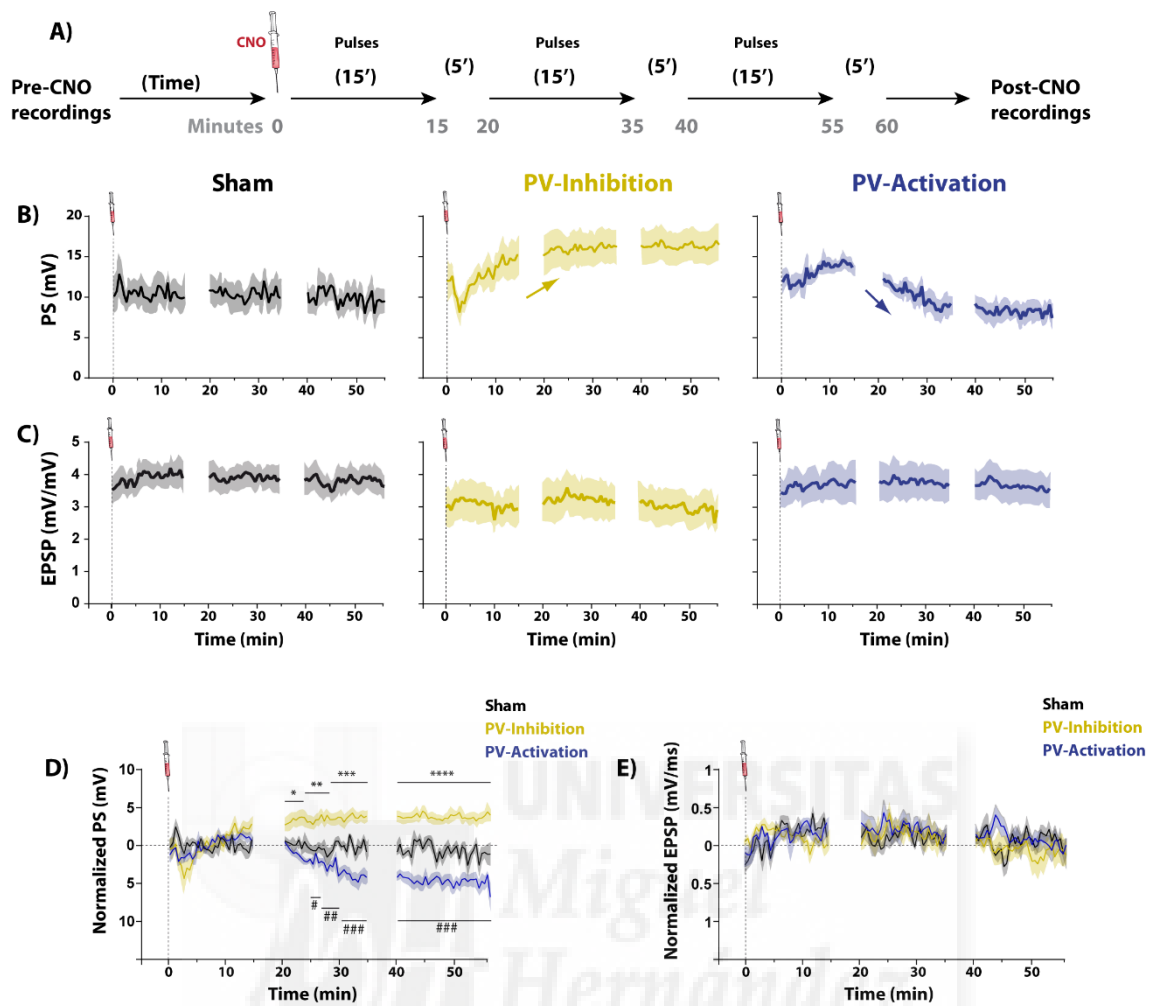
Figure 5.7. Temporal course of single pulse dentate gyrus evoked potentials after CNO injection. A) Scheme of the timeline of the recordings after CNO injection. B) Graphical quantifications of PS amplitude along the time after CNO injection, at minute 0. PS in Sham group remain equal, while it increases in PV-Inhibition group, and decrease in PV-Activation group. Both effects are evident from 20 to 30 minutes after CNO injection and remain stable afterwards. C) Graphical quantifications of EPSP maximum slope along the time after CNO injection. It remains equal in all the groups. D) Graphical quantification of the normalized data of each group PS with respect the normal value without CNO effects. * < 0.05, ** <0.01, *** < 0.001, **** < 0.0001. * Indicates comparisons between PV-Inhibition group and Sham. # < 0.05, ## <0.01, ### < 0.001, #### < 0.0001. # Indicates comparisons between PV-Activation group and Sham. E) Same than D, but with EPSP maximum slope data. All the groups remain without changes along the time.

Gathering together dentate gyrus electrophysiological data.

So far, Input-Output protocol applied in perforant pathway before and after CNO injection reveal that EPSP, as a reflex of the functional dendritic integration in the dentate gyrus, does not change in any group, and all of them become equally potentiated by LTP. CNO injection in Sham group does not change the PS amplitude recorded in hilus, as reflect of granule cell firing. Hilar PV cells inhibition in experimental groups increases the population spike of granule cells drastically, and decreases moderately the PS when we activate them. Also, PS in Sham and PV-Activation group increases after LTP induction, while in PV-Inhibition group, LTP induction does not induce any change after CNO injection; PS seems saturated just by

decreasing perisomatic inhibition. Granule cells are under tight control of hilar inhibitory networks[153,154] an observation that may help explain both results, the soft PS decrease in PV-Activation group and the lack of further PS potentiation after LTP in the PV-Inhibition group. CNO effects are evident from 20-25 to 30 minutes after CNO injection, when they become stables.

5.1.2. Polisynaptic propagation in the hippocampus.

PVbc inhibition facilitates propagation in the trisynaptic circuit

In normal conditions, a single pulse stimulation in the perforant pathway barely arrives to the CA1 region (Figure 5.8A-B), generating a small EPSP, and never evokes a PS in CA1. This result is not altered by CNO administration in Sham group ($F_{7,40}$ = 1.21, p = 0.31 and $F_{7,40}$ = 0.1, p = 0.99, for the EPSP and PS, respectively) (Sham group, Figure 5.8C-F, left). However, in PV-Inhibition group, single pulse applied in perforant pathway evoked a huge EPSP in CA1 *stratum radiatum* after hilar PVbc inhibition [$F_{7,40}$ = 127, p < 0.0001, η_p^2 = 0.48, 1-β = 0.96] at all the stimulation intensities ranging from 0.2 mA [t_{40} = 16.68, p < 0.0001], 0.4 mA [t_{40} = 24.05, p < 0.0001], 0.6 mA [t_{40} = 24.34, p < 0.0001], 0.8 mA [t_{40} = 24.34, p < 0.0001] 1 mA [t_{40} = 24.41, p < 0.0001] and 1.2 mA [t_{40} = 26.67, p < 0.0001] (Figure 5.8C-D, middle). Importantly, there is not only an increased CA1 EPSP in PV-Inhibition group, but also a CA1 PS in this group, something that is not seen in any other circumstance when stimulating perforant pathway (3 synapses away) with single pulses. PS in CA1 before CNO injection is virtually inexistent, but after hilar PVbc inhibition it is evident, and with great amplitude [$F_{7,40}$ = 17.31, p < 0.0001, η_p^2 = 0.42, 1-β = 0.96] at all the stimulation intensities from 0.2 mA [t_{40} = 5.76, p < 0.0001], 0.4 mA [t_{40} = 7.31, p < 0.0001], 0.6 mA [t_{40} = 7.88, p < 0.0001], 0.8 mA [t_{40} = 8.77, p < 0.0001] 1 mA [t_{40} = 8.75, p < 0.0001] and 1.2 mA [t_{40} = 11.16, p < 0.0001] (Figure 5.8E-F). When activating hilar PV interneurons, the light EPSP recorded in CA1, in spite its finesse, is reduced after CNO injection [$F_{7,40}$ = 3.61, p = 0.0042, η_p^2 = 0.26, 1-β = 0.96]. It is evident lightly at 0.2 mA [t_{40} = 3.04, p = 0.03], but robustly at 0.4 mA [t_{40} = 3.87, p = 0.0031], 0.6 mA [t_{40} = 4.19, p = 0.0012], 0.8 mA [t_{40} = 4.84, p = 0.0002], 1 mA [t_{40} = 5.34, p < 0.0001] and 1.2 mA [t_{40} = 5.15, p < 0.0001] (Figure 5.8C-D, right). On the other hand, CA1 PS in PV-Activation group doesn't change [$F_{7,40}$ = 0.86, p = 0.54] (Figure 5.8E-F, right); as it is virtually zero from basal conditions, its EPSP reduction doesn't evoke any decrease in PS.

These data show that CNO alone does not induce any observable change in the trisynaptic propagation (as expected) in Sham group, while the hilar PVbc inhibition causes a huge increase of both the trisynaptic EPSP slope and the PS amplitude in CA1, likely due to the increase in dentate gyrus PS amplitude —or decreasing its latency, or both—. Increasing PVbc inhibition in the hilus causes a further depression of CA1 EPSP slope (in spite being already low in basal conditions) and no observables changes on its PS, which is virtually zero before CNO injection.
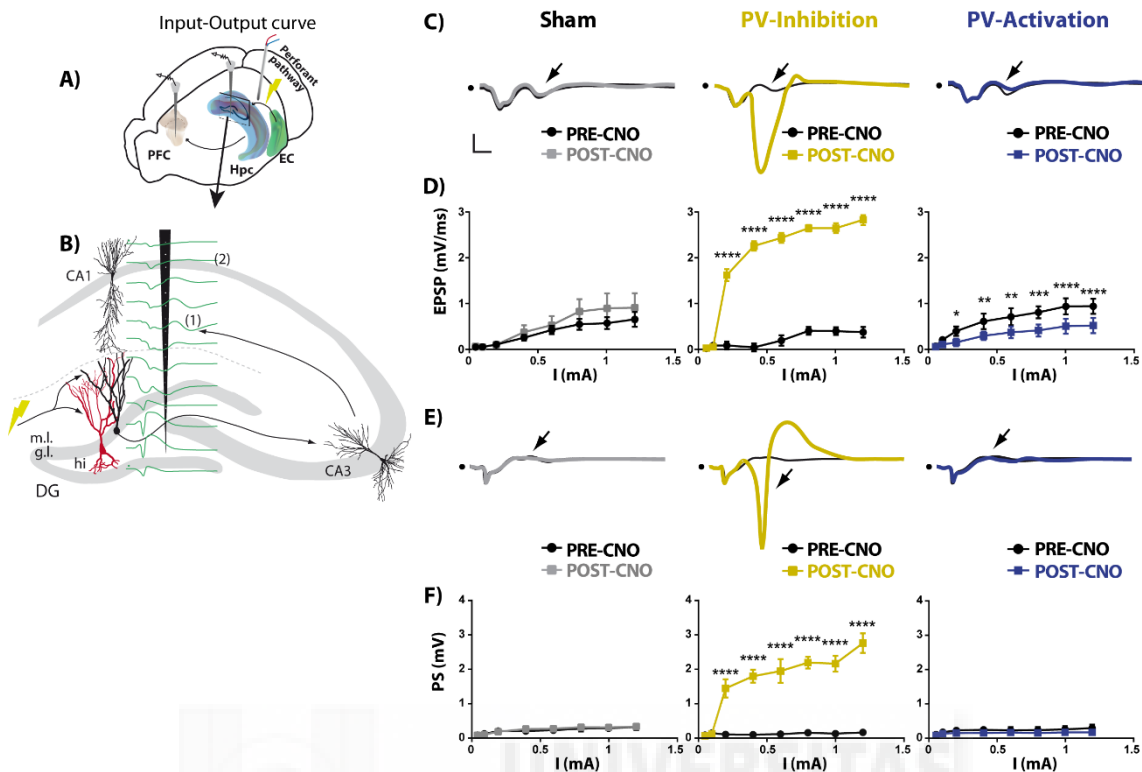
Figure 5.8. Evoked potentials in CA1 after hilar PV modulation when stimulating perforant pathway. A) Schematic representation of the stimulation preparation during the Input-Output protocol applied. B) Schematic representation of the recording probe placed in the hippocampus and dentate gyrus with over-imposed evoked potential after perforant pathway stimulation (in green). (1) Indicates the channel extracted for evaluating CA1 EPSP slope, represented in C-D. (2) Indicates the selected channel for evaluating PS amplitude, represented in E-F. C) Representative waveforms of the EPSP recorded in CA1 *stratum radiatum* before (in black) and after CNO injection (in colour) (1 mg/kg, i.p.). Scalebars indicates 4 ms and 0.5 mV. D) Quantifications of the EPSP maximum slope of the evoked potential associated with the trisynaptic circuit, indicated by the arrow in C. E) Representative waveforms of the CA1 pyramidal layer PS. F) Quantification of the CA1 PS amplitude associated to the trisynaptic circuit, indicated by the arrow in E. * < 0.05, ** <0.01, *** < 0.001, **** < 0.0001. Sham n = 6, PV-Inhibition n = 6, PV-Activation group n = 6.

CA1 single pulse recordings post-CNO injection after dentate gyrus LTP induction.

Single pulse stimulation in perforant pathway after LTP induction in dentate gyrus granule cells dendrites (Figure 5.9A-B) slightly increases the EPSP evoked potential in *CA1 stratum radiatum* in control group [$F_{7,40}$ = 2.43, p = 0.03, η_p^2 = 0.23, 1-β = 0.95], evident at 0.2 mA [t_{40} = 3.34, p = 0.014], 0.4 mA [t_{40} = 4.12, p = 0.0014] and 0.6 mA [t_{40} = 4.2, p = 0.0011] (Figure 5.9C-D, left). However, it is not enough either to induce any change in the CA1 PS, that is virtually zero before and after LTP induction in dentate gyrus post-CNO injection [$F_{7,40}$ = 0.1, p = 0.99] (Figure 5.9E-F, left). In PV-Inhibition group, EPSP and PS in CA1 become already saturated after CNO injection so that LTP induction in perforant pathway does not induce any change in the maximum slope in the EPSP [$F_{7,40}$ = 1.86, p = 0.17] (Figure 5.9C-D, middle), in spite it seems to have even a reduction in the amplitude of the EPSP evoked signal (Figure 5.9C, middle). LTP induction does not alter the PS drastically either (Figure 5.9E-F, middle), in spite of there is one significantly different point increased in PS [$F_{7,40}$ = 2.38, p = 0.03, η_p^2 = 0.22, 1-β = 0.32] at 1 mA

[t_{40} = 3.14, *p* = 0.02]. However, 1-β, as inverse indicator of type 1 error, in such statistical analysis is too low to make this difference trustable, and it is not very consistent in spite its significant *p* value. I personally would reject it based on its low statistical confidence, and I would assume those value as not possible to stablished differences (Figure 5.9F, middle, #). On the other hand, PV-Activation group acts as the Sham-control one; the trisynaptic-associated EPSP recorded in CA1 *stratum radiatum* slightly increases after LTP induction in dentate gyrus [$F_{7,40}$ = 2.40, *p* = 0.03, η_p^2 = 0.4, 1-β = 0.89] (Figure 5.9C-D, right), being tendency at 0.2 mA [t_{40} = 2.56, *p* = 0.1], but evident at 0.4 mA [t_{40} = 3.47, *p* = 0.009], 0.6 mA [t_{40} = 3.05, *p* = 0.03] and 0.8 mA [t_{40} = 3.37, *p* = 0.01]. However, EPSP increases due to the LTP does not induce any changes in the virtually zero CA1 PS in PV-Activation group [$F_{7,40}$ = 0.26, *p* = 0.96].

Taken together these data indicate that LTP induction in perforant pathway increases the trisynaptic propagation into CA1, in the form of sleeper slope of the EPSP recorded in *stratum radiatum* in Sham group and PV-Activation, whitout changes in the CA1 pyramidal cell PS. In PV-Inhibition group, previously enhanced trisynaptic propagation due to PVbc inhibition seems not to be affected after LTP induction in perforant pathway; there is no changes in the EPSP slope, nor in the PS, and both seems to be already saturated.
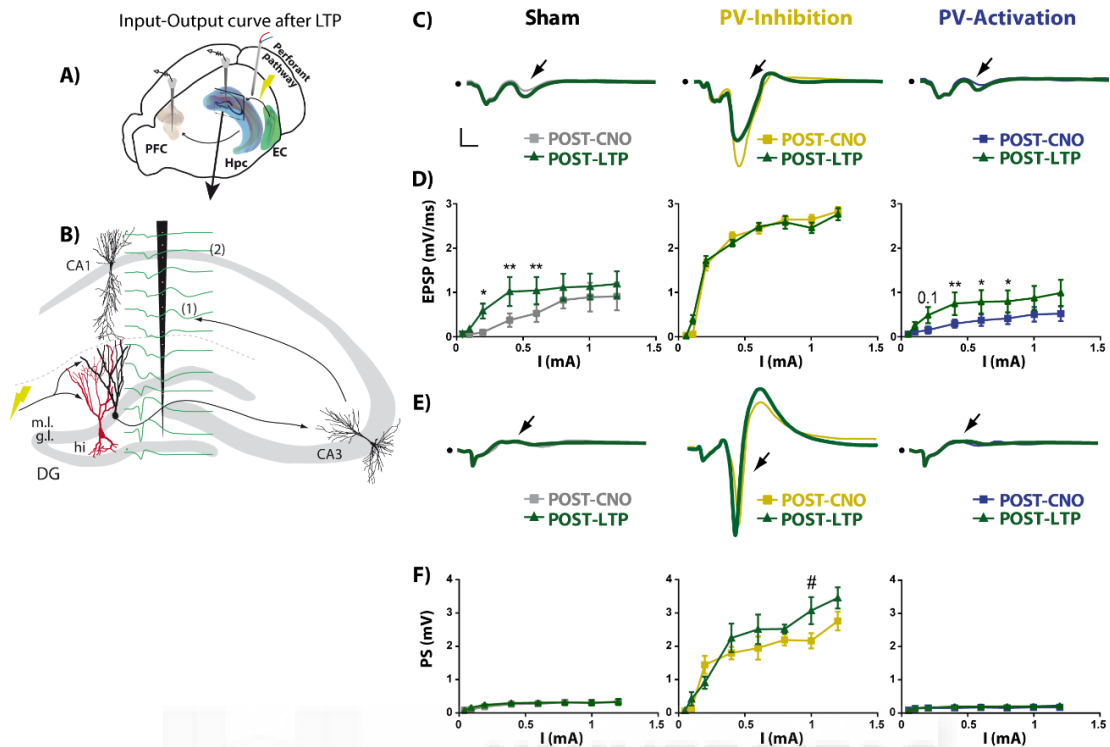
Figure 5.9. Trisynaptic-associated evoked potentials in CA1 after LTP induction in dentate gyrus, post-CNO injection. A) Schematic representation of the stimulation preparation during the Input-Output protocol applied 60 minutes after LTP induction. B) Schematic representation of the recording probe placed in the hippocampus and dentate gyrus with over-imposed evoked potential after perforant pathway stimulation (in green). (1) Indicates the channel extracted for evaluating CA1 EPSP slope, represented in C-D. (2) Indicates the selected channel for evaluating PS amplitude, represented in E-F. C) Representative waveforms of the EPSP recorded in CA1 *stratum radiatum* post-CNO but before (in colour; grey, yellow and blue) and after LTP (green). Scalebars indicates 4 ms and 0.5 mV. D) Quantifications of the EPSP maximum slope of the evoked potential associated to the trisynaptic circuit, indicated by the arrow in C. E) Representative waveforms of the CA1 pyramidal layer PS, same colour code than in C. F) Graphical quantification of the CA1 PS amplitude associated to the trisynaptic circuit, indicated by the arrow in E. * < 0.05, ** <0.01, *** < 0.001, **** < 0.0001. # Indicates a statistical significant value (p = 0.02), but with very low confidence (1-β = 0.32), which make it not trustable. Sham n = 6, PV-Inhibition n = 6, PV-Activation group n = 6.

Disynaptic activity propagation remains constant in all the groups.

In CA1 region, before the trysinaptic associated evoked potential arrives, we record also a disynaptic volume propagation as reflect of the stimulation of the direct projection from EC to CA3 (Figure 5.10A-B). As expected, but importantly, disynaptic activation of CA1 remains constant in the Sham group [$F_{7,40}$ = 0.65, p = 0.70], the PV-Inhibition group [$F_{7,32}$ = 0.79, p = 0.59] and the PV-Activation group [$F_{7,40}$ = 0.28, p = 0.95], comparing before and after CNO injection when we applied a Input-Output protocol (Figure 5.10C-D). One animal from PV-Inhibition group was discarded for this analysis due that dentate gyrus PS volume propagation was so strong that changed the waveform of disynaptic activation in CA1, making its analysis not trustable.

These data point to the non-involvement of CA3 region in the electrophysiological changes observed downstream in the CA1 associated network. The lack of changes in disynaptic activation point that the disynaptic circuit, *per se*, seems not to be functionally affected by our experimental manipulation.

Disynaptic volumen propagation into CA1.
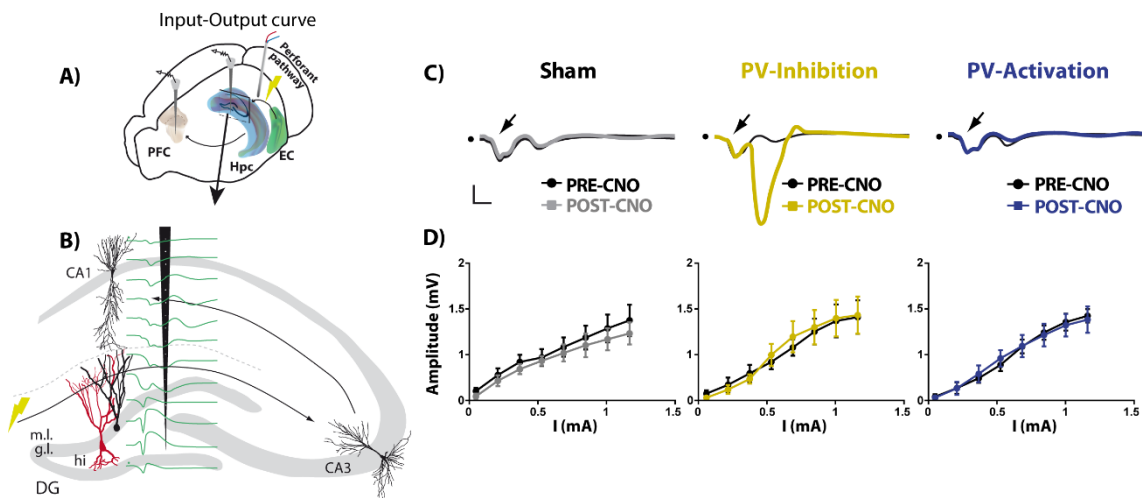
Figure 5.10. Disynaptic propagation into CA1 after perforant pathway stimulation. A) Schematic representation of the stimulation preparation. B) Schematic representation of the recording probe placed in the hippocampus and dentate gyrus with over-imposed evoked potential after perforant pathway stimulation (in green). Arrow indicates the disynaptic circuit after perforant pathway stimulation. C) Representative waveforms of the evoked potential recorded in CA1 *stratum radiatum* before (in black) and after CNO injection (in colour) (1 mg/kg, i.p.). Arrows indicates the disynaptic volume propagation, prior to the trisynaptic one. Scalebars indicates 4 ms and 0.5 mV. D) Graphical quantifications of the disynaptic propagation amplitude indicated by the arrow in C. No differences before and after CNO injection in any group. Sham n = 6, PV-Inhibition n = 5, PV-Activation group n = 6.

Compilation of electrophysiological data recorded in CA1.

CA1 electrophysiological data probe that in standard condition (Sham group), single pulse stimulation in perforant pathway barely arrives at CA1 in the form of EPSP, and only at high intensities; not in the form of PS. Nevertheless, the hilar PVbc inhibition causes to drastically increase not only the trisynaptic-associated EPSP but also the CA1 PS, elicited by single pulse stimulation in the perforant pathway. Hilar PVbc activation, by impairing dentate gyrus firing, further decreases the trisynaptic propagation (Figure 5.8). LTP induction in the perforant pathway increases propagation in all groups, not affecting the CA1 PS. In good agreement with the lack of further potentiation DG activity in the PV-Activation group after LTP induction, no increased trisynaptic propagation was observed (Figure 5.9). Importantly, these changes are associated with the trisynaptic circuit propagation because the analysis of the disynaptic volume propagation amplitude in CA1 reveals no differences before and after CNO injection (Figure 5.10), in any group.

5.1.3.- Propagation of hippocampal activity to the prefrontal cortex

The hippocampus connects with the prefrontal cortex through its ventral part[283,284] (reviewed in Takita et al., 2013[285]), and this connection has been shown to be fundamental for memory formation (reviewed in Preston and Eichenbaum, 2013[286]; Morici et al., 2015[287]). Long-range propagation of activity from the hippocampus to other extra-hippocampal areas, however, requires stimulation frequencies in the theta-beta frequency range[279]. Single or low-frequency stimulation of the perforant pathway does not recruit neurons in the prefrontal cortex[288].

Accordingly, in our experiments, stimulation of the perforant pathway at 1Hz (Figure 5.11A) do not provoke any observable evoked potential in the prefrontal cortex of Sham group, not before nor after CNO injection [$F_{9,50}$ = 0.79, p = 0.62]. However, when decreasing hilar PVbc perisomatic inhibitory tone in the PV-Inhibition group, the same stimulation paradigm elicits a clear evoked potential in prefrontal cortex [$F_{9,30}$ = 2.82, p = 0.01, η_p^2 = 0.29, 1-β = 0.79] being tendency in the pulse number 4 of the train [t_{30} = 2.72, p = 0.1], but significant in the pulses number 5 [t_{30} = 3.6, p = 0.012], 6 [t_{30} = 4.23, p = 0.002], 7 [t_{30} = 4.02, p = 0.003], 8 [t_{30} = 4.21, p = 0.002], 9 [t_{30} = 3.89, p = 0.005] and 10 [t_{30} = 3.73, p = 0.007]. It is interesting to note that the PFC responds to the hippocampal input with an evoked potential oscilating at gamma frequency. When we increase the perisomatic PVbc inhibition over granule cells, in the PV-Activation group, we don't find evoked responses in prefrontal cortex [$F_{9,50}$ = 0.48, p = 0.87] (Figure 5.11B-C).

Evoked potential in PFC after 1Hz train stimulation in perforant pathway.
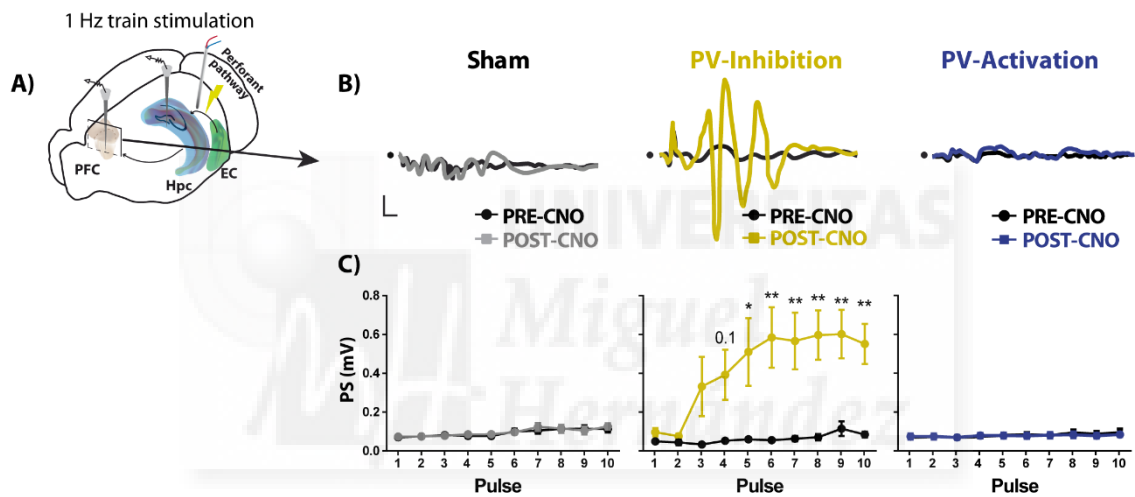
Figure 5.11. Prefrontal cortex activity propagation after perforant pathway stimulation and hilar PV cells inhibition. A) Schematic representation of the surgery preparation for electrophysiological recordings. B) Examples of waveforms extracted from prefrontal cortex during 1Hz train stimulation the in perforant pathway before (in black) and after (in colour) CNO injection. Waveforms were extracted from the 10th pulse of the train. Scalebars indicates 5 ms and 0.1 mV. C) Quantifications of the first wave amplitude of the evoked potential recorded in the prefrontal cortex, when applying 1 Hz train stimulation in the perforant pathway, before (in black) and after (in colour) CNO injection (1 mg/kg, i.p.). * < 0.05, ** <0.01. Sham n = 6, PV-Inhibition n = 4, PV-Activation group n = 6.

Collation of electrophysiological data.

Taken together the electrophysiological data probed that hilar PV interneurons regulate the firing of granule cells by controlling inhibitory perisomatic tone, not affecting its synaptic integration.

By decreasing the hilar PVbc interneurons activity, granule cells fire easily, as evidenced by the increases PS amplitude and its decreases latency; while PVbc activation obstructs the granule cell firing. The increased firing of granule cells causes a disproportionately increase in the trisynaptic communication, allowing CA1 pyramidal neurons to fire even in response to single pulse stimulation in the perforant pathway. Increased CA1 firing is accompanied by an increased extrahippocampal propagation evidenced by the elicited evoked potential in the prefrontal cortex. Knowing that hippocampal efferences reached a rich network of extrahippocampal structures, we next investigated long range hippocampal functional connectivity using fMRI.

5.2-. fMRI results.

fMRI combined with intracranial electrical stimulation allows the quantitative analysis of effective connectivity in brain networks[277,288,289]. Stimulation of the perforant pathway in rats at 10 and 20 Hz demonstrated to activate the dentate gyrus and hippocampus effectively[290]. After LTP induction in the perforant pathway, the same stimulation also recruit structures in the prefrontal cortex, nucleus accumbens and perirhinal cortex[136]. Accordingly, in our experiments, in control conditions (Sham and all pre-CNO data), 20 or 10 Hz train stimulation in the perforant pathway evocate a BOLD response observable only in the hippocampus and dentate gyrus (Figure 5.12 for 20 Hz, and Figure 5.13 for 10 Hz). One-way ANOVA between groups for pre-CNO data results in no differences ([$F_{2,13}$ = 0.67, p = 0.52] for 20 Hz data and [$F_{2,13}$ = 0.01, p = 0.98] for 10 Hz data). Because of that, for simplicity, pre-CNO data in the bar histograms (Figure 5.12D and Figure 5.13B) are represented grouped. Within groups statistical comparisons, before vs after CNO injection, were made using paired t-test analysis.

4.2.1.- fMRI BOLD response when stimulating at 20 Hz.

CNO injection does not change BOLD response in Sham group (Figure 5.12C, up) in any Region Of Interest (ROI). Activation is restricted to the hippocampus [t_5 = 0.41, p = 0.88], although some active voxels are observed in medial temporal lobe structures, mainly subiculum and entorhinal cortex. It can be explained by re-entering activity into the hippocampal formation during 20Hz train stimulation or by direct perforant pathway antidromic activation. After CNO injection, BOLD response does not change in hippocampal ROI [t_5 = 1.54, p = 0.172], nor in the the global activation of the brain [t_5 = 0.32, p = 0.72] in Sham group. Extrahippocampal activation in the prefrontal cortex or subcortical areas is not observed.

In PV-Inhibition group, before CNO injection, BOLD response is restricted to hippocampal ROI. But when inhibiting the hilar PVbc interneurons, BOLD signal is not only enhanced in hippocampal ROI [t_5 = 4.32, p = 0.0076, r^2 = 0.78, 1-β = 0.96], but, most importantly, it is found in structures of the medial temporal lobe [t_5 = 8.11, p = 0.0005, r^2 = 0.92, 1-β = 0.99], prefrontal cortex [t_5 = 3.43, p = 0.01, r^2 = 0.69, 1-β = 0.77] and subcortical structures including nucleus accumbens, striatum and amygdala [t_5 = 2.17, p = 0.08, r^2 = 0.48, 1-β = 0.42]. Although the propagation to the latter one is a tendency more than significant, and the 1-β is low, it is interesting to point the signal-to-noise ratio in that region is usually worse due to the susceptibility presence of artifacts, by the proximity of the ear canal[277]. Importantly, the BOLD response in subcortical structures and prefrontal cortex is zero in basal conditions and it is only evident after CNO injection in the PV-Inhibition group. The resulting evoked map (Figure 5.12C, middle) reminds to the one we obtained after LTP induction[136], but in the present case obtained just downregulating the hilar PVbc perisomatic inhibition.

BOLD response in hippocampal ROI of the PV-Activation group is mostly unchanged after CNO administration [t_4 = 1.44, p = 0.24]. It presents low number of active voxels in medial temporal lobe ROI, mainly in subiculum and entorhinal cortex, without variation after CNO injection [t_4 = 0.81, p = 0.45], and no propagation into prefrontal cortex or subcortical structures, which make the total number of the voxels in the brain to remain constant [t_4 = 0.22, p = 0.84]. Although CNO administration is this group produced a slight decrease in the dentate gyrus PS (Figure 5.3), the EPSP remained unchanged (Figure 5.1), a result that helps explain the fMRI result in this group, since BOLD signal mostly correlates with the synaptic activity[136,291].

BOLD response in fMRI after 20Hz stimulation in perforant pathway.
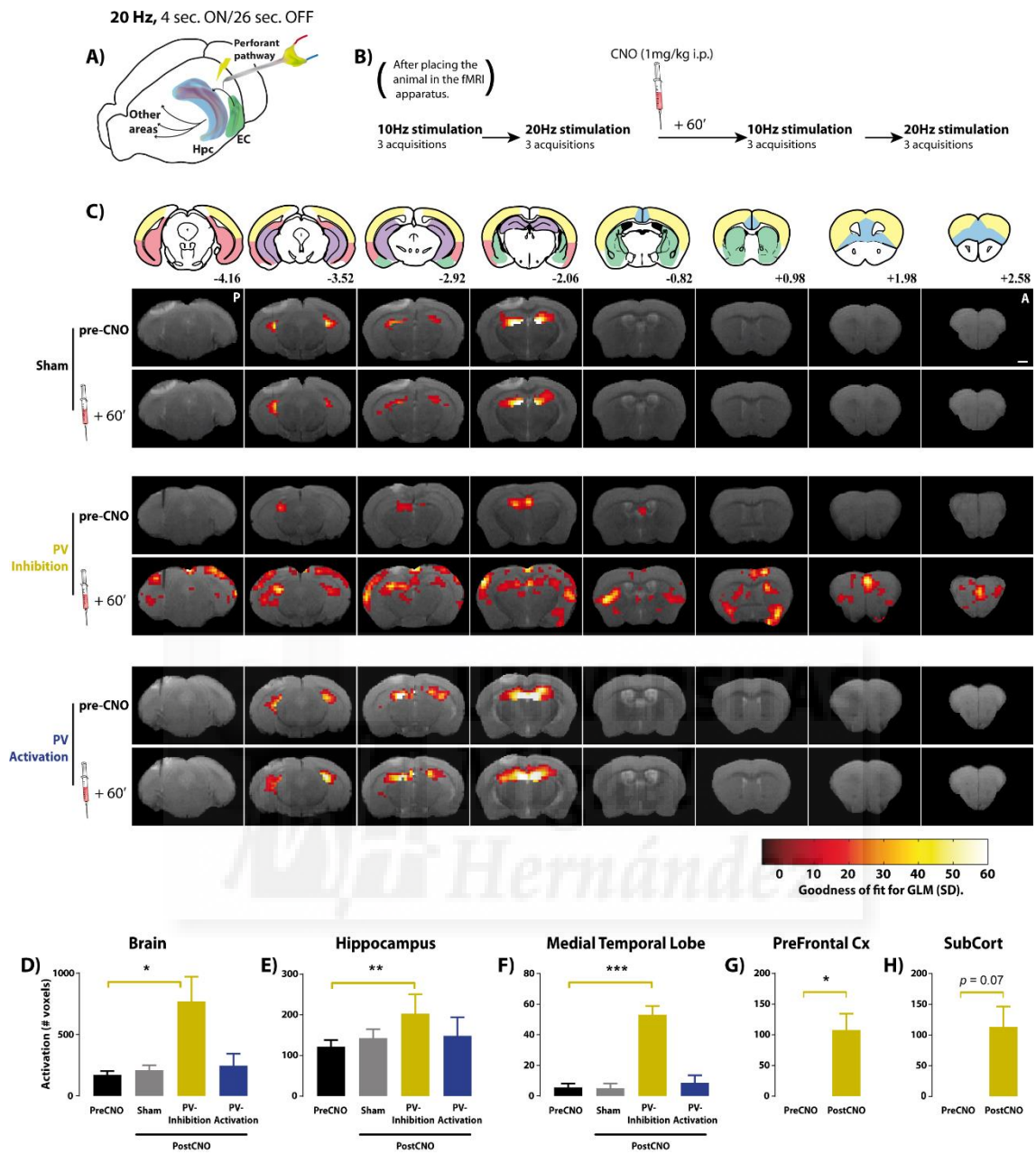
Figure 5.12. fMRI data showing BOLD response after 20 Hz stimulation in the perforant pathway. A) Scheme of the implantation of the carbon fibre electrode in the perforant pathway for fMRI experiments. B) Temporal arrow with the stimulating protocols temporal order after placing the animal inside the fMRI scanner. Post-CNO acquisitions were extracted 60 minutes after its injection. C) First lane indicates the atlas sections (modified from Keith and Paxinos, 2008) correspondent to the approximate fMRI images showed below them. These atlas sections are colour-coded with the ROIs used to group the active voxels according with anatomical and functional criteria. Red = medial temporal lobe, yellow = cortices, purple = hippocampus, green = subcortical structures and blue = prefrontal cortex. Numbers below sections indicate the Anterior (A) – Posterior (P) distance with respect bregma, in mm. Below the atlas section are presented representative T_2-weighted anatomy images with overlaid functional maps evoked after 20 Hz stimulation, per group, before and after CNO-injection. Scale indicates 1 mm. Colourbar indicates the goodness of the fitness for the General Linear Model Applied (GLM) comparing activation during the 20 Hz train (ON period, 4 sec) vs the OFF period (26 sec), with the threshold set on $p = 0.01$. D-H) Bar diagrams represent the number of voxels actives above the threshold during ON period; globally in the whole brain (D), in the hippocampus (E), in the medial temporal lobe structures (F), in the prefrontal cortex (G) and subcortical structures (H). Statistical analysis compares each group of animals with themselves before and after CNO injection. PreCNO data are represented together for simplicity (no differences between groups). * <0.05, ** <0.01, *** <0.001. Sham n = 6, PV-Inhibition n = 6, PV-Activation group n=5.

4.2.2.- fMRI BOLD response when stimulating at 10 Hz.

The stimulation with 10 Hz, instead of 20 Hz, reveals very similar results, which points to the robustness of the finding.

Sham group doesn't show any change before and after CNO injection in hippocampus [t_5 = 0.35, p = 0.75], where the BOLD response activity remain confined (Figure 5.13A, up; Figure 5.13B-C).

PV-Inhibition group evoked maps (Figure 5.13A, middle) evidences also not only and increased hippocampal BOLD signal after PVbc inhibition [t_5 = 4.71, p = 0.0053, r^2 = 0.81, 1-β = 0.96], but also extrahippocampal propagation to medial temporal lobe structures [t_5 = 5.32, p = 0.0031, r^2 = 0.85, 1-β = 0.99], importantly to prefrontal cortex [t_5 = 3.02, p = 0.02, r^2 = 0.64, 1-β = 0.68], and again a tendency to increase activity in subcortical areas [t_5 = 1.97, p = 0.1, critical t value = 1.98, r^2 = 0.43, 1-β = 0.35] (Figure 5.13B-F). Again this tendency, in spite not being significant and having low 1-β, it is worthy to be pointed because voxels in subcortical are not active before CNO injection, and given the higher difficulty for obtaining proper fMRI signals closely to the ear canal[277].

PV-Activation group doesn't change the number of voxels actives in hippocampus after CNO injection [t_4 = 1.44, p = 0.24], where the activation is mostly restricted (Figure 5.13A, bottom; Figure 5.13B-C).

BOLD response in fMRI after 10Hz stimulation in perforant pathway.
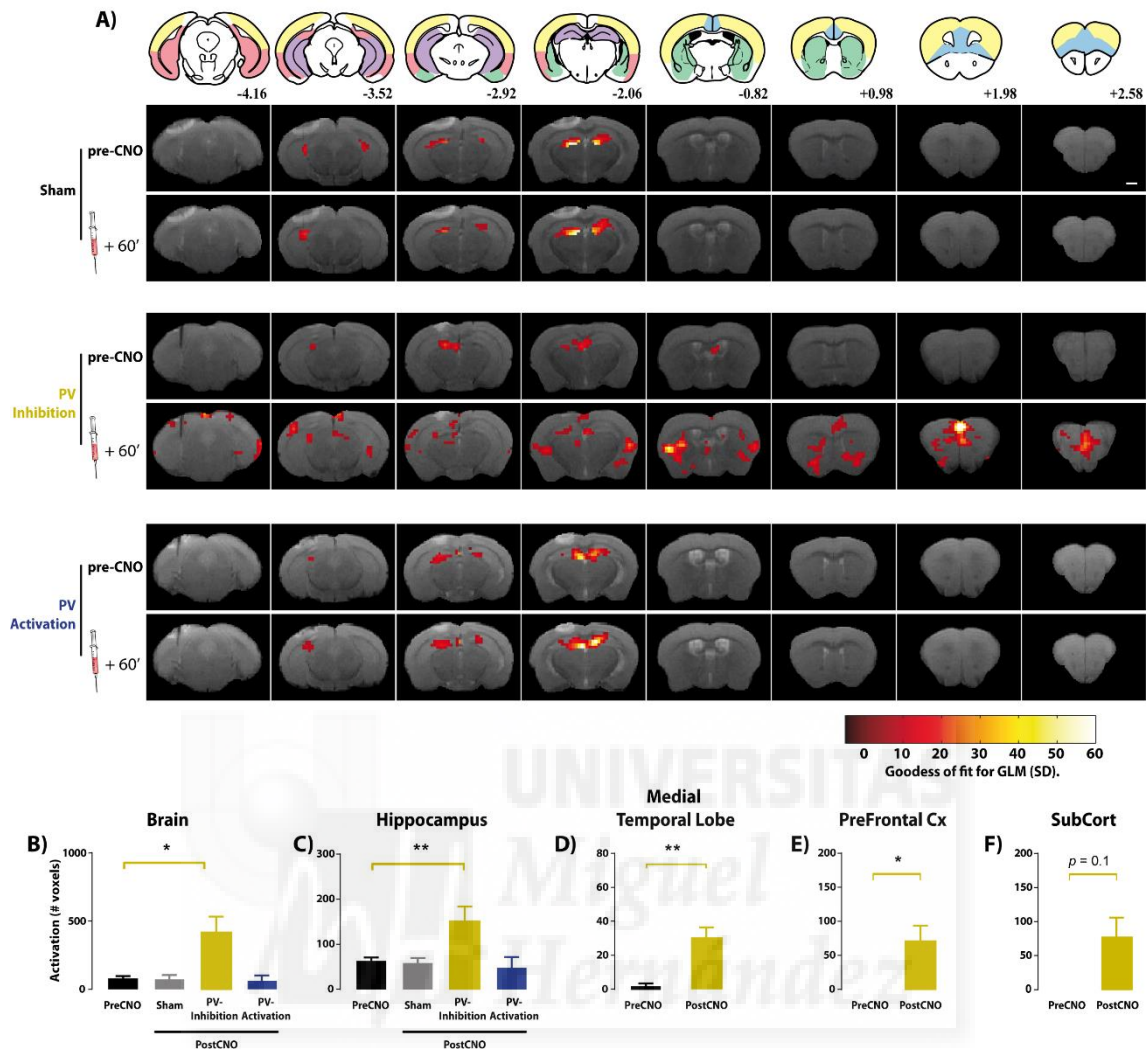
Figure 5.13. fMRI data showing BOLD response after 10 Hz stimulation in the perforant pathway. The stimulation point and temporal protocol to extract data are equal than in previous figure 5.12. A) First lane indicates the atlas sections (modified from Keith and Paxinos, 2008) correspondent to the approximate anatomical fMRI sections showed below them. The atlas sections are colour-coded with the ROIs used to group the active voxels according with anatomical and functional criteria. Red = medial temporal lobe, yellow = cortices, purple = hippocampus, green = subcortical structures and blue = prefrontal cortex. Number below sections indicate the Anterior (A) – Posterior (P) distance with respect bregma, in mm. Representative T_2-weighted anatomy images include overlaid functional maps evoked after 10 Hz stimulation trains in the perforant pathway, organized per group, before and after CNO-injection. Scale indicates 1 mm. Colourbar indicates the goodness of the fitness for the General Linear Model Applied (GLM) comparing activation during the 10 Hz train (ON period, 4 sec) vs the OFF period (26 sec). Significant threshold set on p = 0.01. B-F) Graphics represent the number of voxels actives above the threshold during ON period; globally in the whole brain (B), in the hippocampus (C), in the medial temporal lobe structures (D), in the prefrontal cortex (E) and in subcortical structures (F). Statistical analysis compares each group of animals with themselves before and after CNO injection. Pre-CNO data in B and C are represented together for simplicity (no differences between groups). * < 0.05, ** < 0.01, *** < 0.001. Sham n = 6, PV-Inhibition n = 6, PV-Activation group n = 5.

Compilation of fMRI results.

Overall our results show that (1) CNO injection, *per se*, does not change BOLD responses evoked by electric stimulation, (2) independently of the stimulation frequency applied (10 Hz or 20 Hz), inhibition of hilar PVbc interneurons increases hippocampal long-range functional connectivity, revealing BOLD response in prefrontal cortex (infralimbic, supralimbic and cingulate cortex) —in good agreement with our electrophysiological results—, subcortical structures (as striatum, nucleus accumbens and amygdala) and medial temporal lobe regions (as subiculum and entorhinal cortex), among others. These regions have been associated in the literature with different aspects of memory and learning. Also, comparable functional reorganization was previously reported after LTP induction in the perforant pathway of rats[136,290].

The obtained electrophysiological and fMRI results demonstrate that excitation/inhibition balance in the dentate gyrus controls the distribution of activity in a brain-wide network of mesolimbic dopaminergic and medial prefrontocortical estructures. What is the actual functional role of this PVbc cell operated-mechanis? We next investigated the behavioural consequences of the gain- and loss-of-function in this circuit.

5.3.- Behaviour. Novel Location of the Object task and Elevated Plus maze.

5.3.1.- Hilar PVbc modulation during encoding and no-modulation.

The first task we carried out with the animals was the Novel Location of the Object (NLO), pointed to be dentate gyrus-dependent if challenging to discriminate distances or positions in the space[64]. Animals carried out the task first while modulating hilar PV interneurons during the encoding of the new environmental information regarding objects, and its positions in the space. To do so, we injected CNO 90 minutes before the animal first encounter with the objects (Figure 5.14A, up). During this encoding session, animals explore both objects equally [$F_{2,35}$ = 0.94, p = 0.94]. It means that despite PV cells were being manipulated; animal performed normally. However, the day after, the test session reveal that groups encoded differently —factor group [$F_{2,35}$ = 6.58, p = 0.0037, η_p^2 = 0.27, 1-β = 0.99], factor time, that reflect the differences between familiarization and test 24h [$F_{1,35}$ = 55.86, p < 0.0001, η_p^2 = 0.38, 1-β = 0.99]—. Both, Sham and PV-Inhibition group, explore more the object that had been displaced (Sham [t_{35} = 4.27, p = 0.0004], PV-Inhibition [t_{35} = 8, p < 0.0001]), while the PV-Activation group does not [t_{35} = 0.81, p = 0.8]. Comparison between groups in test sessions demonstrates that PV-Inhibition group mice explore the object in the new location even more than Sham group [t_{70} = 4.66, p = 0.0043] and more than the PV-Activation group [t_{70} = 8.32, p < 0.0001]. Sham group mice explore significantly more the object than PV-Activation group mice [t_{70} = 3.75, p = 0.02]. PV-Activation group mice explore both objects equally, as they did the first time they encounter the objects, as if the objects were new for them (Figure 5.14A).

Figure 5.14. Mice exploratory behaviour during Novel Location of the Object task modulating encoding and in control conditions. A) Schematic representation of the protocol for modulating PVbc during the encoding of new spatial information (up) and quantification of mice's exploration index (time spent exploring displaced object/total time exploring both). B) Schematic representation of same behaviour protocol than in A, but injecting Saline instead of CNO (up), and quantification of mice's exploration index in NLO task. * Indicates comparison within groups, * < 0.05, ** <0.01, *** < 0.001, **** < 0.0001. # Indicates comparison between groups # < 0.05, ### <0.001, #### < 0.001. Fam (familiarization session, related to the encoding) bar (in black) represents data from all the groups, grouped for simplicity (no differences between them). 0.5 of exploratory index indicates equal exploration between objects; < 0.5 indicates more exploration of the static objects; > 0.5 indicates more exploration of the displaced object.

102

One week after, same mice underwent the same task again, with different objects, its position counterbalanced and injecting saline (0'9 %) instead of CNO (Figure 5.14B, up). So the same animals are controls of themselves, as with saline PVbc remain unmodulated. This time all the groups learn normally, as reflected by the increased exploration time in the new object location when tested 24 h after the encoding [$F_{1,35}$ = 29.28, p < 0.0001, η_p^2 = 0.31, 1-β = 1], Sham group [t_{35} = 2.88, p = 0.019], PV-Inhibition group [t_{35} = 2.81, p = 0.023], and PV-Activation group [t_{35} = 3.64, p = 0.0026], without differences between groups [$F_{2,35}$ = 1.05, p = 0.35] (Figure 5.14B, bottom).

5.3.2.- Hilar PVbc modulation during consolidation.

Then we modulate PVbc activity during the consolidation phase of the learning. To do so we repeated the NLO task, with other animals from the same strain, and under same conditions. This time we injected CNO 10' minutes after animals were taken out from the familiarization phase of the learning (after they first encountered objects and its locations, so after the animals encode normally) (Figure 5.15A, up). Injections were done by another trained researcher and in other room, to avoid fear generalization to the test room and apparatus. As CNO takes around 20 minutes to make its effect, injecting CNO 10 minutes after allow us to modulate hilar PV interneurons activity from 30 minutes to several hours after the animals had explored the objects, even if the animal sleep; during the consolidation phase.

A first analysis of object exploration during the familiarization phase shows that all the animals explore equally both object (corresponding to the encoding of the objects' information and its location in space) [$F_{2,39}$ = 2.24, p = 0.13], so we discard bias in exploration from basal conditions. 24 h after the encoding, and having been modulated the PVbc activity during the consolidation, all the groups explore significantly more the displaced object [$F_{1,39}$ = 60.23, p < 0.0001, η_p^2 = 0.38, 1-β = 1], Sham group [t_{39} = 4.49, p = 0.0002], PV-Inhibition group [t_{39} = 5.14, p < 0.0001] and PV-Activation group [t_{39} = 3.95, p = 0.001]. Without differences between groups [$F_{2,39}$ = 1.44, p = 0.25] (Figure 5.15A, bottom).
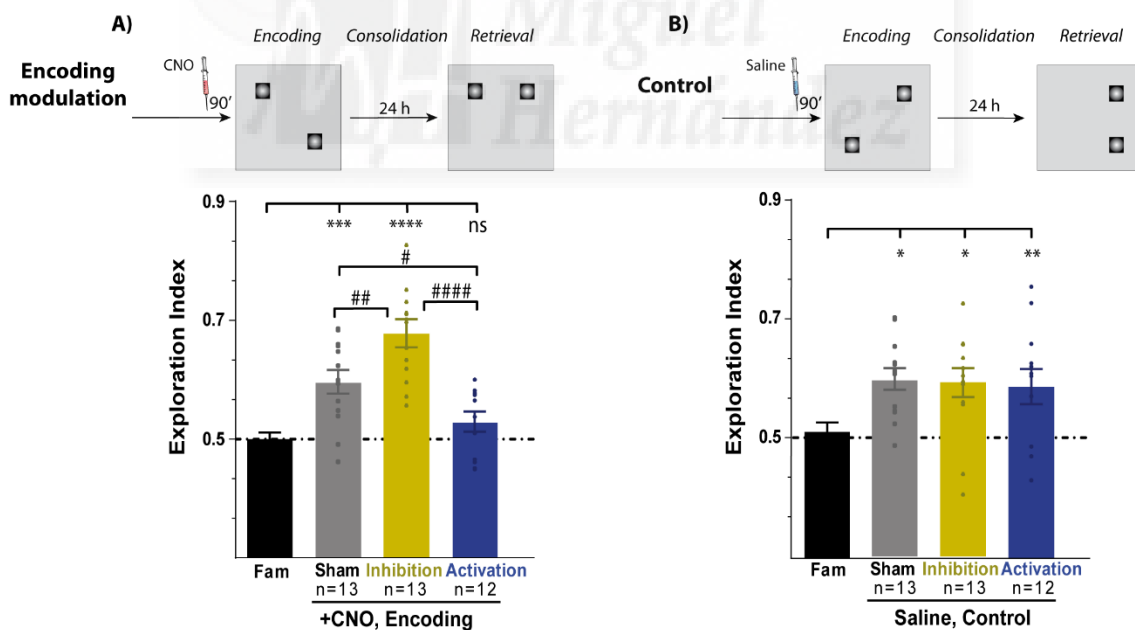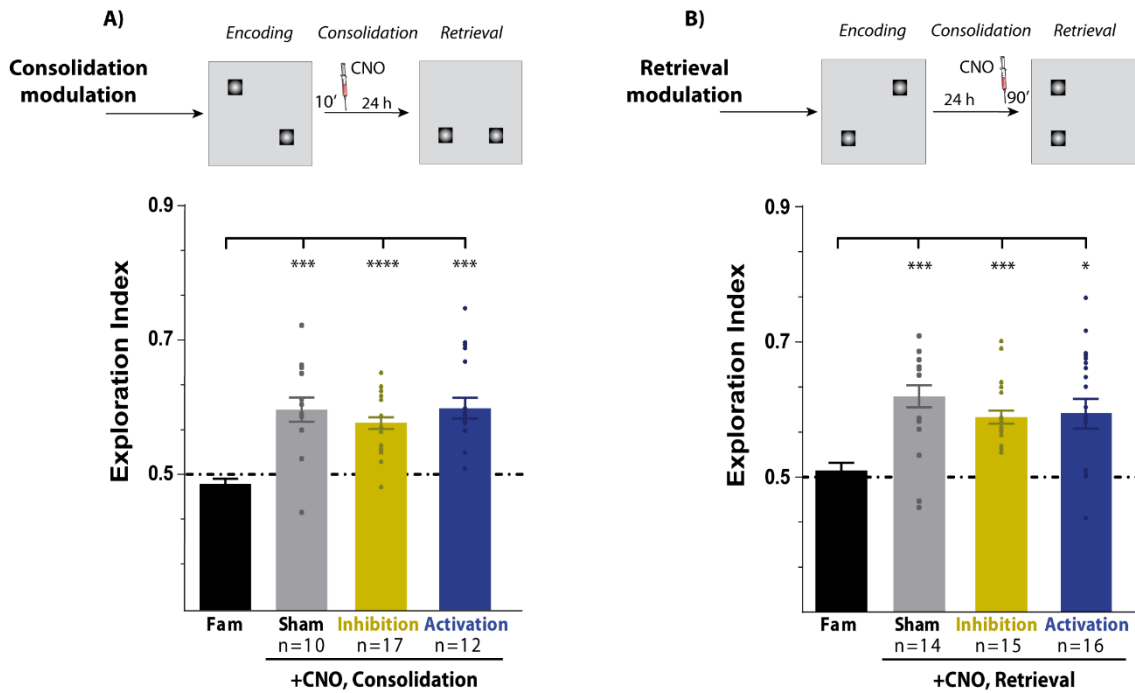
Figure 5.15. Mice exploratory behaviour during Novel Location of the Object task modulating consolidation and retrieval. A) Schematic representation of the temporal procedure for modulating PVbc during the consolidation of new spatial information (up) and quantification of mice's exploration index (time spent exploring displaced object/total exploratory time). B) Schematic representation of the temporal procedure for modulating PVbc during retrieval of previously encoded spatial information (up), and quantification of mice's exploratory index behaviour. Fam (familiarization session, related to the encoding) bar (in black) represents data from all the groups for simplicity (no differences between them). * indicates comparison within groups, * < 0.05, *** < 0.001, **** < 0.0001. 0.5 of exploratory index indicates equal exploration between objects; < 0.5 indicates more exploration of the static objects; > 0.5 indicates more exploration of the displaced object.

5.3.3.- Hilar PVbc modulation during retrieval.

Finally, we repeated the NLO task, under the same conditions than previous experiments, but allowing the animal to encode and to consolidate normally, and then injecting CNO 90 minutes before the animal entered in the arena to carry out the test phase. That way we modulated PVbc activity during the retrieval of previously encoded information of objects and its location (Figure 5.15B, up).

Again, animals explore equally both objects during the first encounter (familiarization phase) [$F_{2,38}$ = 0.89, p = 0.88], which allows us to discard bias from basal conditions and to group familiarization data in Figure 5.15B, in spite the statistical analysis in each group is paired; each group is compared with respect themselves in both sessions. Statistical analysis between familiarization and test sessions probed that all the groups explore more, and equally, the displaced object when tested 24h after the encoding [$F_{1,38}$ = 38.16, p < 0.0001, η_p^2 = 0.33, 1-β = 1]; Sham group [t_{38} = 4.27, p = 0.0004], PV-Inhibition group [t_{38} = 3.95, p = 0.001] and PV-Activation group [t_{38} = 2.51, p = 0.04]. No differences between groups were found [$F_{2,38}$ = 1.03, p = 0.36]. All the groups learn, and were able to retrieve correctly the previously encoded information, discarding PVbc evident involvement during the retrieval.

5.3.4.- Control parameters and anxiety.

Control parameters were evaluated by looking at 1) the movement (distance travelled) in centre vs periphery of the NOL arena, as indirect measure of the anxiety (thigmotaxis) and general locomotion during habituation sessions, with and without CNO during familiarization, and during Test 24h trials (Figure 5.16A); and 2) the animal's behaviour in the Elevated Plus Maze (EPM) after injecting CNO (Figure 5.16B), by evaluating the time spent in its open arms vs time in the closed arms, distance travelled, resting time in each arm and number of entries. EPM classically evaluate anxiety[273,274]. These data allow us to discard anxiety or locomotion general effects on our results, especially when animals are exploring new environments. Control parameters were extracted by Elena Pérez Montoyo using the script developed by her.

Control parameters in NLO task show no differences between groups (Figure 5.16A). Movement between groups, either in the centre as in the periphery, presents one statistically significant difference during the habituation 1 session [$F_{2,68}$ = 3.29, p = 0.043, η_p^2 = 0.08, 1-β = 0.41], between Sham groups animals and PV-Activation group [t_{68} = 3.52, p = 0.04] for periphery distance travelled, but its low partial *eta* square and 1-β values make us reject the alternative hypothesis in this case, accepting the null one; so, considering no differences between groups. Animals move equally in habituation 2 session [$F_{2,68}$ = 1.04, p = 0.97], during familiarization phase when injecting CNO [$F_{2,68}$ = 2.68, p = 0.07], and 24 h later, during the test session [$F_{2,68}$ = 0.19, p = 0.82]. They move also equally when, instead of CNO, we inject saline during familiarization session [$F_{2,68}$ = 0.19, p = 0.82] and during the test 24 h after saline injection [$F_{2,68}$ = 1.79, p = 0.17] (Figure 5.16A).

EPM results reveal no differences in time spent in open/closed arms between groups [$F_{2,114}$ = 0.0003, p > 0.999], nor in the distance travelled, in any arm [$F_{2,114}$ = 0.004, p = 0.995], nor in the resting time [$F_{2,114}$ = 0.052, p = 0.94] and nor in the entries in different zones [$F_{2,114}$ = 0.1, p = 0.89] (Figure 5.16B).

The lack of differences in animals' control parameters, either in NLO locomotor behaviour as in the EPM, indicates that the CNO, and therefore the hilar PV-interneurons modulation, does not affect locomotive behaviour and anxiety. Especially noteworthy is to discard anxiety, due its high impact on memory and spontaneous behaviour, and because it has been related to ventral hippocampus function (reviewed in Bannerman et al. 2004[292]).
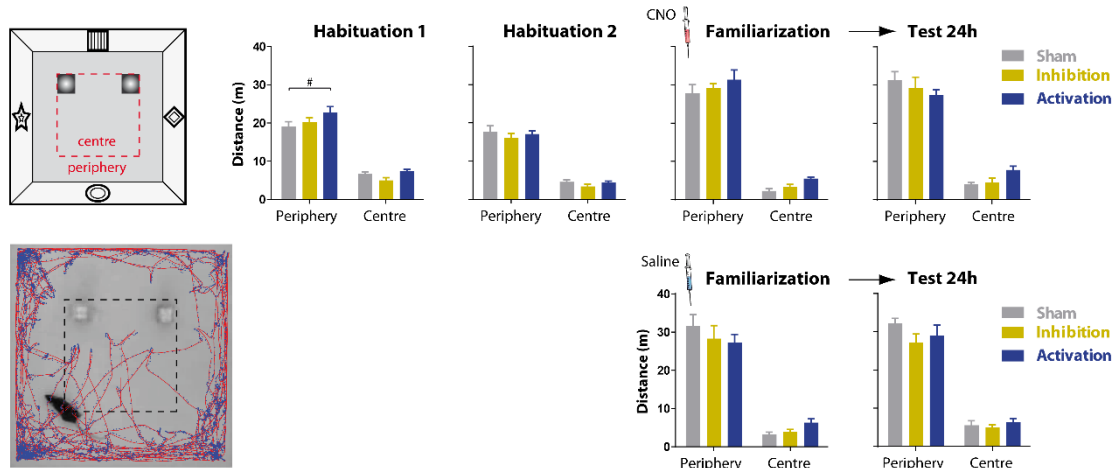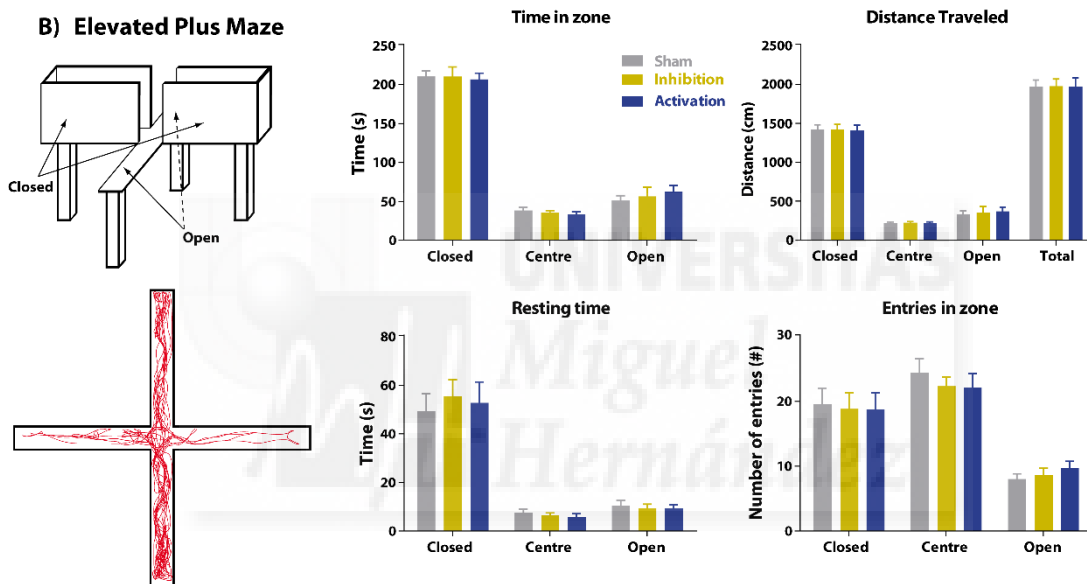
Figure 5.16. Locomotion and anxiety parameters when modulating hilar PV interneurons. A) Mice locomotion in the NLO task in the centre vs periphery of the arena (left, up), analyzed with a custom-made script by Elena Pérez Montoyo (left, bottom). The analysis shows no differences between Sham (n=13) PV-Inhibition (n=12) and PV-Activation group (n=12) in any session, whether we modulate hilar PV interneurons (CNO injection) or not (saline injection). # Indicates p = 0.04, but its low η_p^2 (0.08) and 1-β (0.41) make it not trustable. B) Control parameters in the EPM (left, up) for evaluating anxiety under hilar PV interneuron modulation. No differences were found between groups in the tracking (left, bottom) regarding the time spent, distance travelled, resting time, nor in entries in open vs closed arms or the centre of the arena. Sham (n=14), PV-Inhibition (n=11), PV-Activation (n=13).

Behavioural data collation.

Behavioural data probe that CNO injection, and therefore the hilar PV interneuron modulation, does not change control parameters as locomotion, exploratory behaviour, thigmotaxis and anxiety.

Regarding contextual learning; modulating hilar PV-Interneurons during the encoding of new spatial information modifies memory coding. When injecting CNO before the encoding, Sham animals explore more the new object's location when tested 24h after, indicating that the animals learn normally; PV-Inhibition group animals explore even more the new object's location than Sham ones; while PV-Activation groups animals explore the displaced object and the static one equally. The interpretation is that the hilar PV inhibition, by increasing information transmission in the hippocampus and associated structures, improves spatial learning by facilitating the encoding of new information. Accordingly, activation of PV cells prevents memory formation. As a control, the same group of animals learned normally and homogeneously across groups when injecting saline instead of CNO. Hilar PV-interneurons modulation during consolidation or retrieval of previously encoded spatial information in the NLO task cause no detectable effects on spatial learning, suggesting that these interneurons, and their role in regulating functional connectivity, are not required during the consolidation or retrieval of acquired information.

5.4.- Granule cell cFos expression during NLO task with PVbc modulation.

We have shown that decreasing the inhibitory tone of PV cells in the dentate gyrus increases the excitability of granule cells, facilitates its firing promoting communication in the hippocampus and enhancing the functional coupling in a network of brain structures necessary for memory formation. We have further shown that PV cell inhibition potentiates memory encoding, and its activation prevents memory formation, even though dentate gyrus synapses are functionally intact.

An intriguing question is why the resting inhibitory tone in the dentate gyrus is suboptimal for memory encoding, as our results appear to suggest. Lower inhibitory control of PV interneurons over granule cells firing would render dentate gyrus-dependent learnings more efficiently. One possibility is that the PV-cell population keep the engram of recruited GCs on its optimal size to convey the necessary information for CA3 to encode the memory while assuring that different contexts activate non-overlapping GC engrams. So, preserving pattern separation. Therefore, by inhibiting PV-cells, we may increase the size of the granule cells engram, and so the precision and detail of the encoded context, and therefore facilitating its retrieval during the testing phase, but compromising at the same time the separability of similar context. This hypothesis predicts that the engram size, measured as the number of cFos+ granule cells in the dentate gyrus, should be increased by PV cell inhibition, and decreased by its activation. Therefore, we did the cFos experiments described in material and methods section 3.2 to test this prediction.

5.4.1.- Exploration in NLO task induces cFos expression.

First, we confirmed that our NLO protocol produces a detectable level of cFos expression in the dentate gyrus and the hippocampus, by comparing cFos labelling in Sham animals (that received CNO injection and did the NLO task) with home-cage littermates (that received CNO injection but did not the NLO task) (Figure 5.17A).

Statistical *t*-test comparison probes that animals that underwent NLO task increases the cFos expression in hippocampus compared with those that received CNO, but remain in their home-cage [$t_9 = 3.68$, $p = 0.005$, $r^2 = 0.6$, $1-\beta = 0.98$] (Figure 5.17B).
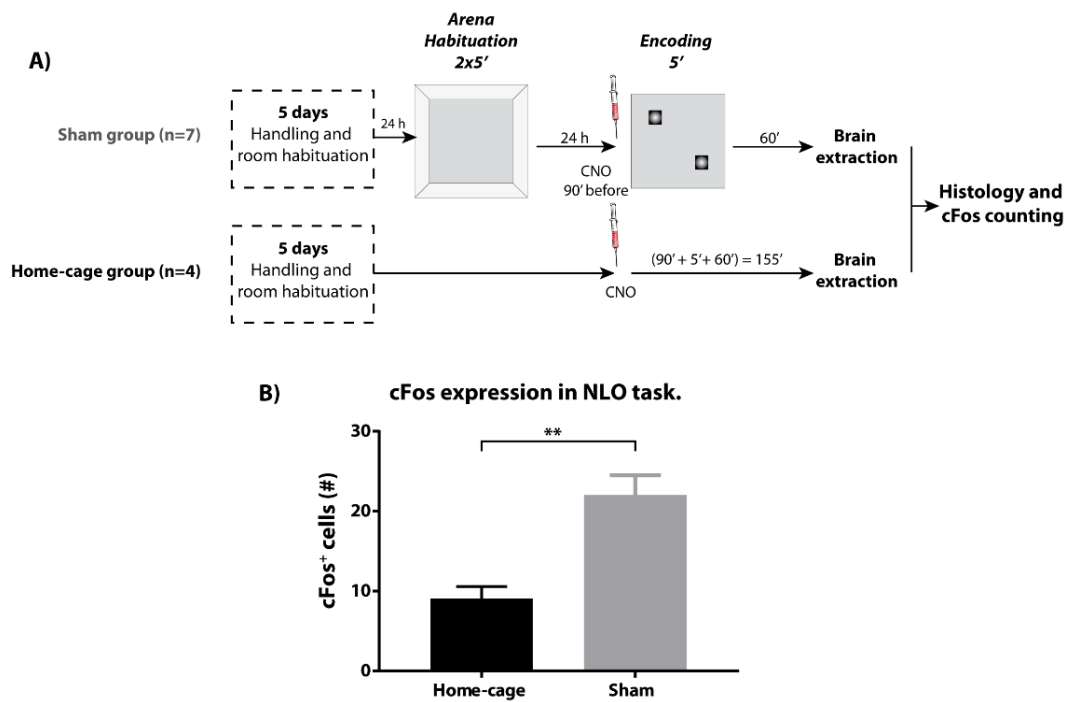
Figure 5.17. cFos expression after spatial encoding in the NLO task. A) Schematic representation of the experimental differences between Sham and home-cage groups. The first one underwent the task while latter one did not. B) Bars diagram representing quantitatively the averaged by group cFos expression in hippocampus. ** indicates $p = 0.005$.

5.4.2.- Granule cells engram's size remains equal when modulating hilar PV cells.

We next investigated whether the total number of cfos+ cells in the dentate gyrus and hippocampus changes under PV-cell activity modulation. Normality test for cFos$^+$ granule cells labelled in dentate gyrus failed in PV-Inhibition and PV-Activation group data (Shapiro-Wilk test; [$W_6 = 0.77$, $p = 0.02$] for PV-Inhibition, and [$W_5 = 0.71$, $p = 0.01$] for PV-Activation group) and the analysis of its kurtosis evidenced a leptokurtic distribution (kurtosis = 3.85 and 4.54 respectively). So that we used a Kruskall-Wallis test instead the ANOVA when comparing cFos$^+$ labelled cells in dentate gyrus. Normality, and rest of the control parameters, in CA3 and CA1 cFos$^+$ data passed the tests and so were analysed with one-way ANOVA.

As before (Figure 5.17), exposure of the animals to the NOL task is sufficient to induce cFos expression (Figure 5.18A-C). But, importantly and unexpectedly, the number of GCs recruited in the memory engram remain equal in all the groups in dentate gyrus [$H_{2,17} = 0.94$, $p = 0.62$], in CA3 [$F_{2,17} = 0.12$, $p = 0.88$] and in CA1 [$F_{2,17} = 1.22$, $p = 0.32$]. Those data were analysed in blind conditions by two different experimenters, and later on, confirmed by counting cFos$^+$ cells automatically. In addition, it was replicated, independently, by an ongoing work in the lab (data not shown).

5.4.3.- Labelling intensity is higher in PV-Inhibition group in DG, but not in CA3.

We also exteracted information about the intensity of the labelling with Imaris software®. The preliminar analysis revealed that all the groups failed in normality test for dentate gyrus data (Sham [W_{49} = 0.94, p = 0.017], PV-Inhibition group [W_{65} = 0.93, p = 0.0017] and PV-Activation group [W_{93} = 0.94, p = 0.0004]), and the two experimental groups failed normality test for CA3 data (PV-Inhibition group [W_{103} = 0.95, p = 0.0013], PV-Activation group [W_{105} = 0.96, p = 0.0068]). Because of that we applied a non-parametric Kruskall-Wallis test.

Comparisons between groups probed that the intensity of the labelling changes in dentate gyrus [$H_{2,208}$ = 26.57, p < 0.0001] but not in CA3 [$H_{2,292}$ = 3.98, p = 0.13], although the number of cells labelled does not when modulating the activity of PV interneurons (previous section). Multiple comparisons revealed that cFos intensity labelling increases in dentate gyrus only in PV-Inhibition group (PV-Inhibition vs Sham, p = 0.01; PV-Inhibition vs PV-Activation, p < 0.0001; Sham vs PV-Activation, p = 0.31) (Figure 5.18D). It was also replicated by an ongoing work in the lab (data not included).
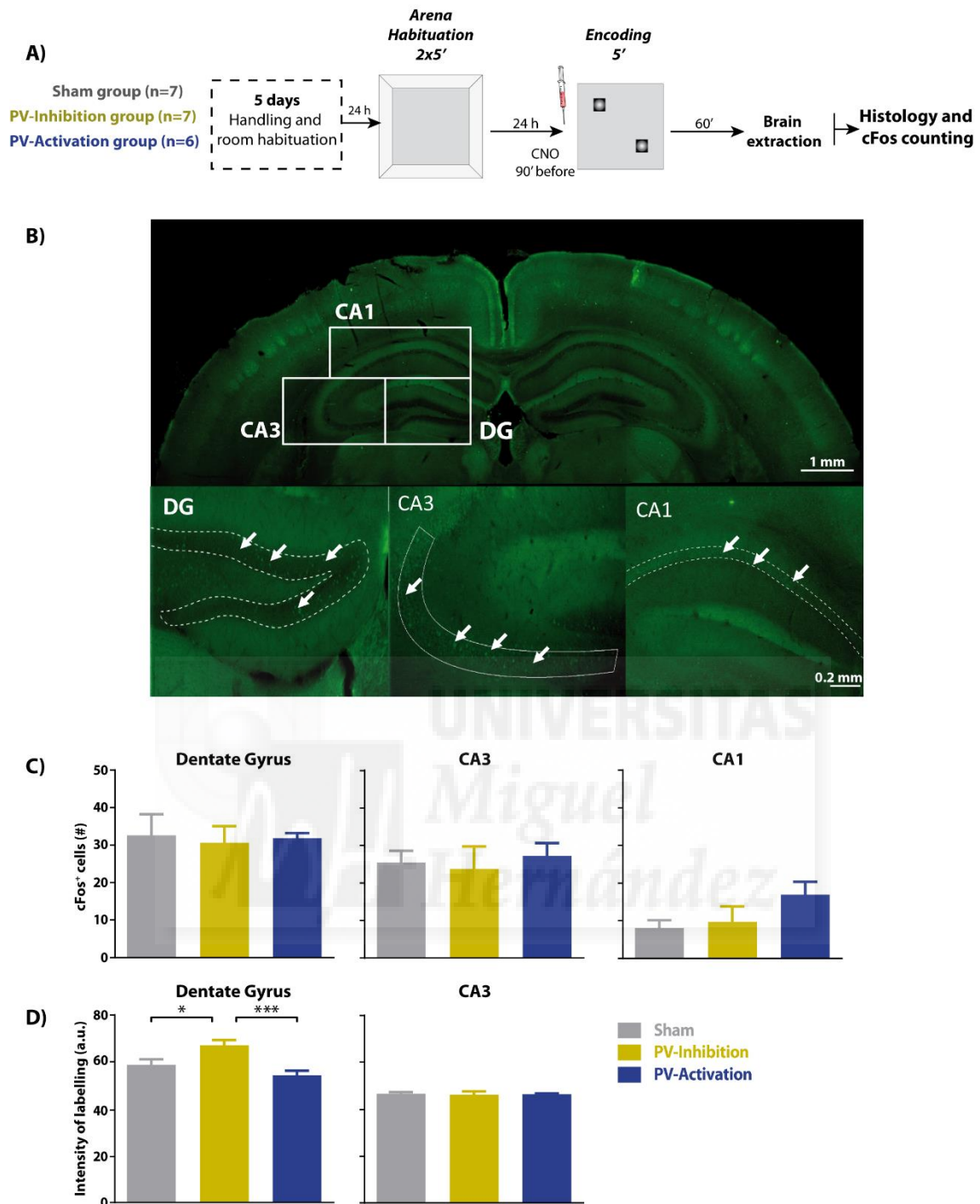
Figure 5.18. cFos expression after spatial encoding in the NLO task when modulating hilar PV interneurons. A) Schematic representation of the experimental procedure. B) Confocal micro-pictures showing the dentate gyrus (DG), CA3 and CA1 region from where cFos positive cells were counted. Micro-pictures taken by Raquel García Hernández. C) cFos counting bars diagrams of labelled granule (DG) or pyramidal cells (CA3 and CA1) averaged by animal and then by group. D) Bars diagram representing quantifications of the labelling intensity of the neurons from two randomize animals per group, each neurons is considered as an individual for the total *n* (dentate gyrus: Sham, n = 51, PV-Inhibition group, n = 67, PV-Activation group, n = 96; CA3: Sham n = 85, PV-Inhibition group, n = 104, PV-Activation group, n = 106). * indicates *p* < 0.05, *** indicates *p* < 0.001.

5.5.- SETAmaze. Spatial Evaluation Task for investigating pattern separation

The cFos results presented in the previous section indicate that PV cell activity does not affect the engram size in the dentate gyrus and hippocampus, at least in our experimental conditions. Following our argument in the previous section, pattern separation in these conditions should not be affected either. We wanted to evaluate pattern separation upon inhibition or activation of PV interneurons. After a search in the databases, we did not find a behavioural test already established and that we consider good enough for our objectives. So that, we decided to develop a new behavioural task. The task and SETAmaze apparatus are described in material and methods section 3.3.

5.5.1.- Control experiments results.

Pattern separation task.

Before the studies with PV cell manipulation, we did a series of experiments to establish the optimal distance at which objects may be gradually moved to calibrate the difficulty of the task (established in 5 cm steps) and to refine the protocol for proper experiments (data not shown). Once optimized, we let control animals to encode a specific position of the objects in the arena and sequentially moved one of the objects, in intervals of 5 min per trial, to evaluate the distance at which animals realize the movement, as evidence of pattern separation. The target was to set the specific distance at which control mice realize this change in the environment when carrying out a short-term memory task involving pattern separation. For half of the animals, the movement of the object was done from the centre to the corner of the arena, and *vice versa* for the other half.

Comparisons between both movements reveal no differences in any position of the objects regarding the total time that animals spend exploring both objects (Figure 5.19A) [$F_{1,15}$ = 0.04, p = 0.94]. The ratio of exploration (exploration index: time exploring displaced object / total time exploring both), along the distinct positions, reveal that the animals explore both objects equally, until the displaced object is separated 15 cm from the original position, whether the movement is from corner-to-centre or from centre-to-corner [$F_{4,60}$ = 18.67, p < 0.0001, η_p^2 = 0.32, 1-β = 1] (corner-to-centre: starting point vs 5cm position [t_{60} = 0.64, p = 0.99], 5 cm vs 10 cm [t_{60} = 0.65, p = 0.99], 10 cm vs 15 cm [t_{60} = 5.8, p = 0.001], 15 cm vs 20 cm [t_{60} = 3.32, p = 0.14]; centre-to-corner: starting point vs 5cm position [t_{60} = 0.01, p > 0.99], 5 cm vs 10 cm [t_{60} = 0.98, p = 0.95], 10 cm vs 15 cm [t_{60} = 5.23, p = 0.004], 15 cm vs 20 cm [t_{60} = 0.48, p = 0.99]) (Figure 5.19B-C). Animals realize the object's movement at 15 cm from original position without statistical differences between groups [$F_{1,15}$ = 0.56, p = 0.46] (Figure 5.19D).

SETAmaze, control experiment. Short-term pattern separation task.
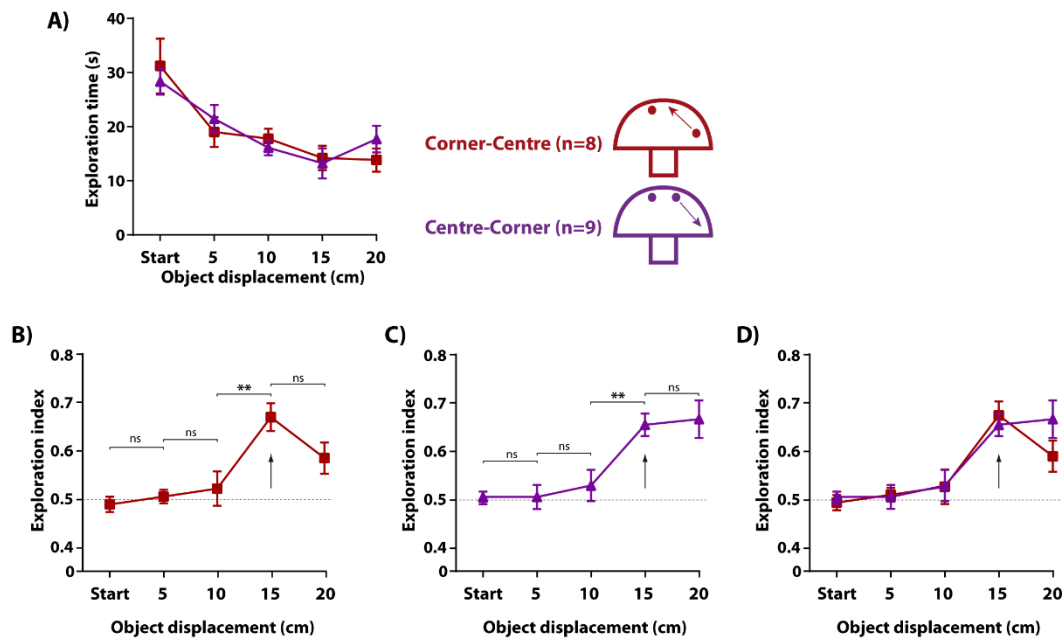
Figure 5.19. SETAmaze pilot studies results; short-term memory pattern separation task. A) Graphical quantification of total time that mice spend exploring both objects during the SETAmaze task, by each position, whether the object's movement is from corner-to-centre or centre-to-corner. B-C) Graphical quantifications of exploration index (time mice spend exploring displaced object divided by total time exploring both), comparing performance on each displacement. D) Same than in B and C, but comparing performance between groups. No statistical differences between groups; all of them realize the object's displacement at 15 cm from starting position. Arrow indicates the point at which animals realize the movement. ** indicates $p < 0.005$.

Long-short term memory interactions in pattern separation task.

Then we compared animal's performance between previously described pilot data (centre-to-corner) with Sham group from the experimental animals. The main difference between both is that pilot animals carried out the task in the same session (purely short-term memory), while Sham animals encoded the object's starting position 90 min after CNO injection, and perform the rest of the trials 24 h later (Figure 5.20A). Two options were possible: 1) If Sham animals use only short-term memory to do the task, —for instance, if they don't remember the object's starting position (encoded 24 h before), or the task does not require to evoke that memory— then animals would realize the object's movement when it is displaced 15 cm from the initial place in the rest of the trials (so, 20 cm away from starting position), or 2) if Sham animals realize object's movement exactly at the same distance than pilot ones (previously set in 15 cm), it necessarily means that they are comparing the new contextual information (related to sequential object's movements) with the object's position previously encoded 24 h before (long-short memory interactions).

Between groups comparison of the total exploration time revealed no differences in general [$F_{1,20} = 1.67$, $p = 0.21$], when taking into account the linear temporal dynamic of the data across the trials. But if we compare between groups only the first movement of the object (5 cm), Sham animals explore a bit less than control ones in pilot studies [$t_{100} = 2.98$, $p = 0.017$] (Figure 5.20B). 5 cm is the first Sham animal's encounter with the object after the 24 h between sessions; it may reflect a loss of saliency or decreased motivation (because they already know the task). Nevertheless, whether we consider the differences in total exploration time at 5 cm

or not (which could be secondary to our research target regarding pattern separation), Sham animals realize the object movement also at 15 cm of displacement from starting point [$F_{4,80}$ = 26.19, p < 0.0001, η_p^2 = 0.44, 1-β = 1]. They spend equal time exploring both object at the starting point vs 5 cm [t_{80} = 1.104, p = 0.93], at 5 cm vs 10 cm [t_{80} = 1.09, p = 0.93], but spend more time exploring the new location when the object is displaced, as in previous pilot studies, 15 cm [t_{80} = 5.47, p = 0.002]; without differences when comparing 15 and 20 cm [t_{80} = 1.94, p = 0.64] (Figure 5.20C). Sham group and previous pilot data present the same progression (Figure 5.20D), without differences between groups at any point [$F_{1,20}$ = 1.79, p = 0.2]. It reveals that all the animals realize the object displacement at 15 cm from the starting position, whether it was encoded 24 h ago, or 5 minutes ago, confirming the previously explained option 2, and allowing us to compare long and short-term memory interactions involving a pattern separation task.

SETAmaze. Long-Short term pattern separation memory interactions control experiment.
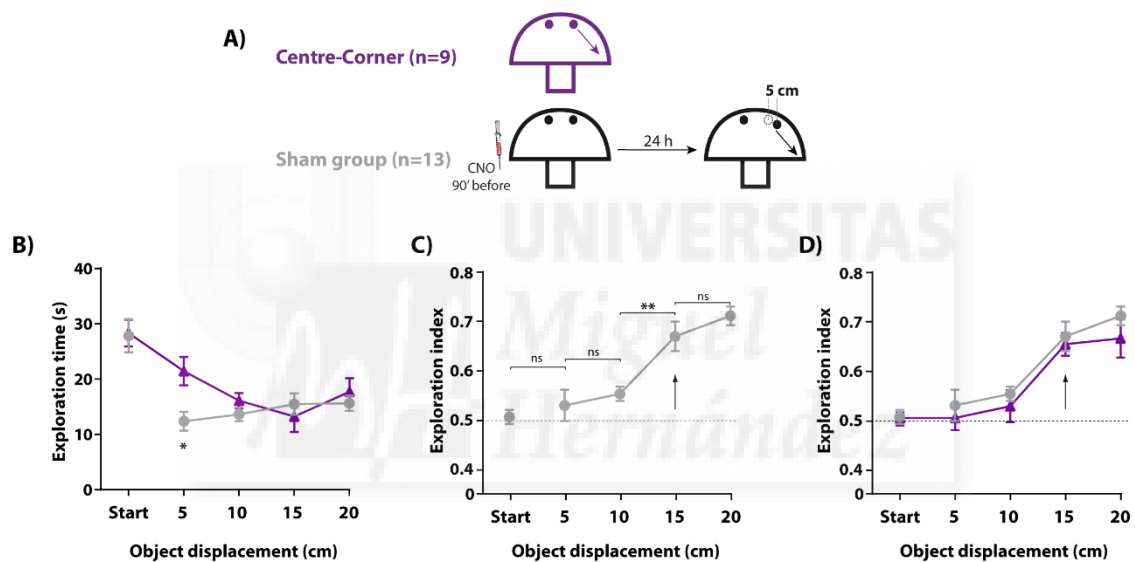
Figure 5.20. Long-short term memory interaction results in the SETAmaze. A) Schematic representation of mice's protocol compared. B) Graphical quantification of total time that mice spent exploring both objects during the SETAmaze task. C) Graphical quantifications of exploration index (time mice spend exploring displaced object divided by total time exploring both), comparing performance on each displacement. D) Same than in C, but comparing performance between groups. No statistical differences between groups; all of them realize the object's displacement at 15 cm from starting position. Arrow indicates the point at which animals realize the movement. * indicates p < 0.05, ** indicates p < 0.005. No connecting line between start and 5 cm position data in Sham group indicates 24 h of delay.

5.5.2.- Hilar PV interneurons modulation does not compromise pattern separation.

In previous data we confirmed that Sham control animals realize the environmental changes at the same point (15 cm from starting position) than pilot ones, even if the first ones encoded the starting position of the object 24 h before the test. Now we compare between experimental animals, in which we modulate hilar PV interneurons (both by activation and by inhibition), and Sham ones (Figure 5.21A); all of them with 24 h of delay between encoding modulation and short-term pattern separation test. Total exploratory time, in absolute terms,

does not change between groups [$F_{2,35}$ = 1.18, p = 0.31] in any temporal point (Figure 5.21B). However, the amount of time that animals spend in each object does vary between groups [$F_{2,34}$ = 3.66, p = 0.03, η_p^2 = 0.1, 1-β = 0.99] (Figure 5.21C); exploration ratio between objects shows that all the groups explore the objects equally in the starting position, at 5 cm and at 10 cm (starting point: Sham vs PV-Inhibition [t_{170} = 0.16, p = 0.99], Sham vs PV-Activation [t_{170} = 0.82, p = 0.83], PV-Inhibition vs PV-Activation [t_{170} = 0.62, p = 0.89]; 5 cm: Sham vs PV-Inhibition [t_{170} = 0.56, p = 0.91], Sham vs PV-Activation [t_{170} = 1.82, p = 0.4], PV-Inhibition vs PV-Activation [t_{170} = 1.18, p = 0.68]; and 10 cm: Sham vs PV-Inhibition [t_{170} = 0.98, p = 0.76], Sham vs PV-Activation [t_{170} = 1.16, p = 0.68], PV-Inhibition vs PV-Activation [t_{170} = 2.09, p = 0.3]), but while Sham group and PV-Inhibition group explore more the displaced object when moved 15 cm from initial position, PV-Activation group does not (Sham vs PV-Activation group [t_{170} = 4.46, p = 0.005]; PV-Inhibition vs PV-Activation [t_{170} = 4.99, p = 0.0015]; Sham vs PV-Inhibition [t_{170} = 0.72, p = 0.86]), presenting no differences between groups at 20 cm of displacement (Sham vs PV-Inhibition [t_{170} = 0.92, p = 0.79], Sham vs PV-Activation [t_{170} = 0.62, p = 0.89], PV-Inhibition vs PV-Activation [t_{170} = 1.52, p = 0.53]).

PV-Activation group requires one object's displacement more (until it reaches 20 cm from starting point) to realize the environmental changes, as evidenced by the repeated measures analysis [$F_{4,136}$ = 44.25, p < 0.0001, η_p^2 = 0.36, 1-β = 1] Sham and PV-Inhibition groups recognize the changes in the displacement at 15 cm (Sham group: starting point vs 5 cm [t_{136} = 1.01, p = 0.95], 5 cm vs 10 cm [t_{136} = 1, p = 0.95], 10 cm vs 15 cm [t_{136} = 5, p = 0.0049] and 15 cm vs 20 cm [t_{136} = 1.77, p = 0.71]; PV-Inhibition group: starting point vs 5 cm [t_{136} = 0.49, p = 0.99], 5 cm vs 10 cm [t_{136} = 2.57, p = 0.36], 10 cm vs 15 cm [t_{136} = 4.33, p = 0.02] and 15 cm vs 20 cm [t_{136} = 1.84, p = 0.68]) while PV-Activation groups does so at 20 cm (starting point vs 5 cm [t_{136} = 1, p = 0.99], 5 cm vs 10 cm [t_{136} = 1.74, p = 0.73], 10 cm vs 15 cm [t_{136} = 1.34, p = 0.87] and 15 cm vs 20 cm [t_{136} = 6.03, p = 0.0003]) (Figure 5.21D-F).
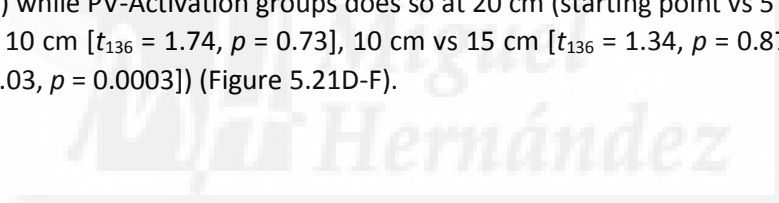
SETAmaze. Hilar PVbc modulation in Long-Short term pattern separation memory interactions.
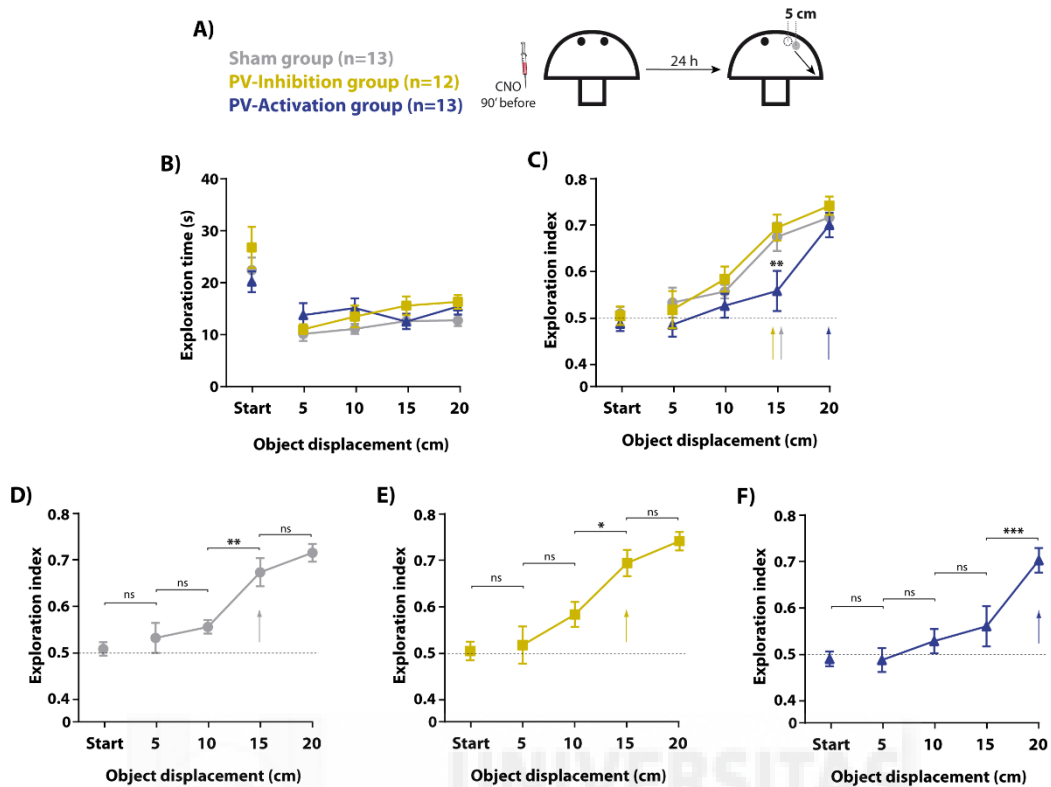
Figure 5.21. Mice performance in the SETAmaze when modulating hilar PV interneurons. A) Schematic representation of behavioural task and groups. B) Graphical quantification of total time that mice spent exploring both objects. C) Graphical quantifications of exploration index (time that the mice explore displaced object divided by total time exploring both). D-F) Same than in C, but comparing performance within groups (repeated measures in Sham group, D, PV-Inhibition group, E, and PV-Activation group, F. Coloured arrows indicate the point in which animals realize object's movement. * indicates $p < 0.05$, ** indicates $p < 0.005$, *** indicates $p < 0.001$. No line between start and 5 cm position indicates 24 h of delay.

Altogether, these data point that hilar PV inhibition does not compromise the pattern separation when comparing new entering spatial information with a previously encoded one, as mice performance in this group is equivalent to Sham mice. While the activation of hilar PV interneurons, again, seems to prevent the encoding of spatial information (when encoding the starting position), so that in the test trials (long-short term memory interaction in the pattern separation task) they require one more displacement to discriminate the object's movement. The result is consistent with the finding of PV interneuron activation impairing memory encoding (section 5.3.1). However, the results obtained in the PV-Inhibition group in the SETAmaze bring an apparent contradiction. We show that this manipulation preserves pattern separation and, in good accordance, the number of cFos cells in the engram is also preserved, so that generalization of memory as a consequence of disinhibition in the system can be discarded. However, we have also shown that this manipulation increases memory encoding in the NLO task, but exploration of the displaced objects in the SETAmaze was undistinguishable between Sham and PV-inhibited animals. Our prediction would have been that, in the presence of intact pattern separation, facilitation of functional connectivity induced by PV-inhibition should have improved memory formation and likely pattern separation in the SETAmaze too. We speculated that the small displacement of the object (5 cm) 24h after the first encoding session was too challenging for the animal to discriminate, and also that this

new and ambiguous short-term representation of the context could have interfered with the posterior sequence of object displacements, resulting in a delayed discrimination. So we repeated the SETAmaze task but now displacing the object 10 cm in the first movement 24h after the encoding phase. We used another different batch of PV-Inhibition group animals, with counterbalanced presentation of the objects and 1 week between experimental (CNO injection) and control (saline injection) experiments. Animals were controls of themselves.

5.5.3.- Hilar PV interneurons inhibition improves long-short term spatial pattern separation.

Statistical analysis within the same group, but comparing PV-Inhibition group animal's performance with CNO injection vs Saline (Figure 5.22A), reveal no differences in absolute time exploring both objects [$F_{1,14}$ = 1.16, p = 0.29] (Figure 5.22B), in any location. Nevertheless, repeated measures analysis shows different exploration ratio between the displaced object and the static one, along the positions [$F_{3,42}$ = 16.07, p < 0.0001, η_p^2 = 0.35, 1-β = 0.99]. When inhibiting hilar PV interneurons, mice realize the object's movement in the first displacement (start position vs 10 cm [t_{42} = 6.85, p < 0.0001], 10 cm vs 15 cm [t_{42} = 0.59, p = 0.97] and 15 cm vs 20 cm [t_{42} = 0.46, p = 0.98]) (Figure 5.22C). While same animals, receiving saline instead CNO, realize object's displacement at the normal 15 cm, as in previous experiments (start position vs 10 cm [t_{42} = 0.28, p = 0.99], 10 cm vs 15 cm [t_{42} = 4.77, p = 0.0087] and 15 cm vs 20 cm [t_{42} = 1.74, p = 0.61]) (Figure 5.22D). Comparisons between groups probe that inhibition of hilar PV interneurons makes the mice to improve the pattern separation when confronting new information with previously memorized (having enhanced its encoding) [$F_{1,14}$ = 5.67, p = 0.0023, η_p^2 = 0.21, 1-β = 0.94], helping them to recognize object's movement at 10 cm, while if hilar PV-Interneurons are not inhibited the animals realize the movement at 15 cm of displacement (PV-Inhibition group vs CNO vs Saline: starting point [t_{56} = 0.77, p = 0.9], 10 cm [t_{56} = 3.52, p = 0.0034], 15 cm [t_{56} = 0.02, p > 0.99]vs 20 cm [t_{56} = 1.42, p = 0.5]) (Figure 5.22E).

SETAmaze. Hilar PVbc inhibition with 10 cm of initial displacement.
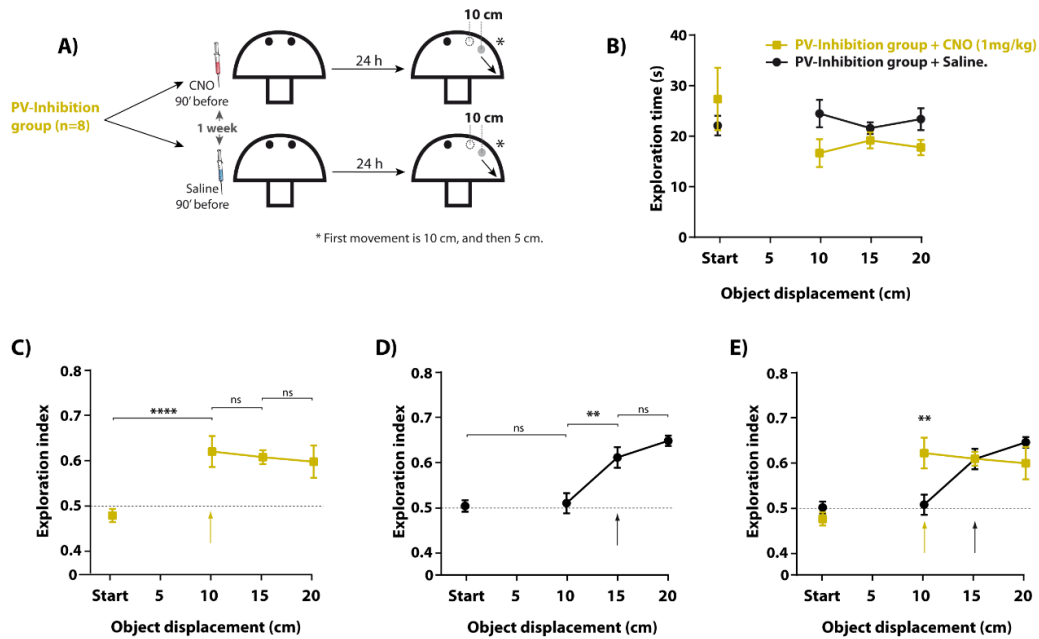
Figure 5.22. Mice performance in the SETAmaze when inhibiting hilar PV interneurons. A) Scheme of the behavioural task. Same animals used for both experiments but injecting CNO or Saline. One week between experiments. B) Quantification of total time that mice spent exploring both objects. C) Quantifications of exploration index (time mice explore displaced object divided by total time exploring both) when inhibiting hilar PVbc for the encoding of the starting position. D) Same than in C but without PVbc inhibition. E) Same data than in C and D but for between groups comparisons. Coloured arrows indicate the point in which animals realize object's movement. ** indicates $p < 0.01$, **** indicates $p < 0.0001$. No line between start and 10 cm position indicates 24h of delay.

SETAmaze data collation.

As collation of SETAmaze results, first, we can say that we have developed a successful new task to evaluate the pattern separation when it requires to compare information in a short-term memory task (as realizing soft changes in the environment) with previously encoded spatial memories. We did so to answer the question about how our experimental manipulation over the hilar PV interneurons affect the pattern separation (dentate gyrus associated function), given the previous results prevented herein and motivated by the lack of proper tasks in the bibliography.

Once tested the mice's performance in pilot studies, we carried out the SETAmaze with experimental mice; modulating hilar PV interneurons. The activation of hilar PV interneurons precludes memory encoding (replicating previous data presented in section 5.3), while hilar PV interneuron inhibition enhances memory encoding (also replicating previous data), which leads to better discrimination of soft changes in the environment, improving the pattern separation function.

VI.- DISCUSSION.

Synaptic changes in the dendrites vs inhibitory modulation.

By far, the largest amount of work in the physiology of memory has focused on the study of synaptic plasticity in excitatory synapses. However, compelling evidence has also accumulated indicating that other cell types and neurotransmitters, notably inhibition, as well as different mechanisms, such as cell excitability changes, are also fundamental in this process. Even from the very beginning of the LTP studies (and maybe neglected), Bliss and Lomo (1973) declared that *the potentiation observed in the PS couldn't be explained wholly in terms of potentiation of the EPSP on excitatory synapses exclusively*. Something more needs to be involved on that. In that sense, LTP induction causes both, a well-known increase in the transmission between excitatory synapses, but also a transitory decrease of the inhibitory tone[290,293]. Understanding how inhibition is tuned, and what are its functional implications, could be as critical as the study of the excitatory dendritic changes related to memory. Altering the inhibitory/excitatory ratio may modify dynamically the way in which activity propagates between nodes in the brain network, and for that, interneurons could be more efficient than having different plastic machinery on each dendrite.

In this work, pharmacogenetic manipulation on hilar PV cells modulates the perisomatic inhibition on the granule cells, while preserves the synaptic functionality. It is maybe not surprising, given the PVbc anatomical connectivity, but has significant theoretical implications for the conclusions presented herein, mainly related to the behavioural and cFos experiment data. It also implies that our experimental approach differentiates the study of the inhibitory regulation in the dentate gyrus, from the more common study of excitatory synaptic plastic[110,111].

Regarding inhibition and how our manipulation may be reflected in the circuit, at least two explanations are possible:

1) The local inhibitory activity (dominating the gamma activity, and related to PVbc[162,250]) over-imposes some temporal windows in which, in the theta rhythm (related with inputs integration in dentate gyrus and hippocampus[159,161]), the excitatory neurons may spike. It has been called the theta-gamma coupling and is thought to underlie neuronal synchronization[164,165]. By reducing the inhibitory tone in our experiments, the temporal precision of this mechanism is expected to decrease, compromising synchronic firing. As we did not find any performance deficiency in the animals when reducing the perisomatic inhibition in the dentate gyrus, by contrary, we find enhanced memory formation, we suggest that synchronization though a theta-gamma mechanism could be more relevant in other brain areas, but not the dentate gyrus, or at least not the major physiological function controlled by PV interneurons in this brain structure. After all, the dentate gyrus has a peculiar design; it presents neurogenesis[151,152], low level of auto-associative recursivity in its connections —acting mainly as a transmitter filter for inputs orthogonalization[139]— and specially high levels of hyper-polarization[140].

2) The local inhibitory activity also may act as a filter for stimuli selection[294,295]. Pioneering work in sensory systems (for a review see Letzkus et al., 2015[294]) showed that the interplay between incoming excitatory inputs to the neocortex and the local inhibition recruited in feed-forward and feed-back circuits, sets a threshold for input specificity, so that only sufficiently strong inputs pass the inhibitory control and exert an effective postsynaptic activation that propagates in the system[296]. Accordingly, a high inhibitory tone (as shown in the dentate gyrus) that is tuned by the input activity (feedforward inhibition) may act as a filter to select salient

inputs dynamically (dynamic-range filter[295]). In this context, PV interneurons have been proposed as a critical element of the visual circuits adjusting the input-output relationships[297,298].

Explanations 1 and 2 may not be exclusive, but complementary. Also, their relevance may differ depending on particular local circuits in the brain (for instance, CA1 connectivity may require more coordination in time, so that the inhibitory reduction might impair its functioning). Our data in the dentate gyrus fit with the explanation 2 about how inhibition may tune activity propagation in this circuit. The high input selectivity, together with its highly reliable synaptic contacts onto CA3 pyramidal neurons, may assure efficient information transfer in the network.

Overall, by modulating PV perisomatic inhibitory tone in the dentate gyrus, we may tune inputs selectivity and so increasing or preventing memory encoding.

Inhibitory control over cell firing. The importance of the communication.

In the dentate gyrus, we regulate granule cells spiking by tuning hilar PV interneurons activity, not affecting the dentate gyrus EPSP in any group. When activating them, granule cells population spike decreases. This effect has a moderate magnitude, likely reflecting high inhibitory tone in the dentate gyrus at rest. Accordingly, when inhibiting hilar PV interneurons, granule cells population spike drastically increases. Changes in granule cell firing will affect the next rele in the circuit, the CA3 region. Thus, increased activity after PV inhibition is expected to arrive, as it does, to the CA1 region. However, the population spike in CA1 was enhanced above any expected prediction (Fig. 5.8) involving exclusively the facilitated trysinaptic propagation. It is evident because, for instance, the PS response in CA1 was saturated with medium-low stimulation intensities applied in perforant patway, at which a comparable-in-amplitude PS in dentate gyrus in control conditions (Sham group or pre-CNO) generated no response in CA1 PS. While the mechanism for this supralinear propagation is yet not known, we speculate that It could be achieved by a synergic increasing in the number of granule cells that fire in response to perforant path stimulation while inhibiting basket cells (sharper population spike), or by the coordination in time of inputs arriving to CA1 in the trisynaptic pathway, the disynaptic CA3-CA1 connexion and/or the monosynaptic temporoamonic pathway, because the dentate gyrus PS also advances about 0.5 ms upon PV inhibition.

Although not surprisingly, it is interesting that dentate gyrus PS is faster when inhibiting hilar PV interneurons. It implies that activity propagation also arrives at CA3 and CA1 earlier so that it can be integrated closer in time with the direct entorhinal input to CA3 and the temporo-ammonic input to CA1. In that sense, Puoille and Scanziani (2001)[216] informed about the very narrow temporal window that hippocampal pyramidal cells have for inputs integration (less than 2 ms, but being especially evident at 1 ms). Its short delay is conditioned mainly by feedforward inhibitory local circuits, which are stronger perisomatically than dendritically. It allows the dendrites to sum incoming activity broader in time and enforces the soma to act as a precise temporal coincident detector. So that, coming back to our data, by decreasing perisomatic inhibition in dentate gyrus granule cells, we make them to spike faster, boosting the information flow and overtaking 0.5 ms in dentate gyrus to CA3 transmission. It may accelerate its transfer to CA1, making CA1 integration to be more effective, favouring hippocampus to communicate with other extra-hippocampal structures[216,299].

The importance of the inter-nodal communication is enormous, of current interest for the theory, and underlies to almost all (if not all) cognitive functions in the brain. There exists a theoretical controversy about how a brain encodes new memories. On the one hand, some researches support that we have isolated feature neuronal detectors, emerging mainly from single neurons data, starting with Barlow, in 1954[300]. On the other hand, other researches support the idea that the brain works in a distributed way, interconnecting neurons that tune their activity to process situations by distributed cells assemblies, starting with Lorente de Nó (1934)[83] and Donald Hebb (1949)[15]. These cell assemblies have nodes of particular relevance for a specific cognitive function, so that they may integrate easily feature detectors but not the other way around. For cell assembly supporters, the nodes of particular relevance for encoding memories are inferotemporal cortex, prefrontal cortex and hippocampus[301]. Our experimental manipulation, when inhibiting hilar PV interneurons, increase internodal communication between the hippocampus, other temporal structures and the prefrontal cortex.

The information transmission from the hippocampus to those other nodes, especially with prefrontal cortex, is very important, as it has been related to other aspects of the mnemic process as consolidation[302–304], as well as a linker of memory-related aspect with other cognitive functions as working memory[305,306], emotional regulation[307], attention[308], decision making[307] and many others (for a review; Sekeres et al, 2018[309]). Hilar PVbc inhibition, by boosting hippocampal processing, also increase long-range hippocampal connectivity with other medial temporal lobe structures and with subcortical regions as accumbens nucleus, amygdala and striatum. All of them have been somehow related to different features of the memory[310–313].

Very interestingly, our obtained fMRI evoked maps, after hilar PVbc inhibition, is very similar to the one obtained when inducing LTP in the dentate gyrus[136]. However, we are not inducing LTP; just tuning the perisomatic inhibition. Of particular interest is the BOLD response activation in the prefrontal cortex, matching with our electrophysiological data, and with the theoretically proposed node of especial relevance for memory processing in cell assemblies distributed networks[301]. Connectivity with prefrontal cortex would integrate hippocampal processed information with other high cognitive functions and would mediate in memory consolidation[314,315], while hippocampus and particularly dentate gyrus are mainly involved in encoding.

Hilar PV interneurons control memory encoding.

Since Milner and Scoville informed about HM, medial temporal lobe structures, and especially hippocampus and dentate gyrus, are seen as crucial regions involved in the encoding of new memories. They are mainly related to the ability of encoding events and episodes that take place in a specific location[51,53,62,81]. This implication would be emphasized when the encoding is automatic —not necessary goal-directed— and referred to where, what and when events.

NLO behavioural task was explicitly chosen to study the PVbc regulation of dentate gyrus function associated with memory and learning. This task is dentate gyrus dependent[64] and allows automatic —not goal-directed— spatial memory testing. Also, our approach enables the experimental segregation for modulating hilar PVbc during the encoding, the consolidation or the retrieval.

When inhibiting hilar PVbc during the encoding, mice improve their performance, while its activation prevents memory encoding. However, all the animals perform normally when modulating hilar PVbc interneurons during consolidation or retrieval. Those results match with the theory in pointing the dentate gyrus as critical node for encoding new spatial memories and give one step more by implicating PVbc as critical regulators of its activity, while its implication during consolidation or retrieval is irrelevant, as they depend more from other regions once it has been encoded. At least our data point to a no implication of hilar PV interneurons on consolidation or retrieval of contextual memories. Probably the consolidation would require more the hippocampal-neocortical interactions[49], so that the dentate gyrus inflexion over the already formed distributed circuits maybe be not enough to modulate them. In line with this, Marr's theoretical proposals[98] also point that, once the auto-associative recurrent networks in CA3 are formed, dentate gyrus implication over them is not necessary (its participation would be previous). Our data agree with this interpretation, and dentate gyrus modulation, though perisomatic-inhibitory modulation seems not to have any effect on spatial memory consolidation in a dentate gyrus dependent task.

On the other hand, memory retrieval drive comes directly from distributed networks in the neocortex[316], where information arrives following two options: 1) after being processed first in dentate gyrus and hippocampus, and then transferred to more stable engrams in neocortex[317,318]. Or 2) processed in parallel in dentate gyrus and hippocampus, and in distributed neocortical networks, but the latter one needs to be boosted by hippocampal inputs[56,319,320] to create stable memory traces. Therefore, both under option 1 or 2, our manipulation on the hilar PV interneurons during the retrieval was, according to the above theory, expected to be ineffective on performance since the primary drive comes directly from more stable, and already formed, engrams in distributed regions of the neocortex.

We can modulate especially the encoding because hilar PV interneurons in the dentate gyrus are required for the initial processing of the incoming contextual information. Once the new sensory inputs enter in the system, they reach the entorhinal cortex and enter the dentate gyrus and hippocampus, and at that point, our experimental manipulation may boost (or impair) the propagation of that information in the trisynaptic circuit. After its encoding, for memory consolidation, hippocampus (CA3 and CA1 regions) needs to start a bidirectional communication in distributed networks with neocortical areas[301]. At this time, our modulation of the granule cells activity becomes again inefective, likely because it fails to modulate the already formed engrams[98], as the primary drive may require directly neocortical engrams, without hippocampal formation implication[316].

With the work presented herein, we point to a specific population of interneurons as a critical regulator, at the level of the system, for a particular cognitive aspect of memory, as encoding. Also, importantly, the memory tuning was achieved without affecting the synapses in granule cells dendrites. Plastic changes in the synapses may promote transient changes in excitatory/inhibitory balance, tuning the coordinate activity in the system so that the internodal communication may vary[136,137]. The correct internodal functional connectivity is crucial for maintaining the rhythmicity in the brain and interneuronal integrity has been shown to be critical on this respect[104]. However, our data demonstrates that interneuron's function might even be more diverse than commonly thought[104], and regulation of long-range connectivity, by filtering or boosting information propagation in the network, appears as a strong mechanism to support the formation of memory engrams. Our data probe that by

modulating the perisomatic inhibitory tone directly in granule cells, letting the synapses intact, we may tune a specific memory process; the spatial memory encoding.

Inhibition and engram size.

How to explain the increased efficiency of the dentate gyrus granule cells to support spatial memory encoding when reducing its perisomatic inhibitory tone? One explanation is that the PVbc interneurons help in the recruitment of granule cells, so that its inhibition may increase the size of the engram (measured in the number of neurons activated to participate in one neural processing). This way increased number of neurons would convey the enhanced information to CA3, increasing the precision, but impairing non-overlapping granule cells engrams (the more neurons each engram requires, the more probable some of them may overlap), so compromising pattern separation. However, our results indicate that the number of neurons recruited remains equal whether we reduce hilar PV perisomatic inhibitory tone, or we increase it. At least the cFos labelling, that has been used extensively in the bibliography as neuronal activity marker[321,322], stain equal number of neurons in the dentate gyrus, CA3 and CA1. Interestingly, the intensity of cFos labelling in the dentate gyrus, not in other areas, is higher when inhibiting hilar PVbc than in the rest of the groups. This experiment was repeated twice with identical results.

Some data probe that synaptic variations in dentate gyrus granule cells —modulating hilar somatostatin interneurons instead of PVbc— change the number of cFos labelled granule cells[323]. Because of that, we argue that maybe synapses in the dendrites determine the specific neurons that would be activated for a particular engram; and the perisomatic inhibition determines the efficiency of the excitatory neuron firing and so its impact on their postsynaptic targets. Remarkably, we also find that the same disinhibition strongly enhances polysynaptic transmission. This way, the dendritic modulation, and so LTP, could control memory by selecting the engram members and controlling its size[323], while perisomatic inhibition regulates the efficiency with which the cell assembly transmits the information in the network.

Following this argument, the similar number of neurons labelled in dentate gyrus and hippocampus can be explained by the intact synaptic activity and plasticity found in all groups. Immediate-Early genes, as cFos, are calcium sensitives[324]. Depolarization of the dendrites may induce cFos expression whether or not it may be related to a correct neuronal activity at the level of the system. When activating hilar PVbc interneurons, the spatial memory encoding is prevented, although we obtained an equal number of neurons labelled against cFos. As dendrites of granule cells neurons are intact in this group, calcium may be mobilized inside them normally, only that the increased perisomatic inhibition make them fire with more difficulties, or not coordinated with the rest of the cell assembly.

Mobilizing calcium depending on synaptic integration also explain why PV-Inhibition group present a similar number of neurons for the memory engram, as their synapses remain integral. However, the intensity of the labelling increases because, in addition to the synaptically driven transient of intracellular calcium, the same number of granule cells neurons are more active, and so internally they also may mobilize more calcium as a reflex of that increased activity[325,326]. It could be reflected in higher labelling for cFos immunostaining and

may lead to a higher efficiency of that particular cell assembly over the rest of the circuit in which they are embedded.

Our data indicate that hilar PV interneurons are not regulating engram size in the dentate gyrus, but seems to be implicated in the efficiency of the connectivity in the cell assemblies created therein. So that, when inhibiting hilar PVbc, active granule cells may be better connected in the network, therefore boosting both, intra- and extra-hippocampal activity, but not requiring more neurons to do so. The combination of the equal number of neurons recruited and more efficient communication to the rest of the network would also explain why inhibiting hilar PV cells facilitates pattern separation.

Hilar PV interneurons and pattern separation.

Another important feature we addressed, related with the enhanced/prevented memory encoding, is the effect of our modulation over the pattern separation, another function associated to the dentate gyrus[98,188,189]. The pattern separation helps associative memory networks to discriminate between similar, although different, overlapping sensory inputs. Dentate gyrus was proposed as pattern separator[98,193] by its anatomical and functional peculiarities, and its connectivity over CA3 —a region thought to be involved in pattern completion—. Nevertheless, other authors consider that the pattern separation function may emerge secondary to its encoding function (the better encoded it is, the more segregated from other memories it would be), or secondary to a "binding conjuncture" function for sensorial inputs[200].

Given our initial data proving the hilar PVbc regulation on memory encoding, mainly because the effect of its inhibition that leads to an enhanced memory encoding, our original hypothesis was that a better-encoded memory might cause a lack of ability to detect soft environmental changes. This is so because removing inhibition would recruit more neurons in the engram and, therefore, the level of engram overlapping would increase when the system is presented with two similar, although different, environments. In these conditions, a later reactivation of engrams during memory recall would more easily yield an ambiguous result. However, after cFos experiments showing that the enhanced encoding does not require more neurons recruited, but they are better connected in the circuit instead, it could mean that pattern separation function may also be potentiated when inhibiting hilar PV interneurons.

However, the tasks previously used in the bibliography were thought to be used only in one trial[188,327], not allowing to modulate one particular mnemic point in the task, and them testing its effect on the rest. The latter was a *sine qua non* condition for us. Our research interest required to modulate one particular spatial memory and then to confront it with similar and overlapping environments. To do so, we created the SETAmaze task to measure pattern separation ability (short-term task) when confronting new sensorial information with previously encoded one (long-term memory interactions).

Data probes that Sham animals realize the movement when the object is displaced 15 cm from its initially encoded position. This distance fits with the bibliography when making a spatial task dentate gyrus dependent, as function of the difficulty. Dentate gyrus lesions impair object location recognition when objects displacement are difficult to realize, but they do not affect if the task is more straightforward. The limit for this difficulty-dependent modulation is 15 cm

between objects[64]. Inhibiting hilar PVbc does increases the pattern separation ability when the object is displaced 10 cm directly (instead of the 15 cm required in control conditions). While activating hilar PV interneurons make the animals to need one more position, until 20 cm of object's displacement, to realize object's movement. We interpret the PV-Activation group result as a replication of the prevention of the memory encoding. Therefore, as hilar PVbc activation prevent memory formation in the initial position of the object, mice did not encode the first object's place. Then, mice's first object's position is actually the first object's movement (5 cm), so that they realize the object's displacement 15 cm away (so, 20 cm from starting point). On the other hand, PV-Inhibition group data proving enhanced pattern separation ability are in agreement with the logic of our arguments. If hilar PV interneurons inhibition improves encoding for a particular spatial configuration, not requiring more cells recruited in the dentate gyrus, but making its connections more efficient, then, the memory trace encoded under PVbc inhibition should be more salient than others, facilitating its recognition as differential contextual patterns.

Using this new task, the SETAmaze, we reproduce our initial results by which we enhance, or preclude, spatial memory encoding; giving reliability to these findings. We also probe that PVbc inhibition does not only preserve pattern separation, but also it increases short-term pattern separation, at least when confronting long-term facilitated memories with soft changes in the environment. These data also fit with the bibliography by pointing the high interrelationship between dentate gyrus, memory encoding and pattern separation whether it is as a function *per se*, or secondary to the encoding of spatial and sensorial information[64,188,200].

Inhibition and its importance.

If decreasing inhibitory tone is good for memory encoding, why do we have the inhibition at that high levels? Why is the resting inhibitory tone in the dentate gyrus suboptimal for memory encoding?

A parsimonious explanation could be that maybe the mice inhibitory tone is sufficient to do what mice do, despite decreased inhibitory tone could improve memory encoding. Perhaps it would not have real effects on mice's normal life. I wonder what's the difference between a standard encoding of, for instance, where the nourishment is in the environment and a better encoding of that location (both would lead to the same results; mice would remember that place). Maybe, as long as the location is well-enough encoded, it would be sufficiently optimized. In that sense, to have a better-than-normal spatial memory might not be that good for the mice. Especially when the lack of inhibition, and lawless excitability, is the basis for epilepsy. Probably if mice may encode good-enough spatial information, an optimal brain mechanism for the mice could be the farthest from epilepsy, the better.

When the biological fitness of species relay on more complex cognitive functions, the scenario may change, and all possible strategies to enhance performance would unveil. In that sense, some articles probe that there are less number of GABAergic synapses on the cell bodies in primates than in rodents[328], and also present smaller proportion of pyramidal-like basket cells in the dentate gyrus[329]. Hilar PV interneurons of primates also lack basal dendrites[330,331], a very significant feature because it may reflect a hyper-specialization on feedforward inhibitory regulation of granule cells, a characteristic that based on our results may indicate an

optimization of the system towards more efficient communication. Interestingly, other types of interneurons do not present this specialization, such as dendrite-targeting interneurons, which are similar throughout the phylogenetic scale, from lizards, through rodents, up to primates and humans[91].

Maybe, if the circuit design in the dentate gyrus of the mice fulfils the requirements of whatever function is supported by this structure, optimization might not be required and a "good-enough" design might be stabilized along its evolution. In this line, maybe a decreased inhibition could be the reason by which an ape is considered to have improved cognitive abilities than a mouse. Perhaps the epilepsy is the price we need to pay to have a more efficient system, and the perisomatic inhibition could make the difference for higher cognitive functions, or at least for increasing efficiency in the neuronal system when environmental pressure pushes the organism to develop more complex behaviours.

For sure, to understand how inhibition tunes the neuronal networks is, under my opinion, fundamental; *per se*, for experimental purposes, for understanding information processing in the brain, and, hopefully, for clinical purposes too. Many of the psychological/neurologic disorders are currently being related with dysregulation of the excitatory/inhibitory balance and alterations in one or more interneuron populations[92]. Mental illness, more evident in humans than in other species (at least from our anthropocentric point of view), could also be a secondary price paid by our brain, by sculping inhibitory circuits to developing our cognitive abilities we also developed an Achilles heel. In that sense, inhibition's study should be more than necessary.

To have inhibition is essential for proper neuronal activity. It gives rhythmicity in the circuit and allows flexibility in a very efficient way[332]. This work focuses on the perisomatic inhibition on dentate gyrus as a mechanism to regulate information transmission in this central node for memory encoding. As always, the final goal is to understand how the brain works, on a broader and integrative view. The present thesis work pretended to gives one small step forward in this endeavour, and has provided compelling evidence to suggest that perisomatic inhibition may work as an efficient switch to route information in brain networks. In our experiments, the brain networks involved had to do with memory formation and, accordingly, the functional consequence of this routing was to regulate memory content. We believe, though, that this function of perisomatic enervating interneurons may extrapolate to other circuits in other brain regions. Hopefully, those data could be extrapolated to humans.

At the end of the day, to understand the brain is to understand ourselves.

VII.- CONCLUSIONS.

Conclusions.

1.- Hilar PV interneurons control granule cells firing without affecting the synaptic excitatory postsynaptic potentials, nor synaptic plasticity as measured by LTP induction.

2.- Hilar PV interneurons regulate the intra-hippocampal functional connectivity, most notably in the trisynaptic propagation from dentate gyrus to CA1. Inhibition of PV interneurons largely facilitates the firing of CA1 pyramidal neurons.

3.- Polysynaptic propagation of activity from the dentate gyrus to extra-hippocampal regions is observed after PV interneuron inhibition. Afferent regions include the prefrontal cortex, dorsal and ventral (accumbens) striatum, amygdala, and other cortical areas in the medial temporal lobe, all known for their implication in different aspects of learning and memory.

4.- The functional role of hilar PV interneurons on memory formation was measured in the NLO task demonstrating a bidirectional effect of their activity during encoding, such that inhibition of this cell type enhances memory encoding, while its activation precludes it.

5.- Modulation of PV interneurons activity in the NLO task had no effect on memory consolidation nor retrieval.

6.- Engram size during memory encoding in the NLO task, as measured by the number of positive cFos cells in the dentate gyrus and hippocampus, was not affected by activation or inhibition of hilar PV interneurons.

7.- Memory enhancement after PV interneuron inhibition does not compromise pattern separation; even it is facilitated.
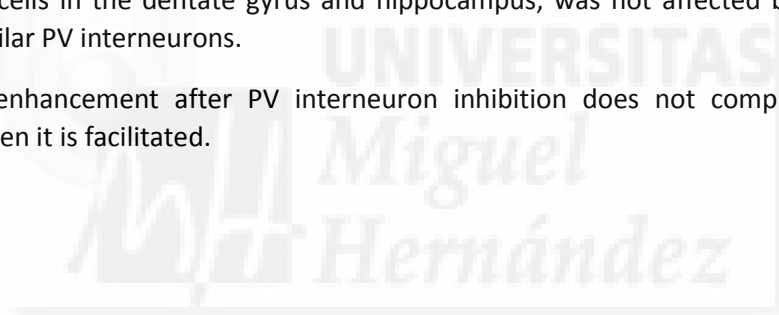
Conclusiones.

1.- Las interneuronas PV del hilus controlan el disparo de las células granulares del giro dentado, sin afectar ni a los potenciales excitatorios post-sinápticos ni a la plasticidad sináptica en giro dentado, como se evidencia tras la inducción de LTP.

2-. Las interneuronas PV del hilus regulan la conectividad hipocampal, especialmente la propagación trisináptica desde el giro dentado a CA1, facilitando el disparo de las neuronas piramidales en CA1.

3.- La propagación de la actividad polisináptica desde giro dentado ha estructuras extrahipocampales se observa tras la inhibición de las interneurons PV del hilus. Las regiones en las que se observa dicha actividad propagada incluyen corteza prefrontal, striado dorsal y ventral (núcleo accumbens), amígdala y otras regiones corticales en el lóbulo temporal medial; todas ellas participan en diferentes aspectos del aprendizaje y la memoria.

4.- El papel que las interneuronas PV del hilus tienen en la formación de memorias es bidireccional y específico sobre la codificación de la nueva información; su inhibición mejora la codificación de la memoria, mientras que su activación la impide.

5.- La modulación de la actividad de las neuronas del hilus en la tarea de conducta del NLO no tuvo efecto ni sobre la consolidación ni sobre la recuperación de la memoria.

6.- El tamaño del engrama, medido como número de células cFos positivas en giro dentado e hipocampo, no cambia ni al inhibir ni al activar a las neuronas PV del hilus.

7.- La potenciación de la memoria tras la inhibición de las interneurons PV del hilus no dificulta la separación de patrones, incluso la facilita.

VIII.- ABBREVIATIONS.

AAV. Adenoassociated virus.

AAV5. Adenoassociated virus, serotype 5.

Ag. Silver.

AMPA. α-amino-3-hydroxy-5-methyl-4-isoxazolepropionic acid receptors.

AP. Antero-Posterior.

BOLD. Blood-Oxygenated Level Dependent signal.

Ca^{2+}. Calcium.

CA1-4. *Cornu Ammonis* hippocampal region, 1-4.

CCK. Cholecystokinin.

Cl. Chlorine.

CNO. Clozapine-N-Oxide.

CSIC. Consejo Superior de Investigaciones Científicas.

DG. Dentate gyrus.

DiI. 1'1-dioctadecyl-3,3,3',3'-tetramethylindocarbocyanine perchlorate.

DREADDs. Designer Receptors Exclusively Activated by Designer Drugs.

DV. Dorso-Ventral.

EC. Entorhinal Cortex.

EPM. Elevated Plus Maze.

EPSCs. Excitatory Post-Synaptic Currents.

EPSP. Excitatory Post-Synaptic Potential.

fMRI. Functional Magnetic Resonance Imaging.

GABA. Gamma-AminoButiric Acid.

GAD. Glutamic acid decarboxylase.

GC. Granule cell.

Gl. Granule cell layer.

GluR1-4. Glutamate receptor types 1-4.

Hi. Hilus.

HICAP cells. Hilar Commisural-Associational Pathway-related interneurons.

HIPP cells. Hilar Perforant Path-associated cells.

hM3D(Gq). Human Muscarinic receptor type 3 DREADD, related to Gq protein.

hM4D(Gi). Human Muscarinic receptor type 4 DREADD, related to Gi protein.

Hpc. Hippocampus.

hSyn. Human synuclein.

IEGs. Immediate Early Genes.

IPSCs. Inhibitory Post-Synaptic Currents.

I.p. Intraperitoneal.

K$^+$. Potasium.

LFPs. Local Field Potentials.

LM. Latero-medial.

LTD. Long-Term Depression.

LTM. Long-Term Memory.

LTP. Long-Term Potentiation.

Mg^{2+}. Magnesium.

mGluR. Metabotropic Glutamate Receptor.

ml. Molecular layer.

NLO. Novel Location of the Object behavioural task.

NMDA. N-Methyl-D-Aspartate receptors.

PS. Population Spike.

PS1. Population Spike evoked by the first pulse in pair pulses protocol.

PS2. Population Spike evoked by the second pulse in pair pulses protocol.

PFC. Prefrontal Cortex.

PV. Parvalbumin.

PVbc. Parvalbumin basket cells.

ROI. Region of interest.

SETAmaze. Spatial Evaluation Task maze.

SPI. Tulving's serial parallel independent framework.

STM. Short Term Memory.

SST. Somatostatin.

VIP. Vasointestinal peptide.

IX.- BIBLIOGRAPHY.

1. Bloch, D. *Aristotle on memory and recollection : text, translation, interpretation, and reception in Western scholasticism*. (Brill, 2007).
2. Broca, P. P. Loss of Speech, Chronic Softening and Parital Destruction of the Anterior Left Lobe of the Brain. *Bull. la Socieété Anthropol.* **2,** 235–238 (1861).
3. Wernicke, C. Der aphasische Symptomencomplex: Eine psychologische Studie auf anatomischer Basis. *Cohn Weigert* (1874).
4. Semon, Richard Wolfgang. *Die Mneme als erhaltendes Prinzip : im Wechsel des organischen Geschehens*. (Engelmann, 1904).
5. Josselyn, S. A., Köhler, S. & Frankland, P. W. Heroes of the Engram. *J. Neurosci.* **37,** 4647–4657 (2017).
6. Ramón y Cajal, S. The Croonian Lecture: La Fine Structure des Centres Nerveux. *Proc. R. Soc. London, Vol. 55, pp. 444-468* **55,** 444–468 (1894).
7. Golgi, C. Sulla sostanza grigia del cervello. *Gazzeta medica Ital.* 90–98 (1873).
8. Ramón y Cajal, S. Estructura del asta de Ammon y fascia dentata. *Ann Soc. Esp. Hist. Nat.* 22 (1893).
9. Sotelo, C. Viewing the brain through the master hand of Ramon y Cajal. *Nat. Rev. Neurosci.* **4,** 71–77 (2003).
10. Harlow, J. M. Passage of an Iron Rod through the Head. *Bost. Med. Surg. J.* **39,** 389–393 (1848).
11. Andersen, P., Morris, R., Amaral, D., Bliss, T. & O'Keefe, J. *The hippocampus book*. (Oxford University Press, 2007).
12. Orbach, J. *The Neuropsychological Theories of Lashley and Hebb.* (University Press of America, 1998).
13. Cohen-Cole, J. Mind as Machine: A History of Cognitive Science. *Isis* **99,** 811–812 (2008).
14. Lorente de Nó, R. Studies on the structure of the cerebral cortex,. I: the area entorhinalis. *J Psychol* (1933).
15. Hebb, D. *The organization of behavior: A neuropsychological theory.* (Wiley Company, 1949).
16. Penfield, W. & Perot, P. The brain's record of auditory and visual experience. A finnal summary and discussion. *Brain* **86,** 595–696 (1963).
17. Scoville, W. B. & Milner, B. Loss of recent memory after bilateral hippocampal lesions. *J. Neurol. Neurosurg. Psychiatry* **20,** 11–21 (1957).
18. Milner, B. *Les troubles de la memoire accompagnant des lesions hippocampiques bilaterales. In Physiologie de l'Hippocampe* (Centre National de la Recherche Scientifique (CNRS), 1962).
19. Florey, E. GABA: history and perspectives. *Can. J. Physiol. Pharmacol.* **69,** 1049–56 (1991).
20. Watkins, J. C. l-glutamate as a central neurotransmitter: looking back. *Biochem. Soc. Trans.* **28,** 297–309 (2000).
21. Ramón y Cajal, S. *Histologie du système nerveux de l'homme & des vertébrés.* (Maloine, 1911).
22. Bliss, T. V & Lomo, T. Long-lasting potentiation of synaptic transmission in the dentate area of the anaesthetized rabbit following stimulation of the perforant path. *J. Physiol.* **232,** 331–56 (1973).
23. Reynolds, G. S. & Skinner, B. F. Technique for reinforcing either of two organisms with a single food magazine. *J. Exp. Anal. Behav.* **5,** 58–58 (1962).
24. Schenk, F. & Morris, R. G. Dissociation between components of spatial memory in rats after recovery from the effects of retrohippocampal lesions. *Exp. brain Res.* **58,** 11–28 (1985).
25. Ennaceur, A. & Delacour, J. A new one-trial test for neurobiological studies of memory in rats. 1: Behavioral data. *Behav. Brain Res.* **31,** 47–59 (1988).
26. Ledoux, J. E., Sakaguchi, A. & Reis, D. J. Strain differences in fear between spontaneously hypertensive and normotensive rats. *Brain Res.* **277,** 137–43 (1983).
27. Jaenisch, R. & Mintz, B. Simian virus 40 DNA sequences in DNA of healthy adult mice derived from preimplantation blastocysts injected with viral DNA. *Proc. Natl. Acad. Sci. U. S. A.* **71,** 1250–4 (1974).
28. Zhang, F. *et al.* Optogenetic interrogation of neural circuits: technology for probing mammalian brain structures. *Nat. Protoc.* **5,** 439–456 (2010).
29. Armbruster, B. N., Li, X., Pausch, M. H., Herlitze, S. & Roth, B. L. Evolving the lock to fit the key to create a family of G protein-coupled receptors potently activated by an inert ligand. *Proc. Natl. Acad. Sci.* **104,** 5163–5168 (2007).
30. Gompf, H. S., Budygin, E. A., Fuller, P. M. & Bass, C. E. Targeted genetic manipulations of neuronal subtypes using promoter-specific combinatorial AAVs in wild-type animals. *Front. Behav. Neurosci.* **9,** 152 (2015).
31. Huang, Z. J., Taniguchi, H., He, M. & Kuhlman, S. Cre-Dependent Adeno-Associated Virus Preparation and Delivery for Labeling Neurons in the Mouse Brain. *Cold Spring Harb. Protoc.* **2014,** 080382 (2014).
32. Deisseroth, K. Optogenetics: 10 years of microbial opsins in neuroscience. *Nat. Neurosci.* **18,** 1213–1225 (2015).
33. Deisseroth, K. & Hegemann, P. The form and function of channelrhodopsin. *Science.* **357,** eaan5544 (2017).
34. Dong, S., Rogan, S. C. & Roth, B. L. Directed molecular evolution of DREADDs: a generic approach to creating next-generation RASSLs. *Nat. Protoc.* **5,** 561–573 (2010).
35. Roth, B. L. DREADDs for Neuroscientists. *Neuron* **89,** 683–694 (2016).
36. Alexander, G. M. *et al.* Remote control of neuronal activity in transgenic mice expressing evolved G protein-coupled receptors. *Neuron* **63,** 27–39 (2009).
37. Ramirez, S. *et al.* Creating a False Memory in the Hippocampus. *Science.* **341,** 387–391 (2013).

38.   Ryan, T. J., Roy, D. S., Pignatelli, M., Arons, A. & Tonegawa, S. Engram cells retain memory under retrograde amnesia. *Science.* **348,** 1007–1013 (2015).

39.   Minatohara, K., Akiyoshi, M. & Okuno, H. Role of Immediate-Early Genes in Synaptic Plasticity and Neuronal Ensembles Underlying the Memory Trace. *Front. Mol. Neurosci.* **8,** 78 (2016).

40.   Baddeley, A. The concept of episodic memory. *Phil. Trans. R. Soc. Lond. B* **356,** 1345–1350 (2001).

41.   Schacter, D. L. & Tulving, E. Memory Systems 1994. (1994).

42.   Squire, L. R. Memory and the hippocampus: a synthesis from findings with rats, monkeys, and humans. *Psychol. Rev.* **99,** 195–231 (1992).

43.   Griffiths, Dickinson & Clayton. Episodic memory: what can animals remember about their past? *Trends Cogn. Sci.* **3,** 74–80 (1999).

44.   O'Keefe, J. & Nadel, L. *The hippocampus as a cognitive map*. (Clarendon Press, 1978).

45.   Everitt, B. J. & Robbins, T. W. Neural systems of reinforcement for drug addiction: from actions to habits to compulsion. *Nat. Neurosci.* **8,** 1481–1489 (2005).

46.   Schultz, W. & Dickinson, A. Neuronal coding of prediction errors. *Annu. Rev. Neurosci.* **23,** 473–500 (2000).

47.   LeDoux, J. The amygdala. *Curr. Biol.* **17,** R868–R874 (2007).

48.   Graf, P. & Schacter, D. L. Implicit and explicit memory for new associations in normal and amnesic subjects. *J. Exp. Psychol. Learn. Mem. Cogn.* **11,** 501–18 (1985).

49.   Wang, S.-H. & Morris, R. G. M. Hippocampal-Neocortical Interactions in Memory Formation, Consolidation, and Reconsolidation. *Annu. Rev. Psychol.* **61,** 49–79 (2010).

50.   Lechner, H. A., Squire, L. R. & Byrne, J. H. 100 years of consolidation--remembering Müller and Pilzecker. *Learn. Mem.* **6,** 77–87

51.   Aggleton, J. P. & Brown, M. W. Episodic memory, amnesia, and the hippocampal-anterior thalamic axis. *Behav. Brain Sci.* **22,** 425-44-89 (1999).

52.   de Haan, M., Mishkin, M., Baldeweg, T. & Vargha-Khadem, F. Human memory development and its dysfunction after early hippocampal injury. *Trends Neurosci.* **29,** 374–381 (2006).

53.   Eichenbaum, H. Hippocampus. *Neuron* **44,** 109–120 (2004).

54.   Miyashita, Y. Cognitive Memory: Cellular and Network Machineries and Their Top-Down Control. *Science.* **306,** 435–440 (2004).

55.   Frey, U. & Morris, R. G. M. Synaptic tagging and long-term potentiation. *Nature* **385,** 533–536 (1997).

56.   Tse, D. *et al.* Schemas and Memory Consolidation. *Science.* **316,** 76–82 (2007).

57.   Fletcher, P. C. & Henson, R. N. Frontal lobes and human memory: insights from functional neuroimaging. *Brain* **124,** 849–81 (2001).

58.   Schneider, W. & Shiffrin, R. Controlled and automatic human information processing: 1. Detection, search, and attention. *Psychol. Rev.* **84,** 1–66 (1977).

59.   Floresco, S. B., Seamans, J. K. & Phillips, A. G. Selective roles for hippocampal, prefrontal cortical, and ventral striatal circuits in radial-arm maze tasks with or without a delay. *J. Neurosci.* **17,** 1880–90 (1997).

60.   Seamans, J. K., Floresco, S. B. & Phillips, A. G. D1 receptor modulation of hippocampal-prefrontal cortical circuits integrating spatial memory with executive functions in the rat. *J. Neurosci.* **18,** 1613–21 (1998).

61.   Nemanic, S., Alvarado, M. C. & Bachevalier, J. The Hippocampal/Parahippocampal Regions and Recognition Memory: Insights from Visual Paired Comparison versus Object-Delayed Nonmatching in Monkeys. *J. Neurosci.* **24,** 2013–2026 (2004).

62.   Eichenbaum, H., Yonelinas, A. P. & Ranganath, C. The Medial Temporal Lobe and Recognition Memory. *Annu. Rev. Neurosci.* **30,** 123–152 (2007).

63.   Akirav, I. & Maroun, M. Ventromedial Prefrontal Cortex Is Obligatory for Consolidation and Reconsolidation of Object Recognition Memory. *Cereb. Cortex* **16,** 1759–1765 (2005).

64.   Gilbert, P. E., Kesner, R. P. & Lee, I. Dissociating hippocampal subregions: double dissociation between dentate gyrus and CA1. *Hippocampus* **11,** 626–36 (2001).

65.   Hunsaker, M. R. & Kesner, R. P. Evaluating the differential roles of the dorsal dentate gyrus, dorsal CA3, and dorsal CA1 during a temporal ordering for spatial locations task. *Hippocampus* **18,** 955–964 (2008).

66.   Hunsaker, M. R., Rosenberg, J. S. & Kesner, R. P. The role of the dentate gyrus, CA3a,b, and CA3c for detecting spatial and environmental novelty. *Hippocampus* **18,** 1064–1073 (2008).

67.   Barker, G. R. I. & Warburton, E. C. NMDA Receptor Plasticity in the Perirhinal and Prefrontal Cortices Is Crucial for the Acquisition of Long-Term Object-in-Place Associative Memory. *J. Neurosci.* **28,** 2837–2844 (2008).

68.   Winters, B. D., Saksida, L. M. & Bussey, T. J. Object recognition memory: Neurobiological mechanisms of encoding, consolidation and retrieval. *Neurosci. Biobehav. Rev.* **32,** 1055–1070 (2008).

69.   Witter, M. P. The perforant path: projections from the entorhinal cortex to the dentate gyrus. in *Progress in brain research* **163,** 43–61 (2007).

70.   Dudai, Y. & Morris, R. G. M. To consolidate or not to consolidate: what are the questions? in *Brain, Perception, MemoryAdvances in Cognitive Neuroscience* 149–162 (Oxford University Press, 2000).

71.   Osada, T., Adachi, Y., Kimura, H. M. & Miyashita, Y. Towards understanding of the cortical network underlying associative memory. *Philos. Trans. R. Soc. Lond. B. Biol. Sci.* **363,** 2187–99 (2008).

72. Nadel, L. & Moscovitch, M. Memory consolidation, retrograde amnesia and the hippocampal complex. *Curr. Opin. Neurobiol.* **7,** 217–27 (1997).

73. Zola-Morgan, S., Squire, L. R. & Amaral, D. G. Human amnesia and the medial temporal region: enduring memory impairment following a bilateral lesion limited to field CA1 of the hippocampus. *J. Neurosci.* **6,** 2950–67 (1986).

74. Smith, C. N. & Squire, L. R. Medial Temporal Lobe Activity during Retrieval of Semantic Memory Is Related to the Age of the Memory. *J. Neurosci.* **29,** 930–938 (2009).

75. Takashima, A. *et al.* Declarative memory consolidation in humans: A prospective functional magnetic resonance imaging study. *Proc. Natl. Acad. Sci.* **103,** 756–761 (2006).

76. Cipolotti, L. *et al.* Long-term retrograde amnesia...the crucial role of the hippocampus. *Neuropsychologia* **39,** 151–72 (2001).

77. Moscovitch, M., Nadel, L., Winocur, G., Gilboa, A. & Rosenbaum, R. S. The cognitive neuroscience of remote episodic, semantic and spatial memory. *Curr. Opin. Neurobiol.* **16,** 179–190 (2006).

78. Nadel, L. & Land, C. Memory traces revisited. *Nat. Rev. Neurosci.* **1,** 209–212 (2000).

79. Rosenbaum, R. S., Winocur, G. & Moscovitch, M. New views on old memories: re-evaluating the role of the hippocampal complex. *Behav. Brain Res.* **127,** 183–97 (2001).

80. Teyler, T. J. & DiScenna, P. The hippocampal memory indexing theory. *Behav. Neurosci.* **100,** 147–54 (1986).

81. Eacott, M. J. & Easton, A. On familiarity and recall of events by rats. *Hippocampus* **17,** 890–7 (2007).

82. Day, M., Langston, R. & Morris, R. G. M. Glutamate-receptor-mediated encoding and retrieval of paired-associate learning. *Nature* **424,** 205–9 (2003).

83. Lorente de Nó, R. Studies on the structure of the cerebral cortex. II. Continuation of the study of the ammonic system. *J. für Psychol.* (1934).

84. Zhang, S.-J. *et al.* Functional connectivity of the entorhinal-hippocampal space circuit. *Philos. Trans. R. Soc. B Biol. Sci.* **369,** 20120516–20120516 (2013).

85. Canto, C. B., Koganezawa, N., Beed, P., Moser, E. I. & Witter, M. P. All Layers of Medial Entorhinal Cortex Receive Presubicular and Parasubicular Inputs. *J. Neurosci.* **32,** 17620–17631 (2012).

86. Yonelinas, A. P. The hippocampus supports high-resolution binding in the service of perception, working memory and long-term memory. *Behav. Brain Res.* **254,** 34–44 (2013).

87. Spellman, T. *et al.* Hippocampal–prefrontal input supports spatial encoding in working memory. *Nature* **522,** 309–314 (2015).

88. van Groen, T., Kadish, I. & Wyss, J. M. Species differences in the projections from the entorhinal cortex to the hippocampus. *Brain Res. Bull.* **57,** 553–6 (2002).

89. van Groen, T., Miettinen, P. & Kadish, I. The entorhinal cortex of the mouse: Organization of the projection to the hippocampal formation. *Hippocampus* **13,** 133–149 (2003).

90. Herreras, O. Local Field Potentials: Myths and Misunderstandings. *Front. Neural Circuits* **10,** 101 (2016).

91. Freund, T. F. & Buzsáki, G. Interneurons of the hippocampus. *Hippocampus* **6,** 347–470 (1998).

92. Pelkey, K. A. *et al.* Hippocampal GABAergic Inhibitory Interneurons. *Physiol. Rev.* **97,** 1619–1747 (2017).

93. Daitz, H. M. & Powell, T. P. Studies of the connexions of the fornix system. *J. Neurol. Neurosurg. Psychiatry* **17,** 75–82 (1954).

94. Wyss, J. M., Swanson, L. W. & Cowan, W. M. The organization of the fimbria, dorsal fornix and ventral hippocampal commissure in the rat. *Anat. Embryol. (Berl).* **158,** 303–16 (1980).

95. Köhler, C. A projection from the deep layers of the entorhinal area to the hippocampal formation in the rat brain. *Neurosci. Lett.* **56,** 13–9 (1985).

96. Köhler, C. Intrinsic projections of the retrohippocampal region in the rat brain. I. The subicular complex. *J. Comp. Neurol.* **236,** 504–522 (1985).

97. Steward, O. & Scoville, S. A. Cells of origin of entorhinal cortical afferents to the hippocampus and fascia dentata of the rat. *J. Comp. Neurol.* **169,** 347–370 (1976).

98. Marr, D. Simple memory: a theory for archicortex. *Philos. Trans. R. Soc. Lond. B. Biol. Sci.* **262,** 23–81 (1971).

99. Amaral, D. G. & Witter, M. P. The three-dimensional organization of the hippocampal formation: a review of anatomical data. *Neuroscience* **31,** 571–91 (1989).

100. Strüber, M., Sauer, J.-F., Jonas, P. & Bartos, M. Distance-dependent inhibition facilitates focality of gamma oscillations in the dentate gyrus. *Nat. Commun.* **8,** 758 (2017).

101. Yuan, M. *et al.* Somatostatin-positive interneurons in the dentate gyrus of mice provide local- and long-range septal synaptic inhibition. *Elife* **6,** (2017).

102. Sauer, J.-F., Strüber, M. & Bartos, M. Impaired fast-spiking interneuron function in a genetic mouse model of depression. *Elife* **4,** (2015).

103. Gan, J., Weng, S., Pernía-Andrade, A. J., Csicsvari, J. & Jonas, P. Phase-Locked Inhibition, but Not Excitation, Underlies Hippocampal Ripple Oscillations in Awake Mice In Vivo. *Neuron* **93,** 308–314 (2017).

104. Buzsáki, G. *Rhythms of the brain*. (Oxford University Press, 2006).

105. Alcami, P. & Marty, A. Estimating functional connectivity in an electrically coupled interneuron network. *Proc. Natl. Acad. Sci.* **110,** E4798–E4807 (2013).

106. Bird, C. M. & Burgess, N. The hippocampus and memory: insights from spatial processing. *Nat. Rev. Neurosci.* **9,** 182–194 (2008).

107. Cooke, S. F. & Bliss, T. V. P. Plasticity in the human central nervous system. *Brain* **129,** 1659–1673 (2006).

108. Klein, M. & Kandel, E. R. Presynaptic modulation of voltage-dependent Ca2+ current: mechanism for behavioral sensitization in Aplysia californica. *Proc. Natl. Acad. Sci. U. S. A.* **75,** 3512–6 (1978).

109. Padamsey, Z. & Emptage, N. Two sides to long-term potentiation: a view towards reconciliation. *Philos. Trans. R. Soc. B Biol. Sci.* **369,** 20130154–20130154 (2013).

110. Malenka, R. C. & Bear, M. F. LTP and LTD. *Neuron* **44,** 5–21 (2004).

111. Morris, R. G. M. NMDA receptors and memory encoding. *Neuropharmacology* **74,** 32–40 (2013).

112. Andersen, N., Krauth, N. & Nabavi, S. Hebbian plasticity in vivo : relevance and induction. *Curr. Opin. Neurobiol.* **45,** 188–192 (2017).

113. Bliss, T., Collingridge, G. L. & Morris, R. G. M. Synaptic plasticity in hippocampus. in *The Hippocampus Book* (eds. Andersen, P., Morris, R. G. M., Amaral, D., Bliss, T. & O'Keefe, J.) 343–444 (Oxford University Press, 2007).

114. Andersen, P., Sundberg, S. H., Sveen, O. & Wigström, H. Specific long-lasting potentiation of synaptic transmission in hippocampal slices. *Nature* **266,** 736–7 (1977).

115. McNaughton, B. L., Douglas, R. M. & Goddard, G. V. Synaptic enhancement in fascia dentata: cooperativity among coactive afferents. *Brain Res.* **157,** 277–93 (1978).

116. Barrionuevo, G. & Brown, T. H. Associative long-term potentiation in hippocampal slices. *Proc. Natl. Acad. Sci. U. S. A.* **80,** 7347–51 (1983).

117. Herron, C. E., Lester, R. A. J., Coan, E. J. & Collingridge, G. L. Frequency-dependent involvement of NMDA receptors in the hippocampus: a novel synaptic mechanism. *Nature* **322,** 265–268 (1986).

118. Volianskis, A. *et al.* Long-term potentiation and the role of N-methyl-d-aspartate receptors. *Brain Res.* **1621,** 5–16 (2015).

119. MacDermott, A. B., Mayer, M. L., Westbrook, G. L., Smith, S. J. & Barker, J. L. NMDA-receptor activation increases cytoplasmic calcium concentration in cultured spinal cord neurones. *Nature* **321,** 519–22 (1986).

120. Harris, E. W. & Cotman, C. W. Long-term potentiation of guinea pig mossy fiber responses is not blocked by N-methyl D-aspartate antagonists. *Neurosci. Lett.* **70,** 132–7 (1986).

121. Bliss, T. V. P. & Cooke, S. F. Long-term potentiation and long-term depression: a clinical perspective. *Clinics (Sao Paulo).* **66 Suppl 1,** 3–17 (2011).

122. Lynch, G. S., Dunwiddie, T. & Gribkoff, V. Heterosynaptic depression: a postsynaptic correlate of long-term potentiation. *Nature* **266,** 737–9 (1977).

123. Levy, W. B. & Steward, O. Synapses as associative memory elements in the hippocampal formation. *Brain Res.* **175,** 233–45 (1979).

124. Wagner, J. J. & Alger, B. E. Homosynaptic LTD and depotentiation: do they differ in name only? *Hippocampus* **6,** 24–9 (1996).

125. Kemp, A. & Manahan-Vaughan, D. Hippocampal long-term depression: master or minion in declarative memory processes? *Trends Neurosci.* **30,** 111–118 (2007).

126. Connor, S. A. & Wang, Y. T. A Place at the Table. *Neurosci.* **22,** 359–371 (2016).

127. Oliet, S. H., Malenka, R. C. & Nicoll, R. A. Two distinct forms of long-term depression coexist in CA1 hippocampal pyramidal cells. *Neuron* **18,** 969–82 (1997).

128. Moser, E. I., Krobert, K. A., Moser, M. B. & Morris, R. G. Impaired spatial learning after saturation of long-term potentiation. *Science* **281,** 2038–42 (1998).

129. Traub, R. D. *et al.* Transient Depression of Excitatory Synapses on Interneurons Contributes to Epileptiform Bursts During Gamma Oscillations in the Mouse Hippocampal Slice. *J. Neurophysiol.* **94,** 1225–1235 (2005).

130. Lu, Y. M., Mansuy, I. M., Kandel, E. R. & Roder, J. Calcineurin-mediated LTD of GABAergic inhibition underlies the increased excitability of CA1 neurons associated with LTP. *Neuron* **26,** 197–205 (2000).

131. Laezza, F., Doherty, J. J. & Dingledine, R. Long-term depression in hippocampal interneurons: joint requirement for pre- and postsynaptic events. *Science* **285,** 1411–4 (1999).

132. Castillo, P. E. Presynaptic LTP and LTD of Excitatory and Inhibitory Synapses. *Cold Spring Harb. Perspect. Biol.* **4,** 005728 (2012).

133. McBain, C. J., Freund, T. F. & Mody, I. Glutamatergic synapses onto hippocampal interneurons: precision timing without lasting plasticity. *Trends Neurosci.* **22,** 228–35 (1999).

134. Lawrence, J. J. & McBain, C. J. Interneuron Diversity series: Containing the detonation – feedforward inhibition in the CA3 hippocampus. *Trends Neurosci.* **26,** 631–640 (2003).

135. Shew, T., Yip, S. & Sastry, B. R. Mechanisms Involved in Tetanus-Induced Potentiation of Fast IPSCs in Rat Hippocampal CA1 Neurons. *J. Neurophysiol.* **83,** 3388–3401 (2000).

136. Canals, S., Beyerlein, M., Merkle, H. & Logothetis, N. K. Functional MRI Evidence for LTP-Induced Neural Network Reorganization. *Curr. Biol.* **19,** 398–403 (2009).

137. Alvarez-Salvado, E., Pallares, V., Moreno, A. & Canals, S. Functional MRI of long-term potentiation: imaging network plasticity. *Philos. Trans. R. Soc. B Biol. Sci.* **369,** 20130152–20130152 (2013).

138. Desmond, N. L. & Levy, W. B. Granule cell dendritic spine density in the rat hippocampus varies with spine shape and location. *Neurosci. Lett.* **54,** 219–24 (1985).

144

139. Schmidt, B., Marrone, D. F. & Markus, E. J. Disambiguating the similar: The dentate gyrus and pattern separation. *Behav. Brain Res.* **226,** 56–65 (2012).

140. Pernía-Andrade, A. J. & Jonas, P. Theta-Gamma-Modulated Synaptic Currents in Hippocampal Granule Cells In Vivo Define a Mechanism for Network Oscillations. *Neuron* **81,** 140–152 (2014).

141. Witter, M. P. Connectivity of the Hippocampus. in *Hippocampal Microcircuits* 5–26 (Springer New York, 2010).

142. Lübke, J., Deller, T. & Frotscher, M. Septal innervation of mossy cells in the hilus of the rat dentate gyrus: an anterograde tracing and intracellular labeling study. *Exp. brain Res.* **114,** 423–32 (1997).

143. Borhegyi, Z. & Leranth, C. Distinct substance P- and calretinin-containing projections from the supramammillary area to the hippocampus in rats; a species difference between rats and monkeys. *Exp. brain Res.* **115,** 369–74 (1997).

144. Kiss, J., Csáki, A., Bokor, H., Shanabrough, M. & Leranth, C. The supramammillo-hippocampal and supramammillo-septal glutamatergic/aspartatergic projections in the rat: a combined [3H]D-aspartate autoradiographic and immunohistochemical study. *Neuroscience* **97,** 657–69 (2000).

145. Pickel, V. M., Segal, M. & Bloom, F. E. A radioautographic study of the efferent pathways of the nucleus locus coeruleus. *J. Comp. Neurol.* **155,** 15–41 (1974).

146. Swanson, L. W. & Hartman, B. K. The central adrenergic system. An immunofluorescence study of the location of cell bodies and their efferent connections in the rat utilizing dopamine-beta-hydroxylase as a marker. *J. Comp. Neurol.* **163,** 467–505 (1975).

147. Conrad, L. C., Leonard, C. M. & Pfaff, D. W. Connections of the median and dorsal raphe nuclei in the rat: an autoradiographic and degeneration study. *J. Comp. Neurol.* **156,** 179–205 (1974).

148. Claiborne, B. J., Amaral, D. G. & Cowan, W. M. Quantitative, three-dimensional analysis of granule cell dendrites in the rat dentate gyrus. *J. Comp. Neurol.* **302,** 206–219 (1990).

149. Nakashiba, T. *et al.* Young Dentate Granule Cells Mediate Pattern Separation, whereas Old Granule Cells Facilitate Pattern Completion. *Cell* **149,** 188–201 (2012).

150. Kitamura, T. & Inokuchi, K. Role of adult neurogenesis in hippocampal-cortical memory consolidation. *Mol. Brain* **7,** 13 (2014).

151. Abrous, D. N. & Wojtowicz, J. M. Interaction between Neurogenesis and Hippocampal Memory System: New Vistas. *Cold Spring Harb. Perspect. Biol.* **7,** a018952 (2015).

152. Deng, W., Aimone, J. B. & Gage, F. H. New neurons and new memories: how does adult hippocampal neurogenesis affect learning and memory? *Nat. Rev. Neurosci.* **11,** 339–350 (2010).

153. Marin-Burgin, A., Mongiat, L. A., Pardi, M. B. & Schinder, A. F. Unique Processing During a Period of High Excitation/Inhibition Balance in Adult-Born Neurons. *Science.* **335,** 1238–1242 (2012).

154. Piatti, V. C., Ewell, L. A. & Leutgeb, J. K. Neurogenesis in the dentate gyrus: carrying the message or dictating the tone. *Front. Neurosci.* **7,** 50 (2013).

155. Rapp, P. R. & Gallagher, M. Preserved neuron number in the hippocampus of aged rats with spatial learning deficits. *Proc. Natl. Acad. Sci. U. S. A.* **93,** 9926–30 (1996).

156. Kempermann, G., Kuhn, H. G. & Gage, F. H. More hippocampal neurons in adult mice living in an enriched environment. *Nature* **386,** 493–495 (1997).

157. Kempermann, G. & Gage, F. H. Closer to neurogenesis in adult humans. *Nat. Med.* **4,** 555–7 (1998).

158. Kowalski, J., Gan, J., Jonas, P. & Pernía-Andrade, A. J. Intrinsic membrane properties determine hippocampal differential firing pattern in vivo in anesthetized rats. *Hippocampus* **26,** 668–82 (2016).

159. Stewart, M. & Fox, S. E. Firing relations of lateral septal neurons to the hippocampal theta rhythm in urethane anesthetized rats. *Exp. brain Res.* **79,** 92–6 (1990).

160. Freund, T. F. & Antal, M. GABA-containing neurons in the septum control inhibitory interneurons in the hippocampus. *Nature* **336,** 170–3 (1988).

161. Buzsáki, G. Theta oscillations in the hippocampus. *Neuron* **33,** 325–40 (2002).

162. Bartos, M., Vida, I. & Jonas, P. Synaptic mechanisms of synchronized gamma oscillations in inhibitory interneuron networks. *Nat. Rev. Neurosci.* **8,** 45–56 (2007).

163. Bragin, A. *et al.* Gamma (40-100 Hz) oscillation in the hippocampus of the behaving rat. *J. Neurosci.* **15,** 47–60 (1995).

164. Lisman, J. E. & Jensen, O. The Theta-Gamma Neural Code. *Neuron* **77,** 1002–1016 (2013).

165. Fries, P. Neuronal Gamma-Band Synchronization as a Fundamental Process in Cortical Computation. *Annu. Rev. Neurosci.* **32,** 209–224 (2009).

166. Varga, C., Golshani, P. & Soltesz, I. Frequency-invariant temporal ordering of interneuronal discharges during hippocampal oscillations in awake mice. *Proc. Natl. Acad. Sci. U. S. A.* **109,** E2726-34 (2012).

167. Orgy Buzsáki, G. & Wang, X.-J. Mechanisms of Gamma Oscillations. *Annu. Rev. Neurosci* **35,** 203–25 (2012).

168. Schmidt-Hieber, C., Jonas, P. & Bischofberger, J. Subthreshold Dendritic Signal Processing and Coincidence Detection in Dentate Gyrus Granule Cells. *J. Neurosci.* **27,** 8430–8441 (2007).

169. Krueppel, R., Remy, S. & Beck, H. Dendritic Integration in Hippocampal Dentate Granule Cells. *Neuron* **71,** 512–528 (2011).

170. Carnevale, N. T., Tsai, K. Y., Claiborne, B. J. & Brown, T. H. Comparative electrotonic analysis of three classes of rat hippocampal neurons. *J. Neurophysiol.* **78,** 703–20 (1997).

171. Claiborne, B. J., Amaral, D. G. & Cowan, W. M. A light and electron microscopic analysis of the mossy fibers of the rat dentate gyrus. *J. Comp. Neurol.* **246,** 435–458 (1986).

172. Ribak, C. E., Seress, L. & Amaral, D. G. The development, ultrastructure and synaptic connections of the mossy cells of the dentate gyrus. *J. Neurocytol.* **14,** 835–57 (1985).

173. Acsády, L., Kamondi, A., Sík, A., Freund, T. & Buzsáki, G. GABAergic cells are the major postsynaptic targets of mossy fibers in the rat hippocampus. *J. Neurosci.* **18,** 3386–403 (1998).

174. Amaral, D. & Lavenex, P. The Hippocampus Book. in *The Hippocampus Book* (eds. Andersen, P., Morris, R. G. M., Amaral, D., Bliss, T. & O'Keefe, J.) 1–852 (Oxford University Press, 2007).

175. Struble, R. G., Desmond, N. L. & Levy, W. B. Anatomical evidence for interlamellar inhibition in the fascia dentata. *Brain Res.* **152,** 580–5 (1978).

176. Sik, A., Penttonen, M. & Buzsáki, G. Interneurons in the hippocampal dentate gyrus: an in vivo intracellular study. *Eur. J. Neurosci.* **9,** 573–88 (1997).

177. Vida, I., Bartos, M. & Jonas, P. Shunting inhibition improves robustness of gamma oscillations in hippocampal interneuron networks by homogenizing firing rates. *Neuron* **49,** 107–17 (2006).

178. Morrison, J. H., Benoit, R., Magistretti, P. J., Ling, N. & Bloom, F. E. Immunohistochemical distribution of pro-somatostatin-related peptides in hippocampus. *Neurosci. Lett.* **34,** 137–42 (1982).

179. Boyett, J. M. & Buckmaster, P. S. Somatostatin-immunoreactive interneurons contribute to lateral inhibitory circuits in the dentate gyrus of control and epileptic rats. *Hippocampus* **11,** 418–22 (2001).

180. Amaral, D. G. & Dent, J. A. Development of the mossy fibers of the dentate gyrus: I. A light and electron microscopic study of the mossy fibers and their expansions. *J. Comp. Neurol.* **195,** 51–86 (1981).

181. Walker, M. C., Ruiz, A. & Kullmann, D. M. Do mossy fibers release GABA? *Epilepsia* **43 Suppl 5,** 196–202 (2002).

182. Chandy, J., Pierce, J. P. & Milner, T. A. Rat hippocampal mossy fibers contain cholecystokinin-like immunoreactivity. *Anat. Rec.* **243,** 519–23 (1995).

183. Chandler, K. E. *et al.* Plasticity of GABA(B) receptor-mediated heterosynaptic interactions at mossy fibers after status epilepticus. *J. Neurosci.* **23,** 11382–91 (2003).

184. Sperk, G. *et al.* Glutamate decarboxylase 67 is expressed in hippocampal mossy fibers of temporal lobe epilepsy patients. *Hippocampus* **22,** 590–603 (2012).

185. Hafting, T., Fyhn, M., Molden, S., Moser, M.-B. & Moser, E. I. Microstructure of a spatial map in the entorhinal cortex. *Nature* **436,** 801–806 (2005).

186. Witter, M. P., Groenewegen, H. J., Lopes da Silva, F. H. & Lohman, A. H. Functional organization of the extrinsic and intrinsic circuitry of the parahippocampal region. *Prog. Neurobiol.* **33,** 161–253 (1989).

187. Hargreaves, E. L., Rao, G., Lee, I. & Knierim, J. J. Major Dissociation Between Medial and Lateral Entorhinal Input to Dorsal Hippocampus. *Science.* **308,** 1792–1794 (2005).

188. Leutgeb, J. K., Leutgeb, S., Moser, M.-B. & Moser, E. I. Pattern Separation in the Dentate Gyrus and CA3 of the Hippocampus. *Science.* **315,** 961–966 (2007).

189. Kesner, R. P. An analysis of the dentate gyrus function. *Behav. Brain Res.* **254,** 1–7 (2013).

190. de Almeida, L., Idiart, M. & Lisman, J. E. The Input-Output Transformation of the Hippocampal Granule Cells: From Grid Cells to Place Fields. *J. Neurosci.* **29,** 7504–7512 (2009).

191. Lisman, J. E. Relating hippocampal circuitry to function: recall of memory sequences by reciprocal dentate-CA3 interactions. *Neuron* **22,** 233–42 (1999).

192. Hunsaker, M. R., Mooy, G. G., Swift, J. S. & Kesner, R. P. Dissociations of the medial and lateral perforant path projections into dorsal DG, CA3, and CA1 for spatial and nonspatial (visual object) information processing. *Behav. Neurosci.* **121,** 742–750 (2007).

193. Rolls, E. T. A theory of hippocampal function in memory. *Hippocampus* **6,** 601–20 (1996).

194. Bakker, A., Kirwan, C. B., Miller, M. & Stark, C. E. L. Pattern Separation in the Human Hippocampal CA3 and Dentate Gyrus. *Science.* **319,** 1640–1642 (2008).

195. Burke, S. N., Wallace, J. L., Nematollahi, S., Uprety, A. R. & Barnes, C. A. Pattern separation deficits may contribute to age-associated recognition impairments. *Behav. Neurosci.* **124,** 559–573 (2010).

196. Gilbert, P. E. & Kesner, R. P. The amygdala but not the hippocampus is involved in pattern separation based on reward value. *Neurobiol. Learn. Mem.* **77,** 338–53 (2002).

197. Kesner, R. P. & Gilbert, P. E. The role of the medial caudate nucleus, but not the hippocampus, in a matching-to sample task for a motor response. *Eur. J. Neurosci.* **23,** 1888–94 (2006).

198. Buckmaster, P. S. & Schwartzkroin, P. A. Hippocampal mossy cell function: a speculative view. *Hippocampus* **4,** 393–402 (1994).

199. Morris, A. M., Weeden, C. S., Churchwell, J. C. & Kesner, R. P. The role of the dentate gyrus in the formation of contextual representations. *Hippocampus* **23,** 162–168 (2013).

200. Lee, J. W. & Jung, M. W. Separation or binding? Role of the dentate gyrus in hippocampal mnemonic processing. *Neurosci. Biobehav. Rev.* **75,** 183–194 (2017).

201. Hetherington, P. A., Austin, K. B. & Shapiro, M. L. Ipsilateral associational pathway in the dentate gyrus: An excitatory feedback system that supportsN-methyl-D-aspartate—dependent long-term potentiation. *Hippocampus* **4,** 422–438 (1994).

202. Ambros-Ingerson, J., Granger, R. & Lynch, G. Simulation of paleocortex performs hierarchical clustering. *Science.* **247,** 1344–1348 (1990).

203. Kesner, R. P. A behavioral analysis of dentate gyrus function. in *Progress in brain research* **163,** 567–576 (2007).

204. Rolls, E. T. & Kesner, R. P. A computational theory of hippocampal function, and empirical tests of the theory. *Prog. Neurobiol.* **79,** 1–48 (2006).

205. Spanswick, S. C. & Sutherland, R. J. Object/context-specific memory deficits associated with loss of hippocampal granule cells after adrenalectomy in rats. *Learn. Mem.* **17,** 241–245 (2010).

206. Morris, A. M., Churchwell, J. C., Kesner, R. P. & Gilbert, P. E. Selective lesions of the dentate gyrus produce disruptions in place learning for adjacent spatial locations. *Neurobiol. Learn. Mem.* **97,** 326–331 (2012).

207. Aimone, J. B., Wiles, J. & Gage, F. H. Potential role for adult neurogenesis in the encoding of time in new memories. *Nat. Neurosci.* **9,** 723–727 (2006).

208. Emerich, D. F. & Walsh, T. J. Selective working memory impairments following intradentate injection of colchicine: attenuation of the behavioral but not the neuropathological effects by gangliosides GM1 and AGF2. *Physiol. Behav.* **45,** 93–101 (1989).

209. Wiebe, S. P. & Stäubli, U. V. Dynamic filtering of recognition memory codes in the hippocampus. *J. Neurosci.* **19,** 10562–74 (1999).

210. Aika, Y., Ren, J. Q., Kosaka, K. & Kosaka, T. Quantitative analysis of GABA-like-immunoreactive and parvalbumin-containing neurons in the CA1 region of the rat hippocampus using a stereological method, the disector. *Exp. brain Res.* **99,** 267–76 (1994).

211. Woodson, W., Nitecka, L. & Ben-Ari, Y. Organization of the GABAergic system in the rat hippocampal formation: a quantitative immunocytochemical study. *J. Comp. Neurol.* **280,** 254–71 (1989).

212. Markram, H. *et al.* Interneurons of the neocortical inhibitory system. *Nat. Rev. Neurosci.* **5,** 793–807 (2004).

213. Bartos, M. & Elgueta, C. Functional characteristics of parvalbumin- and cholecystokinin-expressing basket cells. *J. Physiol.* **590,** 669–681 (2012).

214. Baude, A., Bleasdale, C., Dalezios, Y., Somogyi, P. & Klausberger, T. Immunoreactivity for the GABAA Receptor 1 Subunit, Somatostatin and Connexin36 Distinguishes Axoaxonic, Basket, and Bistratified Interneurons of the Rat Hippocampus. *Cereb. Cortex* **17,** 2094–2107 (2007).

215. Miles, R., Tóth, K., Gulyás, A. I., Hájos, N. & Freund, T. F. Differences between somatic and dendritic inhibition in the hippocampus. *Neuron* **16,** 815–823 (1996).

216. Pouille, F. & Scanziani, M. Enforcement of temporal fidelity in pyramidal cells by somatic feed-forward inhibition. *Science* **293,** 1159–63 (2001).

217. Bezaire, M. J. & Soltesz, I. Quantitative assessment of CA1 local circuits: knowledge base for interneuron-pyramidal cell connectivity. *Hippocampus* **23,** 751–85 (2013).

218. Donato, F., Rompani, S. B. & Caroni, P. Parvalbumin-expressing basket-cell network plasticity induced by experience regulates adult learning. *Nature* **504,** 272–276 (2013).

219. Jonas, P., Bischofberger, J., Fricker, D. & Miles, R. Interneuron Diversity series: Fast in, fast out – temporal and spatial signal processing in hippocampal interneurons. *Trends Neurosci.* **27,** 30–40 (2004).

220. Doischer, D. *et al.* Postnatal differentiation of basket cells from slow to fast signaling devices. *J. Neurosci.* **28,** 12956–68 (2008).

221. Bartos, M. *et al.* Fast synaptic inhibition promotes synchronized gamma oscillations in hippocampal interneuron networks. *Proc. Natl. Acad. Sci. U. S. A.* **99,** 13222–7 (2002).

222. Glickfeld, L. L. & Scanziani, M. Distinct timing in the activity of cannabinoid-sensitive and cannabinoid-insensitive basket cells. *Nat. Neurosci.* **9,** 807–15 (2006).

223. Emri, Z., Antal, K., Gulyás, A. I., Megías, M. & Freund, T. F. Electrotonic profile and passive propagation of synaptic potentials in three subpopulations of hippocampal CA1 interneurons. *Neuroscience* **104,** 1013–26 (2001).

224. Nörenberg, A., Hu, H., Vida, I., Bartos, M. & Jonas, P. Distinct nonuniform cable properties optimize rapid and efficient activation of fast-spiking GABAergic interneurons. *Proc. Natl. Acad. Sci. U. S. A.* **107,** 894–9 (2010).

225. Hu, H., Martina, M. & Jonas, P. Dendritic Mechanisms Underlying Rapid Synaptic Activation of Fast-Spiking Hippocampal Interneurons. *Science.* **327,** 52–58 (2010).

226. Dingledine, R., Borges, K., Bowie, D. & Traynelis, S. F. The glutamate receptor ion channels. *Pharmacol. Rev.* **51,** 7–61 (1999).

227. Geiger, J. R. *et al.* Relative abundance of subunit mRNAs determines gating and Ca2+ permeability of AMPA receptors in principal neurons and interneurons in rat CNS. *Neuron* **15,** 193–204 (1995).

228. Lamsa, K., Irvine, E. E., Giese, K. P. & Kullmann, D. M. NMDA receptor-dependent long-term potentiation in mouse hippocampal interneurons shows a unique dependence on Ca $^{2+}$ /calmodulin-dependent kinases. *J. Physiol.* **584,** 885–894 (2007).

229. Aponte, Y., Bischofberger, J. & Jonas, P. Efficient Ca 2+ buffering in fast-spiking basket cells of rat hippocampus. *J Physiol* **5868,** 2061–2075 (2008).

230.   Han, Z. S., Buhl, E. H., Lörinczi, Z. & Somogyi, P. A high degree of spatial selectivity in the axonal and dendritic domains of physiologically identified local-circuit neurons in the dentate gyrus of the rat hippocampus. *Eur. J. Neurosci.* **5,** 395–410 (1993).

231.   Halasy, K. & Somogyi, P. Subdivisions in the multiple GABAergic innervation of granule cells in the dentate gyrus of the rat hippocampus. *Eur. J. Neurosci.* **5,** 411–29 (1993).

232.   Soriano, E., Nitsch, R. & Frotscher, M. Axo-axonic chandelier cells in the rat fascia dentata: Golgi-electron microscopy and immunocytochemical studies. *J. Comp. Neurol.* **293,** 1–25 (1990).

233.   Freund, T. F., Martin, K. A., Smith, A. D. & Somogyi, P. Glutamate decarboxylase-immunoreactive terminals of Golgi-impregnated axoaxonic cells and of presumed basket cells in synaptic contact with pyramidal neurons of the cat's visual cortex. *J. Comp. Neurol.* **221,** 263–78 (1983).

234.   Buckmaster, P. S. & Schwartzkroin, P. A. Interneurons and inhibition in the dentate gyrus of the rat in vivo. *J. Neurosci.* **15,** 774–89 (1995).

235.   Amaral, D. G. A Golgi study of cell types in the hilar region of the hippocampus in the rat. *J. Comp. Neurol.* **182,** 851–914 (1978).

236.   Gulyás, A. I., Miettinen, R., Jacobowitz, D. M. & Freund, T. F. Calretinin is present in non-pyramidal cells of the rat hippocampus--I. A new type of neuron specifically associated with the mossy fibre system. *Neuroscience* **48,** 1–27 (1992).

237.   Somogyi, P. *et al.* Different populations of GABAergic neurons in the visual cortex and hippocampus of cat contain somatostatin- or cholecystokinin-immunoreactive material. *J. Neurosci.* **4,** 2590–603 (1984).

238.   Bakst, I., Avendano, C., Morrison, J. H. & Amaral, D. G. An experimental analysis of the origins of somatostatin-like immunoreactivity in the dentate gyrus of the rat. *J. Neurosci.* **6,** 1452–62 (1986).

239.   Tóth, K. & Freund, T. F. Calbindin D28k-containing nonpyramidal cells in the rat hippocampus: their immunoreactivity for GABA and projection to the medial septum. *Neuroscience* **49,** 793–805 (1992).

240.   Miettinen, R., Gulyás, A. I., Baimbridge, K. G., Jacobowitz, D. M. & Freund, T. F. Calretinin is present in non-pyramidal cells of the rat hippocampus--II. Co-existence with other calcium binding proteins and GABA. *Neuroscience* **48,** 29–43 (1992).

241.   Kosaka, T. *et al.* GABAergic neurons containing CCK-8-like and/or VIP-like immunoreactivities in the rat hippocampus and dentate gyrus. *J. Comp. Neurol.* **239,** 420–30 (1985).

242.   Hajos, N., Acsady, L. & Freund, T. F. Target selectivity and neurochemical characteristics of VIP-immunoreactive interneurons in the rat dentate gyrus. *Eur. J. Neurosci.* **8,** 1415–31 (1996).

243.   Jiang, X. *et al.* Principles of connectivity among morphologically defined cell types in adult neocortex. *Science.* **350,** 9462 (2015).

244.   Merker, B. Cortical gamma oscillations: the functional key is activation, not cognition. *Neurosci. Biobehav. Rev.* **37,** 401–417 (2013).

245.   Lewis, D. A., Hashimoto, T. & Volk, D. W. Cortical inhibitory neurons and schizophrenia. *Nat. Rev. Neurosci.* **6,** 312–324 (2005).

246.   Uhlhaas, P. J. & Singer, W. Neural Synchrony in Brain Disorders: Relevance for Cognitive Dysfunctions and Pathophysiology. *Neuron* **52,** 155–168 (2006).

247.   Herreras, O. Local Field Potentials: Myths and Misunderstandings. *Front. Neural Circuits* **10,** 101 (2016).

248.   Colgin, L. L. Rhythms of the hippocampal network. *Nat. Rev. Neurosci.* **17,** 239–249 (2016).

249.   Belluscio, M. A., Mizuseki, K., Schmidt, R., Kempter, R. & Buzsaki, G. Cross-Frequency Phase-Phase Coupling between Theta and Gamma Oscillations in the Hippocampus. *J. Neurosci.* **32,** 423–435 (2012).

250.   Gloveli, T. *et al.* Orthogonal arrangement of rhythm-generating microcircuits in the hippocampus. *Proc. Natl. Acad. Sci.* **102,** 13295–13300 (2005).

251.   Mann, E. O., Radcliffe, C. A. & Paulsen, O. Hippocampal gamma-frequency oscillations: from interneurones to pyramidal cells, and back. *J. Physiol.* **562,** 55–63 (2005).

252.   Oren, I., Mann, E. O., Paulsen, O. & Hajos, N. Synaptic Currents in Anatomically Identified CA3 Neurons during Hippocampal Gamma Oscillations In Vitro. *J. Neurosci.* **26,** 9923–9934 (2006).

253.   Cardin, J. A. *et al.* Driving fast-spiking cells induces gamma rhythm and controls sensory responses. *Nature* **459,** 663–667 (2009).

254.   Sohal, V. S., Zhang, F., Yizhar, O. & Deisseroth, K. Parvalbumin neurons and gamma rhythms enhance cortical circuit performance. *Nature* **459,** 698–702 (2009).

255.   Akam, T. & Kullmann, D. M. Oscillations and Filtering Networks Support Flexible Routing of Information. *Neuron* **67,** 308–320 (2010).

256.   de Almeida, L., Idiart, M. & Lisman, J. E. A Second Function of Gamma Frequency Oscillations: An E%-Max Winner-Take-All Mechanism Selects Which Cells Fire. *J. Neurosci.* **29,** 7497–7503 (2009).

257.   Kobayashi, K. & Poo, M. Spike train timing-dependent associative modification of hippocampal CA3 recurrent synapses by mossy fibers. *Neuron* **41,** 445–54 (2004).

258.   Davies, C. H., Starkey, S. J., Pozza, M. F. & Collingridge, G. L. GABA autoreceptors regulate the induction of LTP. *Nature* **349,** 609–11 (1991).

259.   Pavlides, C., Greenstein, Y. J., Grudman, M. & Winson, J. Long-term potentiation in the dentate gyrus is induced preferentially on the positive phase of theta-rhythm. *Brain Res.* **439,** 383–7 (1988).

260. Hyman, J. M., Wyble, B. P., Goyal, V., Rossi, C. A. & Hasselmo, M. E. Stimulation in hippocampal region CA1 in behaving rats yields long-term potentiation when delivered to the peak of theta and long-term depression when delivered to the trough. *J. Neurosci.* **23,** 11725–31 (2003).

261. Colgin, L. L. Theta–gamma coupling in the entorhinal–hippocampal system. *Curr. Opin. Neurobiol.* **31,** 45–50 (2015).

262. Bott, J.-B. *et al.* Spatial Reference Memory is Associated with Modulation of Theta–Gamma Coupling in the Dentate Gyrus. *Cereb. Cortex* **26,** 3744–3753 (2016).

263. White, D. J., Congedo, M., Ciorciari, J. & Silberstein, R. B. Brain Oscillatory Activity during Spatial Navigation: Theta and Gamma Activity Link Medial Temporal and Parietal Regions. *J. Cogn. Neurosci.* **24,** 686–697 (2012).

264. Buzsáki, G. & Draguhn, A. Neuronal oscillations in cortical networks. *Science* **304,** 1926–9 (2004).

265. Engel, A. K. & Singer, W. Temporal binding and the neural correlates of sensory awareness. *Trends Cogn. Sci.* **5,** 16–25 (2001).

266. Korotkova, T., Fuchs, E. C., Ponomarenko, A., von Engelhardt, J. & Monyer, H. NMDA Receptor Ablation on Parvalbumin-Positive Interneurons Impairs Hippocampal Synchrony, Spatial Representations, and Working Memory. *Neuron* **68,** 557–569 (2010).

267. Howard, M. W. *et al.* Gamma oscillations correlate with working memory load in humans. *Cereb. Cortex* **13,** 1369–74 (2003).

268. Lisman, J. E. & Grace, A. A. The Hippocampal-VTA Loop: Controlling the Entry of Information into Long-Term Memory. *Neuron* **46,** 703–713 (2005).

269. Paulsen, O. & Moser, E. I. A model of hippocampal memory encoding and retrieval: GABAergic control of synaptic plasticity. *Trends Neurosci.* **21,** 273–8 (1998).

270. Dudai, Y. The Neurobiology of Consolidations, Or, How Stable is the Engram? *Annu. Rev. Psychol.* **55,** 51–86 (2004).

271. Wess, J., Nakajima, K. & Jain, S. Novel designer receptors to probe GPCR signaling and physiology. *Trends Pharmacol. Sci.* **34,** 385–392 (2013).

272. Leger, M. *et al.* Object recognition test in mice. *Nat. Protoc.* **8,** 2531–7 (2013).

273. Pellow, S., Chopin, P., File, S. E. & Briley, M. Validation of open:closed arm entries in an elevated plus-maze as a measure of anxiety in the rat. *J. Neurosci. Methods* **14,** 149–67 (1985).

274. Pellow, S. & File, S. E. Anxiolytic and anxiogenic drug effects on exploratory activity in an elevated plus-maze: a novel test of anxiety in the rat. *Pharmacol. Biochem. Behav.* **24,** 525–9 (1986).

275. Andersen, P., Holmqvist, B. & Voorhoeve, P. E. Entorhinal activation of dentate granule cells. *Acta Physiol. Scand.* **66,** 448–60 (1966).

276. Stäubli, U., Scafidi, J. & Chun, D. GABAB receptor antagonism: facilitatory effects on memory parallel those on LTP induced by TBS but not HFS. *J. Neurosci.* **19,** 4609–15 (1999).

277. Pérez-Cervera, L. *et al.* Mapping Functional Connectivity in the Rodent Brain Using Electric-Stimulation fMRI. in *Methods in molecular biology (Clifton, N.J.)* **1718,** 117–134 (2018).

278. Shyu, B.-C., Lin, C.-Y., Sun, J.-J., Sylantyev, S. & Chang, C. A method for direct thalamic stimulation in fMRI studies using a glass-coated carbon fiber electrode. *J. Neurosci. Methods* **137,** 123–131 (2004).

279. Moreno, A., Morris, R. G. M. & Canals, S. Frequency-Dependent Gating of Hippocampal–Neocortical Interactions. *Cereb. Cortex* **26,** 2105–2114 (2016).

280. Franklin, K. B. J. & Paxinos, G. *Paxinos and Franklin's The mouse brain in stereotaxic coordinates*. (2012).

281. George, D. & Mallery, M. *SPSS for Windows Step by Step: A Simple Guide and Reference, 17.0 update*. (Pearson, 2010).

282. Cohen, J. *Statistical Power Analysis for the Behavioral Sciences*. (Elsevier, 1977). doi:10.1016/C2013-0-10517-X

283. Condé, F., Maire-lepoivre, E., Audinat, E. & Crépel, F. Afferent connections of the medial frontal cortex of the rat. II. Cortical and subcortical afferents. *J. Comp. Neurol.* **352,** 567–593 (1995).

284. Jay, T. M., Glowinski, J. & Thierry, A.-M. Selectivity of the hippocampal projection to the prelimbic area of the prefrontal cortex in the rat. *Brain Res.* **505,** 337–340 (1989).

285. Takita, M., Fujiwara, S.-E. & Izaki, Y. Functional structure of the intermediate and ventral hippocampo–prefrontal pathway in the prefrontal convergent system. *J. Physiol.* **107,** 441–447 (2013).

286. Preston, A. R. & Eichenbaum, H. Interplay of Hippocampus and Prefrontal Cortex in Memory. *Curr. Biol.* **23,** R764–R773 (2013).

287. Morici, J. F., Bekinschtein, P. & Weisstaub, N. V. Medial prefrontal cortex role in recognition memory in rodents. *Behav. Brain Res.* **292,** 241–251 (2015).

288. Canals, S., Beyerlein, M., Merkle, H. & Logothetis, N. K. Functional MRI Evidence for LTP-Induced Neural Network Reorganization. *Curr. Biol.* **19,** 398–403 (2009).

289. Tolias, A. S., Keliris, G. A., Smirnakis, S. M. & Logothetis, N. K. Neurons in macaque area V4 acquire directional tuning after adaptation to motion stimuli. *Nat. Neurosci.* **8,** 591–593 (2005).

290. Alvarez-Salvado, E., Pallares, V., Moreno, A. & Canals, S. Functional MRI of long-term potentiation: imaging network plasticity. *Philos. Trans. R. Soc. B Biol. Sci.* **369,** 20130152–20130152 (2013).

291. Logothetis, N. K., Pauls, J., Augath, M., Trinath, T. & Oeltermann, A. Neurophysiological investigation of the basis of the fMRI signal. *Nature* **412,** 150–157 (2001).

292. Bannerman, D. . *et al.* Regional dissociations within the hippocampus—memory and anxiety. *Neurosci. Biobehav. Rev.* **28,** 273–283 (2004).

293. Kullmann, D. M. & Lamsa, K. P. LTP and LTD in cortical GABAergic interneurons: Emerging rules and roles. *Neuropharmacology* **60,** 712–719 (2011).

294. Letzkus, J. J., Wolff, S. B. E. & Lüthi, A. Disinhibition, a Circuit Mechanism for Associative Learning and Memory. *Neuron* **88,** 264–276 (2015).

295. Carandini, M. & Heeger, D. J. Normalization as a canonical neural computation. *Nat. Rev. Neurosci.* **13,** 51–62 (2012).

296. Isaacson, J. S. & Scanziani, M. How Inhibition Shapes Cortical Activity. *Neuron* **72,** 231–243 (2011).

297. Atallah, B. V., Bruns, W., Carandini, M. & Scanziani, M. Parvalbumin-Expressing Interneurons Linearly Transform Cortical Responses to Visual Stimuli. *Neuron* **73,** 159–170 (2012).

298. Wilson, N. R., Runyan, C. A., Wang, F. L. & Sur, M. Division and subtraction by distinct cortical inhibitory networks in vivo. *Nature* **488,** 343–348 (2012).

299. Pouille, R. & Scanziani, M. Routing of spike series by dynamic circuits in the hippocampus. *Nature* **429,** 717–723 (2004).

300. Martin, K. A. A brief history of the "feature detector". *Cereb. Cortex* **4,** 1–7

301. Eichenbaum, H. Prefrontal–hippocampal interactions in episodic memory. *Nat. Rev. Neurosci.* **18,** 547–558 (2017).

302. Siapas, A. G. & Wilson, M. A. Coordinated interactions between hippocampal ripples and cortical spindles during slow-wave sleep. *Neuron* **21,** 1123–8 (1998).

303. Wiltgen, B. J., Brown, R. A. M., Talton, L. E. & Silva, A. J. New Circuits for Old Memories. *Neuron* **44,** 101–108 (2004).

304. Tompary, A. & Davachi, L. Consolidation Promotes the Emergence of Representational Overlap in the Hippocampus and Medial Prefrontal Cortex. *Neuron* **96,** 228–241.e5 (2017).

305. Wirt, R. & Hyman, J. Integrating Spatial Working Memory and Remote Memory: Interactions between the Medial Prefrontal Cortex and Hippocampus. *Brain Sci.* **7,** 43 (2017).

306. O'Neill, P.-K., Gordon, J. A. & Sigurdsson, T. Theta Oscillations in the Medial Prefrontal Cortex Are Modulated by Spatial Working Memory and Synchronize with the Hippocampus through Its Ventral Subregion. *J. Neurosci.* **33,** 14211–14224 (2013).

307. Hiser, J. & Koenigs, M. The Multifaceted Role of the Ventromedial Prefrontal Cortex in Emotion, Decision Making, Social Cognition, and Psychopathology. *Biol. Psychiatry* **83,** 638–647 (2018).

308. Konishi, S. *et al.* Transient activation of inferior prefrontal cortex during cognitive set shifting. *Nat. Neurosci.* **1,** 80–84 (1998).

309. Sekeres, M. J., Winocur, G. & Moscovitch, M. The hippocampus and related neocortical structures in memory transformation. *Neurosci. Lett.* (2018). doi:10.1016/j.neulet.2018.05.006

310. Schacter, G. B., Yang, C. R., Innis, N. K. & Mogenson, G. J. The role of the hippocampal-nucleus accumbens pathway in radial-arm maze performance. *Brain Res.* **494,** 339–49 (1989).

311. Morris, M. K., Bowers, D., Chatterjee, A. & Heilman, K. M. Amnesia following a discrete basal forebrain lesion. *Brain* **115 (Pt 6,** 1827–47 (1992).

312. Kim, M. & McGaugh, J. L. Effects of intra-amygdala injections of NMDA receptor antagonists on acquisition and retention of inhibitory avoidance. *Brain Res.* **585,** 35–48 (1992).

313. Graybiel, A. M. The Basal Ganglia and Chunking of Action Repertoires. *Neurobiol. Learn. Mem.* **70,** 119–136 (1998).

314. Manenti, R. *et al.* Strengthening of Existing Episodic Memories Through Non-invasive Stimulation of Prefrontal Cortex in Older Adults with Subjective Memory Complaints. *Front. Aging Neurosci.* **9,** 401 (2017).

315. Ravishankar, M. *et al.* Cortical-hippocampal functional connectivity during covert consolidation sub-serves associative learning: Evidence for an active 'rest' state. *Brain Cogn.* (2017). doi:10.1016/j.bandc.2017.10.003

316. Rajasethupathy, P. *et al.* Projections from neocortex mediate top-down control of memory retrieval. *Nature* **526,** 653–659 (2015).

317. Squire, L. R. & Alvarez, P. Retrograde amnesia and memory consolidation: a neurobiological perspective. *Curr. Opin. Neurobiol.* **5,** 169–177 (1995).

318. Carpenter, G. A. & Grossberg, S. Normal and amnesic learning, recognition and memory by a neural model of cortico-hippocampal interactions. *Trends Neurosci.* **16,** 131–7 (1993).

319. Frankland, P. W. & Bontempi, B. The organization of recent and remote memories. *Nat. Rev. Neurosci.* **6,** 119–130 (2005).

320. Squire, L. R., Genzel, L., Wixted, J. T. & Morris, R. G. Memory consolidation. *Cold Spring Harb. Perspect. Biol.* **7,** a021766 (2015).

321. Josselyn, S. A., Köhler, S. & Frankland, P. W. Finding the engram. *Nat. Rev. Neurosci.* **16,** 521–534 (2015).

322. Tonegawa, S., Pignatelli, M., Roy, D. S. & Ryan, T. J. Memory engram storage and retrieval. *Curr. Opin. Neurobiol.* **35,** 101–109 (2015).

323. Stefanelli, T., Bertollini, C., Lüscher, C., Muller, D. & Mendez, P. Hippocampal Somatostatin Interneurons Control the Size of Neuronal Memory Ensembles. *Neuron* **89,** 1074–1085 (2016).

324. Morgan, J. I. & Curran, T. Regulation of c-fos Expression by Voltage-Dependent Calcium Channels. in *Cell Calcium Metabolism* 305–312 (Springer US, 1989).

325. Fields, R. D., Eshete, F., Stevens, B. & Itoh, K. Action potential-dependent regulation of gene expression: temporal specificity in ca2+, cAMP-responsive element binding proteins, and mitogen-activated protein kinase signaling. *J. Neurosci.* **17,** 7252–66 (1997).

326. Li, C.-Y. *et al.* Estradiol suppresses neuronal firing activity and c-Fos expression in the lateral habenula. *Mol. Med. Rep.* **12,** 4410–4414 (2015).

327. Kirk, R. A., Redmon, S. N. & Kesner, R. P. The ventral dentate gyrus mediates pattern separation for reward value. *Behav. Neurosci.* **131,** 42–45 (2017).

328. Seress, L. & Ribak, C. E. Ultrastructural features of primate granule cell bodies show important differences from those of rats: axosomatic synapses, somatic spines and infolded nuclei. *Brain Res.* **569,** 353–7 (1992).

329. Seress, L. & Pokorny, J. Structure of the granular layer of the rat dentate gyrus. A light microscopic and Golgi study. *J. Anat.* **133,** 181–95 (1981).

330. Seress, L. & Frotscher, M. Basket cells in the monkey fascia dentata: a Golgi/electron microscopic study. *J. Neurocytol.* **20,** 915–28 (1991).

331. Seress, L., Gulyáas, A. I. & Freund, T. F. Parvalbumin- and calbindin D $_{28K}$ -immunoreactive neurons in the hippocampal formation of the macaque monkey. *J. Comp. Neurol.* **313,** 162–177 (1991).

332. Sterling, P. & Laughlin, S. *Principles of neural design*. (The MIT Press) (2015).

X.- ANNEX.

Mapping Functional Connectivity in the Rodent Brain Using Electric-Stimulation fMRI.

Laura Pérez-Cervera[1], José María Caramés[1], Luis Miguel Fernández-Mollá[2], Andrea Moreno[1,3], Begoña Fernández[1], Elena Pérez-Montoyo[1], David Moratal[2], Santiago Canals[1], Jesús Pacheco-Torres[1]

[1] Instituto de Neurociencias, Consejo Superior de Investigaciones Científicas, Universidad Miguel Hernández, Sant Joan d'Alacant 03550, Spain

[2] Center for Biomaterials and Tissue Engineering, Universitat Politècnica de València, Valencia 46022, Spain

[3] Centre for Cognitive and Neural Systems, University of Edinburgh, EH8 9JZ, UK.

ABSTRACT

Since its discovery in the early 90s, BOLD signal-based functional Magnetic Resonance Imaging (fMRI) has become a fundamental technique for the study of brain activity in basic and clinical research. Functional MRI signals provide an indirect but robust and quantitative readout of brain activity through the tight coupling between cerebral blood flow and neuronal activation, the so-called neurovascular coupling. Combined with experimental techniques only available in animal models, such as intracerebral micro-stimulation, optogenetics or pharmacogenetics, provides a powerful framework to investigate the impact of specific circuit manipulations on overall brain dynamics. The purpose of this chapter is to provide a comprehensive protocol to measure brain activity using fMRI with intracerebral electric micro-stimulation in murine models. Preclinical research (especially in rodents) opens the door to very sophisticated and informative experiments, but at the same time imposes important constrains (i.e. anaesthetics, translatability, etc.), some of which will be addressed here.

1. INTRODUCTION

Neuroscience is currently one of the most challenging areas of biomedical research. The human brain and its function remain one of the last frontiers for modern science. Furthermore, there is a growing belief that its scientific understanding will have a profound effect on human progress, not only because of the improvement in treating neurologic and psychiatric

disorders, but also because of the impact that a deep understanding of the brain would have on fields ranging from education, interpersonal relationships, the prolongation of a full physical and intellectual life and also for the development of a neuro-inspired ICT society. In order to achieve this major goal, scientists need techniques that allow proper monitoring of brain function. Ideally, these techniques should satisfy the following criteria:

a) Applicable *in vivo* to study the intact brain.

b) To provide adequate temporal and spatial resolution.

c) To reflect the electrical activity of neurons as close as possible.

d) To be applicable in human and non-human animal models.

Over the past few decades, multiple non-invasive *in vivo* imaging methodologies have been developed to study brain function, although none of them has been able to fulfil all of the above mentioned criteria. These attempts can be classified on the basis of their strategies for measuring brain activity: either directly assessing the electrical activity of the brain, or indirectly through surrogate measures as calcium transients, hemodynamic and/or metabolic changes associated to neuronal activity. Amongst the former we can include electroencephalography (EEG) and magnetoencephalography (MEG), which present excellent temporal resolution but have its particular *Achilles' heel* in the spatial resolution. The second category includes, amongst others, Positron Emission Tomography (PET) and Magnetic Resonance Imaging (MRI). Functional PET applications relay in the use of radioactively-labelled compounds metabolically active (15-Oxygen, Fludeoxyglucose) whose measurement reports changes in blood flow, oxygen and/or glucose consumption, which are surrogates of neuronal activity. PET presents the highest sensitivity of all the aforementioned techniques, but the necessary use of radioactive compounds -with their short half-life and the relatively low spatial resolution- has hindered his widespread for neurological imaging purposes (see ref [1] for a review on neuroimaging techniques).

Functional magnetic resonance imaging (fMRI) utilizes MRI technology to indirectly measure brain activity by detecting changes associated with it. The best-known form of fMRI uses the blood-oxygen-level dependent (BOLD) contrast [2]. It relies on the brain's ability to locally modulate blood flow and volume to satisfy the increased energetic needs during neuronal activation. The relationship between increased local neural activity and changes in cerebral blood flow (CBF) is known as neurovascular coupling (or functional hyperemia). The correlation between BOLD signals and concomitantly recorded electrophysiological measures is well established [3,4], although the exact molecular mechanism remains unclear [5] and its homogeneity throughout brain regions debated [4]. Functional MRI allows imaging brain activations with a spatial resolution as low as a few hundreds of microns (limited by the low intrinsic sensitivity of MRI, the small expected changes in signal intensity and the point spread function; for a review see [6]) and with a temporal resolution of seconds or even shorter (limited by the nature of the hemodynamic response itself).

It is important to stress that BOLD signals do not measure neuronal activity, but changes in neuronal activity (see [6] for a deeper discussion on the fundamentals of BOLD). Nevertheless, these changes in neuronal activity can occur spontaneously whilst the subject is not involved in any specific task. In those conditions the changes are of small amplitude and are referred to as *resting state* activity. Alternatively, the change in activity can be boosted by introducing a specific paradigm that defines an expected low activity state (baseline) and a high activity state (activation) that are subsequently contrasted statistically. Common paradigms include the presentation of sensory stimuli, the introduction of a cognitive task, the administration of chemical substances, or the direct stimulation of the brain's parenchyma. In animal models, the availability of a larger repertoire of neuronal stimulation strategies allows the precise control of the stimulation parameters and neuronal populations being targeted. These strategies include intracerebral direct electrical micro-stimulation and optogenetic or pharmacogenetic stimulation or inhibition of specific neuronal populations. These might overcome some of the limitations of sensory and task stimulation when the focus of the study is to unveil the precise neuronal circuits involved in a certain functional state. For instance, whilst activation of primary sensory structures is in some cases readily available by sensory stimulation, recruitment of other regions as some subcortical nuclei is more challenging. Also, the polysynaptic propagation of activity in intricate brain networks initiated by sensory stimuli or cognitive tasks makes it harder to investigate direct relationships or causality. Direct activation of a specific pathway or a neuronal population greatly eases such studies, allowing to study the consequences of precisely timed and accurately localized manipulation on the overall response of brain-wide networks.

Highly sophisticated and rich experiments can be done in animal models by the combination of fMRI with electrophysiological, optogenetic and pharmacogenetic tools. However, the use of animals (especially small animals as rats and mice) imposes certain limitations that need to be considered carefully. Spatial resolution issues, due to the smaller size of rodent's brains compared to primates, have been partially countervailed by the implementation of systems with ultrahigh magnetic fields and stronger radiofrequency gradients, yet still the obtained resolution is coarse for imaging certain subcortical structures. Therefore, partial volume effects need to be seriously considered. Also, the need for the absolute immobility of the subject during image acquisition has favored the used of anesthetized animals in most of the studies. Besides the obvious impact of anesthesia on neuronal activation, additional factors need to be considered in fMRI studies since anesthetics could directly impact on the hemodynamic response and the neurovascular coupling (discussed in detail in section 3.1)[7] amongst other neuronal activation features. Some alternatives to avoid anesthetics are present, e.g. habituation training protocols which allow to do fMRI experiments in non-anesthetized rodents [8,9] [1-3]. Although they are very appealing and pave the way to advance in rodent fMRI, the available protocols involve an initial period of severe stress during habituation to the MRI environment which could interfere with the particular scientific question at hand. Finally, further complications derived from the combination of fMRI

with other recording or stimulation techniques include the need for MRI-compatible materials in all implants and devices required in the experiment.

The present protocol describes, stepwise, how to perform a BOLD fMRI experiment with intracerebral electric micro-stimulation, which has allowed us to (1) perform precise and controlled activations of selected brain regions, (2) reproducibly acquire data within and between animals in rats and mice, (3) to investigate the frequency-dependence of activity propagation in brain networks and (4) to provide several insights into the synaptic plasticity control of long range connectivity.

2. MATERIALS

2.1. Carbon electrode preparation

1. Theta-shaped glass capillary (World Precision Instruments, Florida, USA).

2. Carbon fibres (Goodfellow Cambridge Limited, UK).

3. Micropipette puller (e.g., Sutter Instrument, Novato, CA, USA).

4. Bunsen burner.

5. Standard forceps, straight (e.g., Fine Science Tools part no. 11000-13; Foster City, CA, USA).

6. London forceps, angled (e.g., Fine Science Tools part no. 11080-02; Foster City, CA, USA).

7. Epoxy resin (fast drying) (Araldite, Huntsman Advanced Materials GmbH, Switzerland).

8. Silver conductive epoxy resin (RS Components, UK).

2.2. Electrode implantation surgery

1. Isoflurane (Braun Medical S.A., Barcelona, Spain).

2. Urethane (Sigma-Aldrich, Missouri, USA).

3. Bupivacaine (Braun Medical S.A., Barcelona, Spain).

4. Stereotaxic frame (Narishige, Tokyo, Japan) and stereotaxic micromanipulator (SM-15, Narishige, Japan).

5. Ophthalmic gel (Lipolac,Angelini Farmaceutica S.A., Barcelona, Spain).

6. Heating pad with rectal thermal probe.

7. Surgical instruments:

a) Small surgical scissors, straight (e.g., Fine Science Tools part no. 14084-08; Foster City, CA, USA).

b) Standard forceps, straight (e.g., Fine Science Tools part no. 11000-13; Foster City, CA, USA).

c) Dumont forceps, straight (e.g., Fine Science Tools part no 11251-20; Foster City, CA, USA).

d) Scalpel handle, straight (e.g., Fine Science Tools part no 10004-13; Foster City, CA, USA).

e) Non-sterile scalpel blade, curved, 22 (e.g., Fine Science Tools part no 10022-00; Foster City, CA, USA).

f) Micro curette, straight (e.g., Fine Science Tools part no 10081-10; Foster City, CA, USA).

g) Micro drill trephine (e.g., Fine Science Tools part no 18004-23; Foster City, CA, USA).

8. Sterile saline solution and hydrogen peroxide.

9. High-temperature Cautery kit (Bovie Medical Corporation, NY, USA).

10. Cotton.

11. Shaver (e.g., Remington, Ellwangen, Germany).

12. Permanent marker (e.g., Staedtler, Germany).

13. 20G and 25G needles (e.g., BD Microlance, Becton Dickinson, Madrid, Spain).

14. Tissue adhesive (Vetbond, 3M Animal Care products, Minnesota, USA).

15. Bone acrylic (Palacos, Heraeus Medical GmbH, Wehrheim, Germany).

16. Super-Bond C&B dental acrylic (Sun Medical Co. Moriyama, Shiga, Japan).

2.3. fMRI

The additional materials listed here are required to produce electrical brain stimulation in the rat whilst it remains in the magnet and acquire and process imaging data.

1. MRI magnet. We use a horizontal 7 Tesla scanner with a 30 cm diameter bore (Biospec 70/30v, Bruker Medical, Ettlingen, Germany). The

system has a 675 mT/m actively shielded gradient coil (Bruker, BGA 12-S) of 11.4 cm inner diameter. Data is acquired and pre-processed with a Hewlett-Packard console running Paravision 5.1 software (Bruker Medical GmbH, Ettlingen, Germany) operating on a Linux platform.

2. <u>MRI coil.</u> It is not indispensable, but it highly convenient. The expected signal changes are in the range of 1-3% of the total signal intensity, thus it will critically contribute to achieve the highest possible signal to noise ratio (SNR). We employ a ^{1}H rat brain receive-only phase array coil with integrated combiner and preamplifier, no tune/no match, in combination with the actively detuned transmit-only resonator (BrukerBioSpin MRI GmbH, Germany)

3. <u>Physiological monitoring and control system.</u> We use a MRI-compatible temperature control unit (MultiSens Signal conditioner, OpSens, Quebec, Canada). Other physiological parameters as heart rate (optimal values, 300 ± 50 beats per minute), oxygen saturation (>95%) and breathing rate (90 ± 10 breaths per minute) are monitored (see note [1]) throughout the session using an MRI-compatible sensor with foot clip (MouseOx, Starr Life Sciences, Oakmont, US). Physiological parameters can be used to feed the analysis of BOLD signals (used as nuisance factors) which might be especially important in resting state experiments.

4. <u>Heating system.</u> It is crucial to keep the animal's temperature in the physiological range, and to maintain it stable (37±0.5 ºC) in order to preserve vascular reactivity in response to neuronal activation. We use a water blanket connected to a water bath (Thermo Scientific SAHARA Heated Bath Circulators S5P) controlled by a temperature regulatory system (Thermo Scientific STANDARD Series Thermostats SC150) (see note [2]).

In the above system, precise control of the animal's temperature requires the constant attention of dedicated personnel to manually vary the temperature in the heating bath. In order to automate this process, a home-made and inexpensive closed loop regulation system has been developed to adjust water bath temperature to keep a constant body temperature in the animal (see details in note [3]).

1

Alternatively, breathing rate can be monitoring alone using a simple custom designed piezoelectric device (sensitive to pressure) positioned in the chest of the animal.

2

Water bath is non-MRI compatible, so this was positioned outside the 5 Gauss security area. The bath is connected to the water blanket through two 5 meters long silicon tubes.

3

The automatic temperature control system is based on the Arduino microcontroller (Arduino MEGA 2560, Arduino S.r.l., Italy). To maintain the physiological temperature of the animal stable automatically, a PID (Proportional-Integral-Derivative) has been developed. The microcontroller obtains, through serial communication (using a RS232 Shield V2, LinkSprite Technologies, Inc., Longmont, CO), the temperature of the animal from the signal conditioner and it generates a control action that is

5. <u>Pulse generator</u> and current source (STG2004, Multichannel Systems, Reutlingen, Germany) for electric micro-stimulation.

6. <u>Digital Oscilloscope</u> (TDS 2004B, Tektronix, Beaverton, United States) to check electrode functionality.

7. <u>Eye ointment</u> (even if it is an acute procedure).

8. <u>MRI-compatible stereotaxic device</u> with ear- and bite-bars.

9. Agarose (0.5%) in saline. It is prepared and introduced in a 10 cc syringe. Can be storage in the fridge before its use (see note [4]).

10. Gradient Echo (GE)-Echo Planar Imaging (EPI) sequence providing adequate temporal and spatial resolution (see note [5] and [6]).

11. T_2-weighted anatomical images. We use a Rapid Acquisition Relaxation Enhanced sequence (RARE) (see note [7]).

12. Image analysis software. There are some commercially available software tools for fMRI analysis. In our case, fMRI data are analysed offline using our own software developed in MatLab, which included Statistical Parametric Mapping package (SPM8, http://fil.ion.ucl.ac.uk/spm), Analysis of Functional NeuroImages (AFNI, http://afni.nimh.nih.gov/afni) and FSL Software (FMRIB http://fsl.fmrib.ox.ac.uk/fsl).

---

transmitted to the thermostat (using a USB Host Shield V2.0 for Arduino) to control the temperature of the fluid pumped to the bed. This control system allows automatic temperature control, maintaining almost stable the temperature of the body of the animal being scanned. The technician can interact with the automatic temperature control system through a keypad and a display (LCD Keypad Shield for Arduino), being able to set the desired temperature for the animal.

4

Agarose can be prepared in deuterated water, so it will be invisible for MRI. Nevertheless, based on our experience, there are no benefits in terms of fMRI maps acquisition.

5

Sequence parameters for GE-EPI images: Field of View (FOV), 25 × 25 mm; slice thickness, 1 mm; 15 slices; matrix, 96 × 96; segments, 1; Flip angle, 60°; Echo Time (TE), 15 ms; Repetition Time (TR), 2000 ms and 4 dummy scans.

6

Alternatively you could use a Spin Echo (SE) sequence with similar parameters. There is extensive literature reviewing the impact of the employed sequence methodology in the obtained fMRI results [6]. Briefly, SE is more specific to microvasculature changes but less sensitive whereas GE is more influenced by changes in macrovasculature but overall more sensitive.

7

Sequence parameters for RARE images: FOV, 25 × 25 mm; slice thickness, 1 mm; 15 slices; matrix, 192 × 192; RARE factor, 8; Effective TE (TE_{eff}), 56 ms; TR, 2000 ms.

3. METHODS

All animal work should be carried out *only* upon review and approval of the methods by your institution's Animal Care and Use Committee [10,11]. For those new to MRI and small animal surgery, prior to initiating any studies, training and advice should be sought from experts in the field.

Due to the presence of strong magnetic fields, surgery is performed in an area separated from the magnet room. Thus, it will be necessary to fix the stimulating and/or recording electrode to the animal's skull so that the animal can be safely transferred to the magnet room at the end of the surgery. Furthermore, due to the common use of surface coils in fMRI experiments, both the electrode positioning and its fixations must be done in such a way that allow maximal proximity between the MRI coil and the brain of the animal. Special care must be taken with bleeding during surgery, because any trace of blood will have a deep impact in the image quality, making it very difficult to obtain a reliable BOLD signal.

3.1. Anesthesia

As previously introduced, most fMRI experiments in rodents are performed in anesthetized animals. Different anesthetics have been introduced for fMRI studies in rodents, each of which presents its particular advantages and drawbacks (for a review see [7]) and all of them having an impact on the neurovascular coupling. At this point, it is important to emphasise that, in our experience; at least 80% of a successful fMRI experiment in rodents relies on maintaining the animal's physiology at adequate and steady-state values. Body temperature (37±0.5 ºC), oxygen saturation (>95%), CO_2 (35-50 mmHg) levels and blood pressure (130-140 mm Hg) need to be fine-tuned. While precise monitoring of some of this values require invasive interventions (i.e. blood pressure and accurate CO_2 measurements require femoral artery cannulation and tracheotomy, respectively) or direct blood sampling difficult to implement in longitudinal studies, pilot experiments with full monitoring of the animal's physiology are strongly recommended in setting up new anaesthetic protocols.

The final election of an anesthetic method will depend on multiple factors like the species utilized (i.e. rats [12] *vs*. mice [13]), the duration of the experiment [14], whether it is an acute or longitudinal experiment, and even the type of stimuli used [15]. As a general rule, injectable anaesthetics provide a stable imaging condition for up to 2 h, whereas inhaled anaesthesia allows longer imaging sessions. An exception to this rule is urethane, which provides a stable and long-lasting (more than 8h) anesthetized state with a single intraperitoneal injection and minimal cardiovascular effects [16]. Importantly, urethane also preserves most of the characteristic electrophysiological rhythms recorded in the hippocampus and other neocortical regions [17]. In the present protocol of electric stimulation fMRI, urethane has been the choice based on the above advantages [17]. However, urethane is restricted to terminal experiments due to its hepatotoxic and carcinogenic effects, for which it is compulsory to

euthanize the animal at the end of the experiment. For chronic rat experiments and when working with mice, dexmedetomidine is the usual election [5]. It allows animal recovery but provides, in our hands, shorter periods of stable anesthesia (in the range of 1.5-2 h). An alternative administration regime for dexmedetomidine has been proposed to extend this period [18]. We have found significant differences between different rats and mice strains. So we do recommend a pilot study in order to choose the most convenient anesthesia for each particular model.

3.2. Electric stimulation

Stimulating electrodes dedicated to MRI experiments have been developed based on existing protocols [19]. Previous studies have shown the utility of iridium [20] or platinum-iridium electrodes [21] for this purpose. Nevertheless, these electrodes produce large susceptibility artefacts around the electrode's location, especially patent in EPI images, precluding the possibility to study functional responses in the area close to the implant. To overcome this problem, we have introduced glass-coated carbon fiber bipolar electrodes in our setup, which present several advantages: most importantly the absence of susceptibility artefacts in the acquired brain images, but also the possibility to produce very thin bipolar electrodes (up to 7 µm tip diameter) [17].

To prepare carbon-fiber electrodes, we use bundles of fibers inserted into a theta-shaped glass capillary previously pulled to form 7 mm long pipettes with ~200 µm tip diameter and adjusted to produce an electrical impedance of 40–65 kΩ (see note [8]). A regular wire with a pin connector is attached to the pipette, connected to the carbon fibers using silver conductive epoxy resin (RS Components, UK), and isolated with clear epoxy resin [17].

Depending on the configuration used in the MRI, the glass electrode can be bent in order to accommodate the receiver coil, minimizing its distance to the brain and maximizing the signal to noise ratio (SNR) (see details in section 3.4).

3.3. Stimulation protocols

In previous work applying electric-stimulation fMRI to study the frequency response of the perforant pathway, the major neocortical input to the hippocampus [22], we showed the existence of an activity threshold to elicit a detectable fMRI response. More specifically, we showed that (1) a certain level of activity, in an approximately constant population of neurons, must be reached in order to start a detectable BOLD signal, (2) the activity-threshold for BOLD elicitation can be reached by applying trains of pulses at relatively low frequencies (4-5 Hz for the perforant path), (3) once the

---

[8] Small electrode tips will cause less tissue damage during implantation, but the higher electric impedance would require higher voltages to inject a same amount of current and therefore the possibility to overheat and damage the tissue. Thus, there is a compromise between these two parameters. In our experience, an electrode tip of ~200 µm render good stimulation while minimizing tissue damage.

threshold is crossed, the BOLD signal (magnitude and extension of the activation) is linearly correlated with the stimulating current, (4) at current intensities evoking a half-maximal neuronal spiking response, the activity spreads polysynaptically, with increasing stimulation frequencies up to 20 Hz. Thus, stimulation protocols often consisted in 6 to 10 trains of electrical pulses (100 µs biphasic pulses) repeated every 30 to 60 s (total duration of the trial 180 to 600 s) and trials repeated 3 to 5 times per condition. The duration of the stimulation train can be adjusted to the specific needs, but durations between 2 and 6 s at frequencies ranging from 4-20 Hz produce BOLD responses of excellent amplitude (larger than 4% change) in a variety of preparations [22,21,17,23,24]. Off periods between stimulation trains sufficiently long as to allow a full recovery of the hemodynamic response (25-30 s in rats and mice) increase the SNR of the response and the statistical power of the analysis. A good coordination between image acquisition and timing of stimulus presentation is necessary and easily achievable using the TTL signals generated by the imaging protocols to synchronize the pulse generator (see Figure 1). Duration of the stimulation train, pulse shape and intensity, frequency, and any stimulus other parameter can be systematically varied for specific purposes [25].

Within each EPI acquisition, it is advisable to acquire long-enough baselines (4 to 8 volumes) before the first stimulation train that will facilitate posterior quantifications of BOLD signal change.

3.4. Intracerebral electrode implant for fMRI

Most of the BOLD based fMRI experiments are acquired using EPI images, which are very sensitive to T_2^* changes. Practically speaking, a number of factors can confabulate causing a deterioration of the quality of the functional images. When working with surgically manipulated animals, especially in acute preparations, extreme care has to be taken to minimize bleeding. After the surgery and before cementing the implant to the skull (see below) thorough cleaning of the exposed cranium is mandatory.

In order to improve the SNR, the tip of the electrode was bent using a Bunsen burner and some forceps to form a 90º angle, so it could go inside the brain leaving the main body of the pipette outside parallel to the head of the rat, minimizing the implant's height and allowing a closer proximity between the MRI array coil and the head of the animal.

The method described here is based on standard procedures used in electrophysiological experiments adapted to the MRI requirements. Similar protocols are used for mice.

   1. Weigh the animal.

   2. Dissolve urethane in sterile 0.9% saline. Warm it to room temperature before injection.

3. Place the animal in an induction chamber, and induce anaesthesia with 4% isoflurane in 100% oxygen (1L/min). Wait until the animal is superficially sedated (see note [9]).

4. Inject urethane intraperitoneally (1.3 g/Kg dose for rats and 1.5 g/kg dose for mice, see note [10]). Wait until the total absence of withdrawal reflexes. Induction time is heterogeneous across animals and strains. If after one hour of the initial dose the animal shows reflexes, additional doses (10-20% of initial dose) can be injected. In our experience, adjustment of the initial dose is necessary for different strains. The slow process of induction of anaesthesia ensures a steady-state anesthesia (with stable vital constants) during more than 8 h.

5. Upon induction, place the animal in a heating pad to maintain the animal's body temperature at 37 ºC. Use a rectal temperature probe with lubricating jelly to monitor the temperature.

6. Shave the head around the incision area.

7. When the animal reaches an appropriate level of anesthesia, fix the animal's head in a stereotaxic frame.

8. Inject subcutaneous local anesthetic (200 uL Bupivacaine, 0.5%) in the incision points, using a 1cc syringe with a 20G needle tip.

9. In order to prevent eye damage, employ ophthalmic gel (Lipolac) on each eye. The gel needs to be reapplied during the surgery to ensure that eyes are covered at all times.

10. Make an incision (~1 cm long) at the top of the head by pressing firmly with a scalpel in an antero-posterior direction. Remove excess skin to expose the skull. Cauterize the skin rims, avoiding burning the skull to prevent image artefacts, and apply hydrogen peroxide to remove any source of bleeding.

> a) In our experience, when working with mice, the complete removal of the skin over the skull significantly increases the quality of the fMRI images. To do that, gently cut with surgical scissors the skin over the head. Remove the excess skin, cauterize borders (with extreme caution to avoid overheating the skull) and apply hydrogen peroxide to clean the area. Carefully remove any trace of blood.

9

Some animal strains are more susceptible of anesthetics mixture and can be affected by the interaction of urethane and isofluorane. In this case, we recommend injecting the animal without previous exposure to other anesthetic.

10

Usually, urethane is injected at doses in the range of 1.2 to 1.4 g/Kg for rats and 1.4 to 1.6 for mice.

11. Calculate the goal stereotaxic coordinates. Modern tools have been developed to facilitate electrode localization [26].

12. Once the target site is located, trephine holes are made using a manual drill. First-time used drill-bits require deep cleaning to remove metal traces that can detach and enter the craniotomy producing large image artefacts.

a) Carefully rotate the drill bit over the skull until achieving a circular craniotomy (2 mm diameter).

b) Delicately pinch the dura using a curved 25G needle. For mice, it is better to avoid this step to minimize bleeding. The dura can be broken directly when introducing carefully the electrode in step 13.

c) Add saline to the craniotomy once dura is pierced to avoid dryness.

13. Slowly lower the MRI-compatible electrode until it reaches the desired ventral coordinate (see notes [11] and [12]).a) If the dura is not broken by the electrode in the case of mice, do not force it (the electrode can be broken or the brain damaged). Go back to step 12.b. and pinch it with the needle.

14. Deeply clean the skull using a dry cotton swab, eliminating any bleeding. Add a small drop of tissue adhesive (Vetbond) to seal the tissue, and wait for 10 minutes.

15. Fix the electrode with several layers of acrylic (Palacos for rats and Super-Bond for mice).

a) Pay special attention to the first layer of acrylic. This is the critical one and should cover as much surface of the skull, including the electrode, as possible. Use less viscous cement in this first layer than in next ones. Wait until it the layer is completely dry (~20 min) before applying more cement.

b) In mice the first layer is crucial. The skull is smaller compared with rats, and the cement has less surface to weld in. Thus, the electrode is more exposed being susceptible of movements and/or breakages. In order to minimize these, we

---

11

For instance, to stimulate the CA3 region of the dorsal hippocampus in the rat the coordinates, referenced to Bregma, are: 3.5 mm anteroposterior and 3.5 mm lateral, initial position 3.6 mm ventral to the dural surface.

12

The same procedure can be followed to insert a recording electrode in the desired area to be sure about stimulation electrode positioning. Nevertheless, care must be taken when placing the recording electrode to minimize brain damage. Ideally, this recording electrode should be placed in a region not fundamental for the fMRI study.

recommend generously covering the section of the electrode closer to the mouse's head using Super-Bond acrylic.

c) Apply extra layers around the implant until fully embedding it, preventing post-surgical movement and protecting it during the transport of the animal to the MRI room. Avoid contact of the cement with the skin during the whole process. This precaution will minimize the probability of bleeding during the imaging session.

16. When the cement is completely dry, remove the electrode holder.

17. Detach the animal from the stereotaxic frame and place it in a transfer cage. In order to avoid temperature dropping, maintain the animal in the heating pad until its transport to the imaging facility.

3.5. fMRI

In order to prevent temperature drop, preheat the magnet's heating system before the animal arrives to the facility.

1. Place the animal in the MRI bed.

2. Check that the correct level of anesthesia has been maintained.

3. Insert the rectal temperature probe using lubricating jelly and tape it in place.

4. Fix the animal's head in an MRI-compatible stereotaxic device.

5. Place the physiological monitoring device (MRI-compatible sensor with foot clip) or the breathing piezoelectric sensor.

6. Cover the exposed skull and the implant with agarose, with special emphasis in filling all the possible empty spaces between the head of the animal and the coil (see notes [13]).

7. Connect the electrode to the current source.

8. Using the oscilloscope, cross-check the impedance of the electrode that should match the value obtained during its fabrication, discarding a possible breakdown in the process of implantation or during the accommodation of the animal in the MRI setup.

9. Fix the coil in the MRI bed over the head of the animal, as close

---

13

EPI images are highly sensible to abrupt changes in magnetic susceptibility originating artifacts in the border where the variation occurs. Due to the specific configuration used in our set up, when the phase array coil is positioned, there is an empty space between the surface coil and the head of the animal. We fill this space with agarose using a syringe previously filled with agarose 0.5%.

as possible to the skull (see note [14]).

10. Place the animal inside the RF coil aligning the approximate center of the brain with the magnet isocenter.

11. Acquire T2-weighted (T2w) anatomical images in the three orthogonal planes.

12. Even when the animal positioning is accurate, there can be small inter-animal differences when defining an exact position. In order to do grouped analyses, it is interesting to minimize this variability. Thus, we recommend using anatomical landmarks to position EPI slices always in the same orientation. A possible strategy is:

a) Take the plane that cut the base of cerebellum and the anterior commissure (see Figure 2a).

b) Take the midline plane that separates the brain in left and right hemispheres (Figure 2b and 2c).

c) Use the above anatomical planes to define the angle and positioning of the slices for functional imaging. In our case, 15 slices are positioned perpendicular to the planes with the 6th more anterior slice containing the anterior commissure (Figure 2d).

13. Use a shimming procedure to adjust field homogeneity in the brain. In our case, we use the MapShim macro implemented by Bruker.

14. Adjust the EPI images according to the landmarks mentioned in step 12 (see note[15]) and use saturation slices around the brain. Acquire a set of EPI images without stimulation to check proper image acquisition (no folding, ghosts, etc.)

15. Acquire an anatomical image with the same geometry than the EPI images but higher (at least double) in plane spatial resolution. It will help to identify anatomical landmarks (Figure

---

14

 Avoid excessive pressure between the coil and electrode. Usually electrodes are fragile and break easily during the experiment if there is some of pressure on them.

15

 The employed FOV usually exceeds the cross section of the subject to prevent artifacts from image folding. The slice thickness is 1 mm for rats and 0.8 mm for mice, but depending on the SNR and the expected level of activation, it could be decreased.

3) and co-registration of brain templates for grouped analysis.

16. Start data acquisition.

3.6. Data analysis

The development of either commercial or open-source software tools for fMRI analysis has greatly facilitated the applicability of fMRI and has contributed to its massive widespread. Nevertheless, due to the complex mathematical work behind the generation of brain activation maps, it is important to apply proper and robust statistical methods, e.g. to avoid false positives [27]. For a deep discussion about the analysis see refs [28,29]. The workflow for the data analysis used in our laboratory implies linear detrending, temporal (0.015–0.2 Hz) and spatial filtering (3 × 3 full width at half maximum gaussian kernel of 1.5 sigma) of voxel time series, a general linear model or cross-correlation analysis with a simple boxcar model shifted forward in time (typically by the employed TR), or a boxcar convolved with the hemodynamic response function (HRF). Typical functional maps obtained in one of our electric-stimulation fMRI experiments are shown in Figure 3.

4. NOTES

1. Alternatively, breathing rate can be monitoring alone using a simple custom designed piezoelectric device (sensitive to pressure) positioned in the chest of the animal.

2. Water bath is non-MRI compatible, so this was positioned outside the 5 Gauss security area. The bath is connected to the water blanket through two 5 meters long silicon tubes.

3. The automatic temperature control system is based on the Arduino microcontroller (Arduino MEGA 2560, Arduino S.r.l., Italy). To maintain the physiological temperature of the animal stable automatically, a PID (Proportional-Integral-Derivative) has been developed. The microcontroller obtains, through serial communication (using a RS232 Shield V2, LinkSprite Technologies, Inc., Longmont, CO), the temperature of the animal from the signal conditioner and it generates a control action that is transmitted to the thermostat (using a USB Host Shield V2.0 for Arduino) to control the temperature of the fluid pumped to the bed. This control system allows automatic temperature control, maintaining almost stable the temperature of the body of the animal being scanned. The technician can interact with the automatic temperature control system through a keypad and a display (LCD Keypad Shield for Arduino), being able to set the desired temperature for the animal.

4. Agarose can be prepared in deuterated water, so it will be invisible for MRI. Nevertheless, based on our experience, there are no

benefits in terms of fMRI maps acquisition.

5. Sequence parameters for GE-EPI images: Field of View (FOV), 25 × 25 mm; slice thickness, 1 mm; 15 slices; matrix, 96 × 96; segments, 1; Flip angle, 60°; Echo Time (TE), 15 ms; Repetition Time (TR), 2000 ms and 4 dummy scans.

6. Alternatively you could use a Spin Echo (SE) sequence with similar parameters. There is extensive literature reviewing the impact of the employed sequence methodology in the obtained fMRI results [6]. Briefly, SE is more specific to microvasculature changes but less sensitive whereas GE is more influenced by changes in macrovasculature but overall more sensitive.

7. Sequence parameters for RARE images: FOV, 25 × 25 mm; slice thickness, 1 mm; 15 slices; matrix, 192 × 192; RARE factor, 8; Effective TE (TE_{eff}), 56 ms; TR, 2000 ms.

8. Small electrode tips will cause less tissue damage during implantation, but the higher electric impedance would require higher voltages to inject a same amount of current and therefore the possibility to overheat and damage the tissue. Thus, there is a compromise between these two parameters. In our experience, an electrode tip of ~200 μm render good stimulation while minimizing tissue damage.

9. Some animal strains are more susceptible to anaesthetics mixture and can be affected by the interaction of urethane and isoflurane. In this case, we recommend injecting the animal without previous exposure to other anaesthetic.

10. Usually, urethane is injected at doses in the range of 1.2 to 1.4 g/Kg for rats and 1.4 to 1.6 for mice.

11. For instance, to stimulate the CA3 region of the dorsal hippocampus in the rat the coordinates, referenced to Bregma, are: 3.5 mm anteroposterior and 3.6 mm lateral, initial position 3.8 mm ventral to the dural surface.

12. The same procedure can be followed to insert a recording electrode in the desired area to be sure about stimulation electrode positioning. Nevertheless, care must be taken when placing the recording electrode to minimize brain damage. Ideally, this recording electrode should be placed in a region not fundamental for the fMRI study.

13. EPI images are highly sensible to abrupt changes in magnetic susceptibility originating artifacts in the border where the variation occurs. Due to the specific configuration used in our set up, when the phase array coil is positioned, there is an empty space between the surface coil and the head of the animal. We fill this space with agarose using a syringe previously filled with agarose 0.5%.

14. Avoid excessive pressure between the coil and electrode. Usually electrodes are fragile and break easily during the experiment if there is some of pressure on them.

15. The employed FOV usually exceeds the cross section of the subject to prevent artefacts from image folding. The slice thickness is 1 mm for rats and 0.8 mm for mice, but depending on the SNR and the expected level of activation, it could be decreased.

ACKNOWLEDGEMENTS

REFERENCES

1. Crosson B, Ford A, McGregor KM, Meinzer M, Cheshkov S, Li X, Walker-Batson D, Briggs RW (2010) Functional imaging and related techniques: an introduction for rehabilitation researchers. Journal of rehabilitation research and development 47 (2): vii-xxxiv.

2. Ogawa S, Lee TM, Kay AR, Tank DW (1990) Brain magnetic resonance imaging with contrast dependent on blood oxygenation. Proceedings of the National Academy of Sciences of the United States of America 87 (24):9868-9872.

3. Logothetis NK (2008) What we can do and what we cannot do with fMRI. Nature 453 (7197):869-878.

4. Moreno A, Jego P, de la Cruz F, Canals S (2013) Neurophysiological, metabolic and cellular compartments that drive neurovascular coupling and neuroimaging signals. Frontiers in neuroenergetics 5:3.

5. Jego P, Pacheco-Torres J, Araque A, Canals S (2014) Functional MRI in mice lacking IP3-dependent calcium signaling in astrocytes. Journal of cerebral blood flow and metabolism: official journal of the International Society of Cerebral Blood Flow and Metabolism 34 (10):1599-1603.

6. Greve JM (2011) The BOLD effect. Methods in molecular biology 771:153-169.

7. Masamoto K, Kanno I (2012) Anesthesia and the quantitative evaluation of neurovascular coupling. Journal of cerebral blood flow and metabolism: official journal of the International Society of Cerebral Blood Flow and Metabolism 32 (7):1233-1247.

8. Liang Z, Watson GD, Alloway KD, Lee G, Neuberger T, Zhang N (2015) Mapping the functional network of medial prefrontal cortex by combining optogenetics and fMRI in awake rats. NeuroImage 117:114-123.

9. Harris AP, Lennen RJ, Marshall I, Jansen MA, Pernet CR, Brydges NM, Duguid IC, Holmes MC (2015) Imaging learned fear circuitry in awake mice using fMRI. The European journal of neuroscience 42 (5):2125-2134.

10. National Research Council (2011) Guide for the Care and Use of Laboratory Animals. National Academies Press, Washington (DC).

11. European Convention for the Protection of vertebrate animals used for experimental and other scientific purposes (2006) Appendix A. Guidelines for accommodation and care of animals (Article 5 of the Convention).

12. Hendrich KS, Kochanek PM, Melick JA, Schiding JK, Statler KD, Williams DS, Marion DW, Ho C (2001) Cerebral perfusion during anesthesia with fentanyl, isoflurane, or pentobarbital in normal rats studied by arterial spin-labeled MRI. Magnetic resonance in medicine 46 (1):202-206.

13. Schroeter A, Schlegel F, Seuwen A, Grandjean J, Rudin M (2014) Specificity of stimulus-evoked fMRI responses in the mouse: the influence of systemic physiological changes associated with innocuous stimulation under four different anesthetics. NeuroImage 94:372-384.

14. Sonnay S, Just N, Duarte JM, Gruetter R (2015) Imaging of prolonged BOLD response in the somatosensory cortex of the rat. NMR in biomedicine 28 (3):414-421.

15. Paasonen J, Salo RA, Shatillo A, Forsberg MM, Narvainen J, Huttunen JK, Grohn O (2016) Comparison of seven different anesthesia protocols for nicotine pharmacologic magnetic resonance imaging in rat. European neuropsychopharmacology: the journal of the European College of Neuropsychopharmacology 26 (3):518-531.

16. Maggi CA, Meli A (1986) Suitability of urethane anesthesia for physiopharmacological investigations in various systems. Part 2: Cardiovascular system. Experientia 42 (3):292-297.

17. Moreno A, Morris RG, Canals S (2016) Frequency-Dependent Gating of Hippocampal-Neocortical Interactions. Cerebral cortex 26 (5):2105-2114.

18. Pawela CP, Biswal BB, Hudetz AG, Schulte ML, Li R, Jones SR, Cho YR, Matloub HS, Hyde JS (2009) A protocol for use of medetomidine anesthesia in rats for extended studies using task-induced BOLD contrast and resting-state functional connectivity. NeuroImage 46 (4):1137-1147.

19. Shyu BC, Lin CY, Sun JJ, Sylantyev S, Chang C (2004) A method for direct thalamic stimulation in fMRI studies using a glass-coated carbon fiber electrode. Journal of neuroscience methods 137 (1):123-131.

20. Sultan F, Augath M, Murayama Y, Tolias AS, Logothetis N (2011) esfMRI of the upper STS: further evidence for the lack of electrically induced polysynaptic propagation of activity in the neocortex. Magnetic resonance imaging 29 (10):1374-1381.

21. Alvarez-Salvado E, Pallares V, Moreno A, Canals S (2014) Functional MRI of long-term potentiation: imaging network plasticity. Philosophical transactions of the Royal Society of London Series B, Biological sciences 369 (1633):20130152.

22. Canals S, Beyerlein M, Murayama Y, Logothetis NK (2008) Electric stimulation fMRI of the perforant pathway to the rat hippocampus. Magnetic resonance imaging 26 (7):978-986.

23. Godino Mdel C, Romera VG, Sanchez-Tomero JA, Pacheco J, Canals S, Lerma J, Vivancos J, Moro MA, Torres M, Lizasoain I, Sanchez-Prieto J (2013) Amelioration of ischemic brain damage by peritoneal dialysis. The Journal of clinical investigation 123 (10):4359-4363.

24. Hadar R, Vengeliene V, Barroeta Hlusicke E, Canals S, Noori HR, Wieske F, Rummel J, Harnack D, Heinz A, Spanagel R, Winter C (2016) Paradoxical augmented relapse in alcohol-dependent rats during deep-brain stimulation in the nucleus accumbens. Translational psychiatry 6 (6): e840.

25. Tehovnik EJ, Tolias AS, Sultan F, Slocum WM, Logothetis NK (2006) Direct and indirect activation of cortical neurons by electrical microstimulation. Journal of neurophysiology 96 (2):512-521.

26. Pallares V, Moya J, Samper-Belda FJ, Canals S, Moratal D (2015) Neurosurgery planning in rodents using a magnetic resonance imaging assisted framework to target experimentally defined networks. Computer methods and programs in biomedicine 121 (2):66-76.

27. Eklund A, Nichols TE, Knutsson H (2016) Cluster failure: Why fMRI inferences for spatial extent have inflated false-positive rates. Proceedings of the National Academy of Sciences of the United States of America 113 (28):7900-7905.

28. Poldrack RA, Mumford JA, Nichols TE (2011) Handbook of Functional MRI Data Analysis. Cambridge University Press.

29. Ashby FG (2011) Statistical Analysis of FMRI Data. MIT Press.